

THE DYNAMICS OF THE LOW ENERGY PLASMA IN THE JOVIAN MAGNETOSPHERE

by

RALPH L. MCNUTT, JR.

B.S., Texas A & M University

(1975)

SUBMITTED IN PARTIAL FULFILLMENT  
OF THE REQUIREMENTS FOR THE  
DEGREE OF

DOCTOR OF PHILOSOPHY

at the

MASSACHUSETTS INSTITUTE OF TECHNOLOGY

JULY, 1980

© Massachusetts Institute of Technology 1980

Signature of Author \_\_\_\_\_ Department of Physics, July 25, 1980

Certified by \_\_\_\_\_ Thesis Supervisor

Accepted by \_\_\_\_\_ Chairman, Department Committee

ARCHIVES  
MASSACHUSETTS INSTITUTE  
OF TECHNOLOGY

SEP 24 1980

LIBRARIES



Room 14-0551  
77 Massachusetts Avenue  
Cambridge, MA 02139  
Ph: 617.253.2800  
Email: docs@mit.edu  
<http://libraries.mit.edu/docs>

## **DISCLAIMER OF QUALITY**

Due to the condition of the original material, there are unavoidable flaws in this reproduction. We have made every effort possible to provide you with the best copy available. If you are dissatisfied with this product and find it unusable, please contact Document Services as soon as possible.

Thank you.

**Some pages in the original document contain pictures, graphics, or text that is illegible.**

## THE DYNAMICS OF THE LOW ENERGY PLASMA IN THE JOVIAN MAGNETOSPHERE

by

RALPH L. MCNUTT, JR.

Submitted to the Department of Physics  
on July 25, 1980 in partial fulfillment of the requirements  
for the Degree of Doctor of Philosophy.

## ABSTRACT

Positive ion data gathered by the Voyager Plasma Science experiment in the dayside Jovian magnetosphere are analyzed to obtain densities, velocity components, and temperatures of the low energy plasma population. This reduced data set is discussed in the context of the outstanding questions concerning this plasma population and its dynamics.

Specifically, we find that on the dayside, there exists a plasma population of temperature  $\sim 100$  electron volts which moves azimuthally but does not rigidly corotate with the planet. The plasma mass density is everywhere dominated by heavy ions and the density gradient is consistent with outward plasma diffusion via flux tube interchange. We also find a local time asymmetry in the plasma data which we interpret as being magnetic field aligned flow away from the magnetic equator on the dayside and toward it on the nightside. The flow is presumably driven by the asymmetry in the magnetosphere produced by the solar wind.

The plasma tends to be concentrated in a plasma sheet, which is associated with the current sheet inferred from Voyager Magnetometer measurements. The sheet plasma is relatively cool, and apparently diffuses outward from the Io torus. Although the plasma sheet itself forms a time stationary pattern, plasma contained therein is in a dynamical state which affects momentum balance across the sheet. The inertia of the sheet apparently causes the lack of corotation of the dayside magnetosphere. In addition, the plasma flow in the sheet is super-Alfvénic, although this condition does not result in a planetary wind outflow, as some investigators have theorized.

The observed plasma provides the inertia in the Jovian magnetosphere, inside of approximately 40 Jovian radii. This is ultimately responsible for plasma transport, angular momentum transport, and the magnetic field line configuration in the dayside magnetosphere.

Thesis Supervisor: John W. Belcher

Title: Associate Professor of Physics

To Nancy

And to my parents

## TABLE OF CONTENTS

	PAGE
ABSTRACT	
CHAPTER I. THE JOVIAN MAGNETOSPHERE BEFORE VOYAGER	8
A. Introduction	8
B. Radio Observations	9
C. Magnetosphere Models Before Pioneer	12
1. Corotation	13
2. Flux Tube Interchange	16
3. The Centrifugal Instability	17
4. Plasma Spatial Distribution	19
5. Pre-Pioneer Expectations	21
D. Earth Based Optical Observations	22
E. Pioneer Observations	23
1. Spacecraft and Trajectory	23
2. Global Structure	24
3. Energetic Particle Anisotropies	27
4. Low Energy Plasma Measurements	28
F. Magnetospheric Models after Pioneer	30
1. Magnetodisc Models	30
2. Planetary Wind Models	33
3. Clock Model	35
4. Sources of Magnetospheric Plasma	36
G. Outstanding Problems Before Voyager	37
CHAPTER II. THE VOYAGER PLASMA SCIENCE EXPERIMENT	39
A. The Voyager Spacecraft	39

B.	Plasma Science Instrument Description and Operation	40
C.	Basic Considerations in Data Interpretation	42
D.	Spacecraft Trajectory and Instrument Response During Jupiter Encounter	48
CHAPTER III.	PLASMA OBSERVATIONS IN THE MIDDLE MAGNETOSPHERE	53
A.	Introduction	53
B.	Positive Ion Charge Density	54
C.	Analysis of Highly Resolved Spectra from Voyager 1	57
1.	Constraints on the Analysis	57
2.	Composition and Temperature: Major Ionic Species	59
3.	Composition and Temperature: Minor Ionic Species	63
4.	Limits on the Electrostatic Potential of the Spacecraft	67
5.	Comparison of Results of L-Mode and M-Mode Analyses	69
D.	Survey of L-Mode and M-Mode Spectra	72
E.	Global Parameter Values from Side Sensor Data	76
F.	Global Flow Information from Main Sensor Data	83
G.	Detailed Plasma Sheet Observations	87
CHAPTER IV.	DISCUSSION OF RESULTS	92
A.	Global Variations of Macroscopic Plasma Parameters	92

1. Azimuthal Velocity Component	92
2. Field Aligned Velocity Component	96
3. Plasma Transport: Absence of a "Wind"	99
4. Plasma Transport: Diffusion	101
5. Plasma Density and Marginal Stability for Interchange Motions	103
6. Plasma Temperature	106
B. Physics of the Plasma Sheet	107
C. Correlation With Other Voyager Results	114
D. Comparison With Pioneer 10 Measurements of the Magnetospheric Plasma	117
CHAPTER V. CONCLUSION	120
A. Summary of Results	120
B. Questions and Future Opportunities	122
APPENDIX. NON-LINEAR LEAST SQUARES FIT	125
A.1. Procedure	125
A.2. Error	128
A.3. Currents and Derivatives	130
A.4. Initialization	133
A.5. Assumptions Used in Fits to the Data	137
ACKNOWLEDGEMENTS	139
REFERENCES	140
TABLES	157
FIGURE CAPTIONS	165
FIGURES	178
BIOGRAPHICAL NOTE	232

## CHAPTER I. THE JOVIAN MAGNETOSPHERE BEFORE VOYAGER

## A. INTRODUCTION

The planet Jupiter has been known and its motion observed since the time of the ancient astronomers of Chaldea and Alexandria. Knowledge of the planet itself has only been gathered in recent historical times and the vast majority of that only in the last decade. In 1610 Gallileo was the first to see the planet as more than just a point of light. He discovered the lighter zones and darker belts that encircle the planet and the four Jovian moons, now named in his honor.

The Jovian magnetosphere was discovered only in the second half of this century. In situ investigation of this structure by instrumented spacecraft has only been accomplished within the last decade. In Chapter I of this work, we review the relevant observations of the magnetosphere from Earth and the in situ observations by the Pioneer 10 and Pioneer 11 spacecraft, as well as some of the theoretical models which these observations inspired. We also discuss the outstanding problems which were unresolved before the Voyager encounters in 1979.

The second chapter describes the Plasma Science experiment flown on the more sophisticated Voyager 1 and Voyager 2 spacecraft. We describe the basic measurements possible with the instrument and consider their advantages and disadvantages in the determination of the characteristics of the magnetospheric plasma.

We describe the observations of the low energy plasma population in Chapter III, where we characterize the data and present results of our detailed plasma data analysis.

In the fourth chapter we discuss the global magnetospheric morphology of the low energy plasma population. This includes a discussion of the plasma sheet surrounding Jupiter and the transport of plasma in the dayside magnetosphere. Finally, we compare our findings with those of the other Voyager fields and particle experiments.

The last section summarizes our conclusions, enumerates some of the still unanswered questions, and discusses future opportunities for in situ measurements.

## B. RADIO OBSERVATIONS

In 1954, Burke and Franklin (1955) discovered radio emissions from Jupiter at 22.2 MHz. Previous observations had been made at 18.3 MHz (Shain, 1956), but Jupiter had not been recognized as the source. They found that the emission tends to be right circularly polarized, suggesting influence on the propagation by a Jovian magnetic field. After several years of observations, it became clear that the emission features rotate with the planet but with a period differing slightly from that of the observable clouds. The System III planetary longitude system, rotating with these features, was subsequently adopted by the IAU to coordinate observations of radio emissions.

These emissions gave rise to an entire field of study. The emissions occur as bursts of radio noise of either short (~ millisecond) or long (~ second) time duration. Ground based observations have detected activity from about 3 to 40 MHz, hence the name "decametric radiation". Three main sources of emission were identified. In addition, Bigg (1964) noted that the position of the Galilean satellite Io appears to modulate the emission

probability of some of the sources. The non-Io correlated emissions were related to a range of Zenographic System III longitudes. This range was named the "active hemisphere."

Other radio emissions were observed coming from Jupiter soon after the discovery of decametric emission. In 1958, thermal emission was detected from Jupiter at 9450 MHz (Mayer et al., 1958). A year later, a new non-thermal component was observed at 3000 MHz (Sloanaker, 1959) and within six years, the non-thermal component was observed down to 200 MHz (see Roberts, 1965). This "decimetric emission" is characterized both by its non-thermal spectrum and a large degree of linear polarization.

Accumulated observational evidence strongly supported the theory that the emission was due to synchrotron radiation from electrons trapped in a roughly dipolar, planetary magnetic field. The flux density and polarization of the decimetric component were found to vary with the System III longitude. Variation in the former was ascribed to the beaming of radiation from very energetic electrons. It was postulated that these were trapped in a dipole field tilted with respect to the Jovian rotation axis. In such a configuration, the flux density should (and is observed to) peak twice each Jovian rotation period, i.e., when the "magnetic equator" (symmetry surface of the magnetic field) is viewed edge on. As the earth lies within  $3^\circ$  of Jupiter's rotational equatorial plane, minima in the observed flux density corresponds to the pointing toward and away from Earth, respectively, of the two magnetic poles. Morris and Berge (1962) first noted the variation of the polarization plane by  $\pm 10^\circ$ . Most radiating electrons mirror close to the magnetic equator, implying that the magnetic axis is inclined by  $\sim 10^\circ$  with respect to the rotational axis of the planet. This observation also allowed the deduction of the System III

longitude of the magnetic pole in the northern hemisphere. It was noted, however, that the variation with time of the polarization angle deviated from pure sinusoidal, suggesting that higher multipole moments of the field must be significant in the emission region. Berge (1966) made interferometric observations at 2880 MHz and 1415 MHz to construct a two dimensional brightness temperature map of the decimetric emission. Using several symmetry assumptions he found a brightness peak located about one Jovian diameter from the center of the planet on each side of the magnetic axis, indicating the location and extent of the Jovian radiation belts. In contrast to the decametric radiation, the decimetric radiation has only a very weak circularly polarized component and is not influenced by Io. The longitude distribution of flux density and polarization angle as observed over the years allowed a determination of the mean rotation rate of the decimetric emission sources. In 1967, Komesaroff and McCulloch (1967) found a rotation period within a second of the System III period.

These radio observations gave the first knowledge of the Jovian magnetic field and trapped particle population. Following the initial decametric observations, it was proposed that the decametric emissions occur just above the local electron gyrofrequency in the extraordinary mode (Ellis, 1965). On the basis of the observed frequencies, it was the surface field strength must therefore exceed four gauss (Warwick, 1967; Goldreich and Lynden-Bell, 1969). For the extraordinary mode, right hand circular polarization should be observed if the magnetic field has a component toward the observer. With the knowledge of the System III longitudes of the magnetic poles, this implied that the northern magnetic pole of Jupiter is located in its northern hemisphere. The magnetic field of Jupiter should therefore point southward at its equator, the opposite

situation from that on Earth. Berge (1965) reached the same conclusion from the circularly polarized component of the decimeter radiation.

From the theory of synchrotron emission (Ginzburg and Syrovatskii, 1965) the number and characteristic energy of radiating electrons can be calculated if the magnetic field strength, spectrum and intensity are known. Using the spectrum maximum and intensity measurements a one gauss field implies  $10^{28}$  electrons at 14 MeV. This is consistent with the magnetic field exerting total control over the electron motion for a belt centered on 4 Jovian radii about 2 radii in diameter, as seen in the two dimensional brightness measurements (Berge 1966). The time scale for energy loss is about a year. The radiation belts are an entire field of study in and of themselves. Subsequent to the Pioneer flybys of Jupiter, the subject has been reviewed by Schulz (1979).

### C. MAGNETOSPHERIC MODELS BEFORE PIONEER

The first attempts to model the magnetosphere of Jupiter were based on extrapolating the knowledge of the magnetosphere of the earth. At the time, nothing was known of the solar wind at the orbit of Jupiter. It was generally assumed that the solar wind did flow past the orbit of Jupiter and would be diverted by the presence of the Jovian magnetic field. Using the Parker model of the solar wind, measured solar wind parameters at the earth, and a dipole field for Jupiter, simple calculations gave a standoff value of  $\sim 50 R_J$  (Jovian radii;  $1 R_J = 71,000$  km) for a surface magnetic field strength of  $\sim 10$  gauss (Brice and Ioannidis, 1970). Hence, the Jovian field was considered strong enough not only to form a magnetosphere like the earth's, but also one large enough to encompass all four of the large

Galilean satellites. Balancing the magnetic pressure against the thermal pressure of the solar wind also suggested a long magnetotail for Jupiter with an extent of at least  $100 R_J$ . It was also noted that the open field lines in such a tail should also form a polar cap as at the earth (Brice and Ioannidis, 1970).

At the same time it was recognized that Jupiter's magnetosphere must be inherently different from the earth's, as a result of its higher rotation rate, as emphasized by Ellis (1965). The discussion of the global dynamics of the Jovian magnetosphere has always been related to one of three concepts or mechanisms. These are corotation, flux tube interchange, and the centrifugal instability. The three are, to some degree, inter-related, and of consequence for magnetized planets with "rapid" rotation rates. We discuss these three concepts below.

### 1. COROTATION

The rotation of a planet and of its atmosphere is coupled through its ionosphere to its magnetosphere. Given the velocity of the neutrals in the ionosphere  $\vec{V}_N$ , and the planetary magnetic field  $\vec{B}$ , an electric field:

$$\vec{E} = -\frac{1}{c} \vec{V}_N \times \vec{B}$$

must be established near the planet in order that the net force vanish on the electrons and ions in the ionosphere. In general, the magnetospheric plasma should exhibit infinite conductivity along magnetic field lines and infinite resistivity across them, so that this electric field maps along the field lines into the magnetosphere and imparts a drift velocity to the magnetospheric plasma.

If the viscosity in the neutral atmosphere and the conductivity in the ionosphere are both sufficiently large, the magnetic field in the magnetosphere will, in effect, be rigidly coupled to the planet. In this case, the plasma drift velocity at a location  $\vec{r}$  in the magnetosphere is given by

$$\vec{V} = \vec{\Omega} \times \vec{r}$$

where  $\vec{\Omega}$  is the planetary angular velocity. The magnetosphere is then said to "rigidly corotate" or "corotate" with the planet (Davis, 1947; Davis, 1948; Hones and Bergeson, 1965; Melrose, 1967; Birmingham and Northrup, 1979).

Gold (1964) also noted that all of the planets with a magnetic field will enforce corotation close to the planet.

However, farther from the planet, in the terrestrial magnetosphere, the corotation electric field is not the dominant electric field. The interaction between the magnetosphere and the solar wind leads to plasma flow driven by the solar wind. Given the solar wind velocity  $\vec{V}_{SW}$  and magnetic field  $\vec{B}_{SW}$ , this motion is controlled by the convection electric field

$$\vec{E}_{conv} = - \frac{\vec{V}_{SW}}{C} \times \vec{B}_{SW}$$

induced by the solar wind. Close to the earth the "corotation" electric field (equation (1)) dominates. The magnetic shell (which is also a constant electric potential shell) on which the total electric field is zero is the plasmapause. Tubes of constant magnetic flux inside the

plasmopause corotate with the earth and tend to remain "full" of plasma while those outside "spill" plasma down the magnetotail and tend to remain "empty". Observationally, this boundary in the Earth's magnetosphere occurs inside the magnetopause (the magnetospheric outer boundary), and exhibits a change in plasma number density of as much as two orders of magnitude (Carpenter, 1966). In Jupiter's magnetosphere, using extrapolated solar wind parameters, Brice and Ioannidis (1970) found that the plasmopause and magnetopause should essentially coincide. As a result, Jupiter's flux tubes should remain closed to solar wind plasma, "full" of any plasma created within the Jovian magnetosphere, and should corotate with the planet.

In the case of Jupiter, Gledhill (1967a) noted that corotation should occur unless one or more of the following applies:

- (a) the plasma density becomes so small that parallel electric fields can exist
- (b) the plasma density becomes so large that there is conduction across the lines of force
- (c) the differential motions of the ions and electrons produce currents which appreciably distort the planetary magnetic field
- (d) the viscous interactions at the magnetosphere/solar wind boundary retard the motion
- (e) the plasma density becomes so small that the space charge necessary to produce the corotation electric field cannot be maintained.

Historically, this concept of corotation was first stated in a more general form for magnetic stars by Ferraro (1937). Since stellar atmos-

pheres are fully ionized, the magnetic field is, in fact, rigidly coupled to the stellar surface. However, the angular speed  $\Omega$  of the "surface" material need not be the same everywhere. Ferraro's isorotation law states that  $\Omega$  must be constant along a given magnetic field line. If there exists a magnetic symmetry axis, then the angular velocity must be constant over a magnetic surface formed by revolving a field line about that axis. The same general result is applicable to a planet with a differentially rotating ionosphere.

## 2. FLUX TUBE INTERCHANGE

Flux tube interchange was first proposed by Gold (1959) as a means of plasma transport in the earth's magnetosphere. In the terrestrial case, this interchange is envisioned as being driven by pressure gradient forces. Gold found that interchange will occur if the plasma energy density in a flux tube falls off faster than  $r^{-4}$  in the isothermal case or faster than  $r^{-20/3}$  in the adiabatic case. Such pressure gradient interchange motions were considered in more detail by Sonnerup and Laird (1963).

At Jupiter, it was hypothesized that the centrifugal force seen by corotating plasma dominates, and would drive the interchange (Ioannidis and Brice, 1971). Although flux tube field lines are "frozen" to the magnetospheric plasma, the "feet" of the tubes are free to move in the ionosphere relative to the planet provided the resistivity of the ionosphere is low enough at some ionospheric level. In this case, overloading of plasma in the equatorial plane results in a Rayleigh-Taylor type of instability. A "full" flux tube interchanges with an "empty" one, driving a field aligned current. The gain in energy from the centrifugal potential

is dissipated as Joule heating in the ionosphere. Brice and Ioannidis estimated that the time scale for instability growth is longer than the Alfvén travel time from the equatorial plane to the ionosphere and shorter than the time required to fill a Jovian flux tube. Hence, the necessary field aligned current system can be established and marginal stability maintained. They found that for marginal stability, the equatorial density should decrease as  $r^{-4}$  in a dipole magnetic field. More rapid decreases would be unstable with respect to interchange. This confirmed Melrose's result that the marginally stable density should vary as  $B/r$  at the equator (Melrose, 1967). Hill (1976) has included the effect of counterstreaming protons along the magnetic field lines and found that density decreases more rapid than  $r^{-9/2}$  in the equatorial plane should lead to interchange motion.

In reality, totally "full" flux tubes never interchange with totally "empty" ones and the process should be a diffusive one with convective cells on some small scale. Siscoe has treated the Jovian magnetosphere on this basis. In the case of diffusion, the true plasma density will be given by the marginally stable density distribution.

### 3. THE CENTRIFUGAL INSTABILITY

The centrifugal instability is a particular case of the general plasma instability known as the ballooning mode instability. The instability essentially opens magnetic field lines allowing the escape of plasma along the field. This is in contrast to interchange motion in which the field lines remain closed and plasma transport is perpendicular to the field. For the centrifugal instability to occur, the ionospheric conductivity must effectively be infinite so that interchange motion is not possible.

In the case of a magnetized star, Dungey (1958) observed that corotating plasma at larger distances will experience larger centrifugal forces. This causes the plasma to concentrate at the farthest point from the rotation axis until a "blob" of magnetized plasma breaks away, via a suitable topology alteration of the field, carrying off angular momentum. Hines (1964) related Dungey's remarks to the plasma in the earth's plasma-sphere. He noted that the centrifugal force on the corotating plasma is balanced by a  $\vec{J} \times \vec{B}$  force from an azimuthal current flow ( $\vec{J}$  being the current density). Letting  $n$  be the number density of ions of mass  $m_i$  at distance  $r$  from the spin axis, distortion of the total field from that of a dipole becomes consequential when the kinetic energy density  $1/2 n m_i \omega^2 r^2$  becomes comparable to the local magnetic field energy density  $B^2/8\pi$ . An equivalent statement is that steady state azimuthal flow cannot be super-Alfvénic. By assuming a field geometry, e.g., dipolar, one can then calculate the maximum radial distance from the planet at which the planetary field can contain the plasma.

Gold (1964) also discussed this point, emphasizing that the distance to which a plasma element can corotate is determined by the total balance of forces. This must include the centrifugal and gravitational forces, pressure gradients, and electromagnetic ( $\vec{J} \times \vec{B}$ ) forces in steady state.

This reasoning was first applied to the magnetosphere of Jupiter by Gledhill (1967b). Letting  $r_0$  be the planetary radius,  $B_0$  the equatorial field strength,  $r = r_0 L$  the radial distance,  $\omega$  the planetary angular velocity,  $m$  the ion mass, and  $n_{\max}$  the maximum plasma density, Gledhill found:

$$n_{\max} = \frac{B_0^2}{4\pi m_i \omega^2 r_0^2 L^8}$$

as the maximum plasma density which can corotate in a dipolar magnetic field in the equatorial plane. This result can be obtained from Hines' equation as well. Exceeding this density could, it was supposed, lead to the plasma breaking away or "slipping" with respect to the main field.

The centrifugal instability in a dipole field has also been treated by Michel and Sturrock (1974) and applied to the case of the Jovian magnetosphere. They proposed that the buildup of plasma in the equatorial plane should result in a steady planetary wind in the outer magnetosphere. This idea has been elaborated by Kennel and Coroniti (1975). The most recent treatment of the centrifugal instability, by Hasegawa (1980), includes both the planetary dipole field and a current sheet magnetic field in the calculation. Hasegawa postulates a periodic filling and opening of the magnetosphere as a result of the instability.

#### 4. PLASMA SPATIAL DISTRIBUTION

A major goal of all the magnetosphere modeling attempts was to deduce the density distribution of plasma. Gledhill's model has already been alluded to. Using a dipole field, his relation for the equatorial plasma density, and the assumption of hydrostatic equilibrium (Angerami and Thomas, 1964), he found a disc shaped magnetosphere. The model, which postulated that the decametric radiation emissions occur at the plasma frequency, was criticized on many points. The large density ( $\sim 10^6 \text{ cm}^{-3}$ ) was ruled out by lack of detectable Faraday rotation in the emissions (Warwick, 1967) and on the grounds that recombination would limit the density to much lower values (Ioannidis and Brice, 1971). The model also

predicted excessive exospheric temperature and seemed susceptible to flux tube interchange as well (Mendis and Axford, 1974).

Melrose (1967) showed that the magnetosphere of Jupiter could be divided into an inner gravitationally dominated part and an outer centrifugally dominated part beyond  $2 R_J$ . He concluded that the outer region would be flattened and density limited by flux tube interchange. However, particles with energies high enough to escape the Jovian ionosphere and populate the outer region were shown to result in a two stream instability. Melrose predicted that, as a result, the magnetosphere would be fragmented into "blobs" of plasma beyond 7 to 8 planetary radii.

Piddington and Drake (1968) noted that the centrifugal force on a corotating plasma would set up a ring current such as hypothesized by Hines (above). However, they suggested that such a current, while distorting the magnetic field, would be compatible with flux tube interchange and would not set up a centrifugal instability. Piddington (1969) pointed out that such a field distortion would lead to the inflation of the Jovian magnetosphere as a whole.

In two papers, Brice and Ioannidis discussed the characteristics of the Jovian magnetosphere (Brice and Ioannidis, 1970; Ioannidis and Brice, 1971). They argued that thermal plasma from the Jovian ionosphere would not, of itself, populate the outer centrifugal region. The potential barrier to be crossed was of the order of several electron volts while the ionospheric temperature was thought to be on the order of several hundred degrees Kelvin. They pointed out that appreciable fluxes of photoelectrons in the 10eV to 30eV range were available to drive protons from the ionosphere to the outer region via ambipolar diffusion. The magnetosphere was hypothesized to be in diffusive equilibrium out to about  $8 R_J$  at which

distance the maximum density of  $\sim 100$  protons  $\text{cm}^{-3}$  would fall off as  $r^{-4}$  as a result of flux tube interchange. Finally, they argued that although the ionospheric Pederson conductivity was low enough to allow interchange motion, rigid corotation of the entire magnetosphere should still occur. Mendis and Axford (1974) and Michael and Sturrock (1974) reexamined the Brice and Ioannidis model, elaborated upon it, and came to the same basic conclusions.

## 5. PRE-PIONEER EXPECTATIONS

In summary, from 1955 until 1973, several major discoveries about the particle and field environment of Jupiter were made. These resulted in general conclusions about the near Jovian space which could only be verified by an in situ spacecraft investigation. Observations of the decimetric and decametric emission from Jupiter implied that Jupiter has a magnetic field, that the field is roughly dipolar with a symmetry axis tilted about  $10^\circ$  with respect to the rotational axis, and that the surface equatorial field strength is between 1 and 10 gauss. The field near the planet was known to confine radiation belts emitting synchrotron radiation. The moon Io was known to play an important role in modulating the decametric emissions; these were thought to be generated near the foot of the Io flux tube in the northern hemisphere of Jupiter. This model accounted for both the upper cutoff frequency and polarization of the bursts. Absorption of high energy particles by all of the Galilean satellites was considered possible (Mendis and Axford, 1974).

Scaling of the earth's magnetosphere to that of Jupiter predicted a bow-shock standoff distance of  $\sim 50 R_J$  and a closed magnetosphere, with flux

tubes essentially full of corotating plasma. Protons from the ionosphere would populate the magnetosphere with low energy ( $\lesssim 10$  eV) plasma. A peak of  $\sim 100$  protons  $\text{cm}^{-3}$  at  $\sim 10 R_J$  would be produced as a result of diffusive equilibrium at  $\lesssim 10 R_J$  and flux tube interchange at larger distances. Finally, the interchange mechanism could also diffuse solar wind plasma inward and energize it, populating the radiation belt. It was on the basis of this scenario that planners built and instrumented the Pioneer 10 and Pioneer 11 spacecraft.

#### D. EARTH BASED OPTICAL OBSERVATIONS

Just prior to the Pioneer 10 flyby of Jupiter, Brown and Chaffee (1974) reported observations of neutral sodium D-line emission, associated with the Galilean moon Io. McElroy et al. (1974) proposed that a cloud of sodium and other gases should be present near Io in orbit about Jupiter. They also noted that Io should have a detectable ionosphere and that, if ionized, the neutral sodium could be a source of magnetospheric plasma. After the Pioneer flybys, Trafton (1975) discovered emissions which, when corrected for Io's motion, could be ascribed to potassium resonance lines. By this time, analysis of Pioneer 10 ultraviolet spectrometer data (discussed below) indicated a neutral hydrogen cloud in the same region as the sodium cloud (Carlson and Judge, 1975) and the newly discovered cloud of neutral potassium.

In 1975, Kupo et al. (1976) reported emission from a partial torus of singly ionized sulfur corotating with Jupiter and associated with Io. The sulfur cloud differed in shape from the sodium cloud, being more extended on the side of Jupiter opposite Io. They found the ionized sulfur subject

to large variations and anticorrelated in emission intensity with that of the sodium cloud. This is expected if neutral sulfur is sputtered off of Io and then ionized. Then the appearance of ionized sulfur corresponds to ionization of the sodium, and hence, a drop in the D-line emission from neutral sodium. Kupo et al. also noted that the observations imply periods during which the Jovian magnetosphere contains a significant amount of heavy ion plasma.

Brown (1976) presented a model of the sulfur observations in which ionization occurs via electron collisions. He deduced an electron density of  $3200 \text{ cm}^{-3}$  at a temperature of 2.2 eV in the vicinity of Io.

Mekler and Eviatar (1977) showed that the sulfur is distributed in a partial disk, absent near Io, six Jovian radii in radius and two in thickness. Further, they calculated an electron temperature of 10 eV and a number density of  $500 \text{ ions cm}^{-3}$ , one quarter of which are sulfur.

The most recent observations include detection of sodium emission at  $\sim 35R_j$  from Jupiter (Pilcher and Schempp, 1979) and that of singly ionized oxygen some four to eight Jovian radii from Jupiter, concentrated in the magnetic equatorial plane (Pilcher and Morgan, 1979).

## E. PIONEER OBSERVATIONS

### 1. SPACECRAFT AND TRAJECTORY

The first in situ fields and particle measurements were made at Jupiter by Pioneer 10 and Pioneer 11 in December, 1973 and December, 1974, respectively. Both spacecraft are spin stabilized at 4.8 rpm. Pioneer 10 carries a scientific payload of 11 instruments weighing 33 kg and consuming

24 watts of electrical power (Hall, 1974). Pioneer 11 carries the same instruments as Pioneer 10 (some with minor additions and modifications) as well as an additional high field magnetometer.

Both Pioneers covered roughly the same local times as the Voyagers which followed them, although the latitudinal coverage was quite different. The Pioneers also penetrated well into the region of the radiation belts from which the synchrotron emission is observed. Pioneer 10 approached Jupiter at about 1000 local time from low southern latitudes. The hyperbolic orbit was inclined  $13.8^\circ$  to Jupiter's equatorial plane. Spacecraft periapsis was  $2.85 R_J$ . The prograde orbit covered  $180^\circ$  in the 12 hours centered on the closest approach to Jupiter and the outbound asymptote covered low northern latitude at about 0600 local time. Pioneer 11 was in a retrograde orbit with periapsis at  $1.60 R_J$ , covering  $720^\circ$  in longitude in the 12 hours nearest closest approach. The inbound asymptote was about the same as that of Pioneer 10, but at larger latitudes. The orbital plane was inclined at  $51.8^\circ$  so that the outward asymptote was at mid-latitudes and about noon local time. (Kennel and Coroniti, 1977; Van Allen et al., 1975; Hall, 1975).

## 2. GLOBAL STRUCTURE

The in situ Pioneer measurements provided both basic results unanticipated by theoretical considerations as well as some answers and many new questions. The most striking global discovery was the inflation of the outer Jovian magnetosphere to double the expected size. The Plasma Analyzer (Wolfe et al., 1974) detected the bowshock at  $109 R_J$  inbound on Pioneer 10 and at  $242 R_J$  outbound. Pioneer 11 data showed three inbound

and three outbound shock crossings. The corresponding innermost magnetopause crossings, identified by the plasma analyzer and vector helium magnetometer, occurred in the range of  $40 R_J$  to  $60 R_J$ . The bulk of data used in the analysis of the dynamics of the Jovian magnetosphere came from the magnetometer (Smith et al., 1974; Acuña and Ness, 1976) and the energetic particle experiments (Van Allen et al., 1974; Simpson et al., 1974; Trainor et al., 1974; Filius and McIlwain, 1974). Data from the magnetic field experiments was used to model the internal magnetic field of Jupiter and confirmed the deduction of the radio astronomers, viz. the equatorial field strength of  $\sim 4$  gauss was primarily due to a dipole tilted  $\sim 10^\circ$  to the rotational axis at a System III longitude of  $\sim 200^\circ$ , with opposite polarity of that of the earth. Pioneer 10 also made the unanticipated discovery that outside of  $10 R_J$  a significant additional magnetic field exists, resulting in radial distention of the field lines. In this region, periodic field strength decreases at the Jovian spin period were observed along the spacecraft trajectories, most prominently on Pioneer 10 outbound. The field distortions were interpreted as due to the presence of an annular current sheet, warped but rotating rigidly with the planet. Further, the sheet was postulated to be due to the centrifugal forces acting upon trapped low energy magnetospheric plasma (Smith et al., 1974), the configuration suggested by Piddington (1969). The energetic particle experiments registered regular omnidirectional flux variations also at the spin period of Jupiter. Van Allen noted that the flux maxima were much broader in time than the field minima and that the maxima were best described by a "magnetodisc" (Van Allen et al., 1974) of quasi-trapped energetic particles, the former aligned with the magnetic dipole equator (that plane passing through the planet, perpendicular to the planetary

dipole moment). Van Allen also attributed the field distortion to unseen corotating low energy plasma, with plasma, field, and high energy particles all symmetric about the magnetic dipole equatorial plane (Van Allen et al., 1974). The magnetodisc phenomena were confirmed by the other particle experimenters. Pioneer 11 magnetic field data also showed clear field decreases at a ten hour period, but a simple disc-like magnetosphere was ruled out by high latitude bow shock and magnetopause crossings. In addition, flux maxima were seen by Pioneer 11 inbound, at times corresponding to magnetic field decreases. Outbound at mid-latitudes, the magnetic field did not exhibit a current sheet structure and the particle flux maxima exceeded those seen inbound, a result inconsistent with quasi-trapping in and confinement to the magnetic equatorial plane (Filius et al. 1975; Simpson et al. 1975; Van Allen et al. 1975). Thus, doubts were raised about the magnetodisc picture. Since the inclination of the Pioneer orbits to the Jovian equatorial plane were greater than the tilt of the dipole from the rotation axis, the spacecraft was only expected to pass into the rigid disc once every ten hours and never through it. Large fluxes at high latitudes and lack of phase synchronization of flux maxima with supposed disc entrances (Filius et al., 1975; Simpson et al., 1975; Chenette et al., 1974) led to the hypothesis that the ten hours variation was temporal rather than spatial. In addition, MeV proton and electron fluxes showing ten hour periodicities (Filius 1976; Simpson et al., 1974; Trainor et al., 1974; Trainor et al., 1975; Vasyliunas, 1975) were observed in the solar wind prior and subsequent to the spacecraft Jupiter encounters. These observations formed the basis of the "clock model" as opposed to the "disc model".

The Pioneer 10 Ultraviolet Spectrometer revealed what was reported as an incomplete torus of neutral hydrogen, centered on Io, and in orbit about Jupiter (Carlson and Judge, 1974). The hydrogen discovery was made by the two channel ultraviolet spectrometer on board the spacecraft. (One channel is used for measuring Lyman  $\alpha$  emission at  $1216 \text{ \AA}$  and the other channel the helium resonance line at  $584 \text{ \AA}$ ). The Lyman  $\alpha$  channel detected emission within six Jovian radii of Jupiter. The cloud had a vertical extent of about one Jovian radius with more atomic hydrogen trailing Io than leading it, covering about  $120^\circ$  of Io's orbit (Carlson and Judge, 1975). Sodium ions resulting from the ionization of the neutral sodium cloud were shown to give a negligible contribution to the measured UV signal.

It is worth noting, in view of the Voyager detection of the copious presence of heavy ions, that all Pioneer particle measurements were interpreted as being primarily hydrogen with either the inferred Io hydrogen torus (Carlson and Judge, 1974) or the Jovian ionosphere being the source. Simpson did note that his fission cell detector could be responding to nuclei with  $Z \sim 10$  (Simpson et al., 1974; Simpson et al., 1975), but that other explanations for the signature existed as well.

### 3. ENERGETIC PARTICLE ANISOTROPIES

Additional information on the energetic particle population is available in the form of the measured anisotropy in the particle flux. Both Pioneer spacecraft are spinners, which enabled the particle experiments to measure the angular distribution of the energetic particles in the plane perpendicular to the spacecraft spin axis.

Assuming that the  $\sim$ MeV particles (which the Pioneer experimenter interpreted as being protons above) are isotropic in their rest frame, bulk plasma flow will result in a first order anisotropy in the energetic particle distribution in the spacecraft frame. Although both first order and second order anisotropies were present in the Pioneer data, the former dominated and were consistent in direction and magnitude with corotation of the plasma at less than  $\sim 60 R_J$  (Van Allen et al., 1974; Simpson et al., 1974). However, magnitudes larger than those predicted for corotation above were also seen (Trainor et al., 1974) and the measurements may be affected by field aligned streaming (McDonald et al., 1979). Birmingham and Northrup (1979) reconsidered the theory of flux anisotropies in detail. Applying this theory to Pioneer 10 inbound between  $42.4 R_J$  and  $5.4 R_J$  Northrup et al. (1979) concluded that the corotational anisotropy alone does not explain the data and that there must be some magnetic field aligned flow to explain the observations. This flow was found to be from the equatorial region back toward this planet.

The Pioneer results showed that the first order anisotropy in the energetic particle population at Jupiter is produced by more than just corotation of the plasma. In the magnetospheric environment, additional sources of first order anisotropy exist; hence the bulk motion of the plasma cannot be unambiguously deduced (Birmingham and Northrup, 1979; Northrup and Thomsen, 1980).

#### 4. LOW ENERGY PLASMA MEASUREMENTS

Measurements of the characteristics of the low energy plasma component are possible by either indirect or direct means. It was known that in the

absence of a low energy plasma, high energy particle fluxes could result in the spacecraft acquiring a large electrostatic charge (De Forest, 1972). Near periapsis on Pioneer 11, some instruments underwent uncommanded mode changes which may have been due to electrostatic discharge (Hall, 1975). Scarf (1975) argued that the lack of such charging effects on Pioneer 10 implied the existence of a "thermal" plasma within 6 to 7  $R_J$  of the planet. This gave observational plausibility to the "dynamical" component of the plasma postulated by various investigators (Smith et al., 1974; Van Allen et al., 1974; cf. Piddington, 1969, referred to in Van Allen).

Unfortunately, direct measurement of the "thermal" plasma was a difficult process on the Pioneer spacecraft. The plasma analyzer detected magnetopause crossings by a dropout of signal to background (Wolfe et al. 1974; Mihalov et al. 1975). During the magnetospheric passages, background signals resulting from the large MeV proton and electron fluxes obscured the low energy (<5 keV) plasma signal. Frank et al. (1976) were able to extract a signal from the Pioneer 10 data within 15  $R_J$  of the planet. The analyzed data consist of energy/charge spectra in 24 channels from 100 eV to 4.8 keV. Assuming that the signal was due entirely to protons (unlikely in view of the Voyager results), Frank et al. fit very sub-sonic Maxwellian distributions to the spectra, and extracted densities and temperatures. He reported densities from 10 to 100  $\text{cm}^{-3}$  and temperatures on the order of 100 eV. In addition, an increase in density was observed during the inbound passage of Io's flux tubes. On the basis of the data, Frank hypothesized a ring current in the vicinity of Europa's L-shell as well as a "plasmopause" exterior to Io's L-shell. The latter result was called into question at the time (Neugebauer and Eviatar, 1976). They noted that the density profile in no way resembled the pre-Pioneer predictions (Ioannidis and

Brice, 1971; Mendis and Axford, 1974), although the agreement with theory is better if Io, rather than the ionosphere, is the principal source of plasma (Siscoe and Chen, 1977). At least during the voyager encounters this proved to be the case. In § IV.D. below we will attempt to reconcile these Pioneer results with the Voyager results to be discussed in Chapter III and IV below.

## F. MAGNETOSPHERIC MODELS AFTER PIONEER

### 1. MAGNETODISC MODELS

The Pioneer data guided the development of many new theoretical models of the Jovian magnetosphere. The principal observation upon which the post-Pioneer modeling has been based is that of the "magnetodisc". The thrust of the resultant modeling has been to deduce plasma properties from the measured magnetic field and to deduce the disc topology from the timing of signatures as seen in both magnetic field and high energy particle data.

Smith et al. (1974) identified the magnetodisc as a current sheet and, following Piddington (1969), postulated that the current gave rise to a  $\vec{J} \times \vec{B}$  force which balanced the centrifugal force exerted on an unobserved thermal plasma. They also concluded that the magnetodisc has the shape of a bent annulus about Jupiter. It was envisioned as lying perpendicular to Jupiter's rotation axis in the meridian plane containing both the angular momentum and magnetic dipole vectors, below the rotational equator on one side of the planet and above it on the other. They postulated that the disc rigidly corotates with the planet so that it appears to "flap" up and down to a semi-stationary observer (such as a spacecraft). They found that the

required current could be accounted for by a  $\lesssim 100$  eV proton/electron plasma of  $\sim 1$  particle  $\text{cm}^{-3}$ . The plasma annulus would be  $1 R_J$  thick and stretch from  $20 R_J$  to  $90 R_J$ . They also noted that particles with energies  $> 10$  keV have a scale height larger than the magnetosphere, and so, if isotropic, would fill it.

Northrup et al. (1974) considered the timing of the energetic particle flux maxima and concluded that a rigid magnetodisc could not account for the observations. They showed that the energetic particle flux maxima on the outbound pass of Pioneer 10 are consistent with there being a propagation delay to the outer magnetosphere of the field configuration. Such a delay could result from a low Alfvén speed (Eviatar and Ershkovitch, 1976) or from convection of the field by a plasma wind (Kivelson et al., 1978).

Several investigators have considered in more detail plasma models based on the magnetic field data obtained on the Pioneer 10 outbound pass. Goertz et al. (1976) derived an analytic magnetic field model on the basis of the data set. They found that the current sheet does not bend back toward the rotational equatorial plane, as had been suggested by Smith and his coworkers. Hill et al. (1974) noted that confinement of plasma more closely to the magnetic equatorial plane should result if its thermal energy density is about the same as its corotational energy density or greater. This idea is analyzed in more detail by Goertz (1976b).

Using the Pioneer 10 magnetic field, Goertz (1976b) and Goldstein (1977) derived the properties of the resultant corotating plasma population. Among the results (Goertz, 1979): (a) the plasma is concentrated in the equatorial plane and decreases as  $L^{-5.4}$ , (b) the temperature in the plasma sheet is of the order of several keV and

increases with distance from the planet, and (c) the Alfvénic Mach number exceeds unity in the sheet without giving rise to a planetary wind. Goertz (1976b) notes that this merely reflects the fact that magnetic field line tension, as well as energy density, affects the containment of plasma. Although the temperatures are high, these conclusions foreshadow the Plasma Science observations discussed herein. Goldstein (1977) did note that the predicted temperature gradient could be reduced if the plasma angular velocity decreased as a function of distance from the planet. This was the case at Jupiter during the Voyager flybys of the planet (McNutt, et al., 1979 and this thesis).

Other investigations were carried out by Gleeson and Axford (1976), Vickers (1978), and Sozzou (1978).

More specialized inquiry has been made into the temperature of the plasma sheet. Walker et al. (1978) considered the twelve encounters with the current sheet seen by Pioneer 10 on its outbound pass. Assuming the field depression was a pure diamagnetic effect, they concluded that energetic protons of energy  $>10$  keV are the major constituents of the "thermal" plasma in the Jovian magnetodisc. This result compares favorably with Goldstein's rigid disc model, but not with the Voyager Plasma Science results (§IV.B.). Van Allen (1978) subsequently analyzed his energetic electron data at  $51 R_J$  outbound on Pioneer 10. He found that the characteristic particle energy is  $\sim 100$  keV and that the energetic protons contribute an order of magnitude more to the pressure than do the energetic electrons. Noting that these results depend crucially on how the energy spectrum is extrapolated to lower energies, Goertz et al. (1979) fit the differential energy spectra to an exponential in magnetic rigidity. They reconsidered the  $>300$  keV proton data set used by Walker et al. (1978) and

found that the dominant plasma contributions is from 100 eV to 10 keV protons in the magnetodisc. Such temperatures are still high compared to those measured in the dayside magnetosphere by Voyager (this thesis).

## 2. PLANETARY WIND MODELS

The second large class of post-Pioneer models discussed are those incorporating plasma outflow driven by centrifugal forces. This is essentially a time stationary version of the centrifugal instability (discussed above). The outflow must be accompanied by a change in magnetic field line topology. Parker and Stewart (1967) discussed this change in terms of a model in which the ring current is produced by pressure gradient rather than centrifugal forces. Starting with a dipole field in vacuo, they showed that increasing pressure can finally result in an open field line topology. In general, the various theoretical treatments of radial outflow have rested on the consideration of the full set of MHD equations. Mestel (1961; 1968) has investigated the axisymmetric case in which a centrifugally driven outflow from a magnetic rotator can result. He noted that the outflow will begin just outside of the radius at which the plasma energy density exceeds that of the magnetic field while the plasma corotates inside.

This formulation has been applied to Jupiter by Kennel and Coroniti (1975) in which they compared Jupiter to a pulsar. They noted that the Pioneer 10 measurement of the toroidal field component is, in a time averaged sense, consistent with outflow. In this case, torque must be supplied by the planet to balance the loss of angular momentum. In this context Kennel and Coroniti (1975) raised the question of whether

corotation can be enforced at all on Jupiter's magnetosphere. Only if atmosphere-ionosphere coupling via neutral-ion collisions is strong enough will corotation be enforced on the magnetosphere. They suggested that if radial outflow accounts for the observed azimuthal magnetic field component seen on Pioneer 10 outbound, sufficient torque may not be available from the upward viscous diffusion of angular momentum through Jupiter's neutral atmosphere to enforce corotation.

Kennel and Coroniti (1977) also proposed a variation in which the state of the magnetospheric flow is directly influenced by the ram pressure of the upstream solar wind. They suggested that while super-Alfvénic magnetospheric flow always occurs down the magnetotail, it may also occur in the dayside magnetosphere as well. This, they postulated, happens if the upstream solar wind ram pressure is so low that the magnetosphere expands and the "trans-Alfvén" surface is well inside of the magnetopause. At times of high solar wind ram pressure only a sub-Alfvén planetary "breeze" would develop on the dayside.

Smith et al. (1976) have noted that although the spiraling of the field, as seen by Pioneer 10, is accommodated quite naturally by the outflow models, there are two serious objections against the models when their predictions are compared with the observations. The existence of quasi-trapped particle flux in the magnetodisc seems inconsistent with an outflowing wind. More seriously, a southward component of the field is always observed within the magnetodisc. In Mestel's solution of the MHD equations, such a component implies that within the magnetic surface defined by such field lines, there can be no radial outflow and the plasma must rigidly corotate with the planet.

## 3. CLOCK MODEL

Chenette et al. (1974) found interplanetary bursts of electrons in the energy range 3 to 30 MeV modulated with the spin period of Jupiter. The electron bursts were seen up to 1 AU from Jupiter exhibiting 10 hour periodicities in flux and spectral index and were in phase with variations observed inside the magnetosphere at  $>50 R_j$  from the planet. These facts led Chenette et al. to hypothesize that the outer magnetosphere electron flux is spatially homogeneous and varies temporally rather than spatially. Evidence for such temporal variation in the Pioneer 11 data also were discussed by Simpson and McKibben (1976).

Hill et al. (1974b) postulated such an effect as a result of either the magnetic field geometry or the ionospheric plasma source being longitudinally asymmetric. Such effects would result in a "diurnal trapping region" in which plasma would be quasi-trapped in a given System III longitude range. As this region swept by the nightside of the planet, a burst of relativistic electrons would be emitted, escaping the magnetosphere on field lines connected to the interplanetary field. Vasyliunas (1975) showed that the maximum flux in the interplanetary electrons bursts is observed when the Jovian "active hemisphere" faces the local midnight meridian. Dessler and Hill (1975) found that at these times the longitude of Jupiter in the midnight meridian plane is that at which the latitudinally averaged surface magnetic field has a broad minimum. They suggested that this field variation enables flux tubes at those Zenographic longitudes to preferentially fill with plasma while they rotate through the dayside magnetosphere. When facing the night side these tubes are opened by the centrifugal instability and plasma, including the observed inter-

planetary electrons, is released. Consequences of this model and its extensions have been discussed in a series of papers (Hill and Dessler, 1976a, Carbary et al. 1976, Dessler, 1978, Dessler and Vasylunas, 1979).

#### 4. SOURCES OF MAGNETOSPHERIC PLASMA

Prior to Voyager flybys of Jupiter, the source of magnetospheric plasma for Jupiter had been somewhat of a puzzle. The Jovian ionosphere and the particle torus associated with Io were considered the most likely sources. Self-consistent magnetospheric models (Carbary and Hill, 1978; Hill and Carbary, 1978) indicated that it was difficult to reconcile an ionospheric source with the radially distended magnetic field configuration seen by the Pioneer. At the same time the Jovian ionosphere presented a ready supply of magnetospheric protons while the ultimate source of the torus remained unknown.

Ioannidis and Brice (1971) suggested that the upper Jovian ionosphere populated the magnetosphere with protons. Melrose (1967) had pointed out that such a source would drive a two-stream instability in the outer magnetosphere. Goertz (1976c) showed that this would trap some of the protons there. However, in deriving a model of a rapidly rotating magnetosphere, Carbary and Hill (1978) showed that an ionospheric source leads to an inflation of the magnetosphere rather than to an annular current sheet configuration, such as seen by the Pioneer spacecraft.

Discovery of the particle tori centered on Io led Siscoe and Chen (1977) to postulate that photoionization of the Io hydrogen torus could be a source of the magnetospheric plasma. They noted that the ions could diffuse outward via flux tube interchange while remaining confined close to

the equatorial region. Hill and Michel (1976) investigated the effects on the magnetosphere produced by heavy ions from the atmospheres of the Galilean satellites. They noted that ions of mass  $m$  and temperature  $T$  will be distributed in a dipole field according to the centrifugal scale height

$$H_c = \left( \frac{2kT}{3m\Omega_J^2} \right)^{1/2}$$

where  $\Omega_J$  is the corotation angular speed. For a thermal plasma at a temperature less than 3 eV per amu, the scale height is about  $1 R_J$ . They found that the predominance of such a source would lead to the type of magnetic field distortion observed by Pioneer 10. This would not be true of an ionospheric source. Siscoe (1977) carried out a similar analysis by conserving the first and second adiabatic invariants of plasma originating at the Galilean satellites. The results are in total agreement with those of Hill and Michel. Hill and Carbary (1978) derived a self-consistent magnetospheric configuration for plasma injected at the Galilean satellites. In this case, they found a field configuration resembling that seen by Pioneer 10. The solar wind and the interstellar neutral gas in the solar system can also supply ions to the Jovian magnetosphere. Siscoe (1978) discussed each possible source, noting that heavy ions from Io should have important dynamical effects. Such a population, he noted, should dominate those from other sources in mass density.

#### G. OUTSTANDING PROBLEMS BEFORE VOYAGER

The state of knowledge about Jupiter's magnetosphere prior to the Voyager flybys in March and July of 1979 has been summed up by Goertz and

Thomsen (1979a). They noted the need for characterization of the low energy plasma in the inner magnetosphere ( $<10 R_J$ ). Measurements of the plasma parameters in the energy range below that sampled by Pioneer instruments were needed in the middle ( $\sim 10 R_J$  to  $\sim 40 R_J$ ) and outer ( $>40 R_J$ ) magnetosphere as well. A knowledge of the gross properties of the plasma was needed so that the global dynamics could be better understood. What the density, temperature, and source of the magnetodisc plasma were remained outstanding questions. Answers to these relate directly to the diamagnetic effect in the current sheet and the role of centrifugal versus pressure gradient forces in the sheet dynamics. Finally, and perhaps most importantly, the question of whether the plasma flow resulted in a centrifugally driven wind or a quasi-steady state corotating disc remained to be answered. Analysis of data from the plasma experiment on Voyager 1 and Voyager 2 has resulted in answers, and some surprises, in regard to these fundamental questions.

## CHAPTER II. THE VOYAGER PLASMA SCIENCE EXPERIMENT

## A. THE VOYAGER SPACECRAFT

The Voyager 1 and Voyager 2 spacecraft evolved from Mariner class spacecraft into the most advanced planetary exploration spacecraft yet flown. The Voyagers are three axis stabilized by hydrazine jets and weigh 815 kilograms. The science instrument payload, including 11 scientific experiments, weighs 115 kg and draws some 100 watts of electrical power at encounter.

The spacecraft configuration consists of the spacecraft main frame, a 3.66 meter diameter high gain antenna, a radioisotope thermoelectric generator boom, and the science boom. The science boom carries the Cosmic Ray experiment, the Low Energy Charged Particle experiment, the Plasma Science experiment, and a two axis scan platform. The latter provides precise pointing for the Ultraviolet Spectrometer, Infrared Spectrometer and Radiometer, Photopolarimeter, and Imaging Science (visible light) Subsystem which are all mounted on it. A pair of 10 meter antennas, mounted at right angles on the bus, are used by the Plasma Wave and Planetary Radio Astronomy experiments. The Magnetometer experiment consists of two high field sensors on the frame structure and two low field sensors located along a 13 meter boom.

Both spacecraft were launched by Titan Centaur III-E boosters and inserted into trans-Jupiter orbit with solid field propulsion modules. Voyager 1, launched on September 5, 1977, approached Jupiter to within 4.9  $R_J$  on March 5, 1979. Voyager 2, launched August 20, 1977 on a lower

velocity orbit, achieved a closest approach of  $10.1 R_J$  on July 9, 1979. Both spacecraft are now on their way to Saturn encounters in 1980 and 1981. Voyager 2, in addition, has possible options for an encounter with Uranus in 1986 and with Neptune in 1989.

## B. PLASMA SCIENCE INSTRUMENT DESCRIPTION AND OPERATION

The Plasma Science instrument has been described in detail (Bridge et al., 1977) and only salient points are summarized here. The experiment consists of four modulated grid Faraday cups and the associated electronics package (Figure 1). Three of the cups are arranged in a symmetric configuration to form the main sensor. The symmetry axis parallels that of the high gain antenna which stays locked on the earth except for short intervals during some spacecraft maneuvers. The normals of the main sensor Faraday cups (A,B, and C cups) are tilted at  $20^\circ$  to the symmetry axis and equally spaced  $120^\circ$  in azimuth about it. The side sensor (D-cup) normal is tilted  $90^\circ$  to the symmetry axis and located  $167^\circ$  in azimuth from the A-cup normal. Looking into the cups, A,B, and C are labeled in a clockwise sense. In the same sense the D-cup is located  $262^\circ$  in azimuth from the Canopus tracker on the spacecraft.

All four Faraday cups measure electric currents from positive ions in the energy per charge range of 10 volts to 5950 volts. In addition, the side sensor measures currents from electrons. That analysis in the magnetosphere is discussed elsewhere (Scudder et al., 1981). Measurements are made in a set of discrete continuous voltage windows which, to first order, increase logarithmically with the voltage. Two positive ion

measurement modes are available and have been used in our analysis. The low resolution mode (L-mode) uses 16-voltage windows, each with an energy per charge resolution of  $\approx 29\%$ . The high resolution mode (M-mode) uses 128 voltage windows with an energy per charge resolution of  $\approx 3.6\%$ . During the encounter, a complete L-mode measurement takes 3.84 seconds, with consecutive L-mode energy per charge spectra taken 96 seconds apart. A complete M-mode measurement takes 30.72 seconds; however, only currents from 72 of the measurement channels are telemetered during each measurement sequence of 96 seconds. To obtain a full M-mode spectrum on the ground, it takes two sequence times or 192 seconds. The convention used for our analysis is to form a composite spectrum every 192 seconds in which data in channels 1 to 56 from one measurement sequence are combined with data in channels 57 to 128 from the subsequent sequence. The Plasma Science data occupies 32 of the 3600 bits per second of general science and engineering data which are telemetered to earth during the encounter phase of the missions.

The limiting noise in the measurements is a result of high energy particles in the magnetosphere penetrating the input field-effect transistors. Fluctuations in such a background produce noise at the preamplifier input. This effect was reduced by shielding the input transistors with  $8 \text{ g cm}^{-2}$  of copper. During the encounters the background noise current was about  $5 \times 10^{-13}$  amperes, about an order of magnitude larger than the limiting instrument noise. The maximum current measured was some five orders of magnitude larger. The instrument has four gain states which can be either preprogrammed in the onboard spacecraft computer or commanded from the ground. Gain state changes were ground commanded during both encounters so as to avoid saturation in the measurement chain, yet maintain

a suitably large signal to noise ratio in the data. Some saturation occurred in the L-mode data during the Voyager 1 encounter and one M-mode saturated as well. Neither L-mode nor M-mode saturation occurred during the Voyager 2 encounter.

The Plasma Science instrument fits in a box some 60 cm square by 40 cm deep. The instrument weights 9.9 kilograms and draws 8.1 watts (peak) of electrical power from the spacecraft supply.

### C. BASIC CONSIDERATIONS IN DATA INTERPRETATION

A Faraday cup is an electrostatic device, and therefore measures positive ion properties as a function of energy per charge. The measured electric currents are related to the positive ion distribution function in the following way (Vasyliunas, 1971; Belcher et al., 1980). Consider the response of the cup to an ionic species of mass number  $A$ , charge number  $Z^*$  and distribution function  $f(\vec{v})$ . Let the set of contiguous potentials, provided by the modulation grid to select the energy per charge channels be  $\{\phi_j\}_{j=1}^{K+1}$  where  $K$  is 16 (L-mode) or 128 (M-mode). This defines a corresponding set of particle velocities  $\{V_j\}_{j=1}^{K+1}$  where

$$V_j \equiv (2eZ_i^* \phi_j / A_i m_p)^{1/2} \quad \text{II.1}$$

with  $e$  and  $m_p$  being the proton charge and mass, respectively. In the  $j$ th channel the measured current is due to particles with an average velocity component of

$$V_j = 1/2(V_{j+1} + V_j) \quad \text{II.2}$$

in a velocity window of width

$$\Delta V_j = V_{j+1} - V_j \quad \text{II.3}$$

Given the area of the cup collector  $A_0$  and the response function of the instrument  $R(\vec{v}, \hat{n})$  the current  $I_j$  measured in the  $j$ th channel is

$$I_j = A_0 \int_{V_j}^{V_{j+1}} (Z^* e \vec{v} \cdot \hat{n}) dv_n \iint_{-\infty}^{\infty} f(\vec{v}) R(\vec{v}, \hat{n}) dv_{t1} dv_{t2} \quad \text{II.4}$$

where the subscript  $n$  denotes the component parallel to  $\hat{n}$  in velocity space and the subscripts  $t_1$  and  $t_2$  refer to the orthogonal components perpendicular to  $\hat{n}$ .

To evaluate the integral, assume the distribution function is a convected, isotropic Maxwellian characterized by density  $n$ , thermal speed  $w$ , and bulk velocity  $\vec{u}$ . Then

$$f(\vec{v}) = \frac{n}{w^3 \pi^{3/2}} \exp \left[ - \frac{|\vec{v} - \vec{u}|^2}{w^2} \right] \quad \text{II.5}$$

The thermal speed is related to the plasma temperature by

$$w = (2kT/Am_p)^{1/2} \quad \text{II.6}$$

where  $k$  is Boltzmann's constant. For reasons which we discuss in the next chapter, we are concerned here primarily with the side sensor (D-cup). The response function for the side sensor can be characterized by a transparency  $T$  and a parameter  $\alpha$  of the order of unity (Binsack, 1966; Sittler, 1978; Olbert, private communication, 1980):

$$R(\vec{v}, \hat{n}) = T_0 e^{-\alpha \frac{|\vec{v} \times \hat{n}|^2}{(\vec{v} \cdot \hat{n})^2}} \quad \text{II.7}$$

The integrations over  $v_{t1}$  and  $v_{t2}$  can be carried out analytically and yield the result

$$I_j = T_0 A_0 Z^* e \int_{v_j}^{v_{j+1}} f_M(v_n) \frac{v_n^3}{\alpha w^2 + v_n^2} \exp \left\{ - \left[ \frac{\alpha u_t^2}{\alpha w^2 + v_n^2} \right] \right\} dv_n \quad \text{II.8}$$

where

$$f_M(v) = \frac{n}{\pi^{1/2} w} \exp \left\{ - \frac{(v_n - u_n)^2}{w^2} \right\} \quad \text{II.9}$$

is the one-dimensional distribution function along the cup normal and the bulk flow components normal and transverse to the cup are  $u_n$  and  $u_t$ , respectively.

In principle, both  $u_n$  and  $u_t$  can be extracted from the measured currents. However, the influence of  $u_t$  on the currents is too slight to be observable unless  $u_t > u_n$  (e.g. flow very oblique to the cup normal). In practice, we do not analyze flows which are highly oblique because our confidence in the validity of expression (II.7) for  $R(\vec{v}, \hat{n})$  is low for high angles of incidence. For the cases we consider herein, it is reasonable to assume that the bulk flow is within  $\sim 20^\circ$  of the cup normal; thus  $u_t^2/u_n^2$  is small and the exponential in II.8 can be approximated as unity for those values of  $v_n$  for which  $f_M(v_n)$  gives an appreciable contribution to the integral. This will introduce errors of order  $u_t^2/u_n^2$  in resulting estimates for  $n$ ,  $u_n$ , and  $w$ . The errors introduced are such that estimates for  $u_n$  and  $w$  will be high and estimates for  $n$  low for Mach numbers greater than unity.

If we assume that the transverse flow is negligible, the response function enters the integral of (II.8) only via the factor  $v_n^2 / (\alpha w^2 + v_n^2)$ . In many cases of interest, the ions are supersonic ( $u_n \gg w$ ), and even this term can be taken as unity if we neglect terms of order  $(w/u_n)^2$ . Furthermore, for the high resolution M-mode, the velocity windows are invariably narrow compared to the distribution function ( $\Delta V_j \ll w$ ). With these two additional assumptions, equation (II.8) becomes:

$$I_j = T_0 A_0 Z^* e (\nabla_j \Delta V_j) f_M (\bar{V}_j)$$

Using definitions II.1 through II.3, this yields

$$\frac{I_j}{T_0 A_0 \frac{e^2}{m_p} (\phi_{j+1} - \phi_j)} = \frac{(Z^*)^2}{A} f_M (\bar{V}_j) \quad \text{II.10}$$

Thus, for a supersonic flow within  $\sim 20^\circ$  of the D-cup axis, the currents  $I_j$  as measured in the high resolution M-mode are, to a good approximation, directly related to the reduced distribution function via equation (II-10). If the flow is transonic (Mach numbers of order unity), or if we are dealing with low resolution L-mode data, equation (II.10) is very approximate, and we must return to the integral equation (II.8) to properly relate  $f_M$  and  $I_j$  (e.g., in the least squares fit analysis of L mode data described in Chapter III and Appendix I). In any case, for data display, we plot the quantity shown on the left hand side of equation (II.10). We will loosely refer to this as the "measured distribution function", even though it actually gives the distribution function scaled by  $(Z^*)^2/A$ , and this only approximately so for the transonic case and/or L-mode data.

The plasma in the Jovian magnetosphere has been found to consist of several different ionic species with different masses and different charge states (Bridge, et al., 1979a, Sullivan and Bagenal, 1979). As a result, the measured current in the  $j$ th channel is actually a sum of terms like (II.4), each computed for a particular ionic species. In such a case, a display of the left hand side of (II.8) will yield a superposition of ionic distribution functions, each scaled by the appropriate value of  $(Z)^*/A$ . Furthermore, if a set of ionic species with mass and charge numbers  $\{A_i, Z_i^*\}_{i=1}^N$  are moving into the cup with the same velocity component  $u_n$ , and all species are reasonably supersonic, then the measured distribution function will show a series of peaks at energies per charge of  $A_i/Z_i^*$  times the proton energy per charge. If we can identify the energy per charge of the proton peak, we can determine the mass to charge ratios of ionic species producing peaks at higher energies per charge. For example, doubly ionized sulfur ( $S^{2+}$ ) has a mass to charge ratio of 16, and, if supersonic, will produce a peak in the measured distribution function at 16 times the energy per charge of  $H^+$ . In this case, we refer to the "16 peak" as being  $S^{2+}$ . The number of different mass to charge ratios actually found in the Jovian magnetosphere is small - e.g., 1, 8,  $10\frac{2}{3}$ , 16, 23, 32, and 64, as we discuss in Chapter 3 below. Thus, even if we do not know the energy per charge of protons, we can usually deduce the mass to charge ratios of the heavier ionic species, if two or more are present, by comparison of the various ratios of observed energy per charge. Knowing the mass to charge ratios we can then deduce the common velocity.

From this discussion, it is clear that we can only determine the ratio  $A_i/Z_i^*$ , and not  $A_i$  and  $Z_i^*$  individually. For example,  $O^+$  has the same mass

to charge ratio as  $S^{2+}$ , and will appear at the same energy per charge as  $S^{2+}$  in our measured spectra. This is a basic ambiguity in the measurement. We will use various physical considerations to argue, for example, whether the 16 peaks should be mostly  $O^+$  or  $S^{2+}$ . However, we emphasize that even though we may misidentify  $A_i$  or  $Z_i^*$  separately, as long as we correctly identify the ratio  $\{A_i/Z_i^*\}$  for a set of ionic species, we will obtain the correct total charge and mass density of the plasma. To show this, suppose we have obtained a set of densities and thermal speeds  $\{n_i, w_i\}_{i=1}^N$  for species with mass to charge ratios  $\{A_i/Z_i^*\}_{i=1}^N$  (which we take to be known from comparison of observed energies per charge). Then the total charge density  $N_c$ , in units of the proton charge is

$$N_c = \sum_i Z_i^* n_i \quad \text{II.11}$$

and the total mass density, in units of the proton mass is

$$N_M = \sum_i A_i n_i \quad \text{II.12}$$

From equation (II.9) and (II.10), it is clear that if we know  $A_i/Z_i^*$  then  $Z_i^* n_i / w_i$  is a measured quantity, and thus independent of our individual choice of  $A_i$  and  $Z_i^*$ . But  $w_i$  is also independent of this choice, since all velocities scale as  $(A_i/Z_i^*)^{1/2}$  (see II.1). Thus  $Z_i^* n_i$  is an invariant, as is  $A_i n_i$ , since  $A_i/Z_i^*$  is known. Even though we may incorrectly identify  $A_i$  and  $Z_i^*$  separately, we always arrive at the correct total mass and total charge densities if we know  $A_i/Z_i^*$ .

Thus far we have been assuming that the various species have a high enough Mach number that the energy per charge peaks are well defined for different  $A_i/Z_i^*$ . It is easily seen that the peak in energy per charge of the  $i$ th species will be within a thermal width of the peak of the  $(i + 1)$ th species when

$$W_{i+1}/u_n \approx 1 - (A_i Z_{i+1}^*/Z_i^* A_{i+1})^{1/2} \quad \text{II.13}$$

For  $A_i/Z_i^*$  values of 1 and 8, strong overlap will begin to occur at Mach numbers near unity. However, for values of 8 and 10  $-2/3$ , or 10  $-2/3$  and 16, strong overlap begins at Mach numbers of  $\sim 6$ . Thus we lose resolution in the heavy ions at relatively high Mach numbers, and identification of individual heavy ion peaks becomes difficult. This happens in many of the observed spectra. Even here, however, it is easily seen from equation (II-8) that as long as all species are within our energy range, then

$$\sum I_j = T_0 A_0 e u_n \sum_i n_i Z_i^* \quad \text{II.14}$$

and thus

$$N_c = \sum_i N_i Z_i^* = \sum_j I_j / T_0 A_0 e u_n \quad \text{II.15}$$

Provided that we have an estimate of  $u_n$  from other sources, we can estimate  $N_c$  even though the individual peaks cannot be identified.

#### D. SPACECRAFT TRAJECTORY AND INSTRUMENT RESPONSE AT JUPITER ENCOUNTER

Because of the finite field of view of the various sensors, the direction of the cup normals with respect to the bulk plasma motion is of primary importance for measuring the properties of the magnetospheric

plasma. Except for brief periods of spacecraft maneuvers, the spacecraft attitude is fixed in inertial space. On the basis of pre-Voyager theory (see Introduction), it was expected that the plasma flow would be azimuthal about the planet, locked into Jupiter's rotation. In this case, as the spacecraft rounds Jupiter in its hyperbolic encounter orbit, the flow would appear to an observer on the spacecraft to change direction as a function of time. To make this more explicit, in Figure 2a, we show the Voyager 1 trajectory as projected into the Jovian rotational equatorial plane during encounter. In Figure 3a, the same type of projection is shown for Voyager 2. In each, the sun is to the right, and tic marks are shown along the trajectory every 12 hours with the day of year shown at the start of each day UTC (Universal time, coordinated) day on board the spacecraft. During the encounters, the main sensor symmetry axis (denoted by S in the figures) lay almost in Jupiter's equatorial plane. On the inbound passes, the side sensor cup normal (denoted by D in the figures) also lay almost in the same plane. Past periapsis the spacecraft were rolled about the high gain antenna axis to acquire Arcturus with the Canopus star tracker. This allowed the imaging of a crescent Jupiter with the Image Science television cameras on the outbound leg of the trajectories. In this orientation, the normal of the D-cup pointed northward of the equatorial plane. It is qualitatively obvious from the trajectory plots that during the inbound approach to the planet, supersonic azimuthally flowing plasma would be detected primarily by the side sensor while not being detected by the main sensor. As the spacecraft is accelerated around Jupiter, such flow would be detected by the main sensor cups near closest approach and then lost to the instrument entirely on the outbound trajectory.

These remarks can be made quantitative for Voyager 1 (Figure 2b) and for Voyager 2 (Figure 3b) by plotting the instrument response to a cold, rigidly corotating positive ion beam for three of the Faraday cups. Unit response means that all the particle flux passing through the instrument aperture is detected at the instrument collector. The response of the A,C, and D cups is shown and aberration due to the spacecraft motion has been included. The response of the B cups closely parallels that of the C cup and so has not been shown. The B and C cup normals are near mirror images in the Jovian equatorial plane, pointing to the south and to the north of that plane respectively until the change of reference star to Arcturus.

Starting at 62-2000 (day of year 62, 20 hours, 00 minutes spacecraft UTC), Figure 2b shows that the D cup would "see" the plasma beam, while the other cups would not see it during most of the inbound trajectory leg. Only from ~64-0800 to ~64-1300 could a corotating beam be detected by the main sensor cups. By 64-1800 (the right hand edge of the figure), all cups have a zero response to a cold, corotating plasma. For reference, periapsis is about 64-1204.

In Figure 3b we show the same cup responses during the Voyager 2 encounter from 189-1700 to 191-1500 (periapsis is ~190-2229). Although qualitatively the same as the Voyager 1 cup response, the Voyager 2 D-cup response falls off earlier before closest approach and the A-cup response is appreciable for a longer time around closest approach to the planet. The difference between the cup responses for the two encounters is the result of different encounter trajectory geometries. Operationally, this has helped to limit the number of Voyager 2 D-cup spectra which we have successfully analyzed.

The spacecraft maneuvers alluded to were designed to orient certain of the experiments for special observations, several maneuvers being designed and executed specifically for the Plasma Science investigation. These can be divided into two types: rolls and off-axis maneuvers. In the former, the spacecraft executes a turn about the high gain antenna axis (pointed at the earth). Since the Plasma Science main sensor symmetry axis is parallel to the antenna axis, such maneuvers only affect the side sensor orientation in a fundamental way. Off-axis maneuvers involve turning the spacecraft about one of its other two axes ("pitch" about the spacecraft X-axis, "yaw" about the Y-axis) such that the high bit data rate communications link with the earth is temporarily broken. During these times, data is accumulated on the on-board tape recorder for high rate playback to earth once communication has been reestablished.

The Voyager 1 spacecraft executed seven off-axis maneuvers designed to look for plasma flow in the middle or outer magnetosphere. In each case, the spacecraft was rolled such that the Y-axis lay parallel to Jupiter's rotation axis. A subsequent yaw of  $360^\circ$  scanned the main sensor in a plane parallel to the rotational equatorial plane. The yaws were completed in about 32 minutes so that the symmetry axis of the main sensor moved about  $16^\circ$  between starts of subsequent 96 second measurement sequences. Since the three independent velocity component measurements possible with the main sensor allow the bulk velocity vector to be constructed (Bridge et al., 1977), spectra acquired with the A,B, and C cups would give the full velocity of the plasma if it lay close enough to the rotational equatorial plane. Each maneuver was finished by completing the initial roll so as to bring the spacecraft back to its nominal orientation. Of the two inbound

and five outbound off-axis maneuvers, strong signals in all three main sensor cups were only seen for the second inbound maneuver PLOMAN 2 (Plasma Outflow Maneuver 2) at ~35 Jovian radii inbound. We defer the discussion of results to the data section below. A roll to sweep the side sensor to look for magnetic field aligned plasma flow and the roll to charge reference stars from Canopus to Arcturus were executed as well. Voyager 2 executed no off-axis maneuvers during its Jupiter encounter phase as a result of contingency planning associated with command receiver problems on the spacecraft (Stone and Lane, 1979).

During the outbound leg of Voyager 2 encounter, that spacecraft did execute several roll maneuvers to reorient the side sensor. In each case, the spacecraft was rolled 180°, maintained that orientation for ~10 hours (~ one Jovian rotation period) and then completed the roll to the nominal orientation. Readily analyzable signals were seen only during part of one of these "reversed orientation" periods.

## CHAPTER III. PLASMA OBSERVATIONS IN THE MIDDLE MAGNETOSPHERE

## A. INTRODUCTION

The Plasma Science experiment gathered data continuously during the flybys of Jupiter by the two Voyager spacecraft. Between the last inbound and first outbound magnetopause crossings, the Plasma Science instrument on Voyager 1 telemetered to earth a total of some 66,000 positive ion, energy per charge spectra (L and M modes, all four Faraday cups). Traveling at a lower speed, Voyager 2 spent more time between its last inbound and first outbound magnetopause crossings. During this time it telemetered to earth some 96,000 positive ion spectra. As we have remarked above, processing of these data is contingent upon many different factors. These include the angle between the plasma flow and the cup normals, the ratio of the velocity component into the cup to the thermal speed (effective Mach number,  $M_{\text{eff}}$ ), the level of background current, and the effects of time aliasing. As long as the measured currents are above background and time aliasing is not a problem, the analysis can proceed at various levels depending upon how accurately the response function of the instrument is modeled.

In this thesis, we present an analysis of positive ion data gathered in the dayside middle magnetosphere ( $10 R_J \lesssim r \lesssim 40 R_J$ ). Outside of  $\sim 40 R_J$ , the data are contaminated by noise as a result of low fluxes of positive ions into the cups. The trajectory of Voyager 2 does not penetrate the inner magnetosphere ( $r \lesssim 10 R_J$ ) so that comparison between the two spacecraft there is not possible. More importantly, the inner

region, as sampled by Voyager 1 is dominated by the Io plasma torus and its associated dynamics, which form separate subjects of their own (Bagenal and Sullivan, 1981). For these reasons, we restrict ourselves to a study of the plasma in the middle magnetosphere. As we shall see the plasma dynamics (e.g. cf. the plasma sheet) are very different from those of the inner magnetosphere. The plasma flow in the middle magnetosphere is predominantly azimuthal about the planet, in the same sense as its rotation. As a result, the flow is directed into the D-cup only on the inbound legs of the spacecraft trajectories (§II.D). Under these conditions, we have a good knowledge of the instrument response function and can analyze the D-cup data so as to give quantitative results. This analysis yields only one component of the bulk velocity, although comparison of fluxes in the different cups shows that this is the largest measured component. The other cups notably B and C, still contain a large amount of information. However, the facts that these cups are asymmetric in shape and view the flow at very oblique angles in the middle magnetosphere make the analysis of the data complex. At this time, a method of routine quantitative analysis is not available. The data from the more oblique sensors can be used to make some quantitative statements about the flow direction, which we do below (§III.F).

#### B. POSITIVE ION CHARGE DENSITY

At the lowest level of analysis, we can obtain the total positive ion charge density from the total current measured in the D-cup (§II.B). We assume normal incidence of the flow into the cup so that the response

function is a constant. As long as the plasma is supersonic, the corrections, which go as the second power of the inverse effective Mach number, are small. We assume that within  $17 R_J$  of the planet the plasma rigidly corotates and that outside of the distance the velocity component into the D cup is constant at 200 km/sec. This choice is in reasonable agreement with the results of Bagenal and Sullivan (1981) and McNutt et al. (1979). Such a choice gives excellent agreement between the total positive ion charge density derived from the ratio of flux density to assumed velocity, and the total electron density recorded by the Plasma Science experiment (Scudder et al., 1981).

The results are shown for Voyager 1 in Figure 4 and for Voyager 2 in Figure 5. In each case the total L-mode current and total M-mode current above the noise level were compared and the larger used for the analysis. This tends to minimize time aliasing problems which can occur with the M-mode spectra and also eliminates the L-mode data for those spectra where instrument saturation occurred. Also, in order to best characterize the data through closest approach, the data used are those from that cup for which the sensor response to a cold corotating beam is largest. In approaching the planet densities are, therefore, obtained from the D-cup, then the C-cup, and finally, the A-cup (see Fig. 2a, 3a and discussions). In each figure the spacecraft event time is shown at the bottom with tic marks every hour and the distance from Jupiter's center in planetary radii at the top. (Throughout we have used the pre-encounter value  $1R_J$  (Jovian radius) = 71,372 km (Van Allen et al., 1974). This has been updated to a value of 71,398 km (Smoluchowski, 1976).) Periapsis is marked by CA ("closest approach"). The top panel shows the vertical distance of the

spacecraft in  $R_J$  from the magnetic dipole equator. Crossings of this equator are shown by arrows in the density panel for reference. These do not always coincide with the current sheet crossings as observed by Voyager and the correspondence is worse at larger distances from the planet (Ness et al. 1979a; Ness et al. 1979b).

Globally, the charge density shows two local increases every Jovian rotation period ( $\sim 9^{\text{h}}55^{\text{m}}$ ) (except for Voyager 1 at 64-000, see §III.G). This is in agreement with the magnetodisc interpretation of the Pioneer fields and particles data (§I.F.1). However, the decreases in magnetic field magnitude and increases in plasma density do not always exactly coincide. Hence, the term "magnetodisc" as originally employed (Van Allen, 1974) is not fully descriptive of the plasma data. To be precise in our terminology, we will speak of the "current sheet" in reference to the magnetodisc signature in the magnetic field data and of the "plasma sheet" in reference to the signature in the Plasma Science experiment data.

In the Voyager 1 density profile (Figure 4), at the plasma sheet crossings the density enhancements are pronounced and correlate fairly well with the dipole equator crossings. The correspondence is better at smaller radial distances although the two crossings of the plasma sheet centered on 64-0000 are a notable exception. The density curve, shown by the solid line is in good agreement with the corresponding electron density curve (Scudder et al., 1981). Crosses mark the mass density determinations discussed below (§III.E).

The Voyager 2 data (Figure 5) are displayed in a similar manner. The plasma sheet crossings do not show the regular structure seen in the Voyager 1 data. Pronounced crossings are centered on ~188-2230, ~189-0130,

and ~189-0000. The abrupt crossings at 190-2200 and 191-0930 are also clearly defined, unlike the density enhancement centered on ~189-2230. The Ganymede wake dropout phenomena is readily apparent from 190-0400 through 190-1200 (Bridge, et al. 1979b; Burlaga et al. 1980) and tends to obscure any regular density increases in this region. Again, crosses show the mass density from fits to selected spectra (§III.E).

### C. ANALYSIS OF HIGHLY RESOLVED SPECTRA FROM VOYAGER 1

#### 1. CONSTRAINTS ON THE ANALYSIS

In order to fully characterize the low energy plasma in the middle magnetosphere, we would like to have available the full three dimensional distribution functions of all ion species present. For various reasons we have alluded to, this is not possible in the dayside middle magnetosphere. Using our knowledge of the instrument response (§II.C) and the assumption of local thermodynamic equilibrium, we can fit the positive ion spectra in the D-cup in a non-linear least squares sense (see Appendix). Throughout most of the dayside middle magnetosphere this fit is based on the reduced distribution function measured along the D-cup normal, so that we routinely find only one velocity component. A more detailed analysis with a special simulation computer code using data in the other cups can provide knowledge of the full velocity vector (Belcher et al., 1980). However, computing constraints restrict usage of this analysis and so, in this thesis, we will primarily concern ourselves with the reduced Maxwellian distribution function parameters of the plasma as derived from a non-linear least

squares fit to the positive ion spectra as measured only in the D-cup.

The accuracy with which the positive ion data sets can be fit is strongly dependent upon data quality. The data quality is affected by several factors including plasma temperature, flux into the D-cup and the measurement mode (L or M). The occurrence of spectra constituting the "best" data seems to be related to crossings of the plasma sheet by the spacecraft. One of the best examples of M-mode data from Voyager 1 is shown in Figure 6. We plot distribution function versus energy per charge of the M-mode spectrum taken at 63-1537:35. The spectrum shown is from a ~20 minute period in which the plasma density was high enough and temperatures low enough that the M mode flux is well above the noise level for most channels and all dominant species within the energy per charge scan of the instrument are resolved. We can analyze this spectrum by utilizing a set of assumptions and then checking these for consistency. Following our previous discussions, we assume that the plasma is multicomponent in nature, and further, that each component is well represented by a convected, isotropic Maxwellian distribution function. Since the convective velocity is expected to be almost anti-parallel to the (outwardly directed) normal of the D-sensor and the magnetic field is nearly perpendicular to the normal, we assume that the species have a common velocity component (i.e. they are "comoving") into the sensor. In general, there could be a field-aligned differential streaming among the components, but this should be a negligible effect for spectra measured with the D-cup.

## 2. COMPOSITION AND TEMPERATURE: MAJOR IONIC SPECIES

Although certain parameters of the plasma, such as total mass density and total charge density, are independent of the exact species identification (II.C) others (such as temperature) are not. There are many times when the effective Mach numbers are lower than in the spectrum shown in Figure 6 and the various species are not resolved in the M-mode data; in the L-mode data the heavy ( $A \geq 2$ ) species are never resolved by the wider energy per charge channels. As a result of these limitations, we need to make some definite assumptions as to the plasma composition. This does not strongly affect the M-mode data analysis presented herein, but it does affect the L-mode analysis to follow. As there are ample sources of hydrogen in the Jupiter environment and the lowest mass to charge ratio is that for protons, we assume that the peak at the lowest energy per charge (see Figure 6) is due to protons.

We have noted above that various ions of oxygen and sulfur have also been identified in the Jovian magnetosphere. In particular, the Plasma Science instrument has observed species with mass to charge ratios of 1, 8,  $10 \frac{2}{3}$ , 16 and 23 (Bridge et al., 1979a; Bridge et al., 1979b). Sullivan and Bagenal (1979) have noted that such ratios result from protons, oxygen, sulfur, and sodium. Figure 6 shows these characteristic peaks.

As a guide to analysis, we have listed the ionization potentials of various atoms (Table I) and molecules (Table II) which are possible candidates for detection. We have also indicated the mass to charge ratio and whether the species has been identified in the Plasma Science data. Of

the species which have been possibly observed, the highest ionization potential listed is 47.3 eV for  $S^{4+}$  (mass to charge ratio 8). Observed ion temperatures in the torus range from ~25 eV to ~85 eV (Bagenal and Sullivan, 1981) and characteristic electron temperatures are also in the tens of eV (Scudder et al., 1981). Broadfoot et al. (1979) observed no  $O^{3+}$  (I.P. 54.9 eV,  $A/Z^* = 5 \frac{1}{3}$ ) and the Plasma Science spectra show no characteristic signals at mass to charge ratios of less than 8. Outside of  $\sim 15 R_J$  there are many instances, such as in the spectrum shown, of a peak at  $10 \frac{2}{3}$ . The peak is clearly not at  $11 \frac{1}{2}$  ( $Na^{2+}$ ) and so is most plausibly identified as  $S^{+3}$  with an ionization potential of about 35 eV. These considerations suggest that in its past, the observed plasma populations was exposed to some ionization mechanism of at least 35 eV in characteristic energy but not as large as 54 eV. On this basis, the peak at mass to charge of 8 is most likely oxygen and not sulfur, and we assume the former identification in the analysis of the data. The peak at 16 is more of a problem. Consideration of ionization energies and the fact that there is a significant amount of  $O^{2+}$  and  $S^{3+}$  would suggest that the signal is most probably due to sulfur, with most of the oxygen in the doubly ionized state. However, this is not necessarily true. To put the analysis of this spectrum on a more quantitative basis so as to better investigate the plasma composition, we have used our fit procedure to find number densities, temperatures, and bulk velocity components for the species suggested by the spectrum.

We have fit various parts of the 63-1537 M-mode spectrum with various components using eleven different sets of assumptions. These are enumerated, along with the results, in Table III. Since the peaks at mass

to charge ratios of 8,  $10 \frac{2}{3}$ , and 16 are well defined and dominant, for case 1 (Table III) we fit three comoving, isotropic Maxwellian distributions with independent thermal speeds to the spectrum. Each density is taken as an independent parameter (this is true in all of our analyses). We have assumed a composition of  $O^{2+}$ ,  $S^{3+}$  and  $O^+$  although the 16 peak could as well be  $S^{2+}$  or (as is likely) a combination of  $O^+$  and  $S^{2+}$  with different thermal speeds. In Figure 18, we show the fit currents. Only that part of the spectrum used in the fit is shown. The individual Maxwellians are shown by thin lines (parabolas) and their summed contribution in each channel is shown by crosses. Under case 1 in Table III we show the individual fit parameters including the thermal speed  $w$ , temperature  $T$ , and temperature per proton mass ( $\sim amu$ ) for each component. In this example we obtain a total mass density of  $22.18 \text{ amu cm}^{-3}$  and a total charge density of  $1.67 \text{ cm}^{-3}$ , which gives an average mass to charge ratio of 13.28. These parameters are functions of the mass to charge ratio only and are independent of the assumed composition.

The probable source of sulfur and oxygen is sulfur dioxide venting from Io (Cheng, 1980). Hence, each magnetic flux tube should contain twice as many oxygen as sulfur atoms. If the ionic species have not thermalized with respect to each other, the local number density ratio of oxygen to sulfur should be two. Thermalization implies a higher scale height for oxygen relative to sulfur, decreasing the local ratio somewhat (for discussion, see Bagenal and Sullivan, 1981). With this in mind, we have computed the ratio of oxygen to sulfur atoms assuming the 16 peak is either all  $O^+$  or all  $S^{2+}$  using the case 1 parameters. The numbers are 7.36 and 0.223, respectively. Since we are high by a factor of 3.7 in the all

oxygen case and low by a factor of 9.0 in the all sulfur case, this suggests that the 16 peak is indeed a combination of the two if the ultimate source is sulfur dioxide. If we assume a ratio of 2, then it can be shown that the signal at 16 must contain  $0.554 \text{ O}^+$  ions  $\text{cm}^{-3}$  and  $0.199 \text{ S}^{2+}$  ions  $\text{cm}^{-3}$  if we are seeing all of the oxygen and sulfur present and they have the same thermal speed. It is likely that we are detecting all of the oxygen, which is probably in its first two ionization states only. Furthermore, if we recall the ionization potentials of Table I and our previous arguments, it is likely that the 8 peak is mostly  $\text{O}^{2+}$  and contributions to the currents from  $\text{S}^{4+}$  are negligible. On the other hand, the ionization energy needed to create  $\text{O}^+$  and  $\text{S}^+$  is about the same. Since the latter is out of our energy per charge scan, it has not been included in the analysis, though it probably makes a significant contribution to the plasma population. Hence,  $0.199 \text{ ions cm}^{-3}$  of  $\text{S}^{2+}$  is an upper limit and most of the signal at 16 is probably due to  $\text{O}^+$ .

The thermal speed is usually the most ill-defined quantity since it is dependent upon the complete definition of the peaks. In the fit shown here, the comparison of temperature and temperature per atomic mass unit (amu) for each component shows that these quantities both vary from component to component. Assuming that the peak at 8 is all  $\text{O}^{2+}$  and the peak at  $10 \frac{2}{3}$  is all  $\text{S}^{3+}$ , it appears that the thermal speed rather than the temperature, tends to be the same for each of these components. This is consistent with ionization and pick-up by the magnetic field of a collisionless plasma (Bagenal and Sullivan, 1981). However, the thermal speed of the 16 peak is somewhat lower. As a comparison, for cases 2 and 3 (Table III) we have assumed that the temperature is the same for each

component and that the 16 peak is all  $O^+$  and all  $S^{2+}$ , respectively. The fits are shown in Figures 8 and 9. Although, the temperature so derived varies almost by a factor of 2 from one case to another, it is important to note that the velocity component, total mass density, and total positive charge density, are almost totally unaffected by the different assumptions. These fits show that neither the assumption of a common thermal speed or of a common temperature gives a complete description of the situation. This is true of other resolved M-mode spectra as well.

In case 4 (Table III) we fit an independent Maxwellian distribution to the proton peak in the M-mode and in case 5 we include that peak in a fit using the four resolved peaks and a common velocity component (see §III.C.3 below). It should be noted that the proton thermal speed is far higher than those of the other components and, in fact, the proton and (assumed)  $O^+$  temperatures are comparable (cases 4 and 5; Table III). This seems to be typical in those few spectra in which simultaneous but independent proton and  $O^+$  fits to M-mode spectra are possible.

### 3. COMPOSITION AND TEMPERATURE: MINOR IONIC SPECIES

Ionic species with ratios of mass to charge of 1, 8,  $10\frac{2}{3}$ , and 16 are routinely present in the spectra obtained with the D-cup in the middle magnetosphere. Species of positive ions as higher mass to charge ratios also contribute to the inertia of the plasma (Bagenal and Sullivan, 1980). In general, these are not visible in the data taken with the D-cup due to the low Mach numbers exhibited by the ionic species. For example, when the species at a mass to charge ratio of 16 has a low enough effective Mach

number any signal from  $\text{Na}^+$  is obscured. Species with larger mass to charge ratios are usually above our energy per charge range outside of  $\sim 10 R_J$ .

There is a clear signature of the sodium at a mass to charge ratio of 23 in the cold spectrum of Figure 6 although a peak is not fully resolved. We attempted to fit this species both to gain more understanding of the relative temperature problem (the identification of a 23 peak as  $\text{Na}^+$  is fairly certain) and to estimate by what amount the mass and charge densities are underestimated by excluding  $\text{Na}^+$  in our fits of other spectra. In each attempt (cases 6 and 7) we could not obtain a good fit to the data. This led us to consider what other species might be contributing to the signal in this part of the energy per charge spectrum. There have been reported sightings of neutral potassium in the Jovian magnetosphere (Trafton, 1975; Trafton, 1977), although potassium has never been clearly detected by any spacecraft instrumentation (e.g., Vogt *et al.*, 1979a). However, at a mass to charge ratio of  $19 \frac{1}{2}$ , doubly ionized potassium would tend to contribute to the signal at about the appropriate place in the spectrum. Upon reviewing the high Mach number M-mode spectra, we found that in one Voyager 1 spectrum, taken at 62-1020:47.065 there is a clear shoulder at mass to charge  $\sim 18$  to the side of the 16 peak. The measured flux was low and further analysis needs to be carried out so as to be certain that the signal is real and not an artifact of spacecraft noise. From Table III, we note that the ionization potentials for  $\text{K}^{2+}$ ,  $\text{S}^{3+}$ , and  $\text{O}^{2+}$  are comparable, so that any neutral potassium present at the ionization site would probably have contributed to a  $\text{K}^{2+}$  population. In any case, under the assumption of both  $\text{K}^{2+}$  and  $\text{Na}^+$  being present, good fits to the data could be obtained (cases 9, 10, and 11). There are indications from

the case 9 parameters that the temperatures of  $O^+$  and  $Na^+$  are closer than are their thermal speeds, but there is not enough resolution to come to a solid conclusion. The mass and charge densities of  $Na^+$  and  $K^{2+}$  from the three fits are consistent and represent about 10% and 7%, respectively, of the total mass and charge densities. As we remarked above, usually the plasma is hotter than it is in this spectrum and no signal around a mass to charge ratio of 23 is resolved. In such a case, by assuming only a contribution at 16 the fit parameters will adjust themselves (e.g. by increasing the fit thermal speed) so as to include any density contributions from  $K^{2+}$  and/or  $Na^+$ . The contributions by those (supposed) species in the high Mach number case are, therefore, upper limits to what we will usually neglect by fitting only the 8, 10 2/3 and 16 peaks.

With respect to neglecting contributions to the density, there is only one spectrum in the entire D-cup data set which clearly shows contributions by ion species with mass to charge ratios of 1, 8, 10 2/3, 16, 23, and 32. This is the spectrum taken at 63-1550:23.086 which has been published elsewhere (Sullivan and Bagenal, 1979; Belcher et al., 1980), and is not shown here. The peaks at 8 and 10 2/3 are not as well defined as those in the spectrum whose analysis we have detailed above. Unlike the spectrum at 1537 on day 63, this spectrum gives us the opportunity to estimate the density we neglect by not being able to include the peak at 32 in the analysis. In addition, assuming that the source of all the sulfur and oxygen is  $SO_2$  that the local number density ratio  $n[O]/n[S]$  is 2 and that  $S^{2+}$  and  $O^+$  have the same thermal speed, this is one of 3 spectra taken in the middle magnetosphere which allows us to calculate the relative contribution of  $O^+$  and  $S^{2+}$  to the 16 peak. A set of fit parameters, based

upon several types of fits as detailed above, is shown in Table IV. Again, the  $O^+$  and proton temperatures are in the same range while the  $H^+$ ,  $O^{2+}$ , and  $S^{3+}$  have about the same thermal speed. At this same time the core electron temperature is 10.6 eV (Scudder et al., 1981) comparable to the  $H^+$  and  $O^+$  temperatures. Computing mass and positive ion charge densities we find a total mass density of  $22.5 \text{ amu cm}^{-3}$ . Of that amount  $5.23 \text{ amu cm}^{-3}$  or 23% is contributed by the fits to  $K^{2+}$ ,  $Na^+$ , and  $S^+$ . The contribution increases to 24% if the protons are included. The total positive ion charge density is  $1.69 \text{ cm}^{-3}$ . The charge density from  $K^{2+}$ ,  $Na^+$  and  $S^+$  contributes  $0.197 \text{ cm}^{-3}$  or 12% of the total while that of the protons contribute another 13%. The measured electron charge density at 63-1550:55.486 is  $1.33 \text{ cm}^{-3}$  (Scudder et al., 1981) which is in fair agreement. If we set the local oxygen ion number density to sulfur ion number density ratio to 2 we find that  $0.518 O^+$  ions  $\text{cm}^{-3}$  and  $0.112 S^{2+}$  ion  $\text{cm}^{-3}$  contribute to the 16 peak. In this, we assumed that the 8 peak is all  $O^{2+}$  and the 32 peak all  $S^+$ . This is based on the relatively high energy (47.3 eV) needed to produce  $S^{4+}$  and the relatively low energy (6.6 eV) at which  $O_2^+$  dissociates (Table II). We note that this results in an average charge state of 1.4 and an average mass of 18.2 amu for the positive ions in the plasma. The average mass to charge ratio is 13.3 consistent with the analysis of the 1537 spectrum in which  $S^+$  is neglected.

Including the peak at the mass to charge ratio of 32 still provides only a lower limit to the positive ion mass and charge densities, but the further corrections to these quantities are probably smaller still. From data taken in the torus region it is known that there are heavier ions whose energy per charge is above our scan range in the middle magnetosphere

(Sullivan and Bagenal, 1979). There is no evidence for  $K^+$  at the mass to charge ratio 39. There is evidence for ions at mass to charge ratios of 64, ~104, and ~160 (Sullivan and Bagenal, 1979). The 64 signal is most likely  $SO_2^+$ ; the other species remain unidentified. In the middle magnetosphere these ions probably make less of a contribution than  $S^+$  at 32 and add little to our mass and charge densities.

#### 4. LIMITS ON THE ELECTROSTATIC POTENTIAL OF THE SPACECRAFT

We have also investigated the possible effect of spacecraft charging on the fit parameters. We included the proton peak in the analysis and fit the spectrum at 63-1537 to four independent Maxwellians, letting the bulk velocity component of each be fit independently of the others. For a given species  $i$ , of mass to charge ratio  $A_i/Z_i^*$ , assume the peak in its distribution is measured at some voltage  $\phi$ . Assume further that the instrument has acquired a potential  $\phi_{s/c}$ , that the true bulk component into the sensor is  $U_i$  and that the inferred component, assuming no spacecraft charging, is  $V_i$ . Then we have

$$\frac{1}{2} A_i m_p U_i^2 = Z_i^* e (\phi + \phi_{s/c}) \quad \text{III.1}$$

$$\frac{1}{2} A_i m_p V_i^2 = Z_i^* e \phi \quad \text{III.2}$$

were  $m_p$  is the proton mass and  $e$  the proton charge. If  $V_i$  can be measured for two different species and  $U_i$  is assumed to be the same for both, we can solve for  $\phi_{s/c}$  and  $U_i$ . The results of the fit to the spectrum taken at 63-1537 are shown under case 4 in Table III. The best estimate of possible

charging effects is derived by comparing fits to ionic species with very different mass to charge ratios. This minimizes the effect of errors in the velocity component found from the fit (i.e., in the values of  $V_i$ ). Using the values tabulated in Table III, we can compute values of  $U_i$  and  $\phi_{s/c}$ . If we compare the energy per charge values at heavy ion peaks with that of the protons, the largest spacecraft potential is derived from comparison with the 10 2/3 peak, from which we obtain  $\phi_{s/c} = 30.6$  volts,  $U_i = 198$  km/sec. This is still an upper limit on  $\phi_{s/c}$ , however. Since only 72 M-mode channels are telemetered each measurement cycle, the proton peak was obtained 96 seconds before the heavy ion peaks. On this timescale, variations in the plasma bulk velocity of this magnitude are not uncommon. We have extended this type of analysis to other M-mode spectra as well. All results are consistent with the spacecraft not charging to more than tens of volts at the most and usually to only a few volts (Bridge et al. 1979a; Scudder et al., 1981). The results are inconsistent with the large spacecraft potentials which, it had been hypothesized, would occur (Scarf and Gurnett, 1977). Intercomparison of velocity components found from the heavy ion peaks also give upper limits on the spacecraft potential but with large errors in the determinations. This can be illustrated as follows. The velocity component value for the 10 2/3 peak is off by 1% from those of the 8 and 16 peaks. We can use the velocity component values from the fits to these peaks to calculate  $V_i$  and  $\phi_{s/c}$  and then find what  $V_{H^+}$  ( $V_i$  for the proton signal) should be. From the 10 2/3 and 16 peaks we find  $\phi_{s/c} = -131$  volts and  $U_i = 187$  km/sec. Such high negative potentials are unreasonable because they would repel all low energy electrons from the spacecraft, and this does not happen (Scudder et al., 1981). From the 8 and 10 2/3 peaks

we find  $\phi_{s/c} = 131$  volts and  $U = 203$  km/sec. In this case  $V_{H^+} = 127$  km/sec which is 1.3 thermal widths lower than where the proton component peak is actually seen.

We also note that the high velocity and temperature for the  $10 \frac{2}{3}$  peak could be explained by an admixture of  $Na^{2+}$  ions rather than by spacecraft charging. We consider this unlikely, for although there is a clear signal at 23 of  $Na^+$  ions, it requires 47.3 eV to populate the  $Na^{2+}$  state, which is somewhat high compared to the other ionization potentials that seem to be typical for other ion species in the plasma. Such a characteristic energy at the place of ionization would probably have resulted in  $O^{3+}$  production, but, as we have noted, this ionic species is not seen. Such an energy would also argue for the peak at 8 to be a mixture of  $O^{2+}$  and  $S^{4+}$  (see values in Table III) and further complicate the analysis. For the sake of argument, suppose there were a population of  $Na^{2+}$  at mass to charge ratio  $11 \frac{1}{2}$ . Further, suppose the true velocity component is 195 km/sec but that 197 km/sec is the apparent average velocity from a mixture of  $S^{3+}$  and  $Na^{2+}$ . Then, instead of  $0.128 S^{3+}$  ions  $cm^{-3}$ , we find  $0.0942 S^{3+}$  ions  $cm^{-3}$  and  $0.0526 Na^{2+}$  ions  $cm^{-3}$ , the latter accounting for 26% of the measured current. The high velocity component of the peak at the mass to charge ratio of  $10 \frac{2}{3}$  is probably more indicative of the inherent error in the fit rather than a result of either detection of  $Na^{2+}$  or any spacecraft potential.

## 5. COMPARISON OF RESULTS OF L-MODE AND M-MODE ANALYSES

In Figure 10, we show M-mode spectral data which includes a plasma sheet crossing and the spectra just discussed (63-1537 and 63-1550). The

figure shows a four hour and fifteen minute run of M-mode spectra from 63-1300 to 63-1715 measured in the D-cup on Voyager 1 inbound. The spectra are plotted as current versus channel number. The current scale has been normalized to the largest current seen during the entire time period and the (linear) channel number scale has been labeled with energy per charge tic marks. It should be noted here that the current scale is linear while the individual spectral plots exhibit distribution function plotted on a logarithmic scale.

The figure gives a good representation of the variability of the data. The peak of the species with the mass to charge ratio of 16 in the 63-1537 spectrum is the highest peak on the figure. While individual spectra show peaks which look well defined and Maxwellian, variations in all the fit parameters from spectrum to spectrum can be significant. In this time period, density increases associated with the plasma sheet can be seen centered around 63-1345 and 63-1550 while the magnetic field minimum (indicative of the center of the current sheet) occurs at about 63-1400 (Ness et al., 1979a). The heavy ions occupy the energy per charge range of ~1000 to 6000 volts. The proton signals occur at about 100 volts and, in the sequence shown, only 3 spectra show proton signals prominently above the noise level. This is a typical problem with the proton signal in the M-mode data. It is readily apparent from Figure 10 that most of the M-mode spectra are in the noise and cannot be fit. This situation is remedied to a large extent by the adjacent L-mode spectra. Since the channel widths in energy per charge are larger than for the M-mode (by a factor of ~8), there is a gain in the signal-to-noise ratio, thus improving the proton signal. At the same time, this decreases the energy per charge resolution so that

the plasma parameters for the ionic species other than protons are more uncertain. The situation is illustrated in Figure 11 where we show a spline fit representation for the L-mode data in the same period as shown in Figure 10. To emphasize the proton signal, we have plotted distribution function versus channel number, both on a linear scale.

In Figure 12, we show the L-mode spectrum taken one minute after the 63-1537 M-mode spectrum discussed above. Here the lack of resolution of the heavy ions is apparent. The protons, however, remain as a resolved separate peak. Typically, the L-mode spectra show such a signature, even when the Mach number is lower. In this example, the effect of the 16 peak being clearly separated from the others in the M-mode is clearly reflected in the peak in the 14th channel of the L-mode. In those cases where the M-mode spectra are unresolved, the corresponding L-mode data exhibit two smooth peaks, one from protons and the other from heavy ions.

The L-mode spectra never contain enough information to allow an unambiguous fit to the heavy ion "peak". Even assuming the same velocity component for all species as well as the same temperature for the assumed major contributors ( $O^{2+}$ ,  $S^{3+}$ , and  $O^+$ ) leaves too many free parameters for the fitting procedure (see Appendix) to work with reasonable results.

We have carried out a series of fits to the L-mode spectrum at 63-1538:36.524 shown in Figure 12. This spectrum should yield plasma parameters close to those found in our detailed M-mode analysis discussed above, though as Figures 10 and 11 show there can be great variability on a time scale of one minute. So as to limit the number of fit parameters, we have assumed a constant bulk velocity component and a common temperature for the heavy ion species used in the fit. The fits are illustrated in

Figures 13, 14, and 15 and the parameters listed in Table V. Attempting to fit more than two heavy ion species typically results in one of the densities being driven negative. This occurs because the densities are not constrained to be positive and the information content of the L-mode spectra is relatively low. Of the cases illustrated, case 1 (of Table V) comes closest to reproducing values characteristic of the M-mode analysis detailed in Table III.

#### D. SURVEY OF L-MODE AND M-MODE SPECTRA

As we have indicated, the spectra shown in Figure 6 (M-mode) and Figure 12 (L-mode) are somewhat atypical. Usually, the sonic Mach number is lower and there is less resolution of the peaks. An example from Voyager 1 inbound is shown in Figure 16. Only the peaks at  $10 \frac{2}{3}$  and 16 are resolved; that at mass to charge ratio 8 is a shoulder on the  $10 \frac{2}{3}$  peak, and any proton signal has been lost in the noise. The latter can be recovered from the adjacent L-mode with its higher signal-to-noise ratio (Figure 17). This confirms the identification of  $10 \frac{2}{3}$  and 16 as the correct mass to charge ratios for the resolved peaks. Fitting independent Maxwellians to the resolved peaks, we find bulk velocity components of 204 km/sec and 203 km/sec, respectively. With respect to resolution, we find that the  $10 \frac{2}{3}$  peak exhibits a sonic Mach number of 10.1 as compared to 15.0 for the  $10 \frac{2}{3}$  peak in Figure 6. A sample M-mode from Voyager 2 taken at 189-1921 is shown in Figure 18. A preliminary analysis based on the peaks at 1,  $10 \frac{2}{3}$ , and 16 gave a common velocity component of 210 km/sec (Bridge et al., 1979b). An unsuccessful attempt to use our analysis

program is shown in Figure 19. The assumed composition is ionic species with mass to charge ratios of 1, 8, 10 2/3, and 16. The velocity obtained is 200 km/sec. Only the parameters for the proton peak are well defined (Mach number 2.1, temperature 45.4 eV), while the individual Maxwellian fits to the heavier species bear no relation to even the minimally resolved peaks. More information can be extracted from this spectrum, but a more sophisticated analysis is required. This is typical of many of the Voyager 1 M-mode spectra and almost all of the Voyager 2 M-mode spectra. The corresponding Voyager 2 L-mode spectrum from 189-1921 and a fit to it are shown in Figures 20 and 21. Although the fit to the proton peak is good and the predicted total currents match the measured currents well in most channels, the  $O^+$  number density is negative and the fit to the heavy ion peak overestimates both the density and temperature of  $S^{3+}$ . The velocity component obtained is 209 km/sec, consistent with the M-mode analysis results. The proton temperature is 31 eV and the formal mass and charge densities are  $4.33 \text{ amu cm}^{-3}$  and  $0.593 \text{ cm}^{-3}$ . The electron data gives about  $0.75 \text{ cm}^{-3}$  for the total charge density at this time and  $\sim 26 \text{ eV}$  for the core electron temperature (Scudder et al., 1981). These numbers are fairly consistent and in any case individual spectra about this time indicate the plasma conditions were fluctuating  $\sim 20\%$  or more (cf. Figures 18 and 20 - although taken only 30 seconds apart, the flux levels are quite different). However, since we could not obtain good fits to these spectra we have omitted them in the subsequent analysis. We have included the M-mode velocity determination as it is consistent with the channel locations in which the minimally resolved 10 2/3 and 16 peaks occur.

The best resolved M-mode spectrum was seen by Voyager 2 inbound at 190-0454 and is shown in Figure 22. A fit to it is shown in Figure 23. Again, clear peaks are seen at mass to charge ratios 1,  $10 \frac{2}{3}$ , and 16 although there are apparently contributions at the other indicated mass to charge ratios as well. There is also a high energy shoulder on the proton peak which may be indicative of alpha particles. (Such a signature is even more apparent in the 189-1921 spectrum in Figure 18 and has resulted in the fit velocity component being high.) No such signatures were seen in any of the Voyager 1 data. Unlike the case with the 63-1537 Voyager 1 spectrum, spectra near the Voyager 2 190-0454 spectrum are not resolved. The situation is illustrated in Figure 24 which shows Voyager 2 M-mode spectra from 190-0300 to 190-0715. The format is the same as that used for the Voyager 1 M-mode spectra in Figure 10. The spectrum at 190-0454 dominates all others in this time period which includes some of the "drop-outs" of data (no measured plasma) associated with the Ganymede wake (Bridge et al. 1979b; Burlaga et al., 1980) from the fit in Figure 23, for the 190-0454 spectrum. The measured velocity component is 130 km/sec, implying that during a full 192 sec measurement time, the plasma sampled occupies about  $0.35 R_J$  in space. Siscoe and Summers (1981) have suggested that this is the correct order of magnitude for convection cell size in the plasma, and hence such dramatic variations from spectrum to spectrum are not unreasonable. Analysis of the two L-mode spectra preceding the resolved M-mode spectra and of the two L-mode spectra following it quantifies these variations. The analysis shows that the local density increase is accompanied by a local decrease of temperature and a local increase of the flow component into the D-cup. At ~190-0455 a charge density spike is seen

in the electron data (Scudder et al., 1981), with most of the increase in the core electron component. At this time, the core temperature is locally cooler. In Figure 23, the Maxwellian at a mass to charge ratio of 16 has a Mach number of 9.5 and, assuming  $O^+$ , a temperature of 15.7 eV as compared to a one spectrum drop in the core electron temperature to 9.5 eV (Scudder et al., 1981).

To compare plasma conditions as seen by Voyager 1 and Voyager 2 at the same distance from Jupiter, we show in Figure 29 an M-mode spectrum taken by Voyager 1 inbound at  $16.5 R_J$ , the same distance as the Voyager 2 spectrum at 190-0454 (Figure 22). The Voyager 1 spectrum is of the class of unresolved M-modes with noise contamination of the proton signal. The split arrows in the figure, accompanying the mass to charge ratios, show the peak location for those species indicated on two different fits to the spectrum. The lower determinations of the peak locations result from fitting  $O^{2+}$ ,  $S^{3+}$ , and  $O^+$  with the same velocity component and the same temperature. The larger values are obtained from the same fit constraints but identifying the species at a mass to charge ratio of 16 as  $S^{2+}$  rather than  $O^+$ . In addition, a dashed arrow locates where the 16 peak would have to occur if the species with mass to charge 16 were rigidly corotating with the planet. Even with no clearly resolved peaks, rigid corotation obviously does not occur in this example (cf. III.B.2). For comparison, we show in Figure 32 the L-mode spectrum taken some 35 seconds earlier. Fits to this spectrum under several assumptions are summarized in Table VI. It should be noted that the L-mode fit to  $H^+$ ,  $S^{3+}$ , and  $S^{2+}$  is an example of a fit which has both a negative density and a subsonic fit to the proton peak. This is an example of the inherent ambiguity in much of the L-mode

data as discussed in the Appendix (§A.4). The other two L-mode fits are consistent with the model M-mode fit parameters as well as with the electron charge density (Scudder et al., 1981). In Table VII we show the formal fractional errors to the common velocity component, the density, and the thermal speed in the fit to the L-mode proton peak (§A.2). All formal errors in the parameters are less than 20% in the fit using  $S^{3+}$  and  $O^+$  as the heavy ion species. Note that the formal velocity error is much higher for the bad fit although the formal density error is quite small. We have included the L-mode fit using  $H^+$ ,  $S^{3+}$ , and  $O^+$  in our set of analyzed data discussed below while the unresolved M-mode of Figure 35 has not been included.

On the basis of a general survey of the data we concluded that the ionic species  $H^+$ ,  $O^{2+}$ ,  $S^{3+}$ , and  $O^+$  ( $S^{2+}$ ) are routinely present in the data. Noise tends to obscure the proton signal in the M-mode spectra, so we only fit the three heavy species to those M-mode spectra selected for analysis. On the basis of various fits to the L-mode data we have fit  $H^+$ ,  $S^{3+}$ , and  $O^+$  to the L-mode spectra selected for analysis, with  $S^{3+}$  and  $O^+$  constrained to have the same temperature. As we have detailed above, other schemes are possible but this selection seems to give the most consistent and error free results in a global sense (see §III.E. and §A.5).

#### E. GLOBAL PARAMETER VALUES

The great variability of the data with respect to temperature, composition, and signal-to-noise ratio precludes fitting all dayside middle magnetosphere data with the same level of confidence in the fit parameter

values. The greatest information context is in the resolved M-mode spectra, which give the most reliable estimates of the plasma parameters. In order to obtain the best velocity component values we have included in our global study only those M-mode spectra with at least two clearly resolved peaks. We searched through both the Voyager 1 and Voyager 2 M-mode data sets and found 62 such spectra from the former (including those of Figures 6 and 16) and only 2 from the latter (shown in Figures 18 and 22).

To extend our high confidence level data base, we searched through the L-mode data sets as well. From the Voyager 1 encounters we selected 573 L-mode spectra for analysis. This represents about 30% of the data taken between the last inbound magnetopause crossing at 62-0235 (Bridge et al., 1979a) and the time at which the proton signal dropped below our energy per charge scan range at 64-0430 as the relative plasma/spacecraft speed decreased near closest approach. In some of the plasma sheet crossings, L-mode spectra saturated in one or more channels. This occurred for 52 of the 573 spectra. In these cases, the currents in channels 8 to 16 of the L-mode spectra were computed from the corresponding currents in the most recent M-mode spectra in time sequence. Although this does increase the problem of time aliasing, it allows a first order analysis to be carried out. In each case the saturation occurs in channels containing the heavy ions. Without filling in these saturated channels, a good estimate of certain parameters, e.g., the total mass density, could not be given.

Using the same criteria as for the Voyager 1 L-mode data, we selected 161 Voyager 2 L-mode spectra for analysis. The smaller number of spectra as compared to the number selected from the Voyager 1 data set reflects the

fact that during the Voyager 2 encounter the effective Mach numbers of the various plasma constituents were lower. As a result, fewer spectra are resolved, e.g., sometimes only a proton peak is clearly defined and sometimes only a heavy ion peak. In either case, fits can still be obtained but the uncertainties in the resultant parameters are large enough that we have only included spectra with two peaks in the analysis in this thesis.

We have applied our non-linear least squares fit analysis to these selected Voyager 1 and Voyager 2 spectra (for details see §A.5), to obtain values of the mass density, bulk velocity component into the side sensor, and temperature of the plasma in the dayside middle magnetosphere. The mass density so derived, normalized to the proton mass (i.e., essentially in  $\text{amu cm}^{-3}$ ), from both the L and M modes is shown by the crosses in Figure 4 for Voyager 1 and Figure 5 for Voyager 2. In addition, for completeness, the Voyager 1 plot contains mass density determinations inside of  $10 R_J$  from Bagenal and Sullivan (1981). Comparison with the charge density curve on the Voyager 1 figure shows that the spectra excluded from the analysis tend to lie away from crossings of the plasma sheet. This is consistent with plasma in the sheet being more dense and cooler (see below) and resulting in spectra with less noise and better species resolution. The situation is less clear on the Voyager 2 pass where the plasma sheet crossings are less well defined.

The velocity components as determined from the Voyager 1 M-mode and L-mode analyses are shown in Figure 36. We give the components obtained from the L-mode and M-mode analysis separately because the M-mode determinations are more accurate. These data are shown for the same time

period as used in the density plot (Figure 4). Radial distance from Jupiter is shown at the top. We have also plotted the velocity component which would be measured in the side sensor if the plasma were rigidly corotating with the planet. In general, the velocity component lags the corotation value, with the lag increasing with increasing radial distance. Where the results of both the L-mode and M-mode analyses are available, it can be seen that these are in good agreement and show the trend to constant velocity components outside of  $\sim 20 R_J$ . This is the basis for our velocity model used in computing the charge density curves of Figures 4 and 5.

The deviation from rigid corotation, as deduced from the Voyager 1 M-mode data, is displayed in a different format in Figure 37. We have taken the difference between the velocity component expected for rigid corotation and the measured component and divided by the thermal speed of the component of the plasma with the mass to charge ratio of 16. This quantity is shown by the triangles in the graph. Note that the difference between the expected component and the measured component is always at least one thermal width, except around 63-1930, which is during a plasma sheet crossing. The deviation tends to be less in these crossings but, even here, is still significant (see also §III.G). To estimate the possible error in the velocity component determination as a result of spacecraft charging, we have estimated that error when subsequent analyses of L-mode and M-mode spectra were available. In essence, this repeats the calculation we discussed above for the spectra around 63-1537 shown in Figures 6 and 12 (cf. eqn. III.1 and eqn. III.2). The possible error is computed using a fit to the L-mode proton peak alone and the M-mode

velocity determination (determined by the energy per charge at the heavy ion peaks). We divide this estimated velocity error by the thermal speed of the component with mass to charge ratio 16. The upper limit on the velocity component error due to charging never exceeds 0.2 thermal widths and is usually lower.

The velocity component results for Voyager 2 are shown in Figure 30. The time period covered is the same as that in the Voyager 2 density plot (Figure 5). The discontinuities in the rigid corotation line result from roll maneuvers of the spacecraft which change the spacecraft attitude. Again, the determinations are always lower than those predicted for rigid corotation of the plasma with Jupiter. In both the Voyager 1 and Voyager 2 graphs, the rigid corotation line has been cut off when the response of the D-cup to a corotating cold beam is exceeded by the cold beam response one of the other cups (B or C) (cf. Figures 2b and 3b). Corotation is assumed for the response calculation so as to include aberration from the spacecraft velocity.

The results conclusively show that the lack of corotation is a global effect, not associated with any type of filamentary plasma structure, in agreement with the results in McNutt et al. (1979). In addition, the coverage from both Voyager spacecrafts indicates that lack of rigid corotation, is, qualitatively, a permanent characteristic of the middle Jovian magnetosphere on the dayside.

The temperatures found from the protons during the Voyager flybys are shown in Figures 39 and 40. Figure 39 also contains the  $O^+$  temperature determinations from the M-mode spectra. (Recall that the M-mode  $O^+$  temperatures and L-mode proton temperatures are typically close when inter-

comparison is possible §III.C.5.) The time periods are, again, the same as those used in the density and velocity component graphs. For reference, we have used arrows to indicate the locations of the crossings of the magnetic dipole equatorial plane. These are also given in the density curves (Figures 4 and 5). During both encounters, the temperature of the resolved proton component is usually about 100 eV. The Voyager 1 curve shows large local variations, with the temperature decreasing in the plasma sheet crossings. This variation is not so apparent in the Voyager 2 data. Also, the temperature tends to increase slightly with increasing radial distance. On both the Voyager 1 and 2 passes, the electron temperatures (Scudder et al., 1981) are comparable.

We find that for the Voyager 1 encounter, the resolved M-mode spectra generally occur in the regions where the proton temperature, as found from the L-mode spectra, shows decreases (i.e. in the plasma sheet). This is consistent with the fact that the individual signatures of heavy ions are only resolved at large sonic Mach numbers. Assuming the peak at mass to charge 16 is  $O^+$ , the temperature of this ion in these M-mode spectra ranges from 8 eV to ~100 eV. The absence of decreases in the Voyager 2 proton temperature profile is, therefore, consistent with the general absence of resolved M-mode spectra in the Voyager 2 data set. Comparing the density profile in Figure 4 and the temperature profile in Figure 39, it appears that during the inbound pass of Voyager 1 large thermal gradients existed across the plasma sheet with the low energy plasma being cooler inside the sheet than outside. The lack of a signature of regular and well defined crossings of the plasma sheet in the Voyager 2 density curves (Figure 5), combined with the relatively featureless temperature curve (Figure 40)

seems consistent in light of the temperature and density correlation in the Voyager 1 data. The two plasma sheet crossings seen in the Voyager 2 data at ~190-2100 and ~191-0930 exhibit relatively cold spectra (Figures 45 and 46) similar to the Voyager 1 crossings of the plasma sheet (cf. Figure 44).

Gaps in the two temperature profiles (Figures 39 and 40) result from a selection effect based on the temperature (via the effective Mach numbers). A proton distribution with a sonic Mach number of unity and a bulk speed of 200 km/sec has a temperature of about 200 eV and will not be resolved from the heavy ion signature in the L-mode (eqn. II.13., §II.B). Yet we have selected L-mode spectra for analysis on the basis of their having a resolved proton peak; hence, spectra exhibiting higher temperatures than ~100 eV have effectively been eliminated from the data set. In the gap regions, fits to the unresolved spectra indicate proton temperature of several hundred electron volts but never as high as 1 keV. A higher, but firmer, upper limit on the plasma temperature can be set by considering the signature of the heavy ions in the L-mode spectra. As noted above, the heavy ion peak in the L-mode spectra is assumed to be due to  $S^{3+}$  and  $O^+$ . Furthermore, these are assumed to have the same temperature so as to limit the number of fit parameters (§A.5). This temperature is always an upper limit since the fit parameters compensate for species known to be in the plasma but not included in the analysis of the L-mode spectra (e.g.  $O^{2+}$ ). Comparing the temperature of the heavy ions so derived with that of the peak at a mass to charge ratio of 16 in the M-mode spectra, we find that the former is typically larger by a factor of 3 to 10 where comparisons are possible. Fits to the unresolved spectra give values of this "temperature" which are usually below 3 keV and always below 10 keV. This is consistent

with the fact that in almost all cases, the distribution function of the measured spectra peaks below 6 keV (the top of our energy per charge scan). In those isolated cases where this is not the case, the distribution function shape indicates that this is the result of a locally high velocity component into the D-cup and not a result of heating. For example, a Maxwellian distribution of singly ionized oxygen moving into the D-cup at 300 km/sec would peak at ~7500 volts. There is evidence from resolved protons at ~30  $R_J$  on Voyager 1 that such velocities may occur (though they are still less than those expected for rigid corotation). In any case, all of our data indicates that within 40  $R_J$  of Jupiter the temperature of the magnetospheric plasma never exceeds 10 keV on the dayside and is typically ~1 keV or less.

#### F. GLOBAL FLOW INFORMATION FROM MAIN SENSOR DATA

In addition to the fit parameters, we also have available information about the flow direction which is of a more qualitative nature and is based on data from the main sensor Faraday cups. Since the B and C cups are oriented almost symmetrically about the Jovian equatorial plane (spacecraft attitude referenced to Canopus) (section II.D), the relative fluxes and spectral shapes give information about flow perpendicular to that plane. During both encounters, the main component of plasma flow was oblique to both of these cups except for a brief period near closest approach. Hence, the response function of the instrument is convolved with the plasma distribution function in a non-trivial way in the measured currents. The near symmetric arrangement of the B and C cups with respect to the flow

ensures that the convolution is about the same for the currents measured in each of these cups. It is this fact which makes possible a qualitative analysis based on the relative fluxes and relative spectral shapes.

We compute a north/south flux anisotropy by taking the difference of the flux density of positive ions into the B-cup and the flux density of positive ions into the C-cup and then dividing by the sum of the two flux densities. Since the B-cup opens southward and the C-cup opens northward the anisotropy will be positive if there is flow to the north and negative if there is flow to the south. When the spacecraft attitude is referenced to Arcturus, the calculation can still be performed but with the A-cup and B-cup rather than with the B-cup and C-cup. In Figure 41, we plot this anisotropy for Voyager 1. The plot is linear against spacecraft event time. We indicate radial distance from the planet at the top and local time at the bottom. (12 noon implies the spacecraft lies in the plane containing the Jupiter-sun line which is perpendicular to Jupiter's orbital plane.) The anisotropy scale is on the left. On the plot we have superimposed a graph of the spacecraft position perpendicular to the magnetic equatorial plane (cf. Figure 4). The scale is shown on the right. Recall that passing through this plane essentially marks crossings of the Jovian current sheet, especially within  $20 R_J$  of the planet.

The correlation of anisotropy and spacecraft position is pronounced. On the dayside (before 1800 local time) there is a marked tendency for flow to be northward when the spacecraft is north of the current sheet and southward when the spacecraft is to the south, i.e., there is plasma flow away from the current sheet. This pattern was observed by Pioneer in anisotropy measurements of MeV protons in the dayside magnetosphere (S.E.3;

McDonald et al., 1979; Northrup et al., 1979). The anisotropy amplitude decreases with radial distance and local time along the spacecraft trajectory. On the nightside (after 1800 local time), the spacecraft location and anisotropy are anticorrelated, i.e., there is plasma flow toward the current sheet.

At a more detailed level two additional characteristics of the data should be noted. First there is an almost discontinuous displacement of the anisotropy curve from ~63-1500 to ~63-1830. This feature may be associated with a global expansion of the magnetosphere and will be discussed elsewhere (§IV.C.). A more subtle point concerns the true location of zero anisotropy on the graph. The B-cup and C-cup normals are oriented such that there is slightly more azimuthal flow entering the C-cup on most of the inbound trajectory than there is entering the B-cup. Hence, no north/south flow would still leave a small negative anisotropy in the graph. As the spacecraft nears Jupiter, the azimuthal components of the cup normals decrease such that this effect vanishes near closest approach (~64-1204). As a result, the zero line should have a small positive slope and pass through 0.0 at ~64-1200. After ~65-0300, the spacecraft attitude is referenced to Arcturus and the anisotropy is computed from the A-cup and B-cup data. In this case, the correction to the zero line turns out to be much smaller.

Using the same format as above, we show the B-cup/C-cup anisotropy curve for Voyager 2 in Figure 42. On the dayside, we again observe flow away from the current sheet and, on the nightside, flow toward the current sheet. The trajectory of Voyager 2 takes the spacecraft to the nightside of the planet before the change in spacecraft attitude from Canopus to

Arcturus reference. Again the magnitude of the anisotropy increases with increasing radial distance from the planet. The effect becomes even clearer if we note that, as on Voyager 1, the azimuthal components of the B and C cups change as the spacecraft travels around the planet. As a result, no anisotropy would appear at a negative value on the left side of the graph and at a positive value on the right side of the graph. A depression in the anisotropy curve at ~191-0500 may be related to a global contraction of the magnetosphere.

The effect has been qualitatively investigated using a computer simulation code which includes the full response function for each of the cups (cf. Belcher et al., 1981). This analysis of selected spectra has shown that the data are consistent with bulk plasma flow and cannot be explained by an anisotropic plasma distribution convolved with the instrument response. In addition, the simulation results show that flow from the sheet is accompanied by radially inward flow and flow toward the sheet by outward flow. This is consistent with the north/south anisotropy reflecting flow along magnetic field lines. Specifically, McNutt and Belcher (1981) found that on Voyager 2 at 189-2010 the azimuthal velocity of the plasma was 264 km/sec, the radial velocity was 167 km/sec inward and the vertical component 95 km/sec southward. At the time the spacecraft was 3.3  $R_J$  below the magnetic equatorial plane, 21.5  $R_J$  from Jupiter, and near local noon.

There is one direct measurement of plasma flow into the main sensor in the middle magnetosphere. This occurred on the inbound leg of the Voyager 1 trajectory during the spacecraft maneuver sequence named PLOMAN 2 (see §II.D). We obtained one L-mode spectrum in all three cups of the main sensor which was suitable for analysis which has been detailed elsewhere

(Sullivan et al., 1979). At this time, plasma flow was primarily in the azimuthal direction with a component of 212 km/s as compared to 443 km/s which would be expected on the basis of corotation. The other flow components were 23 km/s outward and 49 km/s northward. At this time the spacecraft was  $35.3 R_J$  from the planet,  $2.3 R_J$  below the magnetic equatorial plane and  $3.2 R_J$  above the centrifugal equatorial plane. The components of the magnetic field indicate the spacecraft was slightly south of the true magnetic equator at the time (Ness, private communication, 1980) so the plasma flow is back toward the current sheet and inconsistent with the global picture at smaller radial distances.

#### G. DETAILED PLASMA SHEET OBSERVATIONS

The plasma sheet is apparently a permanent feature of the Jovian magnetosphere. The fact that it undergoes temporal variations is evidenced by the less regular structure displayed by it during the Voyager 2 encounter as compared with that found during the Voyager 1 encounter (cf. Figures 4 and 5). In addition, the sheet itself exhibits a great deal of fine scale structure in the characteristics of the plasma (cf. the spectral plot covering the Voyager 1 crossing at 63-1400 shown in Figure 10).

The most regular variation in the plasma sheet was seen by Voyager 1 in the crossing at 63-1900. Although the cooling effect is not as pronounced as during other crossings such as the ones around 63-1400, the spectra through the crossings show enough resolution in the L-mode and M-mode that we can analyze this particular crossing in some detail. In Figure 43, we show the M-mode spectra from 63-1700 to 63-2115 as measured

in the Voyager 1 side sensor. The format is the same as for Figures 10 and 24. The heavy ionic species occupy the energy per charge scan from ~600 volts to ~4000 volts. The increase in density and decrease in temperature (resolution into multiple peaks) which defines the sheet crossing are readily apparent. The proton signal is lost in the noise in the M-mode spectra but not in the L-mode spectra. In Figure 44, we plot a representation of the L-mode distribution function for the same time period. The presentation is the same as that used in Figure 11, and shows a well defined proton signature for most of the time period concerned. The heavy ion peak signal is saturated in the L-mode during most of the crossing and does not reflect the M-mode variation (Figure 43). In order to analyze this crossing we fit the L-mode spectra, using the M-mode data to fill in the saturated channels (§III.E.). The parameters from the analysis are shown in Figure 45. In this crossing, the centrifugal and magnetic equators coincide with each other and with the crossing. The System III longitude at the crossing of the magnetic equatorial plane is  $112^\circ$  so that the spacecraft is over the inactive hemisphere (Vasyliunas, 1975). In the plots, crosses indicate parameters from the electron spectral analysis (Scudder et al., 1981), and triangles those from the positive ion analysis. The second panel from the bottom of Figure 45 shows the mass density normalized to the proton mass. The density enhancement which delineates the sheet crossing shows that the plasma sheet is centered on the current sheet crossing (Ness et al. 1979b) at ~63-1900 as well as on the magnetic equatorial plane. The plasma sheet is about 2  $R_J$  thick and shows three smaller density enhancements, the largest being at the center and clearly discernable in Figure 45. The third panel shows the ratio of

the total mass density to that of the protons. From this plot, it can be seen that the first two internal density increases result from large enhancements in the heavy ions relative to the protons. It should also be noted that these places are precisely where the velocity component most nearly approaches the rigid corotation value. The results are characteristic of the other plasma sheet crossings made by Voyager 1. The temperature of the protons from the L-mode spectral analysis and of the (presumed)  $O^+$  from the M-mode analysis are shown in the top panel of Figure 45 along with the core electron temperatures (Scudder et al., 1981). Local cooling occurs at the largest mass density enhancements although not to the same extent as in some of the other Voyager 1 crossings. To obtain an idea of the full plasma flow pattern during this crossing, we can employ measurements of plasma anisotropy as outlined in the previous section (§III.F.). In the bottom panel of Figure 45, we show the ratio of the difference of the flux densities measured in the B-cup and C-cup to their sum. The maximum flux anisotropy coincides with the maximum density and indicates that most of the plasma sheet is moving southward although a large shear in the flow is present. In fact, the first density enhancement at ~1820 may be moving northward. The idea of bulk motion is borne out by consideration of the B-cup and C-cup spectra. At the maximum anisotropy, not only does the B-cup flux exceed that in the C-cup for the crossing but also the B-cup spectra peak at higher energy per charge values than do the spectra measured in the C-cup. Analysis of selected spectra has indicated that the spectra cannot be duplicated by a gyrotropic, but anisotropic, distribution function (§III.F); hence, the positions of the spectral peaks strongly imply that the flux anisotropy is a real bulk motion effect. In

general, outside of the plasma sheet, plasma is moving away from the magnetic equatorial plane at a significant fraction of the local azimuthal velocity.

Flow of the plasma sheet relative to the current sheet is most prominently exhibited in the Voyager 1 data around the beginning of day 64. The M-mode spectra from 63-2200 to 64-0215 are shown in Figure 46. Only one current sheet crossing occurs during the time shown and that at about 64-0000 between the two plasma sheet crossings (Ness et al., 1979a). By itself, each plasma sheet signature is fairly typical and marked by increased density and decreased temperature. Relative differences include resolved peaks at mass to charge 32 (~2000 volts) in the first crossing and resolved protons in the second (~50 volts at the center of the proton signature). The bifurcation of the sheet is made comprehensible by examination of the measured B cup/C cup anisotropy and the corresponding spectra. Again, flow out of the current sheet is indicated; the plasma in the first density enhancement (~63-2315) lies north of the sheet and is moving northward while that in the second enhancement (~64-0130) lies to the south and is traveling southward. Hence, plasma in the "plasma sheet" is in a dynamic state of motion relative to the current sheet and the concept of a static plasma/magnetic field "magnetodisc" is not strictly correct. We discuss this point in more detail in the next chapter. It should be noted that the bifurcation of the sheet at this crossing is not confined only to low energies. The "double crossing" is also clearly visible in the 22.5 MeV proton data from the Cosmic Ray experiment (Vogt et al., 1979a).

As we have remarked, the crossings of the plasma sheet by Voyager 2 were, in general, less regular than the crossings by Voyager 1 detailed

above. The only two well-defined crossings occurred close to perijove. We show the M-mode spectra which includes the inbound crossing in Figure 47 and those including the outbound crossing in Figure 48. The crossings, which occurred at ~190-2200 (Figure 47) and ~191-0930 (Figure 48), are readily identified in the density profile (Figure 5). Although, the density enhancements are sharp, the spectral peaks do not show the clear structure typical of the Voyager 1 data (cf. Figure 43). The B-cup/C-cup anisotropy for the crossing at 191-0930 is consistent with the global observation of flow toward the current sheet on the nightside (Belcher and McNutt, 1980). The crossing at 190-2200 requires more detailed study. It occurs in the dusk meridian when plasma flow is into the main sensor and it exhibits enough structure in the spectra that a good vector velocity determination should be possible. However, close examination of the individual spectra show clear evidence of time aliasing and non-Maxwellian characteristics so that the analysis is somewhat complicated. A study of all of the details of this plasma sheet crossing is beyond the scope of this thesis.

## CHAPTER IV.

## DISCUSSION OF RESULTS

## A. GLOBAL VARIATIONS OF MACROSCOPIC PLASMA PARAMETERS

## 1. AZIMUTHAL VELOCITY COMPONENT

A basic result of this thesis is the observation that the plasma in the middle magnetosphere on the dayside of Jupiter is not locked into rigid corotation with the planet. All previous theoretical treatments had assumed either rigid corotation throughout the magnetosphere or a sudden change to a radially outflowing planetary wind at some distance from the planet. Kennel and Coroniti (1975) did question whether corotation could be enforced, but discussed the issue in a somewhat different context. Their principal thrust was deciding whether the torque transmitted upward through Jupiter's neutral atmosphere would suffice to drive a radial plasma outflow or lead to the formation of a plasmopause (§I.F.2).

Simultaneous to the finding that the plasma is not rigidly corotating with the planet (McNutt et al., 1979), Hill (1979) hypothesized that such a situation might hold. His reasoning was that if the injection of plasma into the magnetosphere occurs rapidly enough, and if the ionospheric (Pederson) conductivity is low enough, a torque sufficient to enforce corotation cannot be transferred to the plasma as it moves outward. Hill derived the angular speed of the plasma as a function of cylindrical distance from Jupiter assuming cross field transport in a dipolar magnetic field. He did not address the question of the transport mechanism.

The Hill model is characterized by one parameter  $L_0$ , which is the scale length for deviation from rigid corotation expressed in units of  $R_J$ ,

the radius of Jupiter. If  $B_0$  is the surface equatorial magnetic field, then in c.g.s. units

$$L_0^4 = \frac{\pi B_0^2 R_J^2 \Sigma_p}{c^2 \dot{M}} \quad \text{IV.1}$$

where  $\dot{M}$  is the mass loading rate at the Io torus,  $\Sigma_p$  is the ionospheric height integrated Pederson conductivity, and  $c$  is the speed of light. Hence, knowledge of two of the three quantities  $L_0$ ,  $\dot{M}$ ,  $\Sigma_p$  allows the third to be calculated.

To first order the bulk plasma motion for Voyager 1 is azimuthal on the dayside (§III.E. and Krimigis et al., 1979a). The case is not as clear for Voyager 2 as for Voyager 1, but again, to lowest order, the plasma flow is azimuthal (Krimigis et al., 1979b) on the dayside, the local angular velocity of the plasma being smaller than that of the planet. In Figure 49, we plot the ratio of the observed velocity component into the side sensor to that which would be measured as a result of rigid corotation. Assuming that all of the bulk motion of the plasma is azimuthal, this gives the ratio of the local plasma angular speed to the planetary angular speed, which can be compared to the ratio as predicted by Hill's theory.

The plots of normalized plasma angular velocity show three main features. First, at a given radial distance, the magnetospheric plasma was rotating more slowly though the dayside during the Voyager 2 passage than during the Voyager 1 passage. Second, there are indications of local maxima at the plasma sheet crossings. This may be a consequence of Ferraro's isorotation law (§I.C.1). If inertial loading is the cause of lack of corotation, then by Ferraro's theorem the plasma angular velocity should still be a constant along any given field line in the magnetosphere.

As we have discussed above (§II.D), the spacecraft moves through the current sheet and plasma sheet as a result of the tilt between the magnetic and rotational axes of Jupiter. In the distorted field geometry near the current sheet the spacecraft will also move through various magnetic L-shells. The shell with (locally) the smallest L-parameter will be that encountered at the true magnetic equator (i.e. the center of the current sheet). The larger the L-parameter the more torque required for corotation and, hence, the less the angular velocity. The largest local angular velocity should, therefore, be that seen during the current sheet crossing. However, Figure 49 shows increases at the plasma sheet crossings which, as we have noted, do not necessarily coincide with the crossings of the center of the current sheet. The increase is most apparent in the Voyager 1 data in the combined crossings of both sheets at  $\sim 17 R_J$ . In the other crossings there is more scatter in the data and the effect is not as discernable. There is an indication that a local azimuthal velocity increase may be occurring in each of the two plasma sheet crossings measured by Voyager 1 at  $\sim 10.5 R_J$  and  $\sim 12.0 R_J$  (cf. Figure 46) although this is difficult to reconcile with any reasonable magnetic field geometry. Consideration of individual spectra and the fits show that the increase in fit velocity (found in the L-mode spectra) may be influenced by the large enhancement of ions with mass to charge ratios of 16 seen in the crossing. Not all of the increase may be real and a more detailed study of all of the spectra in this region is indicated. We emphasize that the fit velocity components in this region are, at worst, upper limits; the plasma outside of  $11 R_J$  was not corotating with the planet. Finally, the fractional angular velocity falls off roughly as  $r^{-1}$  (i.e. the azimuthal velocity component asymptotically goes to a constant) outside of  $\sim 17 R_J$  in the Voyager 1 data. The

case is less clear in the Voyager 2 data although there is again some indication of a decrease with radial distance from Jupiter.

Hill predicts an  $r^{-2}$  decrease in angular velocity at asymptotically large distances since the field can no longer accelerate the plasma there and the plasma conserves angular momentum as it moves outward. The difference between theory and observation can, in large part, be ascribed to Hills' use of a dipole field in his model; at large distances, the actual planetary field is quite non-dipolar. At some radial distance in the equatorial plane, the field lines map back to the ionosphere at lower latitudes than would be true in a dipole field. If  $\theta_s$  is the surface colatitude of a field line, then it can be shown that the available torque goes as  $\cos \theta_s \sin^2 \theta_s \sim \theta_s^2$  for  $\theta_s$  small. The distortion of the field implies the field can transfer torque more efficiently to large distances than it could in a dipole configuration. Hence, a decrease with distance of the angular speed, such as is observed, is a plausible outcome of the theory.

As we noted above, the inertial loading theory connects the ionospheric conductance and the mass loading rate to the decrease of angular speed with distance from the rotation axis of the planet. Departure from rigid corotation occurred inside the middle magnetosphere at  $\sim 7 R_J$  during the Voyager 1 encounter (Bagenal and Sullivan, 1981; Kaiser and Desch, 1980). The scale length for departure  $L_0$  is  $\sim 17 R_J$  if we average over variations in the curve, essentially the conclusion reached by Hill on the basis of our preliminary analysis of the data (Hill, 1980). However, at  $17 R_J$  the field is appreciably distorted by the current sheet (Ness et al., 1979a) and for purposes of calculation the value of  $L_0$  used in eqn. IV.1 should be  $\sim 12 R_J$  (cf. Connerney et al. 1981). Cheng (1980) has suggested

that during the Voyager 1 encounter Io was injecting  $10^8$  g/sec of  $\text{SO}_2$  into the magnetosphere. This yields  $\dot{M} = 6 \times 10^{31}$  amu/sec. Using  $L_0 = 12$ , this gives  $\Sigma_p = .75$  mho, a value in line with Hill's estimate that 0.1 mho is a good lower limit of the conductance of the Jovian ionosphere.

The Voyager 2 data, while sketchy, does indicate that the angular speed of the plasma at a given radial distance was somewhat less during that encounter than during the Voyager 1 encounter. In the context of the inertial loading model this implies a smaller height-integrated ionospheric conductivity  $\Sigma_p$ , a larger mass injection rate  $\dot{M}$ , and/or a less distended magnetic field line configuration on the dayside. A preliminary analysis of one high-Mach number spectrum taken in the Voyager 2 plasma sheet crossing at  $\sim 190$ - $2100$  ( $10.2 R_J$ ; cf. Figure 47) indicates that the plasma azimuthal velocity is only a few per cent below the corotation value. This would imply a larger  $\Sigma_p$ , smaller  $\dot{M}$ , or both. In addition, it is not clear whether this difference in the Voyager 2 data between  $10 R_J$  and  $\sim 16 R_J$  reflects a spatial or temporal change in the magnetosphere. Further detailed study of the data, beyond the scope of this analysis, is clearly needed.

## 2. FIELD ALIGNED VELOCITY COMPONENT

The spectra collected with the D-cup in the dayside magnetosphere allow the direct determination of only one component of velocity (§III.E). However, as we have remarked above (§III.F), the flux levels in the cups of the main sensor do contain information about the other components. In particular, we have shown (§III.F and Belcher and McNutt, 1980) that in the dayside, plasma also tends to flow away from the current sheet. Available

evidence from the fits to the main sensor data from the Voyager 2 encounter indicates that this flow is roughly along the magnetic field lines so that it is also back toward the planet. The flow is observed to reverse in the nightside magnetosphere so as to be from the planet and toward the current sheet. During the Voyager 2 encounter, the high Mach number spectrum in the plasma sheet at  $\sim 190$ - $2100$  (referred to above) occurs near perijove when the plasma flow is into the main sensor (SIID). A preliminary analysis indicates the plasma is almost up to the corotation speed and has only an azimuthal velocity component. However, perijove occurs very near local dusk so that this measurement is not inconsistent with a streaming of plasma synchronized to the local time. This local time asymmetry suggests an MHD pumping mechanism such as that proposed for higher energy particles by Goertz (1978). One interpretation (Belcher and McNutt, 1980) is based on the dayside/nightside asymmetry which results from the dayside magnetosphere being compressed towards the planet by the solar wind. Without such a compression, the low energy plasma would tend to be distributed along field lines such that the pressure gradient is balanced by the component of centrifugal force along the field line in a steady state. The scale height for such a distribution is:

$$H = (2/3)^{1/2} c_s / \Omega \quad \text{IV.2}$$

where  $c_s$  is the sound speed and  $\Omega$  is the local angular speed (Hill and Michel, 1976). A typical scale length for the resolved M-mode spectra is  $\sim 1 R_J$ . Disturbances will propagate at the sound speed, so the time scale for readjustment is  $\sim H/c_s = (2/3)^{1/2} \Omega^{-1}$ . Hence, the dynamic time scale is  $\sim 13\%$  of the rotation period. However, the plasma along a given field line

is disturbed on this time scale as it rotates into the compressed dayside magnetosphere. As a result, the magnetospheric plasma can never adjust to the local time perturbation and must be in a constant state of motion. In particular, in the noon meridian where the magnetosphere is compressed the most by the solar wind, the scale length of the magnetic field along a given field line will exceed the instantaneous plasma scale height so that the plasma will tend to stream along the field lines at a speed  $\sim c_s$ . In addition, at smaller cylindrical distances to the planet, a tube of constant magnetic flux has a smaller cross section area. Hence, the "squeezing" of a flux tube by the solar wind will also tend to accelerate plasma away from the symmetry surface (the current sheet) and along the field lines toward the planet. As the flux tube moves toward the dusk meridian, it will expand and decrease in scale length which will tend to decelerate the plasma flow. In the dusk meridian as the flux tube continues to expand, the plasma will then begin to flow back toward the current sheet. As the flux tube leaves midnight and approaches dawn, it begins to be compressed such that, presumably, at the dawn meridian the plasma inflow changes to outflow and the cycle begins anew. Since perturbation of the magnetosphere by the solar wind decreases with decreasing distance to the planet, so will the flow along the field lines, although the data suggest the effect is appreciable as close as  $\sim 15 R_J$  to Jupiter.

The dynamical state of the magnetospheric plasma has several important consequences which we will discuss in the context of the physics of the plasma sheet (see below §IV.C). A general result is the plasma motion along the curved magnetic field lines can appreciably add to the centrifugal force already exerted by the plasma on the field as a result of

the planetary rotation. In addition, this force is always directed perpendicular to the field and so can add inertial forces on the field perpendicular to the current sheet (see also §IV.C.). If our interpretation of the data is incorrect and we are observing an anisotropic distribution rather than bulk streaming, there are still major dynamical effects. In particular, the parallel pressure would have to be much larger than the perpendicular pressure and the implicit assumption of isotropic pressure in previous theoretical treatments could no longer be invoked.

### 3. PLASMA TRANSPORT: ABSENCE OF A "WIND"

So far we have discussed flow along the magnetic field and perpendicular to the field in the azimuthal direction. The third possible component of the flow involves transport outward from the magnetic symmetry axis. If the decrease of angular speed with distance from Jupiter is an inertial loading effect as we have suggested (§IV.A.1; Hill, 1979; Hill, 1980) then plasma and angular momentum must be continually transported out of the Jovian magnetosphere and deposited into the solar wind. Conceivably, the transport could be convective, e.g. as a continuous centrifugally driven wind (§ I.F.2. and Kennel and Coroniti, 1977) or as an aperiodic instability (§I.C.3 and Hasegawa, 1980), or the transport could be diffusive, e.g. by flux tube interchange (§I.C.2. and references therein). As we shall show, flux tube interchange diffusion is the most probable mechanism, at least in the region of the magnetosphere which we are considering.

With respect to a centrifugally driven plasma wind, evidence from the Plasma Science experiment indicates that there is none either on the dayside or within  $\sim 15 R_J$  of the planet on the nightside. We have already remarked (§IV.A.1) that the principal component of plasma flow in the dayside magnetosphere is azimuthal. Preliminary analysis of Voyager 1 and Voyager 2 data taken during spacecraft maneuvers on the nightside indicate that this is also true within  $\sim 15 R_J$  of the planet on the nightside as well (Sullivan, private communication, 1980). In addition, Pioneer and Voyager magnetic field measurements in the middle magnetosphere (Smith et al., 1974; Smith et al. 1975; Ness et al. 1979a; Ness et al. 1979b) have always shown a closed magnetic topology across the current sheet. This precludes an MHD Weber-Davis type of convective outflow such as Kennel and Coroniti (1975) had suggested for Jupiter. On the basis of these considerations, we feel that a centrifugally driven wind in Jupiter's middle magnetosphere can be ruled out as a transport mechanism.

In consideration of the balloon-mode instability aperiodic transport, it has been remarked throughout the literature that the order of magnitude criterion for marginal stability is given by equating the kinetic energy density of the plasma to the local magnetic field energy density (cf. Hasegawa, 1980, eq. 27). This is equivalent to there being a surface of marginal stability for which the Alfvénic Mach number is unity. It has been implied by some (e.g. Kennel and Coroniti, 1975; Hill and Dessler, 1976a; Hill and Dessler, 1976b) that attaining such marginal stability will lead to an opening of the field line topology, although others (e.g. Goertz, 1976a) have insisted that this concept has been taken too literally (See also §I.A.3). In those cases during the Voyager 1 encounter in which the plasma sheet and current sheet crossings closely coincide, the Alfvénic

Mach number does exceed unity without any noticeable change in flow direction. Away from the sheets, the magnetic field dominates the total energy density. The principal reason for this behavior in the crossings is the reduction of the Alfvén speed which is facilitated by both the increased mass density in the plasma sheet and decreased magnetic field in the current sheet. At the least, this correlation of crossings and equal field and plasma energy densities implies that the low energy plasma component is the dominant cause of the field distortion into a current sheet configuration on the dayside (§I.A.3).

In the Voyager 2 data, decreases of the Alfvén speed are not as pronounced and the observed Alfvénic Mach number never exceeds unity. This difference from the Voyager 1 results is produced by the low azimuthal velocities and lack of large mass density enhancements in the plasma sheet in the middle magnetosphere during the Voyager 2 encounter. As a result, radial pressure gradients could be more important in the magnetosphere during the Voyager 2 encounter during that of Voyager 1, although a detailed consideration is beyond the scope of this thesis. To summarize, available evidence indicates that the balloon-mode instability is not operative in the middle magnetosphere and there is no aperiodic convective plasma transport.

#### 4. PLASMA TRANSPORT: DIFFUSION

The presence in the magnetosphere of elements associated with Io, the configuration of the magnetic field, and the enhanced heavy ion to proton ratio in the plasma sheets strongly suggests that Io is the source of almost all of the magnetospheric inertia (§I.F.4). As a result of venting

from Io this material is continuously injected into and must be continuously transported out from the system. This is corroborated by the observation of heavy ions moving away from Jupiter in the nearby interplanetary medium (Krimigis et al., 1979a; Zwickl et al., 1980). In addition, we have argued that lack of corotation in the dayside magnetosphere is a result of outward plasma transport there (§IV.A.1). As transport is apparently not a result of either a steady or aperiodic "wind" (§IV.A.3), it must be diffusive (Siscoe, 1977; Goertz, 1979).

We can estimate an effective diffusion "velocity" from the continuity equation and the assumption of azimuthal symmetry. Using Hill's best estimate of the injection rate (Hill, 1980) we can estimate the transport in the plasma sheet at, for example, the crossing at ~63-1900 for Voyager 1. Let the plasma sheet thickness be denoted by  $t$ , the L-shell parameter by  $L$ , and the mass density by  $\rho$ . Then from continuity, the outward transport velocity  $V_t$  is given by

$$\dot{M} = 2\pi R_J L t \rho V_t$$

Using values of  $t = 2 R_J$ ,  $L = 17$ ,  $\rho = 70 \text{ amu cm}^{-3}$  and  $\dot{M} = 10^{30} \text{ amu sec}^{-1}$  we obtain  $V_t = 13 \text{ km/sec}$ . This is the right order of magnitude for keeping the plasma flow primarily into the D-cup as observed. Cheng's (1980) mass loading rate gives an outward transport velocity higher by a factor of 60, the value being 780 km/sec. This would imply a "wind" such as has been precluded by the observations (§IV.A.3). Although our estimate of flow is based on only a rough set of numbers, a factor of ~50 is difficult to account for. Cheng's estimate could simply be high. On the other hand, the assumption of azimuthal symmetry in the loss process may be incorrect. As the magnetic field lines stretch out into a magnetotail configuration on

the nightside (Ness et al., 1980), some of the plasma flow toward the current sheet on the nightside (§III.F., IV.A.2., IV.B.) could be reaching into the tail region and escaping the system as a "wind" blowing down the tail (cf. Hill et al., 1974a; Krimigis et al., 1979b). Even in this case, some mechanism must transport the plasma outward to the tail region ( $\sim 30 R_J$  from the planet on the nightside) and the transport must involve the dayside magnetosphere as well or else the plasma would be spun up to rigid corotation with the planet.

#### 5. PLASMA DENSITY AND MARGINAL STABILITY FOR INTERCHANGE

We expect the radial profile of the mass density in the dayside magnetosphere to reflect the transport mechanism responsible for moving plasma from the Io plasma torus outward. The most likely mechanism for transport is flux tube interchange diffusion driven by the centrifugal force on the azimuthally moving plasma.

Ioannidis and Brice (1971) argued that corotation could perhaps be enforced even if interchange motions did occur (see also §I.C.2). Conversely, the observation of the lack of corotation argues that interchange motions will occur, if energetically favored, inasmuch as the same ionospheric conductance which topologically allows breakdown of corotation will also permit interchange motions. Such motions will drive the radial density gradient to a value consistent with marginal stability against the motion. Furthermore, once they are topologically allowed, interchange motions should limit the density well before the centrifugal (balloon-mode) instability becomes operable (Ioannidis and Brice, 1971; Mendis and Axford, 1974). This should be true even in the presence of the current sheet (Piddington and Drake, 1968).

It can be shown that a full flux tube near the planet, surrounded by vacuum and initially corotating with the planet, will move outward by interchange with empty ones, and in doing so, exhibit an angular speed about the planet in accordance with Hill's result (§IV.A.1). However, at some distance  $\sim L_0 R_J$  the outward velocity would equal the azimuthal velocity and the former exceed the latter at even greater distances. As we have noted (§I.C.2) full flux tubes never interchange with total empty ones so this type of reasoning gives an upper limit to the outward transport velocity (the same type of calculation, but under the assumption of rigid corotation, was performed by Mendis and Axford (1974)). On the scale of the magnetosphere, the process must be diffusive, (via convection cells on a small enough scale (Siscoe and Summers, 1981), resulting in a marginal stability value of the plasma density at any given location.

Marginal stability criteria for centrifugally driven interchange motions have been introduced by Melrose (1967) and Hill (1976). Assuming a collisionless plasma counterstreaming along field lines from an ionospheric source Hill finds that marginal stability in the equatorial plane is given by  $n \sim r^{-9/2}$  in a dipole field (§I.C.2) where the number density  $n$ , and distance  $r$  are all referred to their equatorial values. A similar result with slightly different behavior of  $n$  holds if the pressure gradient in the plasma drives the instability (Gold, 1959).

For comparison with these theoretical results, in Figure 50 we have again plotted the mass density from the Voyager 1 data but on a scale which is logarithmic with distance from Jupiter. In the approximation that all of the local increases are due to heavy ions concentrated in the plasma sheet, the slope from those sections of the curve off the sheet indicates the distribution of proton mass density. The profile is closely

approximated by an  $r^{-9/2}$  fall off outside of the torus region ( $\gtrsim 8 R_J$ ).

This is at least suggestive that centrifugally driven flux tube interchange determines the density distribution outside of the plasma sheet. It should be noted that although Hill derived his result assuming an ionospheric source of plasma, the result should be applicable as long as there is a field aligned streaming velocity which increases linearly with distance from the planet. Such field aligned streaming does occur (§IV.A.1) but the flow velocity dependence is not currently known.

These results are suggestive, but not conclusive. Perhaps most importantly, the marginal stability criterion needs to be rederived taking into account the field distortions which result from a current sheet. In addition, we do know that heavy ions as well as protons stream along the field on the basis of some of the example spectra which have been studied (see the example quoted in Belcher and McNutt, 1980). On the other hand, preliminary analysis indicates that the plasma sheet enhancements are due almost entirely to the heavy ions, enhancements of protons in the sheets seems to be minimal; hence, this result may indirectly be indicative of an ionospheric source for most of the protons versus an Io torus source for the heavy ions. Clearly more detailed study of the magnetosphere source problem is required.

With respect to the profile in the plasma sheet (i.e., at the local maxima in the graph), the slower fall off with distance of mass density ( $\sim r^{-3}$ ) must be more intimately related to the dynamics of the system and the rate of outward transport of material. For example, if the sheet thickness and mass injection rate are both roughly constant, continuity implies that the effective transport velocity must increase with radial distance.

In Figure 51 we have plotted the Voyager 2 data on the same scale. The same  $r^{-9/2}$  line is included for comparison of the data sets. The results are again suggestive of interchange diffusion, though they are not nearly so convincing as are the results from the Voyager 1 data set.

## 6. PLASMA TEMPERATURE

To complete the comparison between the Voyager 1 and Voyager 2 data sets, we show the positive ion temperature plotted on a logarithmic distance scale in Figures 52 and 53. This includes the proton temperatures from the L-mode fits, the (presumed)  $O^+$  temperatures from the M-mode fits, and, in the case of Voyager 1, the fit temperature from and inside of the  $I_0$  plasma torus (Bagenal and Sullivan, 1980).

There is apparently a positive radial gradient in the Voyager 1 temperature data. There are less resolved spectra between plasma sheet crossings at larger radial distances. This is consistent with higher temperatures, since resolution is a function of the effective sonic Mach number and the measured velocity component is approximately constant outside of  $17 R_J$  (§IV.A.1). However, the spacecraft makes larger excursions from the magnetic equatorial plane at larger distances (cf. Figure 4) so that the apparent heating with distance may actually be due to the thermal gradient across the plasma sheet (§III.E). To reiterate our previous observations, even where the spectra have not been included in this analysis, the evidence indicates the temperature is never greatly in excess of 1 keV throughout the dayside magnetospheres inside of the last inbound magnetosphere crossing at  $46.7 R_J$  (Bridge, et al., 1979a).

The cooling effect in the plasma sheet is very pronounced in the Voyager 1 data as marked by the temperature decreases to  $\sim 10$  eV outside of  $10 R_J$ . The temperature decrease is present but relatively small in the crossing at  $\sim 63-1930$  ( $16.7 R_J$  - Figures 43, 44, and 45) as compared to those at  $\sim 64-0200$  ( $11.4 R_J$ ),  $\sim 63-2315$  ( $13.6 R_J$  - Figure 46),  $\sim 63-1545$  ( $19.7 R_J$  - Figure 10), and  $\sim 63-0600$  ( $27.2 R_J$ ). A line though the lowest temperatures measured in the last three of these crossings gives a plasma sheet temperature which varies at  $r^{-1/2}$ . A cooling trend with radial distance in the sheet is definitely indicated although the sheet stays hotter than would be expected from conservation of the first adiabatic invariant.

The Voyager 2 data (Figure 53) covers so little radial range that no global variations can be ascertained. The one noticeable temperature decrease is associated with the resolved M-mode spectrum at  $190-0454$  (Figures 22-28) discussed above (§III.D). It is worth noting that the resolved L-mode spectra from the Voyager 2 encounter exhibit temperatures of the same order as their counterparts from the Voyager 1 encounter. Available evidence suggests that the plasma temperature in the dayside magnetosphere was not significantly different during the two encounters (excluding the plasma sheet cooling effect). This suggests that the lack of resolution in the Voyager 2 data set (a result of small effective Mach numbers) is an azimuthal velocity effect rather than a temperature effect.

## B. PHYSICS OF THE PLASMA SHEET

The Jovian plasma sheet, like the current sheet, is, on the basis of the Voyager 1 and Voyager 2 encounters, a permanent feature of the Jovian

magnetosphere. However, as we have continually noted in comparing the two Voyager data sets, the sheet does apparently undergo large temporal variations. The sheet is characterized by enhanced plasma density overall and a relative enhancement of heavy ions with respect to protons (§III.G). In addition, the sheet (at least on the dayside) is relatively cool, i.e., the enhancement of heavy ions relative to the protons is associated with a cooling of all species. This is true of crossings of the sheet by both Voyager 1 and Voyager 2 and can be qualitatively verified from consideration of individual spectra even when quantitative analysis is not available across a sheet crossing (e.g. the crossing centered on 189-1200 in the Voyager 2 data - Figure 5). Comparing crossings of the sheet, there is also a tendency for the more abrupt ones to exhibit lower temperatures. For example, in the Voyager 1 data, the crossing at 63-1930 shows a density increase more extended spatially than do the other crossings, but with a temperature profile which never decreases as much as in the other crossings. In the Voyager 2 data, the crossings at ~190-2200 (Figure 47) and ~191-0930 (Figure 48) exhibit very contained structure and very cold spectra.

Contrary to previous speculation (see §I.F.1), we have found that the plasma sheet is not a simple disc of plasma aligned with the current sheet. Our current interpretation of our data has led us to conclude (§III.F) that the magnetospheric plasma is in a constant state of dynamic agitation, with motion along the magnetic field lines as well as across them azimuthally ( $\vec{E} \times \vec{B}$  drift) and radially (outward flux-tube interchange diffusion). It is conceivable that instead a very large pressure anisotropy with  $P_{\parallel} \gg P_{\perp}$  could account for the observations; however, we consider this unlikely for physical reasons and also because our analysis to date indicates that true

bulk motion is indicated. Our subsequent discussion is, therefore, based upon isotropic plasma distributions with a field aligned component of flow. Based upon this interpretation, if we follow a flux tube as it drifts around the planet and diffuses outward, we will observe plasma flowing along the field lines from the magnetic equator toward the planet on the dayside and from the planet toward the magnetic equator on the nightside (§III.F). If  $\omega$  is the angular speed of the flux tube and  $\tau_D$  is the radial diffusion time, then the field aligned flow varies on a time scale  $\omega^{-1} \ll \tau_D$  and to first order the outward diffusion can be neglected in the motion of the flux tube.

If we consider the Voyager 1 density profile (Figure 4) and flow anisotropy profile (Figure 41) we find that although the crossings of the plasma sheet occur near the magnetic equator (as do the field aligned flow reversals), they are not centered precisely on those locations. We noted above that in the bifurcated plasma sheet crossing centered on  $\sim 64-0000$  (Figure 46) plasma in the earlier crossing is moving northward and in the later crossing is moving southward, i.e., the plasma sheet itself is bifurcated at this local time ( $\sim$ local noon) and the sheet itself is in motion. To first order the plasma sheet is composed of local concentrations of plasma in contiguous flux tubes with the concentrations moving as a unit along the flux tube. So, for example, when we see a plasma sheet signature removed from a current sheet crossing, such as at  $\sim 63-1545$  on Voyager 1 (Figure 10), we do so because the motion of the sheet has displaced it vertically with respect to its equilibrium position near the magnetic equator.

Although the plasma in each flux tube is in continuous motion, the flow is such that the plasma sheet itself can exhibit a time-stationary

structure. To see this we must follow a flux tube as it moves around the planet. As we have suggested before (§III.F) suppose the flux tubes tend to be compressed by the solar wind as they move into the dayside magnetosphere. If there are time concentrations of plasma in the tube as it moves to the dayside, one above and one below their equilibrium point, compression of the tube will tend to move the concentrations farther from the equilibrium point along the magnetic field lines. The field constrains the plasma motion in the perpendicular direction and the compression will be less, farther from the equilibrium position, hence, the plasma will accelerate along the field in much the same way as toothpaste rushes out of a squeezed tube. For a given flux tube the rate of compression will decrease to zero as the tube moves from local dawn to local noon, so the acceleration of the plasma in the flux tube should as well. At local noon, the flux tube will begin to expand and so decelerate the flow which will have achieved its maximum speed along the tube. At local dusk, the still expanding flux tube will have slowed the density concentrations to zero velocity at their greatest separation from each other. As the flux tube moves past local dusk toward the midnight meridian plane, the concentrations will begin to fall back toward each other and the magnetic equator. The largest infall speed will occur at local midnight where the flux tube, at its greatest expansion begins to contract again. At local dawn the concentrations will tend to run into each other but at zero relative closing speed as the contracting flux tube reverses the plasma infall to outflow once again. Equilibrium is never achieved and the plasma motion mimics a forced oscillator rather than occurring in a quasi-static fashion.

The scenario which we have described is illustrated in Figure 54 which shows the plasma sheet configuration. In our description we have followed a simple flux tube around the planet noting the positions of maximum acceleration, velocity, and separation of the plasma concentrations in the tube. A tube at a larger radial distance should exhibit greater maximum values for these quantities as the day-night field asymmetry should be larger. Hence, plasma concentrations in a set of flux tubes in a given meridional plane will exhibit a deviation from the magnetic equatorial plane which will increase with distance from the planet. In our idealization, the plasma location and field aligned velocity is a function of local time only for a given flux tube. Thus, if we take a contiguous set of flux tubes, each of which moves to the position of the next as they drift about Jupiter, the plasma concentrations in each will trace out two loci about the planet. One will be south of the magnetic equatorial plane and the other to the north with the greatest separation between the two in the dusk meridian and with no separation in the dawn meridian. The set of all such loci formed by all contiguous sets of flux tubes in all meridional planes is the plasma sheet. The set splits into a northern part and a southern part with the bifurcation increasing with radial distance and toward local dusk. This pattern results solely from the fact that the solar wind tends to perturb a given flux tube at the same period as it takes the plasma to come to static equilibrium.

The dynamical aspects of this plasma sheet configuration are even more important than the configurational ones. Since the flow is field aligned and the field lines are appreciably curved in the vicinity of the magnetic equator (Connerney et al., 1981), there exists along the sheet an inertial force perpendicular to the magnetic field in a meridional plane. In

general, this results in a component of centrifugal force perpendicular to the magnetic equatorial plane and acting on the field lines so as to distend them away from that plane and increase the thickness of the current sheet. Hence, magnetic tension perpendicular to the magnetic equator is balanced by an inertial force as well as by a pressure gradient force. A description of the sheet based on pressure balance alone, is, therefore, insufficient and will result in an overestimate of the sheet temperature, potentially by orders of magnitude. (Even if there is instead an anisotropy with  $P_{\parallel} \gg P_{\perp}$ , a simple pressure balance analysis of the plasma sheet is still incorrect.)

With respect to temperature in the dynamical plasma sheet, the component of the momentum equation along a field line yields the Bernoulli constant along a field line (see e.g., Heinemann and Olbert, 1978):

$$\frac{1}{2} v_p^2 + \frac{5}{2} c_s^2 - \frac{1}{2} v_{\phi}^2$$

where  $v_p$  is the poloidal bulk speed,  $v_{\phi}$  the toroidal bulk speed, and  $c_s$  the sound speed. As we have shown, outside of  $\sim 17 R_J$ ,  $v_{\phi}$  is approximately constant with radial distance (§III.E. and IV.A.3). Hence, in the adiabatic limit, plasma with the largest field aligned streaming velocity should also be coldest. In our idealized model the temperature should decrease toward the noon-midnight plane and should also decrease with increasing distance from the planet, at constant displacement from the magnetic equatorial plane. More generally, the faster the plasma moves along the field lines the colder it should be.

In reality, the plasma sheet exhibits a distribution in density, streaming velocity, and temperature. Dispersion in the poloidal velocity

and irreversible processes such as internal shocks and effective viscosities (Belcher and McNutt, 1980) will tend to spread out the plasma concentrations, increasing the temperature and scale height of the sheet.

Also, the daytime compression of the magnetosphere by the solar wind, which drives the sheet dynamics, is a time dependent effect. As corotating interaction regions in the solar wind move past Jupiter compression of the magnetosphere to half its nominal extent ( $\sim 100 R_J$ ) can occur on a time scale of hours (Goodrich et al., 1980). During both the Voyager 1 and Voyager 2 encounters with Jupiter there were large global changes in the magnetosphere by the spacecraft (Bridge et al., 1979a; Bridge, et al., 1979b) as evidenced by the multiple crossings of the bowshock and magnetopause. As a result, we expect the day/night asymmetry in the plasma sheet configuration and dynamics also to change on such a timescale. The more compressed state of the dayside magnetosphere during the Voyager 1 encounter as compared with its state during the Voyager 2 encounter is, no doubt, responsible for the more regular nature of the plasma sheet during the former. The exact causal relationship is, however, not clear at this time. The slower rotation of the plasma sheet during the Voyager 2 encounter and the concomitant reduction of centrifugal force is consistent with the reduced current carried in the current sheet during the Voyager 2 encounter (Connerney et al., 1981).

In summary, it is clear that the plasma sheet cannot be treated simply as a spinning annulus of hot plasma as some investigators have suggested (e.g., Walker et al., 1978; Krimigis et al., 1979b). Of itself, the plasma sheet is relatively cold ( $10 \text{ eV} \lesssim T_{\text{ion}} \lesssim 1 \text{ keV}$ ), or at least contains a cold component (see Belcher et al., 1980). It diffuses angular momentum outward rapidly enough that the magnetic field lines threading it slip with

respect to Jupiter at the ionosphere of the planet. The inertia of the sheet apparently suffices to produce the annular current sheet which circles Jupiter. The case is more clear cut for the Voyager 1 encounter during which the Alfvénic Mach number in the plasma sheet on the dayside exceeded unity (§IV.A.1). In addition, there is evidence that the symmetry axis of the dayside current sheet was inclined to the rotational equatorial plane at less of an angle than is the magnetic equatorial plane (Connerney et al., 1981) during the Voyager 1 encounter. Both of these effects highlight the probable dominance of the plasma sheet in determining overall magnetospheric dynamics. Finally, we again emphasize that the field aligned component of velocity of the sheet plasma will contribute everywhere an outward stress on the field lines. In particular, the Plasma Science data indicates that the observed plasma has a very low  $\beta$  ( $\sim 0.01$ ) and can in no way account for static pressure balance across the current sheet (but see §IV.C). However, field aligned streaming results in the coupling of directed kinetic energy into momentum balance across the sheet. This can be a potentially significant contribution depending upon the local field line curvature and field aligned plasma speed. An accurate assessment of momentum balance is needed but is beyond the scope of this thesis.

### C. CORRELATION WITH OTHER VOYAGER RESULTS

The results from the Plasma Science experiment on Voyager have, in general, been confirmed and amplified by the other Voyager experiments. Proper identification of the various ionic species in the Jovian magnetosphere has resulted from a cross correlation of results from the Plasma Science (Bridge et al., 1979a; 1979b), Ultraviolet Spectroscopy

(Broadfoot et al., 1979; Sandel et al., 1979), Cosmic Ray (Vogt et al., 1979a; 1979b) and Low Energy Charged Particle (Krimigis et al., 1979a; 1979b) investigations. The confinement of the heavy ions to a plasma sheet and their characteristic low temperature ( $\lesssim 100$  eV) were indicative of a Galilean satellite source and the observations of the Io torus (Bagenal and Sullivan, 1981 and §IIF.4) identified the source as being Io. Although a problem of continuing investigation, the basic mechanism of the source was found via the discovery of venting of material from Io (Morabito et al., 1979) and the near simultaneous suggestion that tidal heating of Io by Jupiter could result in vulcanism on that moon (Peale et al., 1979).

The basic structure of the middle magnetosphere as being disk shaped and consisting of a current sheet and plasma sheet has been verified by the Magnetometer (Ness et al., 1979a; 1979b), Plasma Science (Bridge et al. 1979a; 1979b, this thesis), Cosmic Ray (Vogt et al. 1979a; 1979b), Plasma Wave (Scarf et al., 1979; Gurnett et al. 1979) and Low Energy Charges Particle (Krimigis et al. 1979a; 1979b) experiments. These investigations have confirmed that the "magnetodisc" is a basic feature of the Jovian magnetosphere which does show definite temporal variations, and that it is roughly aligned with the Jovian magnetic equatorial plane.

There have been some basic disagreements about the nature of the plasma contained in this structure and the resultant dynamics. In particular, Krimigis et al. (1979a; 1979b) analyzed their data for anisotropies (cf. §I.E.3) at energies of about 100 keV. From their anisotropy measurements they deduced that the magnetodisc plasma rigidly corotates with Jupiter out to the magnetopause. On the basis of such velocity component measurements they also fit their data to isotropic convected Maxwellian distribution functions, and they found that the

measured plasma could be characterized by a temperature  $\sim 30$  keV to  $\sim 40$  keV in the magnetosphere.

These conclusions are in basic disagreement with the results of the Plasma Science instrument in those regions in which the data sets can be directly compared. The results of the latter, detailed above, show a plasma consisting of multiple ionic species with a characteristic temperature of  $\sim 100$  eV. Furthermore, the plasma is not locked in rigid corotation with the planet (McNutt et al., 1979; this thesis), as Krimigis et al. have asserted. Belcher et al. (1980) have suggested that there may indeed be both cold and hot components of the magnetospheric plasma, produced by different acceleration and heating mechanisms. This could explain the difference in reported temperatures. There has also been basic disagreement about the number density of ions in the magnetosphere. Again, when comparison of the Plasma Science and Low Energy Charged Particle data sets have been possible, it has been found that the mass density of  $< 6$  keV ions dominates the mass density of  $> 30$  keV ions. The question of the energy range in which most of the thermal energy density resides is still open. As a determination of the total electron density (and, hence, positive ion charge density) is possible from interpretation of the Plasma Wave experiment data (Scarf and Gurnett, 1977), comparison of the data from the three experiments in question should yield definitive results as to the distribution of charge density at greater than 6 keV energies. As the time of this writing, such comparisons have yet to definitely resolve the density controversy.

The reports of rigid corotation of the plasma versus the lack thereof are more difficult to reconcile. Goertz (1980) has emphasized that large pressure gradients could result in measured particle anisotropies at 100

keV energies in the same sense as those produced by bulk plasma motion. These are made explicit in the calculations of Birmingham and Northrup (1979) and of Northrup and Thomsen (1980).

Field aligned streaming, reported by Pioneer investigators, (McDonald et al., 1979; Northrup et al., 1979; §I.E.3), similar to that found by the Voyager Plasma Science investigations (Belcher and McNutt, 1980; and this thesis) also contributes to particle anisotropies and add to the difficulty in properly interpreting  $\gtrsim 100$  keV particle anisotropy data. The Plasma Science experiment, with its proven capability of establishing both direction and magnitude of bulk plasma flow via direct measurement of the distribution function (the measured data are negligibly affected by pressure gradients), remains the only instrument on the Voyager spacecraft capable of unambiguously establishing the plasma bulk flow pattern. Unfortunately, such determinations are limited to the middle and inner magnetosphere when measured fluxes are appreciable and even at these times are, along much of the spacecraft trajectory, (e.g. on the nightside) difficult to make as a result of the sensor geometry (§II.D)

#### D. COMPARISON WITH PIONEER 10 MEASUREMENTS OF THE MAGNETOSPHERIC PLASMA

In light of the results of the analysis of Plasma Science data in the Jovian magnetosphere (this thesis and Bagenal and Sullivan, 1981), it is appropriate to reconsider the results of the similar investigation based on Pioneer 10 data (Frank et al. 1976; §I.E.4). In the Pioneer 10 data the flux density versus energy per charge spectra show peaks well above the corotation energy for protons. Assuming that the magnetospheric plasma was entirely composed of protons, Frank et al. deduced that the plasma must be

subsonic and fit their data accordingly to isotropic Maxwellian distributions. The Voyager Plasma Science results suggest that instead the Pioneer 10 instrumentation detected supersonic sulfur and oxygen ions with magnetospheric protons negligibly contributing to the measured signal. That Frank et al., actually detected heavy ions has been postulated previously by Hill and Michel (1976), Neugebauer and Eviatar (1976), and Goertz and Thomson (1979b). In Figures 5 through 9 of their paper, Frank et al. (1976) show measured spectra and their fit parameters, which we can reinterpret assuming their thermal energy really reflects the bulk flow energy of heavy ions. At  $3.33 R_J$ , Frank et al. find a characteristic plasma energy per charge of 95 eV as compared to a corotational energy of 9.2 eV for protons. Assuming the plasma is cold and corotating at this distance (cf. Bagenal and Sullivan, 1981), we find that the measurements can be explained by corotating ions with an average mass to charge ratio of 10.3. At  $2.85 R_J$ , Frank et al. find a characteristic energy per charge of 105 eV as compared to a corotational energy of 6.5 eV for protons. This implies corotating ions with an average mass to charge ratio of 16.1. These values can easily be explained in terms of a corotating cold plasma primarily consisting of some combination of  $O^+$ ,  $O^{2+}$ ,  $S^{2+}$ , and/or  $S^{3+}$ . We consider this to be likely in view of the Voyager 1 Plasma Science observations inside of the orbit of Io. The densities quoted by Frank et al. ( $60 \text{ cm}^{-3}$  at  $3.33 R_J$  and  $85 \text{ cm}^{-3}$  at  $2.85 R_J$  from their fits) are from a region within the large negative radial gradient in density found by Bagenal and Sullivan and so may be consistent with the ion densities measured by Voyager 1 in the cold region inside of Io's orbit. The spectra taken at  $10.3 R_J$  and  $14.2 R_J$  outbound by Pioneer 10 are not so easily amenable to reinterpretation. The thermal energy, if reinterpreted as a

bulk energy, yields either very small mass to charge ratios for corotating ions or large deviations from corotation of  $0^+$ , much larger than seen by Voyager at a comparable distance.

However, all of these measurements are complicated by the facts that Pioneer 10 is a spin stabilized spacecraft and that the look directions of the positive ion detectors with respect to the local plasma flow drastically affects the positive ion spectral measurements. We have stressed this with respect to the Plasma Science instrument on Voyager (SII.D.) and Neugebauer and Eviatar (1976) have made a similar point with respect to the Pioneer 10 observations just discussed.

The situation is complicated even more by the temporal variability of the magnetosphere. Broadfoot et al. (1979) note that the ultraviolet observations made by Pioneer 10 and by Voyager 1 suggest that a high temperature plasma torus was not present during the Pioneer 10 encounter. This would imply that a ready source of heavy ions was not available at that time. On the other hand, it is conceivable that the torus was present but simply not radiating at wavelengths within the instrument range as a result of changes in the torus temperature. In any case, the numbers we have calculated above, combined with the typical Voyager spectral observations, strongly suggest that heavy ions were present in the magnetosphere during the Pioneer 10 encounter and are responsible for the spectra measured by Frank et al.

## CHAPTER V. CONCLUSION

## A. SUMMARY OF RESULTS

We have presented the first description of the density, bulk flow, and temperature of the low energy plasma in the middle magnetosphere of Jupiter on the dayside of the planet. We have shown that the multicomponent nature of the plasma persists throughout this region and must explicitly be taken into account in any analysis of the data. The dominant species are various ions of sulfur and oxygen. Protons in the magnetosphere contribute about 10% of the positive ion charge density, and  $\sim 1\%$  of the mass density. Hence, they are negligible with respect to global magnetospheric dynamics.

We have shown that the middle magnetosphere does not rigidly corotate with the planet, as had been thought. Injection of plasma from the Io plasma torus to the magnetosphere occurs rapidly enough that sufficient torque cannot be transferred through the Jovian atmosphere/ionosphere to keep the plasma locked to the planetary rotation rate. We have found the observations to be in basic agreement with this mechanism as proposed by Hill. In addition, we have shown that the radial density profile of the plasma is consistent with flux tube interchange diffusion supplying the radial plasma transport needed in Hill's theory. That enough ionospheric resistivity exists to allow the plasma to "slip" with respect to Jupiter's rotation guarantees that the inertial loading which allows this slip will also suffice to allow interchange motions. The temperature of the magnetospheric plasma is always less than a few keV and typically is  $\sim 100$  eV or less. Large variations in the plasma parameters can occur on a distance scale of only a few tenths of a Jovian radius.

We have confirmed the "magnetodisc" model of the magnetosphere which was postulated by Pioneer investigators, but we have shown that this concept is inadequate to describe the actual situation. This "disc" actually consists of a current sheet, as defined by the magnetic field, and a dynamic plasma sheet which contains the carriers of the current. We have found that the plasma sheet consists of a relatively large number of heavy ions relative to protons as compared to the situation away from the sheet. The sheet plasma is relatively cool compared to non-sheet plasma although this effect was more pronounced during the Voyager 1 encounter as compared with the situation during the Voyager 2 encounter.

We have found that the plasma in the magnetosphere is in apparent motion along the magnetic field lines as the plasma drifts around the planet at less than the corotation speed. The plasma streams away from the magnetic equatorial plane on the dayside and toward it on the nightside. It is suggested that the effect is a result of a global day/night asymmetry in the Jovian magnetosphere which is induced by the solar wind. Since the field aligned motion is synchronized to the local time, the plasma sheet itself can form a time stationary pattern although the plasma motion leads to inertial stresses on the magnetic field lines. As a result, the simple assumption of quasi-static pressure balance across the current sheet is invalid and calculations based on this assumption will tend to overestimate the plasma sheet temperature. It is possible that the field aligned motion can lead to energization of some of the plasma, as the plasma diffuses away from the Io torus, as a result of viscous or other effects (see e.g. Goertz, 1978). Some such mechanism is necessary since observationally, the density gradient of energized heavy ions is outward, indicative of a

non-inner magnetospheric source (Vogt et al. 1979b) although the ultimate origin of these ions must be Io.

We do not necessarily see all of the plasma with the Plasma Science experiment. In particular, if there is a hot Maxwellian component of the plasma (as suggested by Belcher et al., 1980), which results from some type of heating, we probably are not observing all of the thermal energy density. However, it is clear that the bulk of the mass density is accounted for. It is also clear that the field aligned streaming of the low energy plasma can contribute substantial inertial stresses perpendicular to the current sheet so that momentum balance across the current sheet must be a combination of inertial effects as well as possible pressure gradient effects resulting from a hot plasma component. Further complexities result if large pressure anisotropies are assumed to occur in the plasma sheet.

## B. QUESTIONS AND FUTURE OPPORTUNITIES

Although the Voyager flybys of Jupiter have answered many questions posed by the Pioneer encounters, they have raised new ones as well. Questions relating to detailed momentum balance in the middle magnetosphere may be answered by more detailed analysis and intercomparison of the fields and particle data sets. For example, the Plasma Science data set can, with more work, yield valuable data on the full vector bulk velocity of the plasma along the spacecraft trajectories. Comparison of Plasma Science and Magnetometer data can be used to treat in detail the problem of balancing plasma inertia with magnetic field line tension, perhaps throwing some light on transport of plasma out of the Jovian system. At a very basic

level, such a study could also help to remove the ambiguity in the radial variation of current density which enters into all magnetic field models for the current sheet (see, e.g. Connerney et al., 1981).

Detailed comparison of Plasma Science, Plasma Wave, and Low Energy Charged Particle data could perhaps yield valuable information on plasma heating and energization as well as on total charge density and non-Maxwellian features in the plasma distribution function. This information is needed, in turn, to compare the effects of inertial forces versus pressure gradient forces in the interaction between the magnetospheric plasma and the total (planetary and current sheet) magnetic field. For example, analysis of the Low Energy Charged Particle Data for both first and second order anisotropies could perhaps help to confirm or refute our interpretation of the Plasma Science data that field aligned flow, rather than gyrotopic anisotropy in the plasma, contributes in a major way to the dynamics of the plasma sheet. In any case, it is abundantly clear that attempting to characterize the magnetosphere on the basis of each one of the Voyager investigations by itself is akin to the story of the blind men, each touching different parts of the elephant and yet each asserting to the others that only he knew the true nature of the animal.

Though a still better understanding of the Jovian magnetosphere is possible by a more refined analysis of the data, some questions will remain unanswered. The four in situ investigations of Jupiter have each indicated that the Jovian system can undergo large temporal changes. These are apparently driven by variations in the injection of plasma by Io and by changes in the dynamic pressure of the solar wind. In addition, the middle magnetosphere on the dusk side has yet to be probed. Likewise, much of the

region near the dawn meridian has not been investigated; only Pioneer 11 actually passed through the dawn meridian and did so deep within the inner magnetosphere. In light of the day/night asymmetry in the (presumed) field aligned plasma flow, these have become regions of particular interest. With respect to local characterization of plasma, the Voyager missions have indicated the need for an in situ mass spectrometer investigation and for probing the plasma properties in the energy range of 6 keV to  $\sim$ 30 keV. The Galileo Jupiter orbiter, if flown, can potentially do much toward answering these questions in the middle magnetosphere. Additional coverage of the dusk side is possible with the International Solar Polar probes as they execute gravity assists at Jupiter, if they are properly instrumented.

The Jovian magnetosphere has proven to be neither earth-like nor pulsar like as some had envisioned. It is instead a unique plasma construct in many ways, apparently as a result of the venting of heavy ions from the Jovian moon Io. This alone makes the Jovian magnetosphere worthy of further scientific inquiry. In addition, its presence in the solar system allows us the unique opportunity of making in situ observations and studies of plasma confined by a fast magnetic rotator, a subject of general physical and astrophysical interest.

## APPENDIX: NON-LINEAR LEAST SQUARES FIT

## A.1. PROCEDURE

In the non-linear least squares fit an iterative procedure is used to solve for the "best" values of the fit parameters. Initial values must be assigned to the fit parameters. Depending on whether we are fitting the L- or M-mode spectra different procedures are used to do this and are discussed in §A.4.

Here we outline the fit procedure used which follows Bevington (1969). Let  $I_j^m$  be the measured current in the  $j$ th channel and  $\sigma_j$  the associated error in the measurement. Further let  $I_{ji}$  ( $n_i, u_{zi}, w_i, u_{ti}$ ) be the current calculated for the  $j$ th channel as contributed by the  $i$ th ionic species described by parameters  $n_i, u_{zi}, w_i, u_{ti}$  with mass to charge ratio  $A_i/Z_i^*$ . Let  $I_j^c = \sum_i I_{ji}$  be the current calculated to be contributed by all species in the  $j$ th channel. The chi-square is given by

$$\chi^2 = \sum_j \frac{(I_j^m - I_j^c)^2}{\sigma_j^2}$$

The "best" values of the fit parameters are those for which  $\chi^2$  is minimized. In the analysis, not all parameters are necessarily kept free. In particular, when the plasma is hot and the multiple peak structure is ill-defined or non-existent, additional assumptions must be made in order to reduce the number of free parameters and assure the convergence of the fit (by "convergence" we refer to approaching the minimum of  $\chi^2$  with

positive values for all the fit parameters). For example, the bulk normal velocity components of several species can be tied to the same value.

We search for the best set of fit parameters as follows. Let the  $n$ th free fit parameter be denoted by  $a_n$  and the corresponding small parameter increment by  $\delta a_n$ .

By expanding the predicted currents to first order in the parameter increments

$$I_j^C = I_{j0}^C + \sum_n \frac{\partial I_{j0}^C}{\partial a_n} \delta a_n$$

and setting  $\partial \chi^2 / \partial \delta a_n = 0$  we find a set of simultaneous linear equations for the fit parameter increments. Adding these to the fit parameters give a new set of parameters which more nearly minimize  $\chi^2$ , providing we started close enough to the minimum of  $\chi^2$  in the first place.

In the first order approximation, let

$$\beta_k \equiv \sum_j \frac{1}{\sigma_j^2} (I_j^m - I_j^C) \frac{\partial I_j}{\partial a_k}$$

$$\alpha_k \equiv \sum_j \frac{1}{\sigma_j^2} \frac{\partial I_j}{\partial a_l} \frac{\partial I_j}{\partial a_k}$$

The set of equations for the  $\delta a_n$  can be written as

$$\vec{\beta} = \vec{\alpha} \cdot \delta \vec{a}$$

In our analysis, the initial guess for the fit parameters is sometimes crude. As a result, we may start the iterations far from the minimum  $\chi^2$  in fit parameter space. To speed the convergence, we use the gradient-expansion algorithm. In this case we solve

$$\vec{b} = \vec{\alpha} \cdot \delta \vec{a}$$

where  $\alpha'_{jk} = \alpha_{jk} (1 + \delta_{jk}\lambda)$ . With the parameter  $\lambda$  small, succeeding iterations converge the fit parameters to the values such that  $\chi^2$  is reduced to its local minimum value. By increasing  $\lambda$ , the diagonal terms of the  $\alpha$  matrix are emphasized and the parameter increments lie along the negative gradient of the  $\chi^2$  hyperplane in the fit parameter space.

This procedure has previously been implemented and successfully used in the analysis of solar wind data. We have adopted it for use in the analysis of the magnetospheric data. The iteration proceeds such that  $\chi^2(a + \delta a)$  is compared to  $\chi^2(a)$ . If the chi-square value has increased,  $\lambda$  is increased by a factor of 10 and  $\delta a$  is recomputed. If the chi-square has decreased,  $\lambda$  is decreased by a factor of 10 and the values  $a_j = a_j + \delta a_j$  are substituted for the new best values in the fit parameter determination. Bevington (1969) following Marquardt, suggests that  $\lambda = 0.001$  is a good initial value. We have verified that this is the case in the magnetospheric analysis by varying it from .01 to .0002 over computer analysis runs of certain segments of the data.

## A.2. ERROR

The formal error  $\sigma_{aj}$  in the value of the fit parameter  $a_j$  can be expressed in terms of the  $\alpha$  matrix described above. Define

$$\sigma_{aj} \equiv (\alpha^{-1})_{jj}$$

and let the parameter set be that which minimizes  $\chi^2$ . Furthermore, let  $\nu$  be the number of degrees of freedom. It can be shown that

$$\chi^2(a_j + \sigma_{aj}^2) = \chi^2(a_j) + 1$$

where  $\chi^2(a) \approx \nu$ . It is in this sense that the  $\sigma_{aj}$ 's estimate the errors in the  $a_j$ 's.

Contributions to error in the fit originate in both the ambient plasma being sampled and the instrument itself. With respect to the ambient plasma, to the extent that there are departures from a convected, isotropic Maxwellian in the various ion distribution functions, a difference between the measured and calculated currents is introduced. Time aliasing will also affect the accuracy of the measurements. For example, measured bulk velocities of the plasma are  $\sim 200$  km/sec, and an entire L-mode spectrum is measured in 3.84 seconds. Hence, spatial inhomogeneities in the plasma on a scale of less than  $\sim 800$  km result in the sampling of different values of the various plasma parameters. In the fitting procedures such effects appear as sources of error. In addition penetrating radiation from high energy particles can interfere with the electronics and increase the instrument noise level.

Instrumental uncertainties include a nominal noise level  $\sigma^2$  and error from the digitization of the measured current for purposes of telemetry. In each gain state current is measured over four decades in 256 logarithmically spaced, quantized steps. It can be shown that this introduces an uncertainty  $\epsilon I_j^m$  in the current measured in the  $j$ th channel where

$$\epsilon = \frac{10^{1/64} - 1}{12^{1/2}}$$

The formal total uncertainty of the  $j$ th channel measurement can then be written as

$$\sigma_j^2 = \sigma^2 + (\epsilon I_j^m)^2$$

In the fit we have only included  $\sigma^2$  in the calculation of  $\chi^2$ . This gives a larger weight to the channels which measure the largest currents rather than more heavily weighting the smallest currents which are affected by the "noise" sources mentioned above. To get another estimate of the error, we assume that parent variance of the fit is approximated by the estimated variance of the fit. In doing this, we assume that convected, isotropic Maxwellians are good representations of the measured data and force the reduced chi-square to be unity. This method is good to the extent that all of the uncertainties in each measurement are not known and that these are the same for each instrument channel. Comparing errors so computed with many spectra and fits to them, we have found this method to be useful in evaluating the goodness of fit on a qualitative basis.

## A.3. CURRENT AND DERIVATIVES

The method employed in our analysis requires analytic expressions for both the current measured in each instrument channel and the derivative of this current with respect to each of the parameters describing the fit.

The current in the  $j$ th channel is given by eqn. II.4. To find the appropriate quantities we must evaluate three integrals  $I_1$ ,  $I_2$ , and  $I_3$ , viz.:

$$I_1 \equiv \int \frac{\frac{V_{j+1}}{w}}{\frac{V_j}{w}} \frac{x^3}{\alpha+x^2} e^{-\left(x - \frac{u_n}{w}\right)^2 - \frac{\alpha}{\alpha+x^2} \left(\frac{u_t}{w}\right)^2} dx$$

$$I_2 \equiv \int \frac{\frac{V_{j+1}}{w}}{\frac{V_j}{w}} \frac{x^3}{\alpha+x^2} \left(x - \frac{u_n}{w}\right) e^{-\left(x - \frac{u_n}{w}\right)^2 - \frac{\alpha}{\alpha+x^2} \left(\frac{u_t}{w}\right)^2} dx$$

$$I_3 \equiv \int_{\frac{V_j}{w}}^{\frac{V_{j+1}}{w}} \frac{x^3}{(\alpha+x^2)^2} e^{-\left(x - \frac{u_n}{w}\right)^2 - \frac{\alpha}{\alpha+x^2} \left(\frac{u_t}{w}\right)^2} dx$$

Defining the factor  $\beta$  via

$$\beta \equiv \frac{T_0 A_0 e}{\pi I_1^2 Z^*}$$

we obtain for the current and its derivatives

$$I_j = \beta n w I_1$$

$$\frac{\partial I_j}{\partial n} = \beta w I_1$$

$$\frac{\partial I_j}{\partial u_n} = 2\beta n I_2$$

$$\frac{\partial I_j}{\partial u_t} = -2\alpha \left(\frac{u_t}{w}\right) \beta n I_3$$

$$\frac{\partial I_j}{\partial w} = \beta n \left[ I_1 - \frac{n}{w} \left\{ \frac{x^3}{\alpha+x^2} e^{-\left(x - \frac{u_n}{w}\right)^2 - \frac{\alpha}{\alpha+x^2} \left(\frac{u_t}{w}\right)^2} \right\} \right]_{x = \frac{V_j}{w}}^{x = \frac{V_{j+1}}{w}}$$

An analytic form for  $I_1$  (and, hence  $I_2$  and  $I_3$  by a differentiation) can be obtained but involved a doubly infinite sum over combinations of Hermite polynomials. The convergence properties of this series are good only for small sonic Mach numbers, whereas, in general, much of the data to be analyzed are characterized by sonic Mach numbers of order unity or greater.

In order to compute the values of these integrals over the detector channel width, we have used a three point Gaussian quadrature. It can be shown (Ralston, 1959) that given a function  $f(x)$  on an interval  $x \in [a,b]$ , the integral

$$I = \int_a^b f(x) dx$$

can be approximated as follows. Introduce the variable  $t$  and function  $\phi$  such that

$$t = \frac{2x - (b+a)}{b-a} \quad \text{and} \quad \phi(t) = f(x)$$

Then the integral becomes

$$I = \left(\frac{b-a}{2}\right) \int_{-1}^1 \phi(t) dt$$

and we find that

$$\int_{-1}^1 \phi(t) dt = \frac{5}{9} \phi\left(-\sqrt{\frac{3}{5}}\right) + \frac{8}{9} \phi(0) + \frac{5}{9} \phi\left(\sqrt{\frac{3}{5}}\right)$$

with the error of order

$$\frac{1}{15,750} \phi^{(vi)}(\xi) \quad , \quad \xi \in (-1,1)$$

so that the error in I is of order

$$\frac{1}{15,750} f^{(vi)}(\eta) \left(\frac{b-a}{2}\right)^6 \quad , \quad \eta \in (a,b)$$

Applying this formalism to  $I_1$ ,  $I_2$ , and  $I_3$ , we see that as long as  $w > \Delta V_j$  for all  $j$  the error will be small.

#### A.4. INITIALIZATION

Automation of a procedure to initialize the fit parameters has proven to be a crucial step in the analysis. Only those L-mode and M-mode spectra with at least two clean peaks in the reduced distribution have been selected out for detailed analysis. Lack of detail and resolution in many of the spectra, especially the low Mach number L-mode spectra, have made it imperative that the initial guesses be close to the best values of the fit parameters, in order that the fit iterations converge (see sA.1 above).

Measurement of the current can lead to ambiguity in the fits if sufficient resolution does not exist in the data and the effective Mach number is not large enough. The instrument is designed such that  $\Delta V_j / \bar{V}_j \approx$

const. The relative variation in the current is then described by a smoothed function

$$I(v) = \frac{n}{w} v^2 e^{-\frac{(v-u_n)^2}{w^2}}$$

with  $n$ ,  $u_n$ , and  $w$  as defined above. The fit is most sensitive to the location of the maximum in this function and less sensitive to its width. It can be shown that in the high sonic Mach number case assumed

$$v_{\max} \approx u + \frac{1}{4} w \left(\frac{w}{u}\right)$$

where

$$\left. \frac{dI}{dv} \right|_{v = v_{\max}} = 0.$$

However, an additional solution for the maximum with

$$v_{\max} \approx w + \frac{1}{2} u$$

also occurs for subsonic flow. In the case of the cold M-mode (large sonic Mach number) spectra this presents no major difficulty as the peaks are clear and the Mach numbers are much greater than unity. However, for plasma flow with effective Mach numbers less than  $\sim 1.5$  the maximum and width of the current spectrum for appropriately chosen subsonic parameters is similar to the true spectrum, and the fit to the L-mode protons can locate the wrong local minimum for  $\chi^2$  in the fit parameter space (identified by relatively large errors in the final fit parameters - see sA.2 above).

The procedure for initializing the M-mode fit parameters proceeds on the assumption that the plasma is cold and the smoothed approximation for the measured current is applicable. The peak current is assumed to occur at the peak of the mass to charge 16 distribution function and we take i.e.  $U_n' = \nabla_{j_{\max}}$ . A search to higher channels is begun until channel  $j_w$  is identified such that

$$\frac{I_{j_w}^m}{\nabla_{j_w}^2} < \frac{1}{e} \frac{I_{j_{\max}}^m}{\nabla_{j_{\max}}^2}$$

Then, the thermal speed is given by

$$(w')^2 = \frac{(\nabla_{j_w} - \nabla_{j_{\max}})^2}{\ln \frac{I_{j_{\max}}^m}{\nabla_{j_{\max}}^2} \frac{\nabla_{j_w}^2}{I_{j_w}^m}}$$

The current in the peak channel gives the value of  $n'/w'$ . The values so derived are valid only for protons and are converted to their proper values via the scalings

$$u_{n \text{ guess}} = (Z^*/A)^{1/2} u_n'$$

$$w_{\text{guess}} = (Z^*/A)^{1/2} w'$$

$$n_{\text{guess}} = A^{1/2} / (Z^*)^{3/2} n'$$

For each additional species we assume the same sonic Mach number and

velocity. By evaluating the current at the location of the predicted peak of the other species the appropriate starting density is then calculated. For the M-mode spectra and L-mode spectra as well, the transverse velocity component  $u_t$  is set to zero (cf. §II.C).

The selected L-mode fit parameters are initialized by using a less refined scheme. The spectra to be analyzed have been selected on the basis of containing a recognizable proton peak. The channel  $j_p$  containing the maximum in the proton relative distribution function is input to the analysis program. Assuming the protons are cold, we can write (cf. eqn. II.10, §II.C):

$$\ln \frac{I_j^m \pi^{1/2}}{T_0 A_0 e V_j \Delta V_j} \approx -\bar{V}_j^2 \left[ \frac{1}{w^2} \right] + \bar{V}_j \left[ \frac{2u_n}{w^2} \right] + \left[ \ln \left( \frac{n}{w} \right) - \frac{u_n^2}{w^2} \right]$$

Fitting a parabola to the reduced distribution function in channels  $j_p - 1$  to  $j_p + 1$  then yields initial estimates of  $n$ ,  $u_n$ , and  $w$  for the protons. The initial normal velocity estimate used for the heavy ions is the same as that used for the protons. The initial thermal speeds of the heavy ions are specified via input of sonic Mach numbers, based upon trial and error analysis runs through parts of the data set. This procedure is followed to find values such that the fit will usually converge. To initialize the densities, a moment density using the five channels centered on that one containing the largest current is calculated. (The maximum current is always found in the second of the two peaks in the analyzed L-mode spectra.) This moment density is scaled by a numerical factor of order unity, again found by trial and error, to make initial density estimates for the heavy ionic species to be fit.

## A.5. ASSUMPTIONS USED IN FITS TO THE DATA

For the L-mode analysis, we fit comoving, isotropic Maxwellian distributions of  $H^+$ ,  $S^{3+}$ , and  $O^+$ , assuming that the sulfur and oxygen ions have the same temperature. In our initialization scheme (§A.4) we have started with an assumed sonic Mach number of 4 for the heavy components and used scale factors of 0.3 and 3, respectively, to initialize the densities of these components. Using the proton velocity estimate we computed the channels in which each of the distributions should peak. We then include in the analysis  $\pm 3$  channels of the proton peak and  ${}_{-5}^{+1}$  channels from the computed peaks for the two heavy ions. This effectively eliminates signals from ions with mass to charge  $\gtrsim 20$ . We iterated 6 times through the non-linear least squares fit procedure (§A.1) and rejected any fits with negative densities and/or formal errors of greater than 10% (§A.2) in the fit velocity component.

The M-mode analysis includes fits to isotropic, comoving Maxwellian distributions of  $O^{2+}$ ,  $S^{3+}$ , and  $O^+$ . The initialization values are found as described in section A.4 above. After predicting the channel in which the peak current for each distribution should occur we include  ${}_{-10}^{+16}$  channels of the  $O^{2+}$  peak,  $\pm 16$  channels of the  $S^{3+}$  peak, and  ${}_{-16}^{+6}$  channels of the  $O^+$  peak. This effectively eliminates contributions from the protons, from noise below the peak at a mass to charge ratio of 8, and from sodium and heavy ions above a mass to charge ratio of  $\sim 20$  while retaining enough information to adequately evaluate the temperatures of the fit species. These parameters are iterated 10 times and in practice, always return

positive densities. The formal velocity component in the errors are  $\lesssim 1\%$  for the Voyager 1 M-mode spectra. This procedure did not yield good densities for any of the selected Voyager 2 M-mode spectra. To try to fit these we included  $H^+$  in the analysis, taking only 6 channels below the  $O^{2+}$  peak and  ${}_{-15}^{+20}$  channels of the proton peak. This did give a good fit the spectrum at 190-0454 as shown in Figure 23, but not to the 189-1921 spectrum as shown in Figure 19. For the latter, we estimated the velocity component value from the two heavy ion peaks (assuming they occur at mass to charge ratios of  $10 \frac{2}{3}$  and 16) as 217 km/sec, which is consistent with the preliminary analysis value (Bridge et al. 1979b). This value is used to locate the arrows shown in Figure 18 and is included in the global parameter graphs.

## ACKNOWLEDGEMENTS

I wish to extend my deepest thanks to Professor John Belcher who, as advisor, collaborator, and friend, has made this work possible.

I am also very grateful to Professor Herbert Bridge, Dr. James D. Sullivan, Dr. Alan Lazarus, and Professor Stan Olbert for the use of the Voyager Plasma Science data, useful discussions, friendship, and encouragement. I thank Dr. Chris Goertz for his insightful conversation and Dr. George Gordon for his programming help.

I acknowledge the useful discussions with my fellow students Dr. Charles Goodrich, Fran Bagenal, and Jim Jessen.

I am indebted to my parents for their advice and support during the years; their encouragement has helped make this work possible. I am indebted as well to my wife, Nancy, for her patience, encouragement and help.

For a work such as this, there are a great many people whose contributions are essential, whether they be typing, operating a computer, or giving a simple word of encouragement. I would like especially to single out and thank Dale Lancaster, Mary Terkoski, Ray Rothrock, Trish Welch, Pamela Milligan, Mary Wright, Leo Da Costa, Ronnie Smith, Anne Bowes, and Sally Skinner.

My thanks also go to the the Voyager mission team at the Jet Propulsion Laboratory for a successful mission to Jupiter and to the American taxpayers who have, in no small way, made the exploration of the planets possible.

My graduate studies at M.I.T. and this thesis were supported by the National Aeronautics and Space Administration under contract 953733 to the Jet Propulsion Laboratory.

## REFERENCES

- Acuña, M.H., and N.F. Ness, The main magnetic field of Jupiter, J. Geophys. Res., 81, 2917, 1976.
- Allen, C.W., Astrophysical Quantities, 3rd ed., The Athlone Press, London, 1976.
- Angerami, J.J., and J.O. Thomas, Studies of planetary atmospheres, 1. The distribution of electrons and ions in the Earth's exosphere, J. Geophys. Res., 69, 4537, 1964.
- Bagenal, F., and J.D. Sullivan, Spatial distribution of plasma in the Io torus, Geophys. Res. Lett., 7, 41, 1980.
- Bagenal, F., and J.D. Sullivan, Direct plasma measurements in the Io torus and inner magnetosphere of Jupiter, submitted to J. Geophys. Res., 1981.
- Belcher, J.W., and R.L. McNutt, Jr., The dynamic expansion and contraction of the Jovian plasma sheet, submitted to Nature, 1980.
- Belcher, J.W., C.K. Goertz, and H.S. Bridge, The low energy plasma in the Jovian magnetosphere, Geophys. Res. Lett., 7, 17, 1980.
- Belcher, J.W., C.K. Goertz, J.D. Sullivan, M.H. Acuña, and N.F. Ness, Plasma observations of the Alfvén wave generated by Io, submitted to J. Geophys. Res., 1981.
- Berge, G.L., An interferometric study of Jupiter at 10 cm and 21 cm, Radio Sci., 69D, 1552, 1965.
- Berge, G.L., An interferometric study of Jupiter's decimetric radio emission, Astrophys. J., 146, 767, 1966.

- Bevington, P.R., Data Reduction and Error Analysis for the Physical Sciences, McGraw-Hill Book Company, New York, 1969.
- Bigg, E.K., The influence of the satellite Io on Jupiter's decametric emission, Nature, 203, 1008, 1964.
- Binsack, J.H., Plasma studies with the IMP-2 satellite, pp. 41-4, Ph.D. thesis, MIT Cambridge, MA, August, 1966.
- Birmingham, T.J., and T.G. Northrop, Theory of flux anisotropies in a guiding center plasma, J. Geophys. Res., 84, 41, 1979.
- Brice, N.M., and G.A. Ioannidis, The magnetospheres of Jupiter and Earth, Icarus, 13, 173, 1970.
- Bridge, H.S., J.W. Belcher, R.J. Butler, A.J. Lazarus, A.M. Mavretic, J.D. Sullivan, G.L. Siscoe, and V.M. Vasyliunas, The plasma experiment on the 1977 Voyager mission, Space. Sci. Rev., 21, 259, 1977.
- Bridge, H.S., J.W. Belcher, A.J. Lazarus, J.D. Sullivan, R.L. McNutt, F. Bagenal, J.D. Scudder, E.C. Sittler, G.L. Siscoe, V.M. Vasyliunas, C.K. Goertz, and C.M. Yeates, Plasma observations near Jupiter: Initial results from Voyager 1, Science, 204, 987, 1979a.
- Bridge, H.S., J.W. Belcher, A.J. Lazarus, J.D. Sullivan, F. Bagenal, R.L. McNutt, Jr., K.W. Ogilvie, J.D. Scudder, E.C. Sittler, V.M. Vasyliunas, and C.K. Goertz, Plasma observations near Jupiter: Initial results from Voyager 2, Science, 206, 972, 1979b.

- Broadfoot, A.L., M.J.S. Belton, P.Z. Takacs, B.R. Sandel, D.E. Shemansky, J.B. Hollberg, J.M. Ajello, S.K. Atreya, T.M. Donahue, H.W. Moos, J.L. Bertaux, J.E. Blamont, D.F. Strobel, J.C. McConnell, A. Dalgarno, R. Goody, and M.B. McElroy, Extreme ultraviolet observations from Voyager 1 encounter with Jupiter, Science, 204, 979, 1979.
- Brown, R.A., A model of Jupiter's sulfur nebula, Astrophys. J. Lett. 206, L179, 1976.
- Brown, R.A., and F.H. Chaffee, Jr., High resolution spectra of sodium emission from Io, Astrophys. J. Lett., 187, L125, 1974.
- Burke, B.F., and K.L. Franklin, Observations of a variable radio source associated with the planet Jupiter, J. Geophys. Res., 60, 213, 1955.
- Burlaga, L.F., J.W. Belcher, and N.F. Ness, Disturbances observed near Ganymede by Voyager 2, Geophys. Res. Lett., 7, 21, 1980.
- Carbary, J.F., T.W. Hill, and A.J. Dessler, Planetary spin period acceleration of particles in the Jovian magnetosphere, J. Geophys. Res., 81, 5189, 1976.
- Carbary, J.F. and T.W. Hill, A self-consistent model of a corotating Jovian magnetosphere, J. Geophys. Res., 83, 2603, 1978.
- Carlson, R.W., and D.L. Judge, Pioneer 10 ultraviolet photometer observations at Jupiter encounter, J. Geophys. Res., 79, 3623, 1974.
- Carlson, R.W., and D.L. Judge, Pioneer 10 ultraviolet photometer observations of the Jovian hydrogen torus: The angular distribution, Icarus, 24, 395, 1975.

- Carpenter, D.L., Whistler studies of the plasmopause in the magnetosphere - 1: Temporal variation in the position of the knee and some evidence on plasma motions near the knee, J. Geophys. Res., 71, 693, 1966.
- Chenette, D.L., T.F. Conlon, and J.A. Simpson, Bursts of relativistic electrons from Jupiter observed in interplanetary space with the time variation of the planetary rotation period, J. Geophys. Res., 79, 3551, 1974.
- Cheng, A.F., Effects of Io's volcanoes on the plasma torus and Jupiter's magnetosphere, Rutgers University Technical Report RU80-198, 1980.
- Connerney, J.E.P., M.H. Acuña, and N.F. Ness, Modeling the Jovian current sheet and inner magnetosphere, submitted to J. Geophys. Res., 1981.
- Davis, L., Jr., Stellar electromagnetic fields, Phys. Rev., 72, 632, 1947.
- Davis, L., Jr., Stellar electromagnetic fields (abstract), Phys. Rev., 73, 536, 1948.
- DeForest, S.E., Spacecraft charging at synchronous orbit, J. Geophys. Res., 77, 651, 1972.
- Dessler, A.J., Longitudinal control of Jovian magnetopause motion, J. Geophys. Res. Lett., 5, 65, 1978.
- Dessler, A.J., and T.W. Hill, High-order magnetic multipoles as a source of gross asymmetry in the distant Jovian magnetosphere, Geophys. Res. Lett., 2, 567, 1975.

- Dessler, A.J. and V.M. Vasyliunas, The magnetic anomaly model of the Jovian magnetosphere: Predictions for Voyager, Geophys. Res. Lett., 6, 37, 1979.
- Dungey, J.W., Cosmic Electrodynamics, Cambridge University Press, Cambridge, 1958.
- Ellis, G.R.A. The decametric radio emissions of Jupiter, Radio Sci., 69D, 1513, 1965.
- Eviatar, A., and A.I. Ershkovich, Plasma density in the outer Jovian magnetosphere, J. Geophys. Res., 81, 4027, 1976.
- Ferraro, V.C.A., Non-uniform rotation of the sun and its magnetic field, Mon. Notices Roy. Astron. Soc., 97, 458, 1937.
- Fillius, R.W., The trapped radiation belts of Jupiter, in Jupiter, edited by T. Gehrels, University of Arizona Press, Tucson, 1976.
- Fillius, R.W., C.E. McIlwain, and A. Mogro-Campero, Radiation belts of Jupiter: A second look, Science, 188, 465, 1975.
- Fillius, R.W., and C.E. McIlwain, Measurements of the Jovian radiation belts, J. Geophys. Res., 79, 3589, 1974.
- Frank, L.A., K.L. Ackerson, J.H. Wolfe, and J.D. Mihalov, Observations of plasmas in the Jovian magnetosphere, J. Geophys. Res., 81, 457, 1976.
- Ginzburg, V.L. and S.I. Syrovatskii, Cosmic magnetobremsstrahlung (synchrotron radiation), Ann. Rev. Astron. Astrophys., 3, 297, 1965.
- Gledhill, J.A., Goddard Space Flight Center Report X-615-67-296, 1967a.
- Gledhill, J.A., Magnetosphere of Jupiter, Nature, 214, 155, 1967b.

- Gleeson, L.J., and W.I. Axford, An analytic model illustrating the effects of rotation on a magnetosphere containing low energy plasma, J. Geophys. Res., 81, 3403, 1976.
- Goertz, C.K., Comments on "Longitudinal asymmetry of the Jovian magnetosphere and the periodic escape of energetic particles" by T.W. Hill and A.J. Dessler, J. Geophys. Res., 81, 5601, 1976a.
- Goertz, C.K., The current sheet in Jupiter's magnetosphere, J. Geophys. Res., 81, 1976b.
- Goertz, C.K., Plasma in the Jovian magnetosphere, J. Geophys. Res., 81, 2007, 1976c.
- Goertz, C.K., Energization of charged particles in Jupiter's outer magnetosphere, J. Geophys. Res., 83, 3145, 1978.
- Goertz, C.K., The Jovian magnetodisk, Space Sci. Rev., 23, 319, 1979.
- Goertz, C.K., Scan plane anisotropies and corotation in Jupiter's magnetosphere, Massachusetts Institute of Technology Technical Report, MIT-CSR-TR-80-3, 1980.
- Goertz, C.K., and M.F. Thomsen, The dynamics of the Jovian magnetosphere, Rev. Geophys. Space Phys., 17, 731, 1979a.
- Goertz, C.K., and M.F. Thomsen, Radial diffusion of Io - injected plasma, J. Geophys. Res., 84, 1499, 1979b.
- Goertz, C.K., D.E. Jones, B.A. Randall, E.J. Smith, and M.F. Thomsen, Evidence for open field lines in Jupiter's magnetosphere, J. Geophys. Res., 81, 3393, 1976.
- Goertz, C.K., A.W. Schardt, J.A. Van Allen, and J.L. Parish, Plasma in the Jovian current sheet, Geophys. Res. Lett., 6, 495, 1979.

- Gold, T., Motions in the magnetosphere of the Earth, J. Geophys. Res., 64, 1219, 1959.
- Gold, T., Fields and particles in interplanetary space, in Space Exploration and the Solar System, edited by B. Rossi, Academic Press, New York, 1964.
- Goldreich P., and D. Lynden-Bell, Io, a Jovian unipolar inductor, Astrophys. J., 156, 59, 1969.
- Goldstein, H., Theory of the plasma sheet in the Jovian magnetosphere, Planet. Space Sci., 25, 673, 1977.
- Goodrich, C.C., J.D. Sullivan, and H.S. Bridge, Voyager predictions of the standoff distance of the Jovian bow shock, Massachusetts Institute of Technology Technical Report CSR-TR-80-4, 1980.
- Gurnett, D.A., W.S. Kurth, and F.L. Scarf, Plasma wave observations near Jupiter: Initial results from Voyager 2, Science, 206, 987, 1979.
- Hall, C.F., Pioneer 10, Science, 183, 301, 1974.
- Hall, C.F., Pioneer 10 and Pioneer 11, Science, 188, 445, 1975.
- Hasegawa, A., Ballooning instability and plasma density limitations in Jovian magnetosphere, Rice University conference on Physics of the Jovian Magnetosphere, 1980.
- Heinemann, M. and S. Olbert, Axisymmetric ideal MHD stellar wind flow, J. Geophys. Res., 83, 2457, 1978.
- Herzberg, G., Molecular Spectra and Molecular Structure I. Spectra of Diatomic Molecules, 2nd ed., D. Van Nostrand Company, Inc., Princeton, New Jersey, 1964.

- Herzberg, G., Molecular Spectra and Molecular Structure III. Electronic Spectra and Electronic Structure of Polyatomic Molecules, D. Van Nostrand Company, Inc., Princeton, New Jersey, 1966.
- Hill, T.W., Interchange stability of a rapidly rotating magnetosphere, Planet. Space Sci., 24, 1151, 1976.
- Hill, T.W., Inertial limit on corotation, J. Geophys. Res., 84, 6554, 1979.
- Hill, T.W., Corotation lag in Jupiter's magnetosphere: Comparison of observation and theory, Science, 207, 301, 1980.
- Hill, T.W., and A.J. Dessler, Longitudinal asymmetry of the Jovian magnetosphere and the periodic escape of energetic particles, J. Geophys. Res., 81, 3383, 1976a.
- Hill, T.W., and A.J. Dessler, Reply, J. Geophys. Res., 81, 5602, 1976b.
- Hill, T.W., and F.C. Michel, Heavy ions from the Galilean satellites and the centrifugal distortion of the Jovian magnetosphere, J. Geophys. Res., 81, 4561, 1976.
- Hill, T.W. and J.F. Carbary, Centrifugal distortion of the Jovian magnetosphere by an equatorially confined current sheet, J. Geophys. Res., 83, 5745, 1978.
- Hill, T.W., A.J. Dessler, and F.C. Michel, Configuration of the Jovian magnetosphere, Geophys. Res. Letters, 1, 3, 1974a.
- Hill, T.W., J.F. Carbary, and A.J. Dessler, Periodic escape of relativistic electrons from the Jovian magnetosphere, Geophys. Res. Lett., 1, 333, 1974b.
- Hines, C.O., Hydromagnetic motions in the magnetosphere, Space. Sci. Rev., 3, 342, 1964.

- Hones, E.W., Jr., and J.E. Bergeson, Electric field generated by a rotating magnetized sphere, J. Geophys. Res., 70, 4951, 1965.
- Ioannidis, G.A. and N.M. Brice, Plasma densities in the Jovian magnetosphere: Plasma slingshot or Maxwell demon? Icarus, 14, 360, 1971.
- Kaiser, M.L. and M.D. Desch, Narrow-band Jovian kilometric radiation: A new radio component, Geophys. Res. Lett., 7, 389, 1980.
- Kennel, C.F. and F.V. Coroniti, Is Jupiter's magnetosphere like a pulsar's or Earth's?, Space. Sci. Rev., 17, 857, 1975.
- Kennel, C.F. and F.V. Coroniti, Jupiter's magnetosphere, Ann. Rev. Astron. Astrophys., 15, 389, 1977.
- Kivelson, M.G., P.J. Coleman, L. Froidevaux, and R.L. Rosenberg, A time dependent model of the Jovian current sheet, J. Geophys. Res., 83, 4823, 1978.
- Komesaroff, M.M. and P.M. McCulloch, The radio rotation period of Jupiter, Astrophys. Lett., 1, 39, 1967.
- Krimigis, S.M., T.P. Armstrong, W.I. Axford, C.O. Bostrom, C.Y. Fan, G. Gloeckler, L.J. Lanzerotti, E.P. Keath, R.D. Zwickl, J.F. Carbary, and D.C. Hamilton, Low-energy charged particle environment at Jupiter: A first look, Science, 204, 998, 1979a.
- Krimigis, S.M., T.P. Armstrong, W.I. Axford, C.O. Bostrom, C.Y. Fan, G. Gloeckler, L.J. Lanzerotti, E.P. Keath, R.D. Zwickl, J.F. Carbary, and D.C. Hamilton, Hot plasma environment at Jupiter: Voyager 2 results, Science, 206, 977, 1979b.

- Kupo, I., Y. Mekler, and A. Eviatar, Detection of ionized sulfur in the Jovian magnetosphere, Astrophys. J. Lett., 205, L51, 1976.
- Mayer, C.H., T.P. McCullough, and R.M. Sloanaker, Observations of Mars and Jupiter at a wavelength of 3.15 cm, Astrophys. J., 127, 11, 1958.
- McDonald, F.B., A.W. Schardt, and J.H. Trainor, Energetic protons in the Jovian magnetosphere, J. Geophys. Res., 84, 2579, 1979.
- McElroy, M.B., Y.L. Yung, and R.A. Brown, Sodium emission from Io: Implications, Astrophys. J. Lett., 187, L127, 1974.
- McNutt, R.L., Jr., and J.W. Belcher, Positive ion observations in the middle magnetosphere of Jupiter, submitted to J. Geophys. Res., 1981.
- McNutt, R.L., Jr., J.W. Belcher, J.D. Sullivan, F. Bagenal, and H.S. Bridge, Departure from rigid co-rotation of plasma in Jupiter's dayside magnetosphere, Nature, 280, 803, 1979.
- Mekler, Y., and A. Eviatar, Jovian sulfur nebula, J. Geophys. Res., 82, 2809, 1977.
- Melrose, D.B., Rotational effects on the distribution of thermal plasma in the magnetosphere of Jupiter, Planet. Space Sci., 15, 381, 1967.
- Mendis, D.A. and W.I. Axford, Satellites and magnetospheres of the outer planets, Ann. Rev. Earth Planet. Sci., 2, 419, 1974.
- Mestel, L., A note on equatorial acceleration in a magnetic star, Mon. Notices Roy. Astron. Soc., 122, 473, 1961.
- Mestel, L., Magnetic braking by a stellar wind-I, Mon. Notices Roy. Astron. Soc., 138, 359, 1968.

- Michel, F.C., and P.A. Sturrock, Centrifugal instability of the Jovian magnetosphere and its interaction with the solar wind, Planet. Space Sci., 22, 1501, 1974.
- Mihalov, J.D., H.R. Collard, D.D. McKibben, J.H. Wolfe, and D.S. Intriligator, Pioneer 11 encounter: Preliminary results from the Ames Research Center plasma analyzer experiment, Science, 188, 448, 1975.
- Morabito, L.A., S. P. Synnott, P.N. Kupferman, and S.A. Collins, Discovery of currently active extraterrestrial volcanism, Science, 204, 972, 1979.
- Morris, D., and G.L. Berge, Measurements of the polarization and angular extent of the decimeter radiation from Jupiter, Astrophys. J., 136, 276, 1962.
- Ness, N.F., M.H. Acuña, R.P. Lepping, K.W. Behannon, L.F. Burlaga, and F.M. Neubauer, Jupiter's magnetic tail, Nature, 280, 799, 1979.
- Ness, N.F., M.H. Acuña, R.P. Lepping, L.F. Burlaga, K.W. Behannon, and F.M. Neubauer, Magnetic field studies at Jupiter by Voyager 1: Preliminary results, Science, 204, 982, 1979a.
- Ness, N.F., M.H. Acuña, R.P. Lepping, L.F. Burlaga, K.W. Behannon, and F.M. Neubauer, Magnetic field studies at Jupiter by Voyager 2: Preliminary results, Science, 206, 966, 1979b.
- Neugebauer, M. and A. Eviatar, An alternative interpretation of Jupiter's "plasmopause", Geophys. Res. Lett., 3, 708, 1976.
- Northrop, T.G. and M.F. Thomsen, Theory of scan plane flux anisotropies, submitted to J. Geophys. Res., 1980.

- Northrop, T.G., C.K. Goertz, and M.F. Thomsen, The magnetosphere of Jupiter as observed with Pioneer 10, 2. Nonrigid rotation of the magnetodisc, J. Geophys. Res., 79, 3579, 1974.
- Northrop, T.G., T.J. Birmingham, and A.W. Schardt, Anisotropies in the fluxes of Pioneer 10 protons, J. Geophys. Res., 84, 47, 1979.
- Parker, E.N., and H.A. Stewart, Nonlinear inflation of a magnetic dipole, J. Geophys. Res., 72, 5287, 1967.
- Peale, S.J., P. Cassen, and R.J. Reynolds, Melting of Io by tidal dissipation, Science, 203, 892, 1979.
- Piddington, J.H., Cosmic Electrodynamics, John Wiley and Sons, Inc., New York, 1969.
- Piddington, J.H. and J.F. Drake, Electrodynamic effects of Jupiter's satellite Io. Nature, 217, 935, 1968.
- Pilcher, C.B. and J.S. Morgan, Detection of singly ionized oxygen around Jupiter, Science, 205, 297, 1979.
- Pilcher, C.B. and W.V. Schempp, Jovian sodium emission from region C<sub>2</sub>, Icarus, 38, 1, 1979.
- Ralston, A., Methods for numerical quadrature, in Mathematical Methods for Digital Computers, edited by A. Ralston and H.S. Wilf, John Wiley and Sons, Inc., New York, 1960.
- Roberts, J.A., Jupiter, as observed at short radio wavelengths, Radio Sci. 69D, 1543, 1965.
- Sandel, B.R., D.E. Shemansky, A.L. Broadfoot, J.L. Bertaux, J.E. Blamont, M.J.S. Belton, J.M. Ajello, J.B. Holberg, S.K. Atreya, T.M. Donahue, H.W. Moos, D.F. Strobel, J.C. McConnell, A. Dalgarno, R. Goody, M.C. McElroy, and P.Z. Takacs, Extreme ultraviolet observations from Voyager 2 encounter with Jupiter, Science, 206, 962, 1979.

- Scarf, T.L., The magnetospheres of Jupiter and Saturn, in The Magnetospheres of the Earth and Jupiter, edited by V. Formisano, D. Reidel Publishing Company, Dordrecht-Holland, 433, 1975.
- Scarf, T.L. and D.A. Gurnett, A plasma wave investigation for the Voyager mission, Space Sci. Rev., 21, 289, 1977.
- Scarf, T.L., D.A. Gurnett, and W.S. Kurth, Jupiter plasma wave observations: An initial Voyager 1 overview, Science, 204, 991, 1979.
- Schulz, M., Jupiter's radiation belts, Space Sci. Rev., 23, 277, 1979.
- Scudder, J.D., E.C. Sittler, Jr., and H.S. Bridge, A survey of the plasma electron environment of Jupiter: A view from Voyager, submitted to J. Geophys. Res., 1981.
- Shain, C.A., 18.3 Mc/s radiation from Jupiter, Australian J. Phys., 9, 61, 1956.
- Simpson, J.A., and R.B. McKibben, Dynamics of the Jovian magnetosphere and energetic particle radiation in Jupiter, edited by T. Gehrels, University of Arizona Press, Tucson, 1976.
- Simpson, J.A., D.C. Hamilton, R.B. McKibben, A. Mogro-Campero, K.R. Pyle, and A.J. Tuzzolino, The protons and electrons trapped in the Jovian dipole magnetic field region and their interaction with Io, J. Geophys. Res., 79, 3522, 1974b.
- Simpson, J.A., D.C. Hamilton, G.A. Lentz, R.B. McKibben, M. Perkins, K.R. Pyle, and A.J. Tuzzolino, Jupiter revisited: First results from the University of Chicago charged particle experiment on Pioneer 11, Science, 188, 455, 1975.

- Siscoe, G.L., On the equatorial confinement and velocity space distribution of satellite ions in Jupiter's magnetosphere, J. Geophys. Res., 82, 1641, 1977.
- Siscoe, G.L., Jovian plasmaspheres, J. Geophys. Res., 83, 2118, 1978.
- Siscoe, G.L. and C.K. Chen, Io: A source for Jupiter's inner plasmasphere, Icarus, 31, 1, 1977.
- Siscoe, G.L. and D. Summers, Centrifugally driven diffusion of Iogenic plasma, submitted to J. Geophys. Res., 1981.
- Sittler, E.C., Studies of the electron component of the solar wind and magnetospheric plasma, p. 56, PhD thesis, MIT Cambridge, MA, February, 1978.
- Sloanaker, R.M., Apparent temperature of Jupiter at a wavelength of 10 cm, Astron. J., 64, 346, 1959.
- Smith, E.J., L. Davis, Jr., D.E. Jones, P.J. Coleman, Jr., D.S. Colburn, P. Dyal, C.P. Sonett, and A.M.A. Frandsen, The planetary magnetic field and magnetosphere of Jupiter: Pioneer 10, J. Geophys. Res., 79, 3501, 1974.
- Smith, E.J., L. Davis, Jr., D.E. Jones, P.J. Coleman Jr., D.S. Colburn, P. Dyal, and C.P. Sonnett, Jupiter's magnetic field, magnetosphere, and interaction with the solar wind: Pioneer 11, Science, 188, 451, 1975.
- Smith, E.J., L. Davis Jr., and D.E. Jones, Jupiter's magnetic field and magnetosphere, in Jupiter, edited by T. Gehrels, University of Arizona Press, Tucson, 788, 1976.
- Smoluckowski, R., Origin and structure of Jupiter and its satellites, in Jupiter, edited by T. Gehrels, University of Arizona Press, Tucson, 3, 1976.

- Sonnerup, B.U.Ö. and M.J. Laird, On magnetospheric interchange instability, J. Geophys. Res., 68, 131, 1963.
- Sozzou, C., A similarity model illustrating the effect of rotation on an inflated magnetosphere, Planet. Space Sci., 26, 311, 1978.
- Sullivan, J.D. and F. Bagenal, In situ identification of various ionic species in Jupiter's magnetosphere, Nature, 280, 798, 1979.
- Sullivan, J.D., H.S. Bridge, J.W. Belcher, A.J. Lazarus, R.L. McNutt, Jr., and F. Bagenal, Morphology of low energy plasma within  $40 R_J$  of Jupiter, EOS Trans. AGU, 60, 920, 1979.
- Stone, E.C. and A.L. Lane, Voyager 2 encounter with the Jovian system, Science, 206, 925, 1979.
- Trafton, L., Detection of a potassium cloud near Io, Nature, 258, 690, 1975.
- Trafton, L., Periodic variations in Io's sodium and potassium clouds, Astrophys. J., 215, 960, 1977.
- Trainor, J.H., F.B. McDonald, D.E. Stilwell, and B.J. Teegarden, Jovian protons and electrons: Pioneer 11, Science, 188, 464, 1975.
- Trainor, J.H., F.B. McDonald, B.J. Teegarden, W.R. Webber, and E.C. Roelof, Energetic particles in the Jovian magnetosphere, J. Geophys. Res., 79, 3600, 1974.
- Van Allen, J.A., On the plasma sheet in Jupiter's dawn magnetodisc, U. of Iowa, 78-29 1978.
- Van Allen, J.A., D.N. Baker, B.A. Randall, and D.D. Sentman, The magnetosphere of Jupiter as observed with Pioneer 10, 1. Instrument and principle findings, J. Geophys. Res., 79, 3559, 1974.

- Van Allen, J.A., B.A. Randall, D.N. Baker, C.K. Goertz, D.D. Sentman, M.F. Thomsen, and H.R. Flindt, Pioneer 11 observations of energetic particles in the Jovian magnetosphere, Science, 188, 459, 1975.
- Vasyliunas, V.M., in Methods of Experimental Physics, Vol. 9B of Plasma Physics, edited by R.H. Lovbergs, p. 49, Academic Press, 1971.
- Vasyliunas, V.M., Modulation of Jovian interplanetary electrons and the longitude variation of decametric emission, Geophys. Res. Lett., 2, 87, 1975.
- Vickers, G.T., A self-consistent model of the Jovian plasma sheet, Planet. Space Sci., 26, 381, 1978.
- Vogt, R.E., W.A. Cook, A.C. Cummings, T.L. Garrard, N. Gehrels, E.C. Stone, J.H. Trainor, A.W. Schardt, T. Conlon, N. Lal, and F.B. McDonald, Voyager 1: Energetic ions and electrons in the Jovian magnetosphere, Science, 204, 1003, 1979a.
- Vogt, R.E., A.C. Cummings, T.L. Garrard, N. Gehrels, E.C. Stone, J.H. Trainor, A.W. Schardt, T.F. Conlon, and F.B. McDonald, Voyager 2: Energetic ions and electrons in the Jovian magnetosphere, Science, 206, 984, 1979b.
- Walker, R.J., M.G. Kivelson, and A.W. Schardt, High  $\beta$  plasma in the dynamic Jovian current sheet, Geophys. Res. Lett., 5, 799, 1978.
- Warwick, J.W., Radiophysics of Jupiter, Space Sci. Rev., 6, 841, 1967.
- Wolfe, J.H., J.D. Mihalov, H.R. Collard, D.D. McKibben, L.A. Frank, and D.S. Intriligator, Pioneer 10 observations of the solar wind interaction with Jupiter, J. Geophys. Res., 79, 3489, 1974.

Zwickl, R.D., S.M. Krimigis, T.P. Armstrong, and L.J. Lanzerotti, Ions of Jovian origin observed by Voyager 1 and 2 in interplanetary space, The Johns Hopkins University, JHU/APL 80-05, 1980.

TABLE I. IONIZATION POTENTIALS OF ATOMS

Element	Charge State				
	+1	+2	+3	+4	+5
H	13.598 (1) $\Delta$				
He	24.587 (4)	54.416 (2) $\Delta$			
O	13.618 (16) $\Delta$	35.117 (8) $\Delta$	54.934 (5 1/3)	77.413 (4)	113.90 (3 1/5)
Na	5.139 (23) $\Delta$	47.296 (11 1/2) $\Delta$	71.64 (7 2/3)	98.91 (5 3/4)	138.40 (4 3/5)
S	10.360 (32) $\Delta$	23.33 (16) $\Delta$	34.83 (10 2/3) $\Delta$	47.30 (8) $\Delta$	72.68 (6 2/5)
K	4.341 (39)	31.63 (19 1/2) $\Delta$	45.72 (13)	60.92 (9 3/4)	82.66 (7 4/5)

Each column shows the energy in electron volts to ionize the element to the charge state indicated. The mass to charge ratio of the resultant ionic species is shown in parentheses.  $\Delta$  = a species with the given mass to charge ratio definitely identified in Plasma Science data.  $\Delta$  = a species with the given mass to charge ratio possibly identified in Plasma Science data. All ionization potentials are from Allen (1976).

TABLE II. IONIZATION POTENTIALS AND DISSOCIATION ENERGIES OF MOLECULES

Molecule	Energy Required for Ionization			Energy Required for Dissociation
O <sub>2</sub>	12.08	(32)	▲	5.115
S <sub>2</sub>				≤ 4.4
SO	12.1	(48)		5.35
SO <sub>2</sub>	12.34	(64)	▲	5.61 (→ SO + O)

Energies are given in electron volts. The mass to charge ratio of the singly charged ion is shown in parentheses. ▲ = a species with the given mass to charge ratio has been identified in the Plasma Science data. Data for S<sub>2</sub> is from Herzberg (1964) and data for SO<sub>2</sub> is from Herzberg (1966). All other data is from Allen (1976).

TABLE III. SUMMARY OF M-MODE SPECTRAL FIT PARAMETERS  
 VOYAGER 1 63-1537:35.085, 19.8 R<sub>J</sub> INBOUND

Case	Component	Assumptions on Fit	n (cm <sup>-3</sup> )	v(km s <sup>-1</sup> )	w(km s <sup>-1</sup> )	T(eV)	T/A (eV)	n <sub>c</sub> (cm <sup>-3</sup> )	n <sub>M</sub> (amu cm <sup>-3</sup> )
1	O <sup>2+</sup> S <sup>3+</sup> O <sup>+</sup> (S <sup>2+</sup> )	Common velocity component; independent thermal speeds	0.139	195	14.0	16.4	1.02	1.67	22.2
			0.143		14.6	35.6	1.11		
			0.951		11.0	10.1	0.631		
			(0.476)		(11.0)	(20.7)	(0.631)		
2	O <sup>2+</sup> S <sup>3+</sup> O <sup>+</sup>	Common velocity component; common temperature	0.150	195	12.7	13.5	--	1.65	22.3
			0.111		8.98				
			1.62		12.7				
3	O <sup>2+</sup> S <sup>3+</sup> S <sup>2+</sup>	Common velocity component; common temperature	0.165	195	16.3	22.2	--	1.66	22.2
			0.124		11.5				
			0.488		11.5				
4	H <sup>+</sup> O <sup>2+</sup> S <sup>3+</sup> O <sup>+</sup>	Four independent, isotropic, Maxwellian dist- ributions	0.185	183	42.4	9.38	9.38	1.89	22.4
			0.194	195	18.9	29.8	1.85		
			0.128	197	13.1	23.7	0.897		
			0.951	195	11.0	10.1	0.631		
5	H <sup>+</sup> O <sup>2+</sup> S <sup>3+</sup> O <sup>+</sup>	Common velocity component; independent thermal speeds	0.162	195	42.3	9.34	9.34	1.83	22.3
			0.138		14.0	16.4	1.02		
			0.148		14.6	35.6	1.11		
			0.949		11.0	10.1	0.631		
6	O <sup>2+</sup> S <sup>3+</sup> O <sup>+</sup> Na <sup>+</sup>	Four independent Maxwellian distributions	0.146	195	17.5	Bad fit on Na <sup>+</sup> velocity component			
			0.0888	195	19.9				
			0.765	195	9.60				
			0.908	143	52.0				
7	O <sup>2+</sup> S <sup>3+</sup> O <sup>+</sup> Na <sup>+</sup>	Common velocity component for O <sup>+</sup> and Na <sup>+</sup> ; all other para- meters independent	0.158	194	15.8	20.8	Bad fit on Na <sup>+</sup> thermal speed		
			0.141	197	14.1	33.2			
			0.879	195	10.4	9.63			
			0.270		50.6	300.			

8	S <sup>3+</sup> O <sup>2+</sup> K <sup>2+</sup> Na <sup>+</sup>	Common velocity component and common temperature for all species fit	0.114 1.03 -0.00301 0.0770	195	9.04 12.8 8.19 10.7	13.6	Bad fit on K <sup>2+</sup> density		
9	S <sup>3+</sup> O <sup>2+</sup> K <sup>2+</sup> Na <sup>+</sup>	Common velocity component; independent thermal speeds	0.170 0.906 0.0321 0.0555	195	16.7 10.2 7.23 8.31	46.6 8.69 10.6 8.29	1.46 0.543 0.273 0.360	Values for K <sup>2+</sup> and Na <sup>+</sup> only 0.120      2.53	
10	S <sup>3+</sup> O <sup>2+</sup> K <sup>2+</sup> Na <sup>+</sup>	Common velocity component; common thermal speed for O <sup>+</sup> , K <sup>+</sup> , and Na <sup>+</sup>	0.168 0.901 0.0374 0.0543	195	16.4 10.2	44.9 8.69 21.2 12.5	1.40 0.543	0.129	2.71
11	O <sup>2+</sup> K <sup>2+</sup> Na <sup>+</sup>	Common velocity component; common thermal speed for K <sup>+</sup> and Na <sup>+</sup>	0.907 0.0352 0.0534	195	10.3 8.78	8.86 15.7 9.25	0.554 0.402	0.124	2.60

Various number of channels above and below the predicted peak of the different ionic species were used in each fit. Data in channels 1 to 56 (i.e. the proton signature) are from the measurement sequence which occurred 95 seconds prior to the time given as that of the spectrum.

TABLE IV. M-MODE SPECTRAL FIT PARAMETERS  
 VOYAGER 1 63-1550:23.086, 19.6 R<sub>J</sub> INBOUND

Component	$n(\text{cm}^{-3})$	$w(\text{km s}^{-1})$	T(eV)	T/A (eV)
H <sup>+</sup>	0.214	25.8	3.47	3.47
O <sup>2+</sup>	0.109	23.6	46.5	2.91
S <sup>3+</sup>	0.107	17.2	49.4	1.54
O <sup>+</sup>	0.742	10.3	8.86	0.554
K <sup>2+</sup>	0.0209	9.75	7.94	0.204
Na <sup>+</sup>	0.0604	9.75	19.4	0.841
S <sup>+</sup>	0.0947	12.8	27.4	0.855

The common velocity component is  $180 \text{ km s}^{-1}$ . These data have been composited from several different fits to the same spectrum.

TABLE V. SUMMARY OF L-MODE SPECTRAL FIT PARAMETERS  
 VOYAGER 1 63-1538:36.525, 19.8, R<sub>J</sub> INBOUND

Case	Component	$n(\text{cm}^{-3})$	$v(\text{km s}^{-1})$	$w(\text{km s}^{-1})$	T (eV)	T/A (eV)	$n_c(\text{cm}^{-3})$	$n_M(\text{amu cm}^{-3})$
1	H <sub>2</sub> <sup>+</sup>	0.231	184	47.1	11.6	11.6	1.8	23.1
	S <sub>3</sub> <sup>+</sup>	0.144		16.1	43.0	1.34		
	O <sup>+</sup>	1.14		22.7	43.0	2.69		
2	H <sub>2</sub> <sup>+</sup>	0.283	177	61.3	19.6	19.6	2.05	27.6
	S <sub>3</sub> <sup>+</sup>	0.0655		34.5	199.	6.21		
	S <sub>2</sub> <sup>+</sup>	0.787		34.5	199.	6.21		
3	H <sub>2</sub> <sup>+</sup>	0.235	183	47.0	11.5	11.5	2.01	24.9
	O <sub>2</sub> <sup>+</sup>	0.235		33.8	95.4	5.96		
	S <sub>2</sub> <sup>+</sup>	0.653		23.9	95.4	2.98		

All fits assume a common velocity for all three species and a common temperature for the two heavy ionic species used in the fit.

TABLE VI. SPECTRAL FIT PARAMETERS  
VOYAGER I INBOUND 16.5 R<sub>J</sub>

MODE	TIME	FIT TO	$v$ (km s <sup>-1</sup> )	T <sub>proton</sub> (eV)	$n_c$ (cm <sup>-3</sup> )	$n_m$ (amu cm <sup>-3</sup> )	FIGURE
H <sup>a</sup>	63-1943:59.003	O <sup>2+</sup> , S <sup>3+</sup> , O <sup>+</sup>	178	----	3.31	42.3	30
H <sup>a</sup>		O <sup>2+</sup> , S <sup>3+</sup> , S <sup>2+</sup>	184	----	3.09	35.8	31
L <sup>a</sup>	63-1943:24.024	H <sup>+</sup> , S <sup>3+</sup> , O <sup>+</sup>	160	80.3	4.93	63.3	33
L <sup>a,b</sup>		H <sup>+</sup> , S <sup>3+</sup> , S <sup>2+</sup>	98.1	160	10.9	203.	34
L <sup>a</sup>		H <sup>+</sup> , O <sup>2+</sup> , S <sup>2+</sup>	190	54.3	3.90	38.2	35
E1, E2 <sup>c</sup>	63-1944:31.404	Core and Halo Distributions	----	T <sub>core</sub> = 17.3 T <sub>Halo</sub> = 136	4.13	---	---

<sup>a</sup> All heavy ions (A>1) are assumed to have the same temperature in each fit. A common bulk velocity component is assumed in each fit.

<sup>b</sup> Bad fit; S<sup>3+</sup> density is negative.

<sup>c</sup> Analysis by Scudder and Sittler (1980) included for comparison.

TABLE VII. FRACTIONAL ERRORS IN L-MODE FIT; VOYAGER 1, 63-1943:24.024

FIT	$\delta v/v$	$\delta w_{H^+}/w_{H^+}$	$\delta n_{H^+}/n_{H^+}$
H <sup>+</sup> , S <sup>3+</sup> , O <sup>+</sup>	0.0145	0.148	0.191
H <sup>+</sup> , S <sup>3+</sup> , S <sup>2+</sup>	0.126	0.510	0.00424
H <sup>+</sup> , O <sup>2+</sup> , S <sup>2+</sup>	0.00978	0.196	0.236

## FIGURE CAPTIONS

- Figure 1: Line drawing of the Voyager Plasma Science experiment. The apertures of the three cups which form the main sensor are visible. The side sensor (D-cup) opens toward the lower left. From the D-cup counterclockwise are located the B-cup, the A-cup, and the C-cup. The symmetry axis of the main sensor lies parallel to the spacecraft high gain antenna and usually points toward the earth.
- Figure 2a: Projection of Voyager 1 encounter trajectory into Jovian equatorial plane. The orbits of the four Galilean satellites are also shown. Projections of the D-cup normal (D) and main sensor symmetry axis (S) of the Plasma Science experiment are also projected into this plane at 30 hour intervals. The beginning of each day (spacecraft event time) is also marked along the trajectory. ( $1R_J \approx 71,372$  km).
- Figure 2b: The response function (velocity interdependent) of the A, C, and D cups of the Plasma Science experiment to a cold corotating beam as a function of time during the Voyager 1 encounter. The day labels occur at 1200 hours on the day indicated. Unit response implies that all beam particles that are intersected by the given cup are measured. Note the necessity of switching the analysis over from the side sensor to the main sensor at 64-0600. The response includes the correction for spacecraft aberration. (Perijove at 64-1204.6 UTC).

- Figure 3a: Same as Figure 2a, but for Voyager 2 during its encounter with Jupiter.
- Figure 3b: Same as Figure 2b, but during the Voyager 2 encounter. Note that the difference in encounter geometry for Voyager 2 as compared to Voyager 1 results in the side sensor response falling off sooner before perijove for Voyager 2 and the main sensor response being appreciable for a longer period of time around perijove (190-2229.0 UTC).
- Figure 4: The bottom section shows the positive ion charge density (calculated from measured currents) and the positive ion mass density (calculated from the fits to individual spectra) as a function of time during the Voyager 1 encounter. The top section shows the perpendicular distance from the magnetic equatorial plane ( $O_4$  model dipole reference) to the spacecraft. The zeros of this curve indicate crossings of the magnetic equatorial plane which are indicated by arrows in the bottom section. The radial distance of the spacecraft from the center of Jupiter is shown in units of Jovian radii across the top. Perijove is marked as "CA" (closest approach).
- Figure 5: Same format as Figure 4, but for the Voyager 2 encounter.

Figure 6: M-mode spectrum taken by the side sensor of the Plasma Science experiment on Voyager 1. The spacecraft was  $19.8 R_J$  from Jupiter on the inbound leg of its encounter trajectory. The format used is the logarithm of the reduced distribution function (see text) plotted against the energy/charge (in volts) scan of the instrument. Peaks in the distribution function are indicative of ionic species with different mass to charge ratios moving into the sensor with the same velocity component. Based on the common velocity component fit to this spectrum (see text), the arrows indicate the location of the distribution function peaks of supersonic ions with mass to charge ratios of 1, 8,  $10 \frac{2}{3}$ , 16 and 23.

Figure 7: A fit to the spectrum shown in Figure 6. Only that spectral data which is being fit is reproduced. The contribution of each individual species being fit is shown by a thin solid line (approximately a parabola). The summed contribution over all fit species are indicated by crosses at the center of each channel; these should be compared to the data in each channel. For this particular fit, we have assumed a composition of  $O^{2+}$ ,  $S^{3+}$ , and  $O^+$ . The densities and temperature are independent of each other, but a common velocity component ("comoving") into the sensor has been assumed.

Figure 8: Another fit to the spectrum of Figure 6. The same as for Figure 7 except that here a common temperature ("isothermal") for the three heavy ionic species has been assumed.

Figure 9: A third fit to the spectrum shown in Figure 6. The fit is to  $O^{2+}$ ,  $S^{3+}$ , and  $S^{2+}$  with a common temperature and a common velocity component into the side sensor.

Figure 10: Plasma sheet crossings by Voyager 1 at ~63-1345 and ~63-1530. Raw data in the form of 160 M-mode spectra are displayed. The plot is linear in instrument channel number, time, and relative flux density (relative positive ion current). The largest current measured in the ~4 1/4 hours depicted was 37,250 femtoamps and the vertical scale has been normalized to this value. Heavy ions (mass/charge  $\gtrsim 8$ ) are responsible for the signal at  $> 1000$  volts. Protons produce signals well above the background noise at ~100 volts for only four spectra around 63-1530. The peak at the mass to charge ratio of 16 in Figure 6 is the tallest peak in this figure. The second tallest peak (also at mass/charge 16) and the most forward of the three prominent proton peaks both belong to the 63-1550 spectrum mentioned in the text.

Figure 11: The same time period covered by Figure 10 but showing L-mode data. The plot here is linear in instrument channel number, time, and relative distribution function. Division by the energy/charge width of each channel (to convert to distribution function) emphasizes the proton signal present in the data. The L-mode spectra span the energy/charge range in only 16 channels;

however for this representation we have spline fit the L-mode data to an effective 128 channels. This allows better comparison with the corresponding M-mode data (Figure 10) and eliminates problems with hidden lines which occur in presenting raw L-mode data in this format.

Figure 12: One of the L-mode spectra shown in Figure 11 taken by Voyager 1. This spectrum was taken ~one minute after the M-mode spectrum of Figure 6 was assembled. The scales are the same as for Figure 6 so the two spectra are directly comparable. The clear separation of the proton signal from that of the heavy ions is readily apparent. Individual heavy ionic species (mass/charge  $\geq 8$ ) are not resolved.

Figure 13: A fit to the L-mode spectrum of Figure 12. Only that part of the spectrum which is being fit is shown. The fit species are  $H^+$ ,  $S^{3+}$ , and  $O^+$ . A common velocity component into the side sensor is assumed for all three and the two heavy ionic species ( $S^{3+}$  and  $O^+$ ) are assumed to have the same temperature. The densities are all independent of each other.

Figure 14: Same as Figure 13 but with  $H^+$ ,  $O^{2+}$ , and  $S^{2+}$  as the assumed components in the fit.

Figure 15: Same as Figure 13 but with  $H^+$ ,  $S^{3+}$ , and  $S^{2+}$  as the assumed components in the fit.

Figure 16: M-mode spectrum from Voyager 1 inbound at  $41.2 R_J$ . The format is the same as for Figure 6. The signature of the protons has been lost in the noise in the low channels.

Figure 17: L-mode spectrum from Voyager 1 taken less than one minute before the M-mode spectrum of Figure 16. The heavy ions are not resolved but the proton signature is clearly present above the noise in the wider L-mode channels.

Figure 18: M-mode spectrum from the side sensor on Voyager 2 at  $22.0 R_J$  inbound. Heavy ion peaks at the mass to charge ratios of  $10 \frac{2}{3}$  and 16 are just resolved. The proton signal is clear but noisy. There is a suggestion of an alpha particle shoulder (mass/charge = 2) on the high side of the proton signature.

Figure 19: Attempted fit to the spectrum of Figure 18. While the total fit distribution function matches the measured data fairly well, the contributions of the individual fit species are badly off. In particular, the temperature of the  $O^+$  distribution has been driven far too high by the fit process.

Figure 20: L-mode spectrum taken ~ half a minute before the M-mode spectrum of Figure 18.

- Figure 21: Attempted fit to the Voyager 2 L-mode spectrum of Figure 20. Although the fit bulk velocity component is good and the total fit is good, the fit procedure drove the temperature of one of the heavy ionic species high and the density of the other negative. No parameters from this fit are included in the discussion of global plasma characteristics.
- Figure 22: M-mode spectrum from Voyager 2 inbound at 16.5  $R_J$ . This is the coldest, best resolved M-mode spectrum seen in the middle magnetosphere by the side sensor of the Plasma Science experiment on Voyager 2. Only ionic species with mass to charge ratios of 1 and 16 are clearly resolved; contributions are definitely present at mass to charge ratios of 8 and  $10 \frac{2}{3}$  as well. Species at 23, 32, and 64 are plausible contributors to this spectrum but not indicated by it.
- Figure 23: Fit to the spectrum of Figure 22. The velocity component found from this fit was used to locate the arrows at the various mass to charge ratios in the previous figure.
- Figure 24: M-mode data from Voyager 2. The format is the same as that of Figure 10. The prominent spectrum at ~190-0500 is that one shown in Figures 22 and 23. These spectra, taken during the period of time in which Voyager 2 was passing through the Ganymede "wake" region, give a good illustration of the time variability of the plasma conditions encountered by the spacecraft.

Figure 25: L-mode spectrum from Voyager 2 acquired just before the M-mode spectrum shown in Figure 22.

Figure 26: Fit to the L-mode spectrum of Figure 25.

Figure 27: L-mode spectrum from Voyager 2 acquired just after the M-mode spectrum shown in Figure 22. Note that the velocity component into the side sensor as well as the densities of the various components have all dropped relative to their values in the spectrum shown in Figure 25.

Figure 28: Fit to the L-mode spectrum of Figure 27.

Figure 29: M-mode spectrum from Voyager 1 inbound at  $16.5 R_J$ . The proton signal is present but contaminated by noise. The heavy ions are unresolved, but the distribution functions are clearly decreasing with energy/charge above  $\sim 3000$  volts. The mass to charge ratios shown are based on the common velocity component found from the fits shown in Figures 30 and 31. A dashed arrow locates where the peak of the mass to charge 16 species would occur if the plasma were rigidly corotating with the planet. Note that this spectrum was taken at the same distance from the planet as the Voyager 2 M-mode spectrum shown in Figure 22.

- Figure 30: A fit to the M-mode spectra shown in Figure 29. The assumed composition is  $O^{2+}$ ,  $S^{3+}$ , and  $O^+$ . A common temperature and velocity component is assumed. The fit velocity component gave the lower estimate of the locations for the various mass to charge ratio arrows shown in Figure 29.
- Figure 31: A fit to the M-mode spectra shown in Figure 29. This fit uses the same assumptions as those used for the fit shown in Figure 30 except here the assumed composition is  $O^{2+}$ ,  $S^{3+}$ , and  $S^{2+}$ . This gives the upper estimate for the locations of the arrows in Figure 29.
- Figure 32: L-mode spectrum from Voyager 1 inbound acquired by the side sensor of the Plasma Science experiment. This spectrum was acquired within the minute before the acquisition of the M-mode spectrum of Figure 29.
- Figure 33: A fit to the spectrum of Figure 32 assuming a composition of  $H^+$ ,  $S^{3+}$ , and  $O^+$ .
- Figure 34: A fit to the spectrum of Figure 32 assuming a composition of  $H^+$ ,  $S^{3+}$ , and  $S^{2+}$ .
- Figure 35: A fit to the spectrum of Figure 32 assuming a composition of  $H^+$ ,  $O^{2+}$ , and  $S^{2+}$ .

Figure 36: Bulk velocity component of the plasma into the side sensor of the Plasma Science experiment during the Voyager 1 encounter. The time period covered is the same as that of Figure 4; radial distance from the center of the planet is shown across the top. The upper panel shows velocity component determinations found from analysis of the resolved M-mode spectra. The lower panel shows velocity component determinations found from analysis of resolved L-mode spectra. In each panel a solid line marks the value of the velocity component which would have been measured if the plasma were locked into rigid corotation with the planet.

Figure 37: Deviations from rigid corotation and error in velocity component determinations from Voyager 1. The time period covered is the same as that of Figure 36. The triangles give the deviations from between the rigid corotation line and the M-mode velocity component determinations (cf. upper panel of Figure 36) expressed in terms of the number of thermal widths of the 16 peak of the corresponding M-mode spectrum. The squares show the maximum possible error in velocity component determinations (expressed in terms of the same thermal widths) as a result of spacecraft charging. This calculation is possible only where there are good velocity component determinations available from timewise adjacent L-mode and M-mode spectra.

Figure 38: Same as Figure 36 but for Voyager 2. The time period covered is the same as that of Figure 5. The breaks in the rigid corotation line occur as the result of a spacecraft roll maneuver.

- Figure 39: Plasma temperature measured along the inbound leg of the Voyager 1 encounter trajectory. The time period covered is the same as that of Figure 4. The plot includes proton temperatures from the L-mode analysis and  $O^+$  temperatures from the M-mode analysis.
- Figure 40: Same as Figure 39 but for Voyager 2. The time period covered is the same as that of Figure 5.
- Figure 41: North/south plasma flux anisotropy during the Voyager 1 encounter. The data trace and the left hand scale shows the plasma flux anisotropy as inferred from the Voyager 1 main sensor during encounter (see text). The smooth curve and right hand scale indicates the distance of the spacecraft from the magnetic equatorial plane. Distance from Jupiter and spacecraft event time are shown across the top; local time is shown across the bottom.
- Figure 42: Same as Figure 41, but for Voyager 2.
- Figure 43: M-mode spectra from the plasma sheet crossing by Voyager 1 centered on  $\sim 63$ -1900. The format is the same as that of Figure 10. The peak current to which the vertical scale has been normalized is 49,680 femtoamps.

- Figure 44: L-mode spectra showing both proton and heavy ion signatures for the same time period as that covered in Figure 43. The format is the same as that of Figure 11. The L-mode channels containing the heavy ion signatures were saturated from ~63-1845 to ~63-1945.
- Figure 45: Plasma parameters for most of the time period covered in Figure 44. The core electron temperatures are from Scudder and Sittler (1980) and are included for comparison. All other parameters are from the positive ion L-mode analysis. The bottom panel shows the north/south plasma flux anisotropy for the period covered. This is essentially an enlargement of the appropriate part of the data trace shown in Figure 41.
- Figure 46: M-mode spectra from the plasma sheet crossings by Voyager 1 at ~63-2330 and ~64-0145. The maximum current measured in any channel (used for normalization) was 121,780 femtoamps. The principal spectral peak occurs at the mass to charge ratio of 16. The signature of  $S^+$  at 32 is visible in some of the spectra at the first crossing and the signature of protons (at < 100 volts) is visible in spectra at the second crossing. The magnetic field minimum occurs at ~64-0000.
- Figure 47: M-mode spectra from the plasma sheet crossing by Voyager 2 at ~190-2100. The normalization current is 819,750 femtoamps. These spectra were measured by the A-cup of the main sensor.

- Figure 48: M-mode spectra from the plasma sheet crossing by Voyager 2 at ~191-0930. The normalization current is 73,470 femtoamps. These spectra were measured by the A-cup of the main sensor.
- Figure 49: Ratio of the measured velocity component to that expected on the basis of rigid corotation, as projected along the normal of the side sensor of the Plasma Science experiment. The plot is against distance for both Voyager 1 and Voyager 2. If the true plasma flow is strictly azimuthal, the ratio gives the angular speed of the plasma expressed as a fraction of the angular speed of Jupiter.
- Figure 50: Log-log plot of positive ion mass and charge densities versus radial distance along the Voyager 1 inbound trajectory. Mass density values inside of  $10 R_J$  are from Bagenal and Sullivan (1981). The dashed line has a slope of  $-9/2$ .
- Figure 51: Same as Figure 50, but for Voyager 2. The dashed line has the same slope and intercept as the one in Figure 50.
- Figure 52: Log-log plot of positive ion temperature versus radial distance along the Voyager 1 inbound trajectory. Values from inside of  $10 R_J$  are from Bagenal and Sullivan (1981).
- Figure 53: Same as Figure 52 but for Voyager 2.
- Figure 54: Line drawing illustrating plasma flow patterns which form an idealized version of the Jovian plasma sheet.

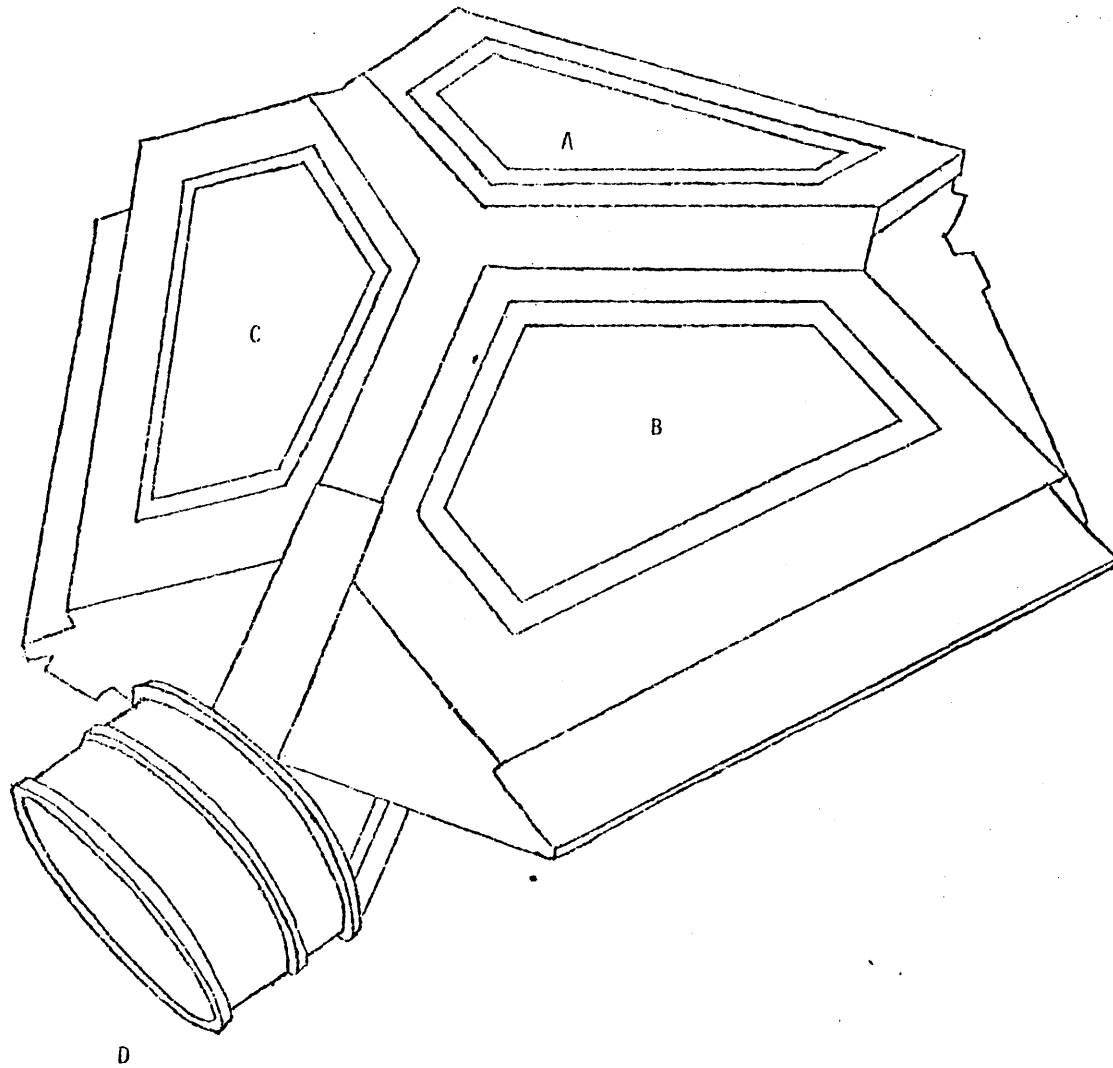


FIGURE 1

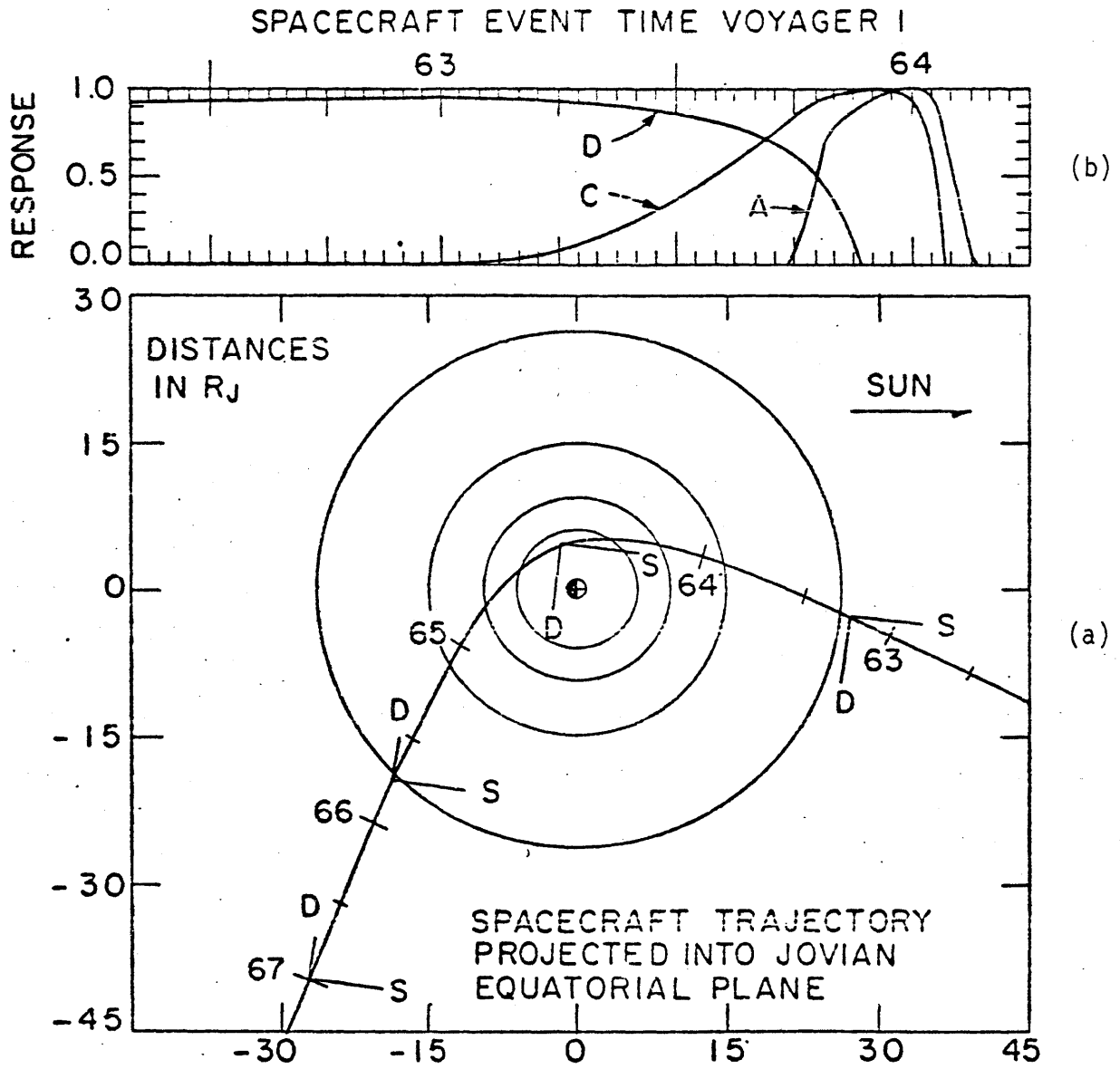


FIGURE 2

SPACECRAFT EVENT TIME VOYAGER 2

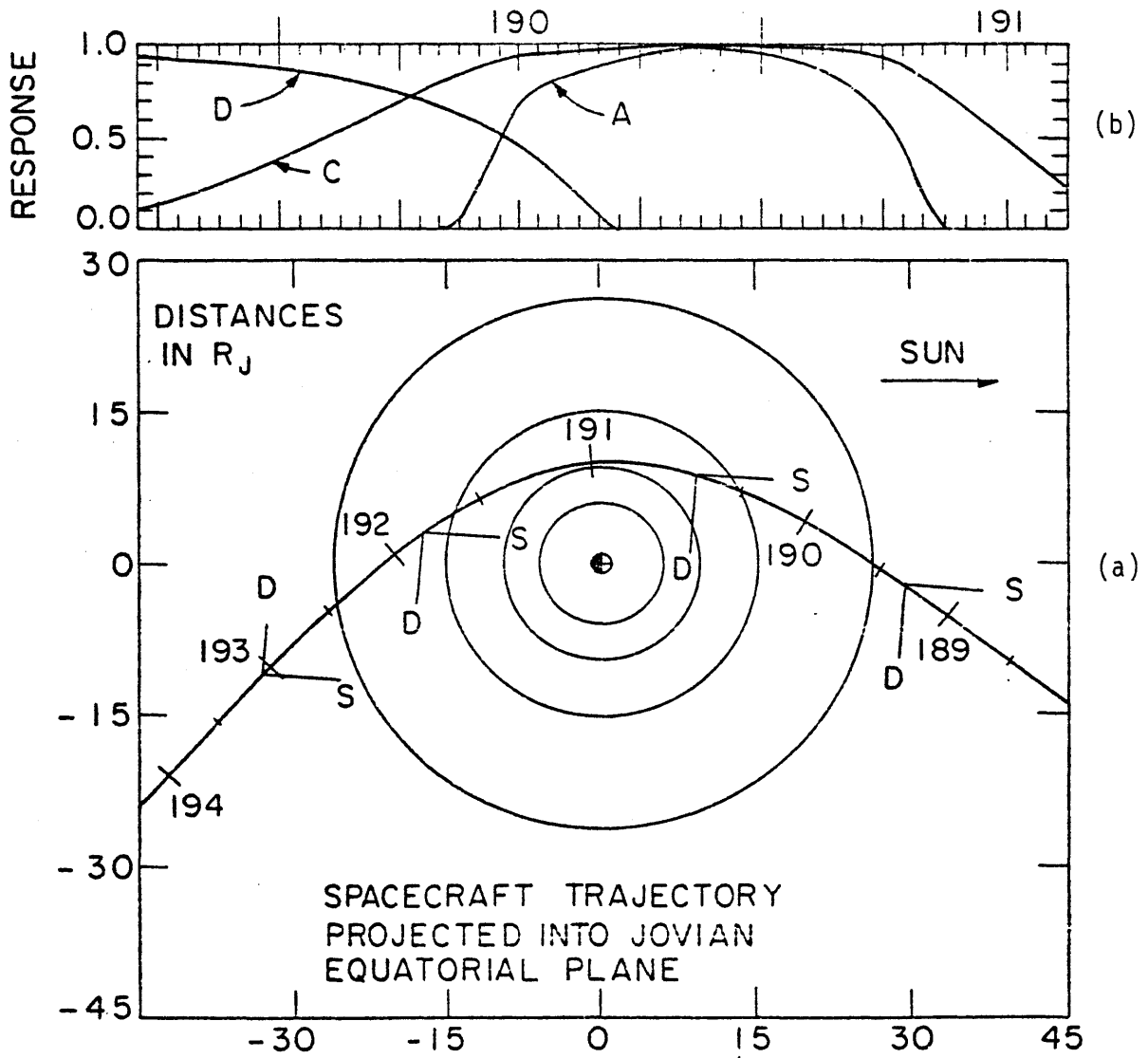


FIGURE 3



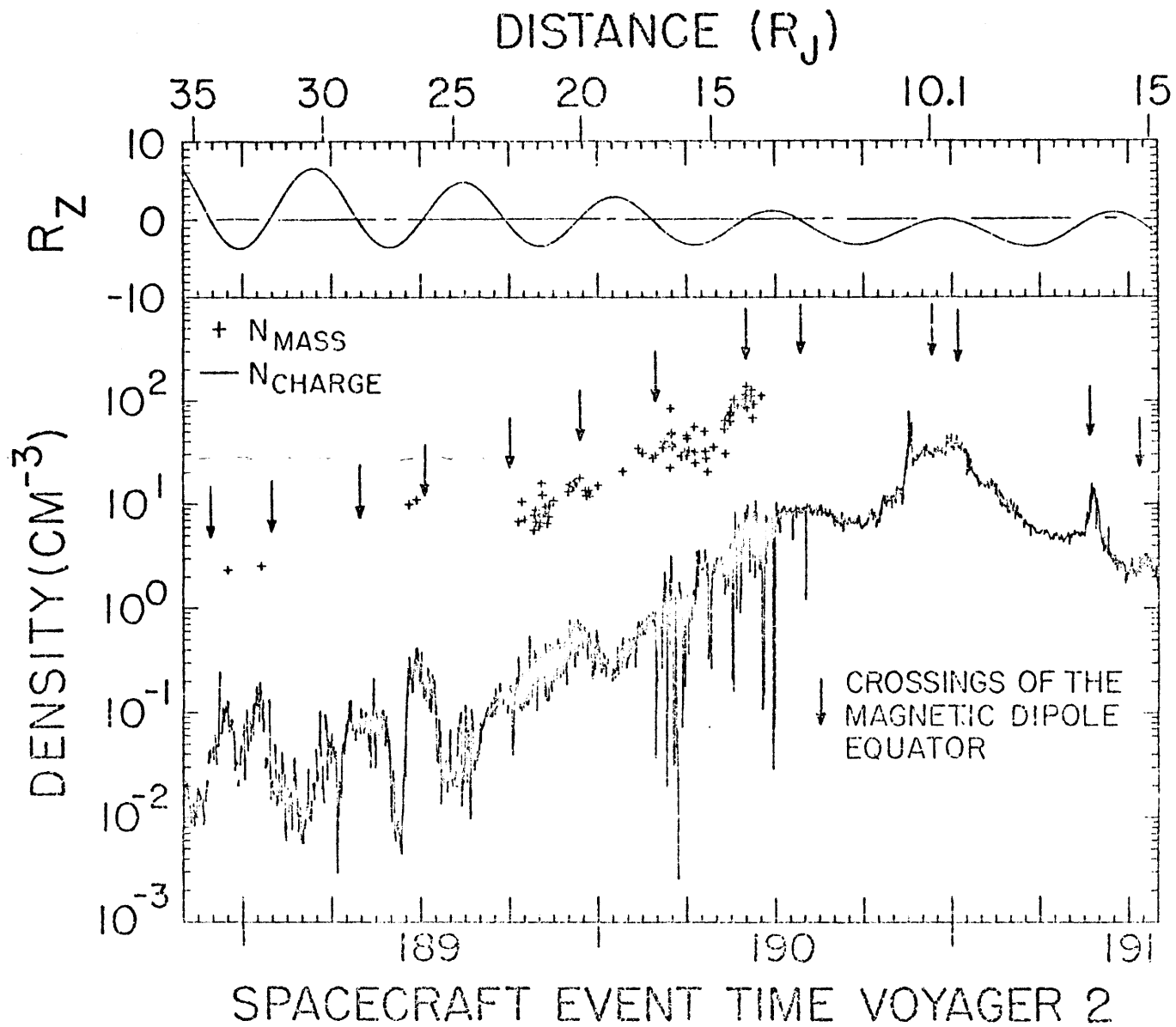


FIGURE 5

VOYAGER 1 INBOUND 19.8R<sub>J</sub>  
1979 63 1537:35.085

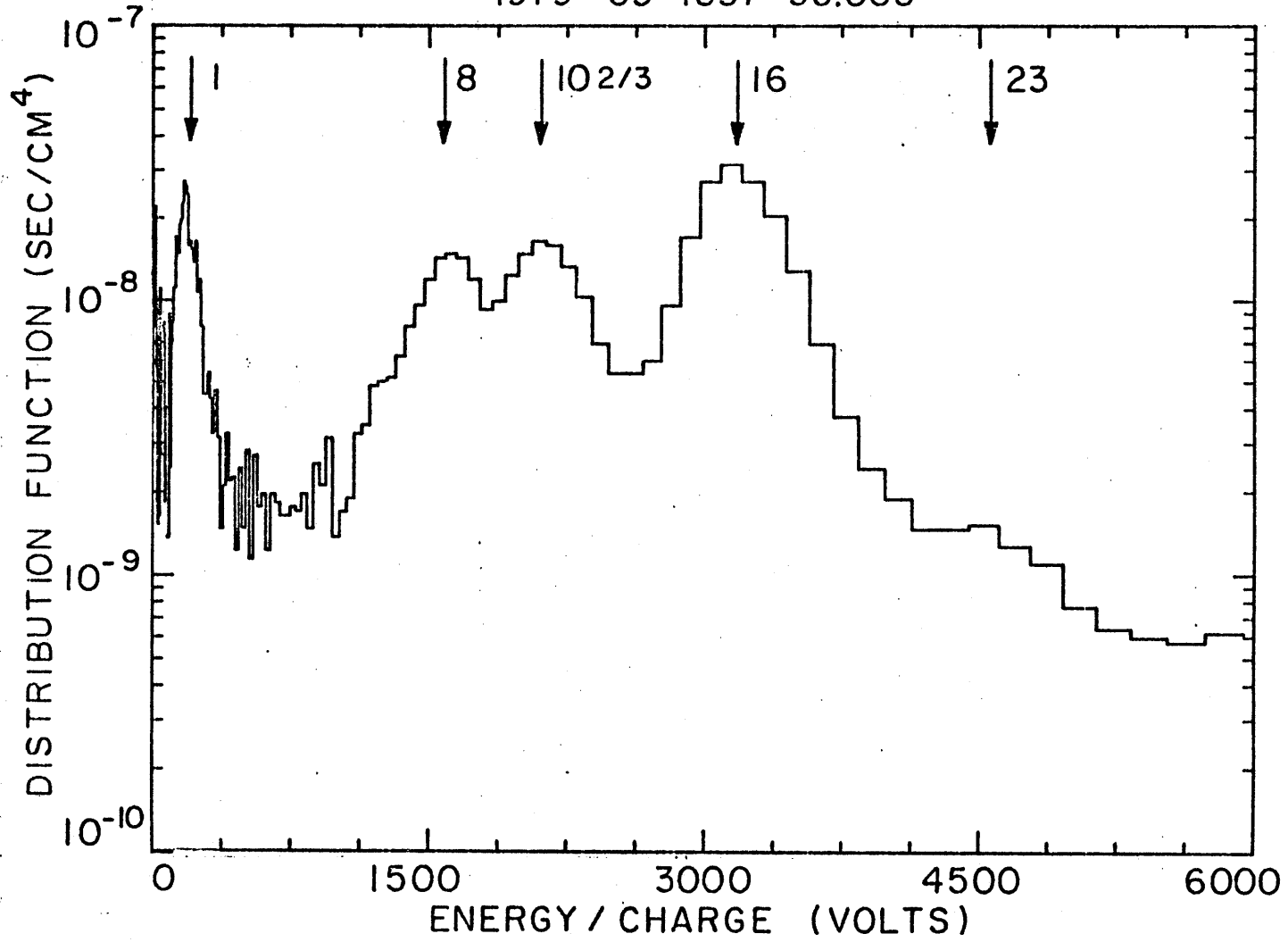


FIGURE 6

1979 63 1537:35.085

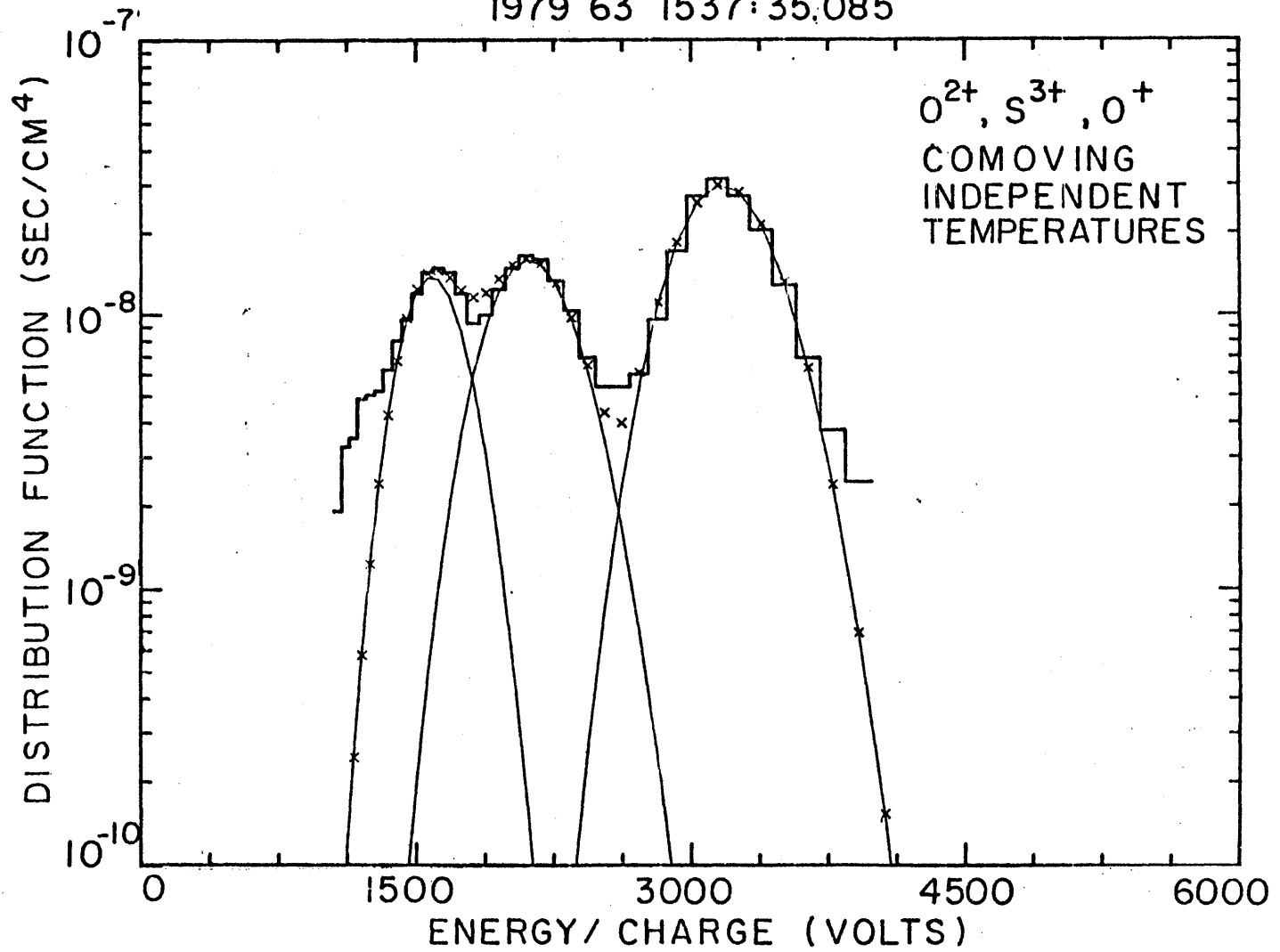


FIGURE 7

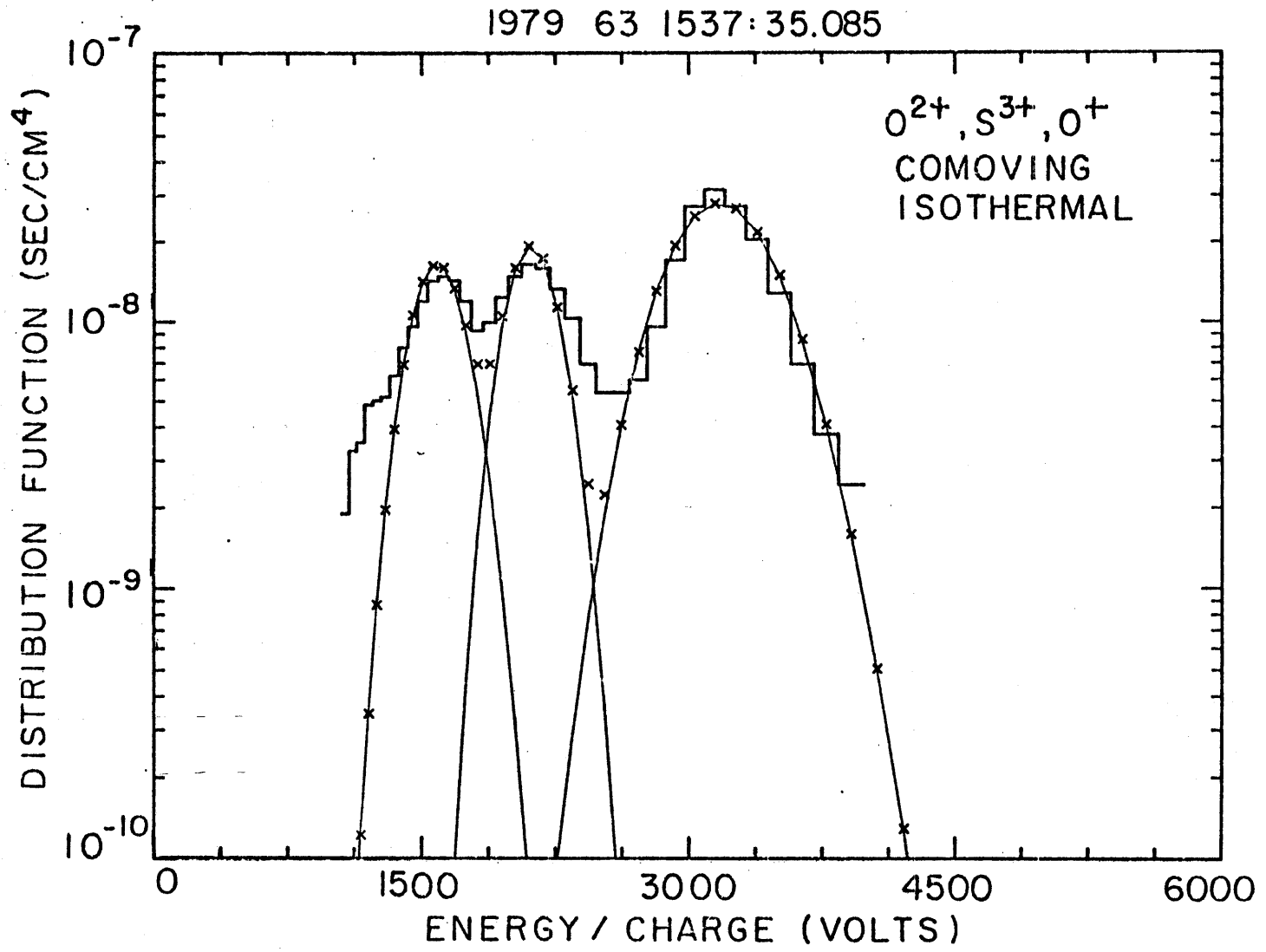


FIGURE 8

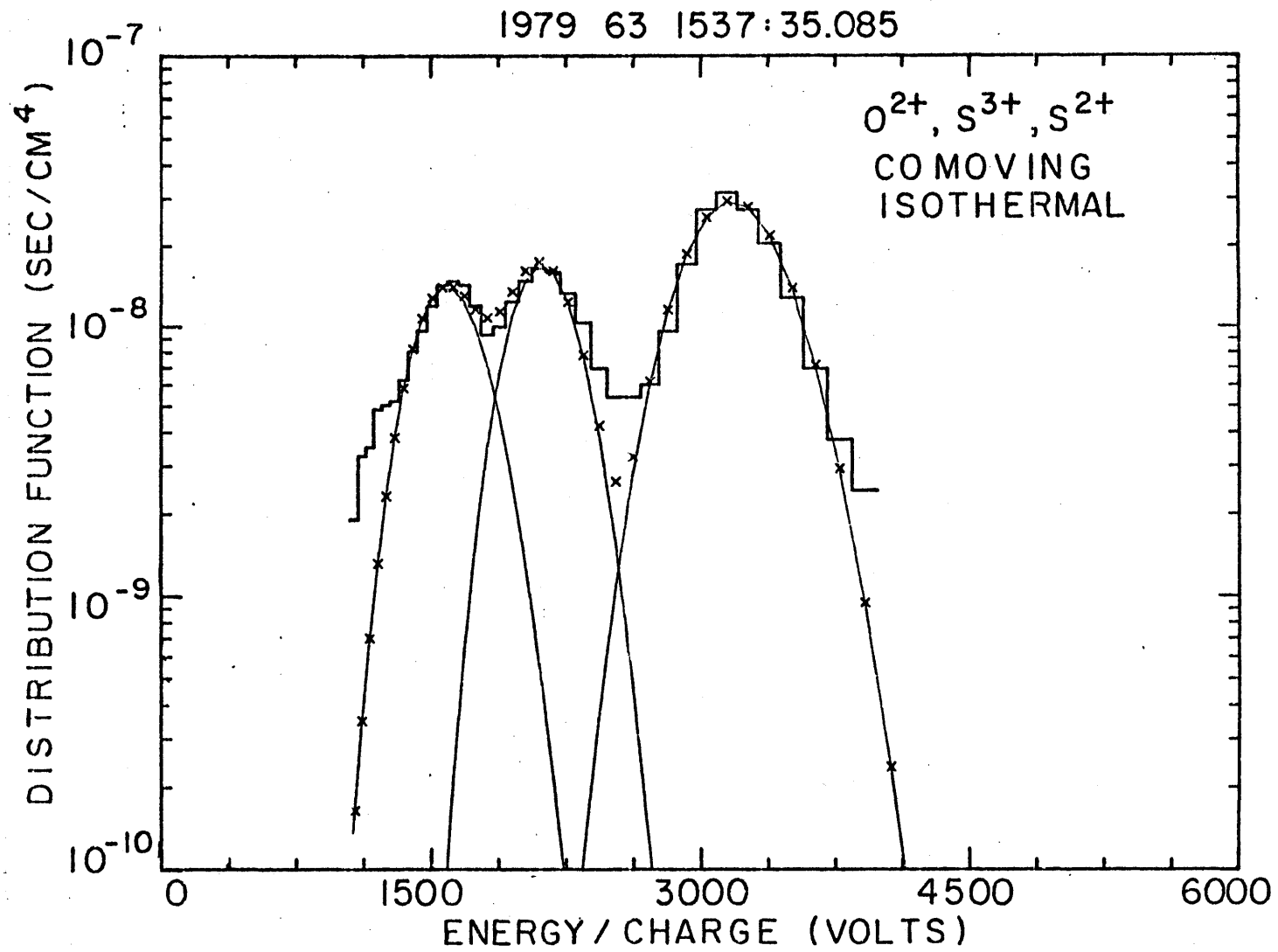


FIGURE 9

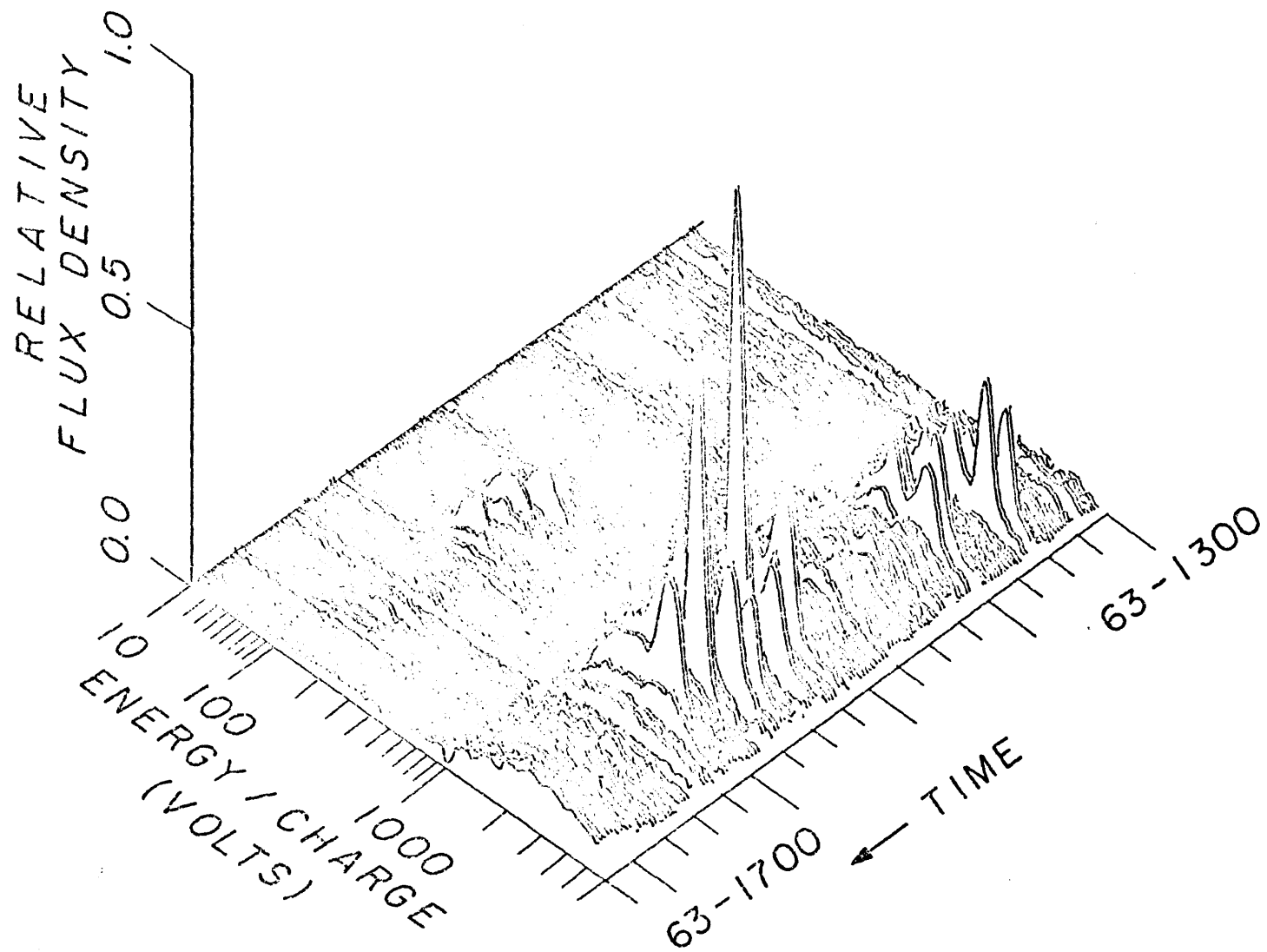


FIGURE 10

# L-MODE SPLINE

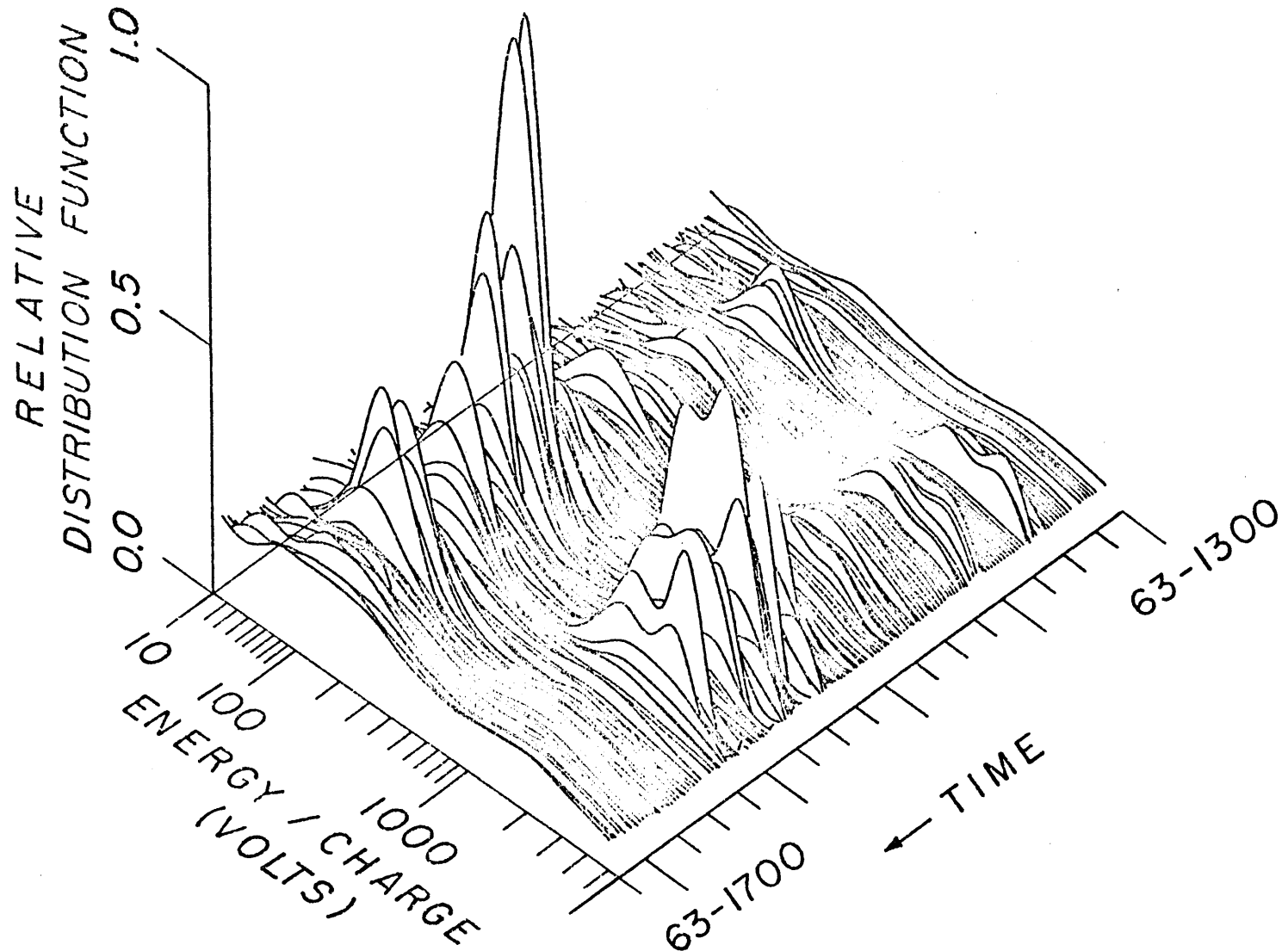


FIGURE 11

VOYAGER 1 INBOUND 19.8 R<sub>J</sub>  
1979 63 1538:36.524

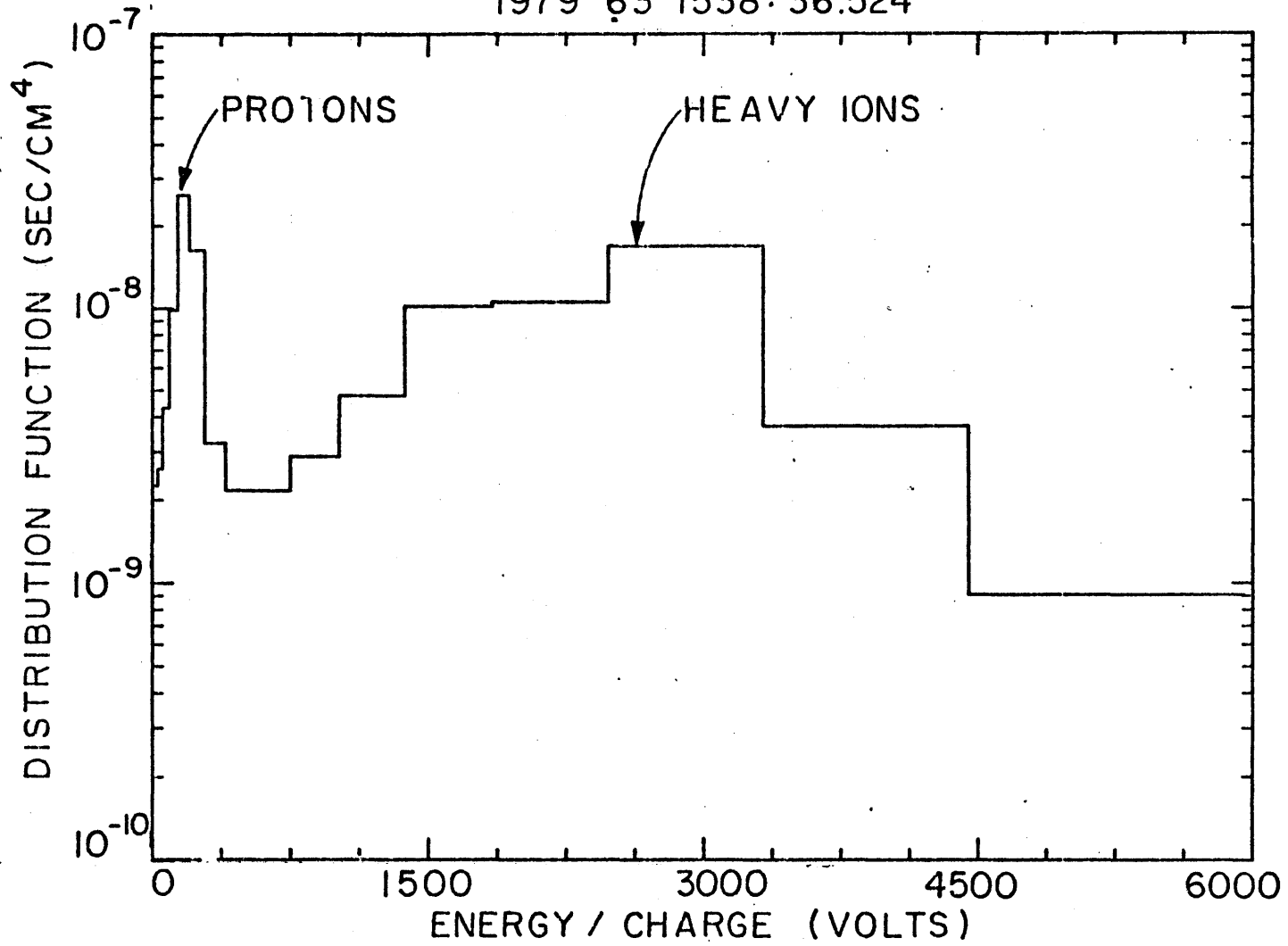


FIGURE 12

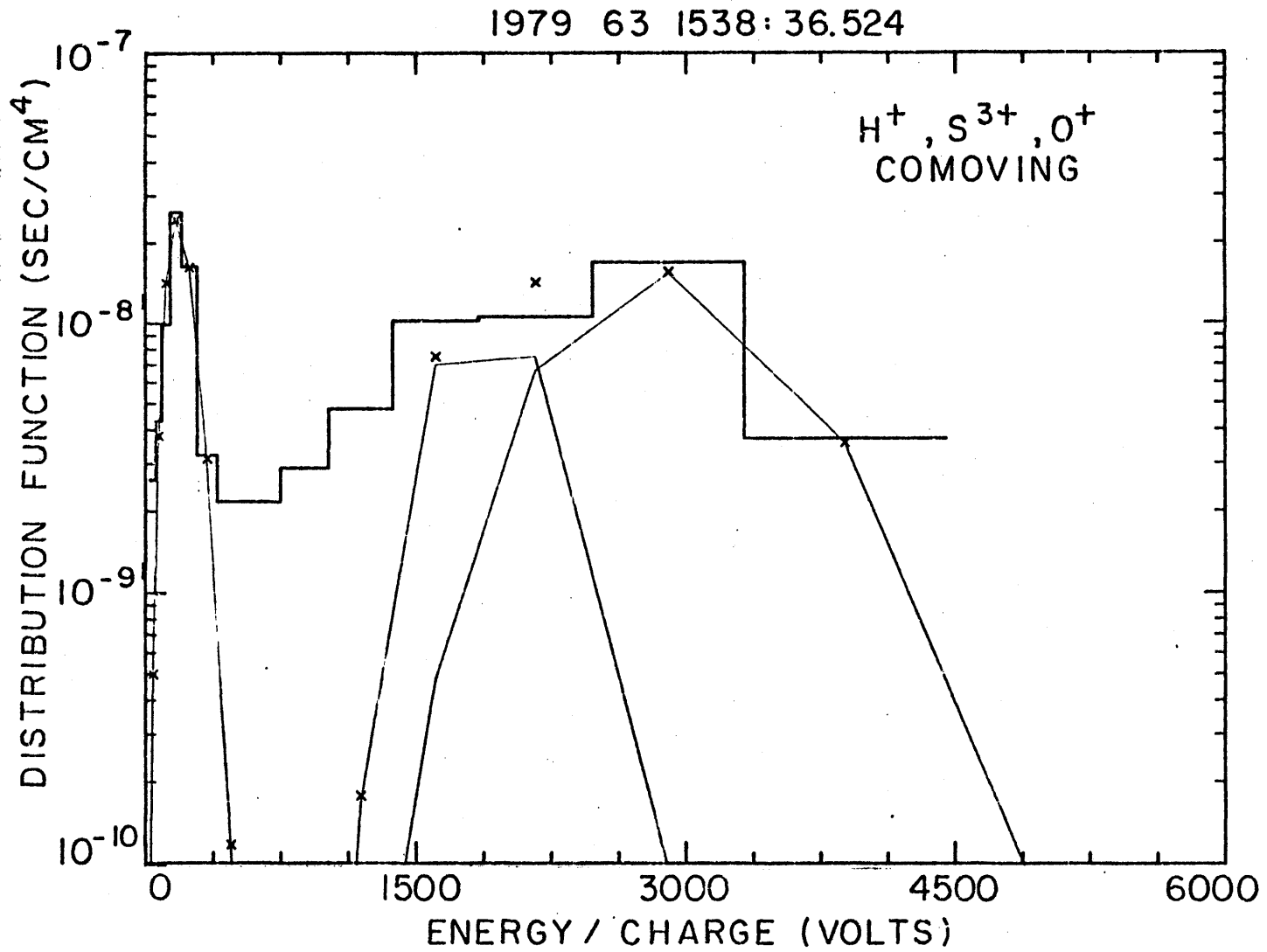


FIGURE 13

1979 63 1538:36.524

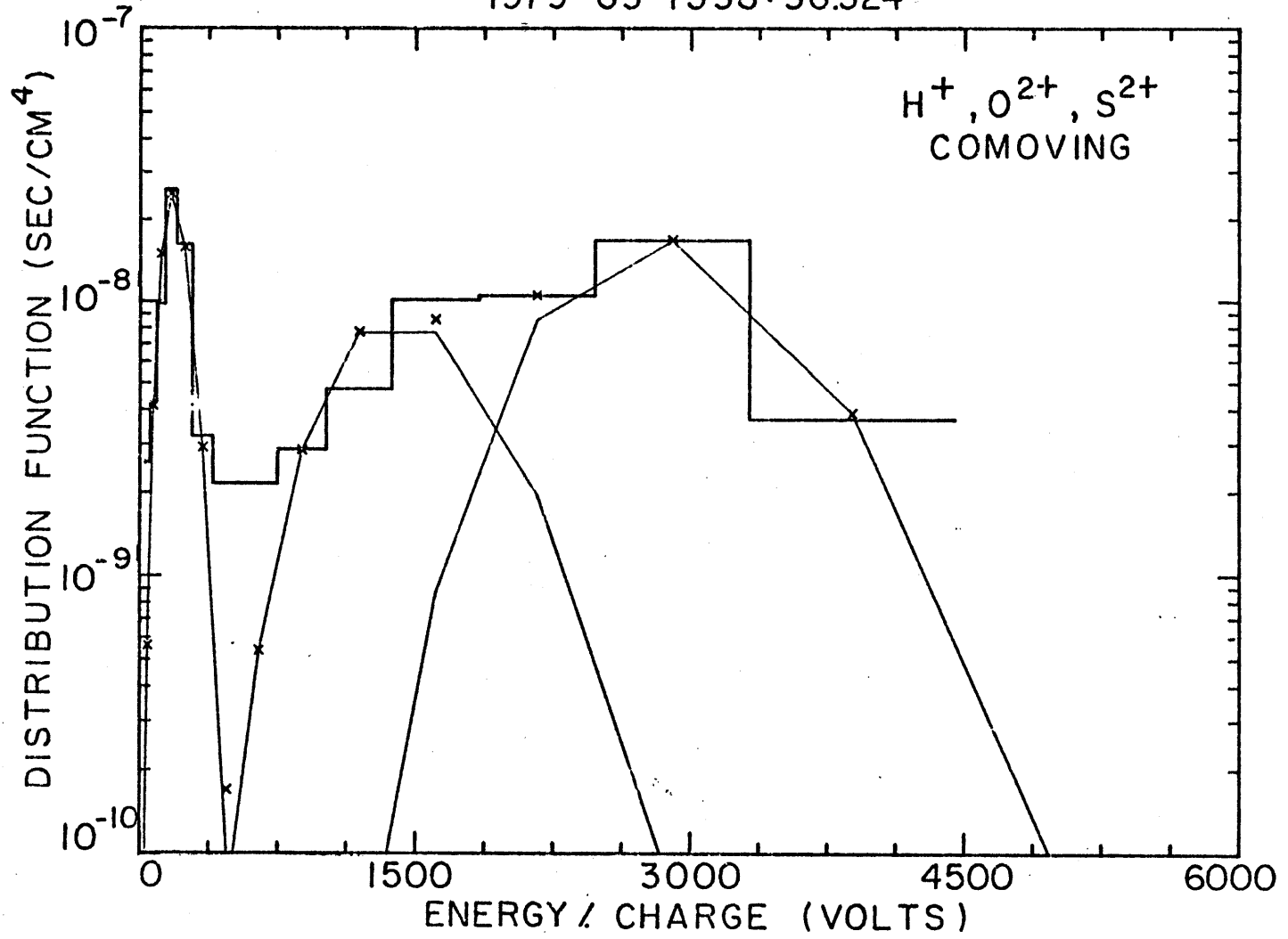


FIGURE 14

1979 63 1538:36.524

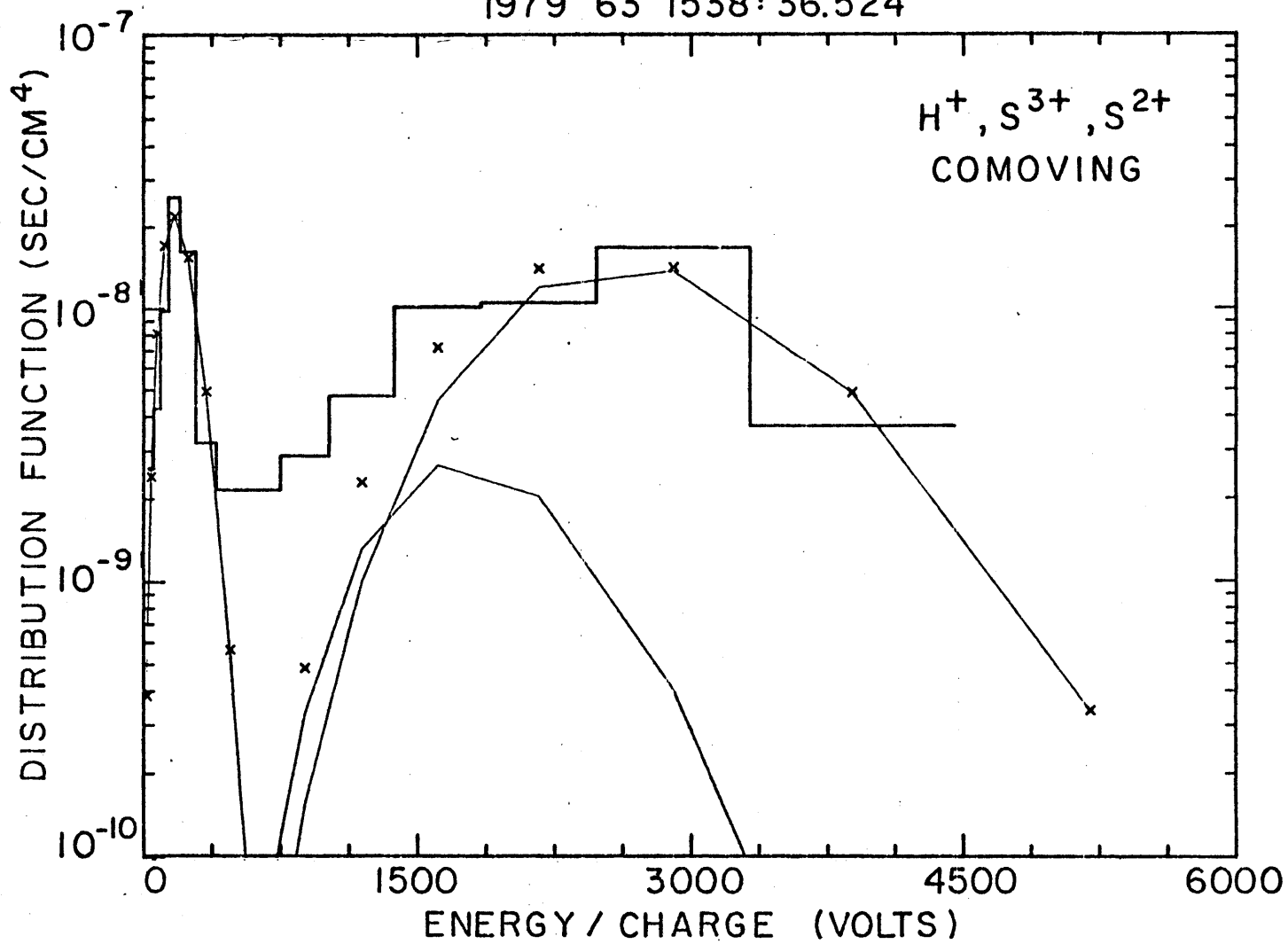


FIGURE 15

VOYAGER 1 INBOUND 41.2 R<sub>J</sub>  
1979 62 1027:11.065

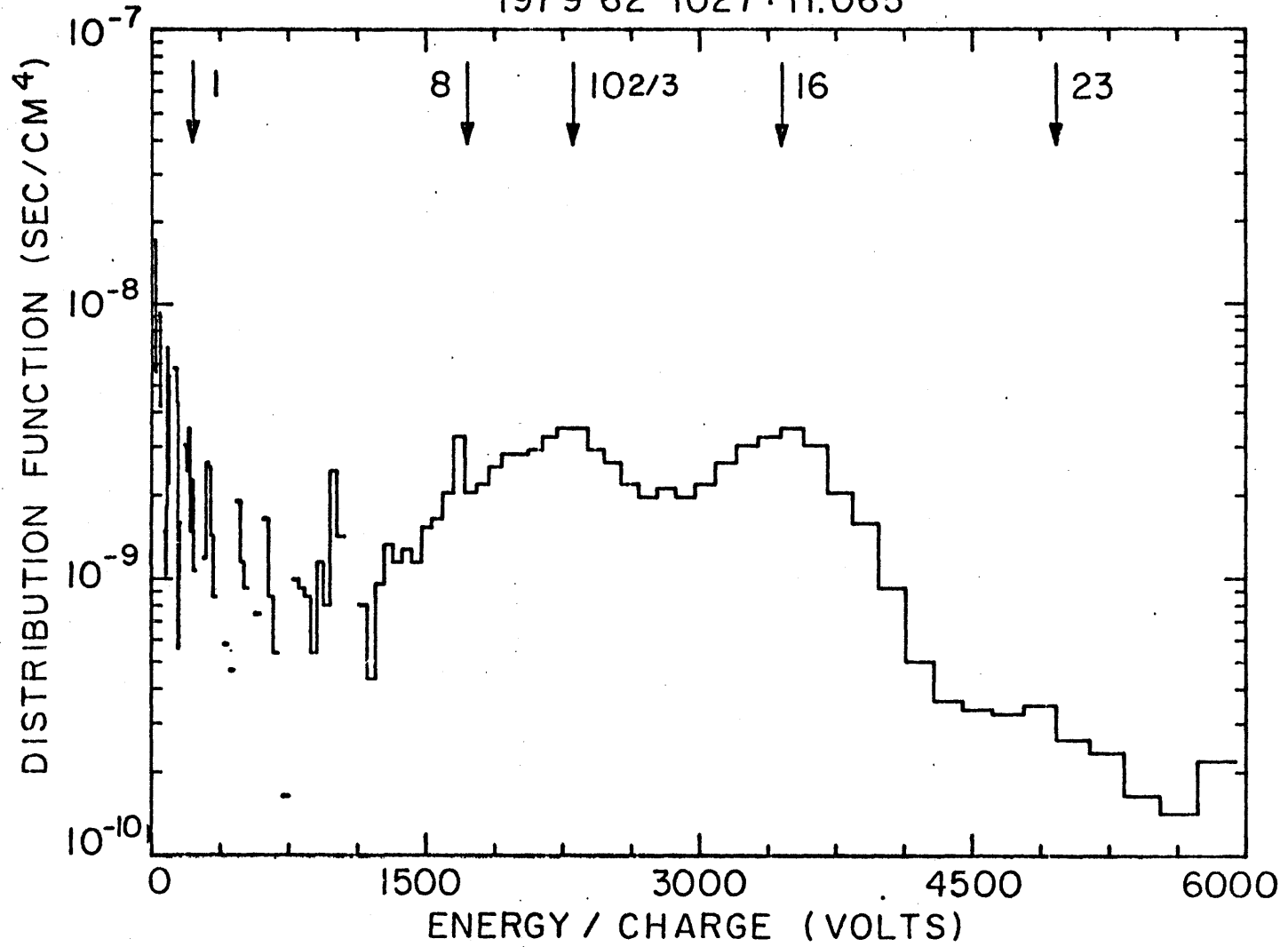


FIGURE 16

VOYAGER 1 INBOUND 41.2 R<sub>J</sub>  
1979 62 1026:36.504

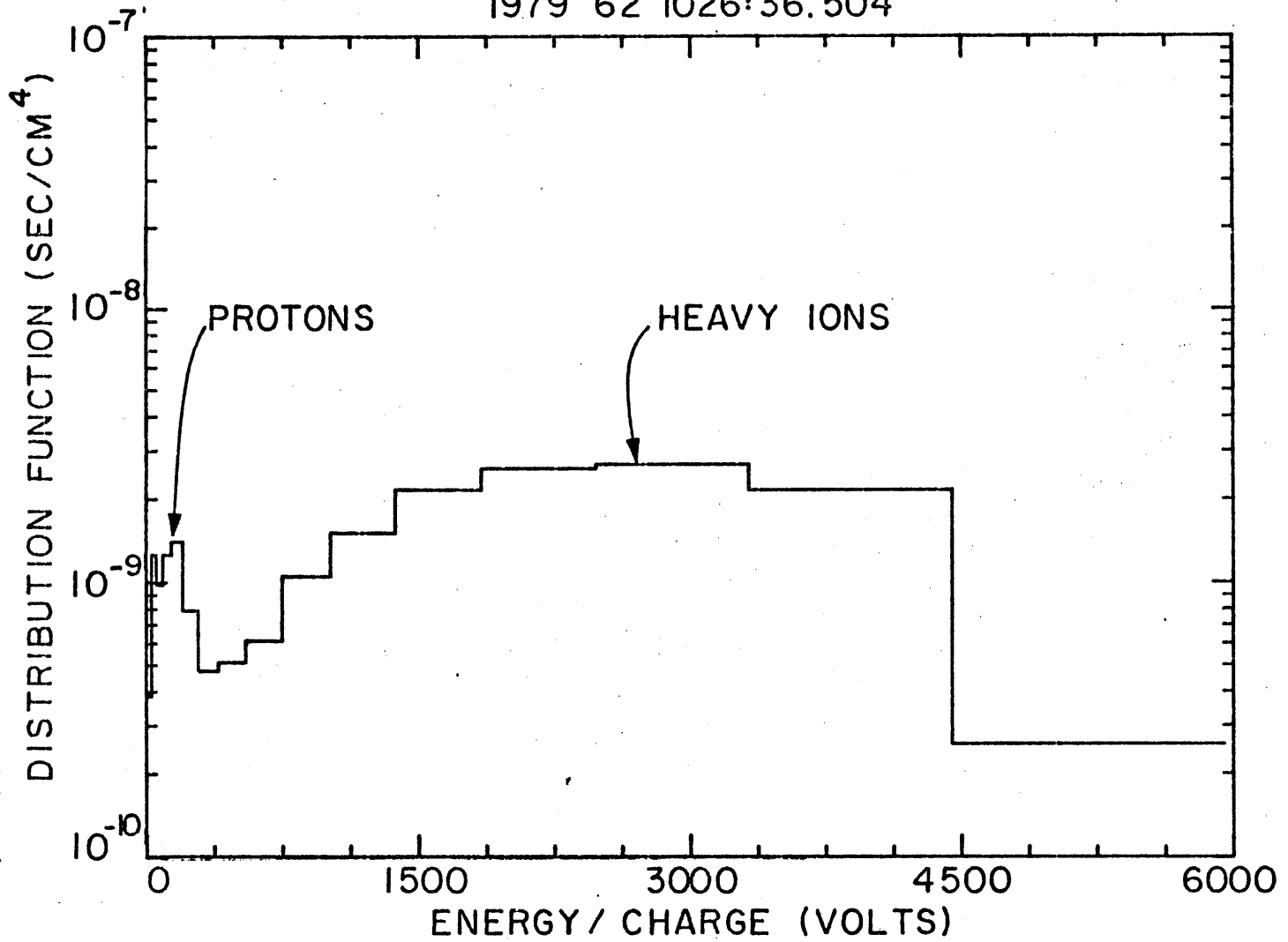


FIGURE 17

VOYAGER 2 INBOUND 22.0 R<sub>J</sub>  
1979 189 1921:46.110

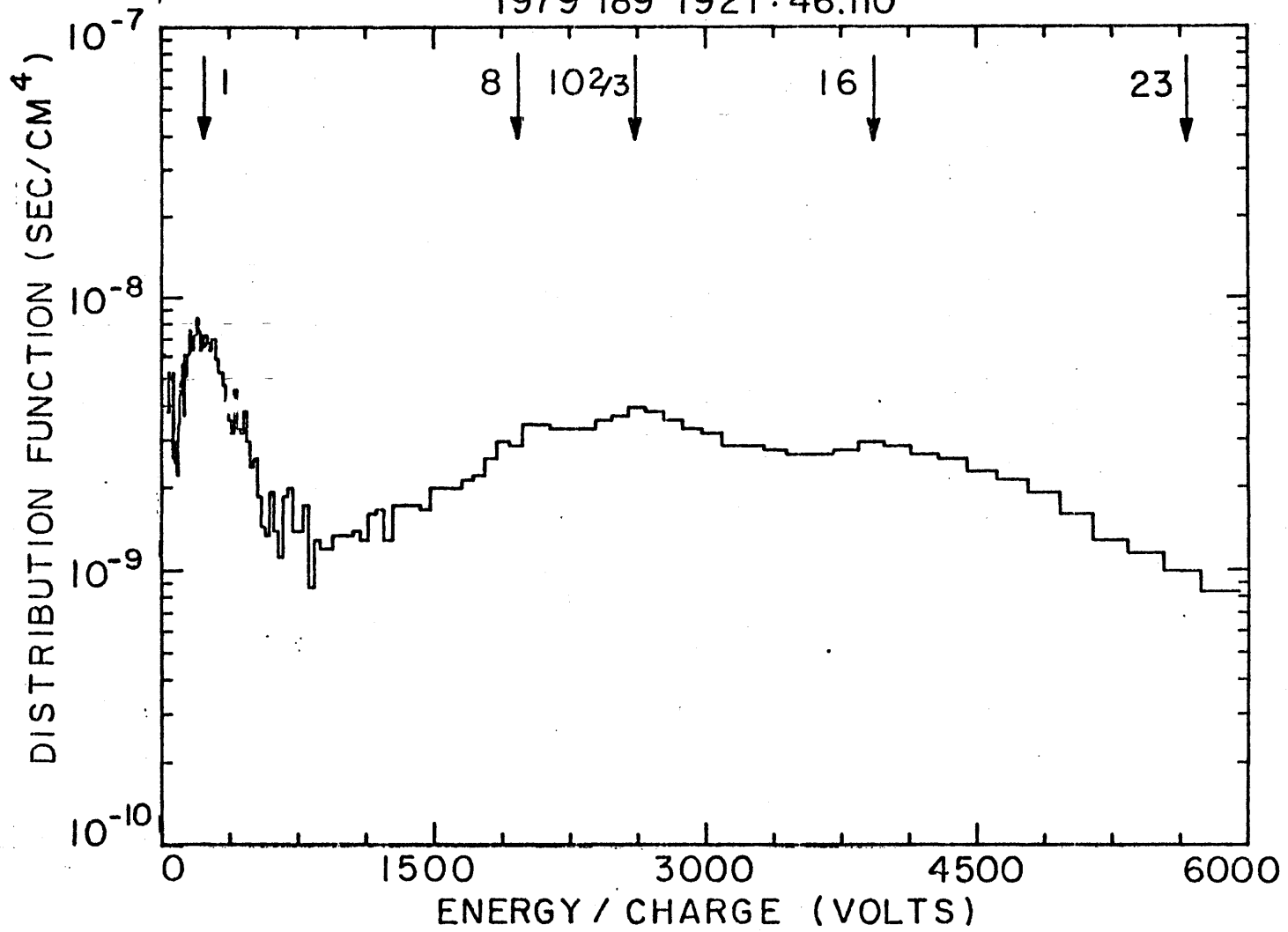


FIGURE 18

1979 189 1921:06.110

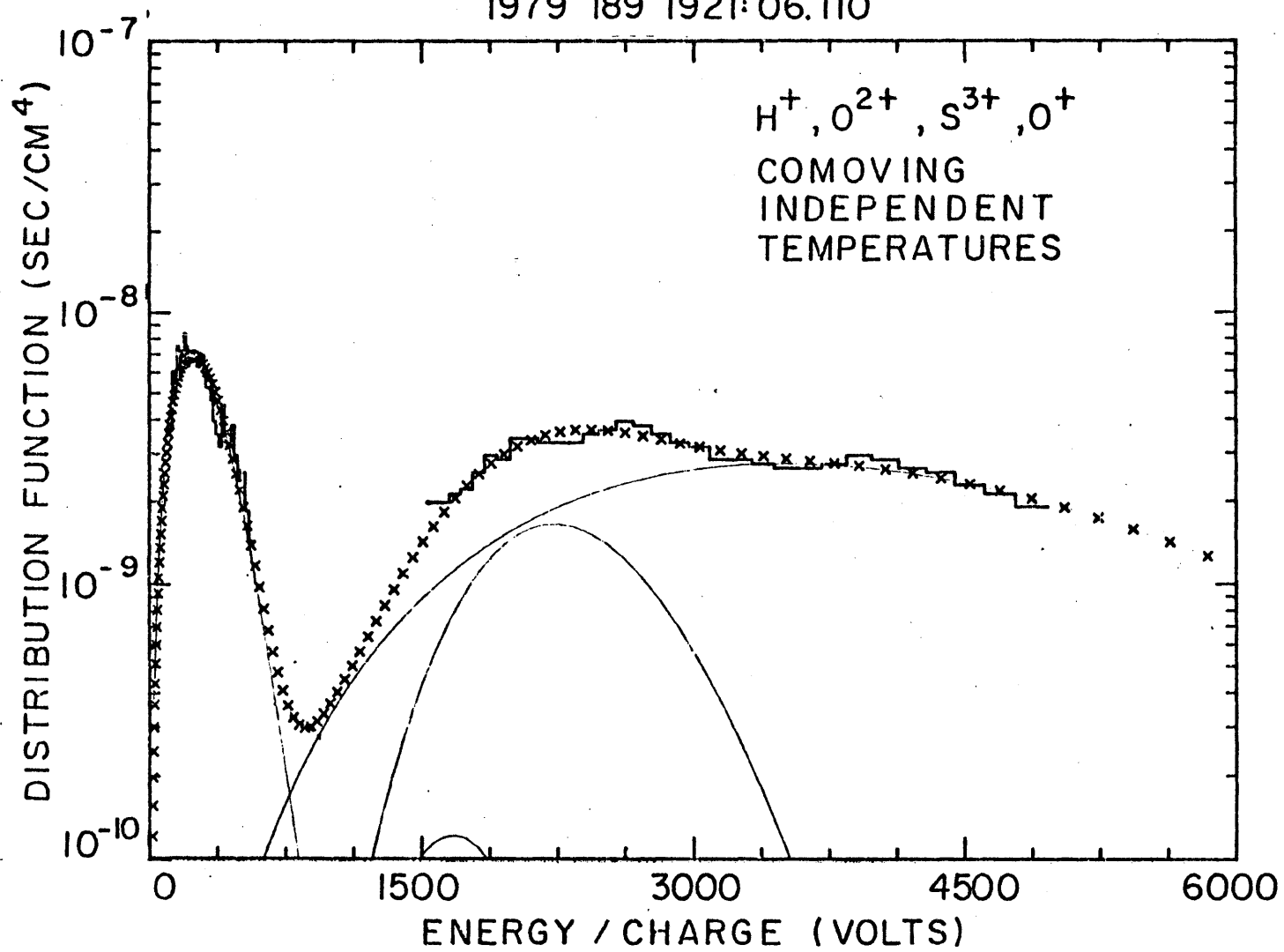


FIGURE 19

VOYAGER 2 INBOUND 16.5 R<sub>J</sub>  
1979 189 1921: 11.549

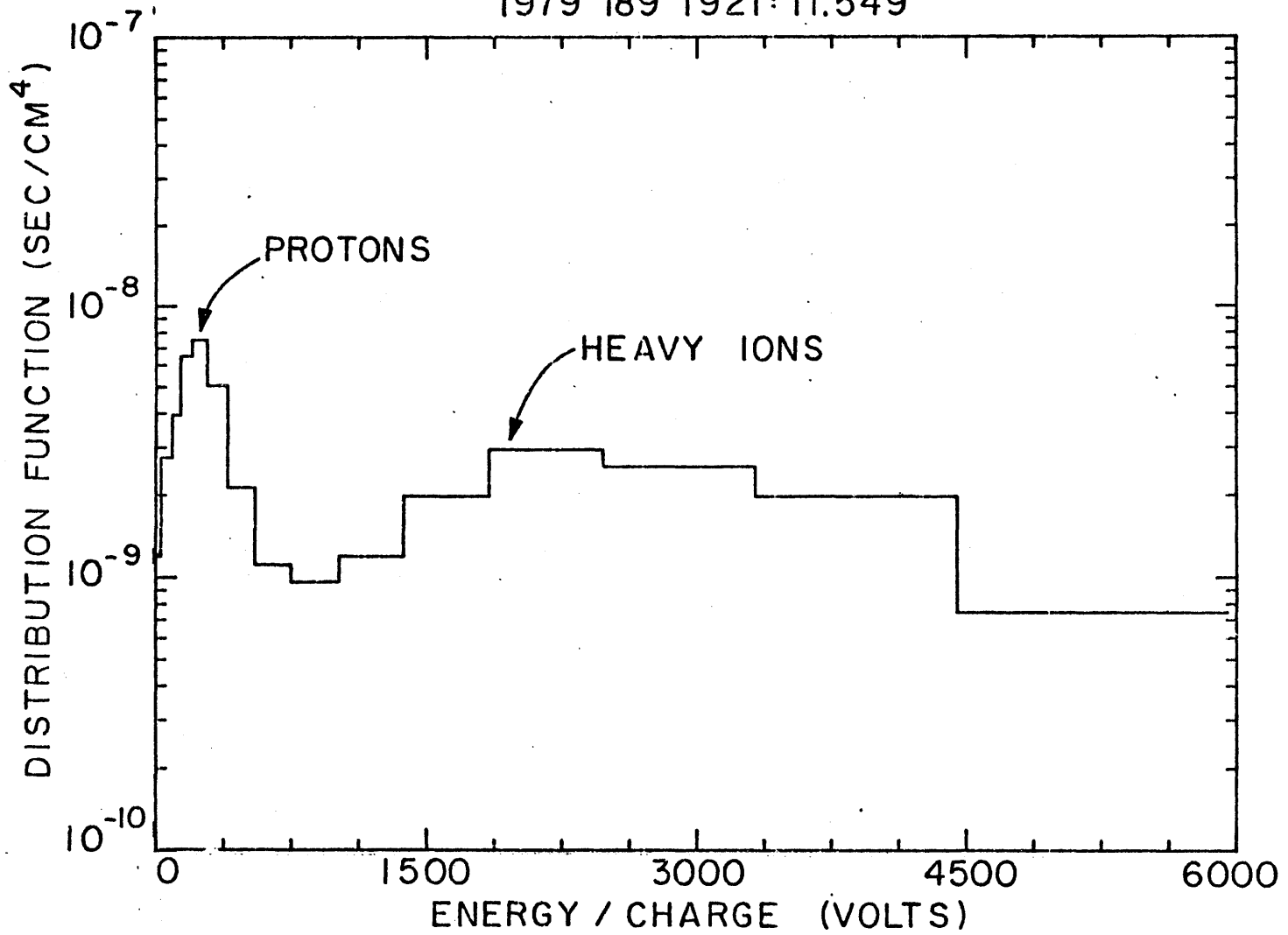


FIGURE 20

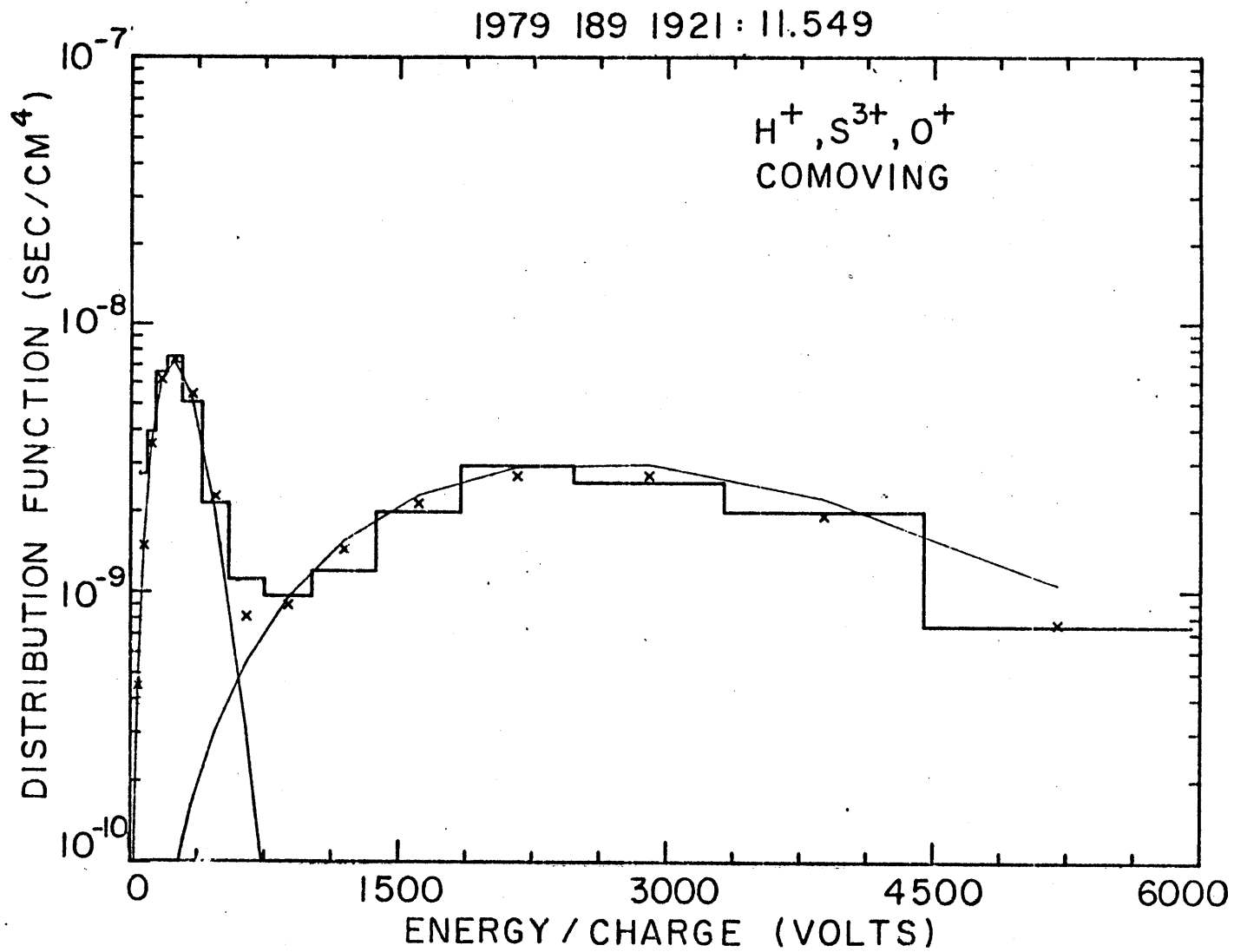


FIGURE 21

VOYAGER 2 INBOUND 16.5 R<sub>J</sub>  
1979 190 0454:34.085

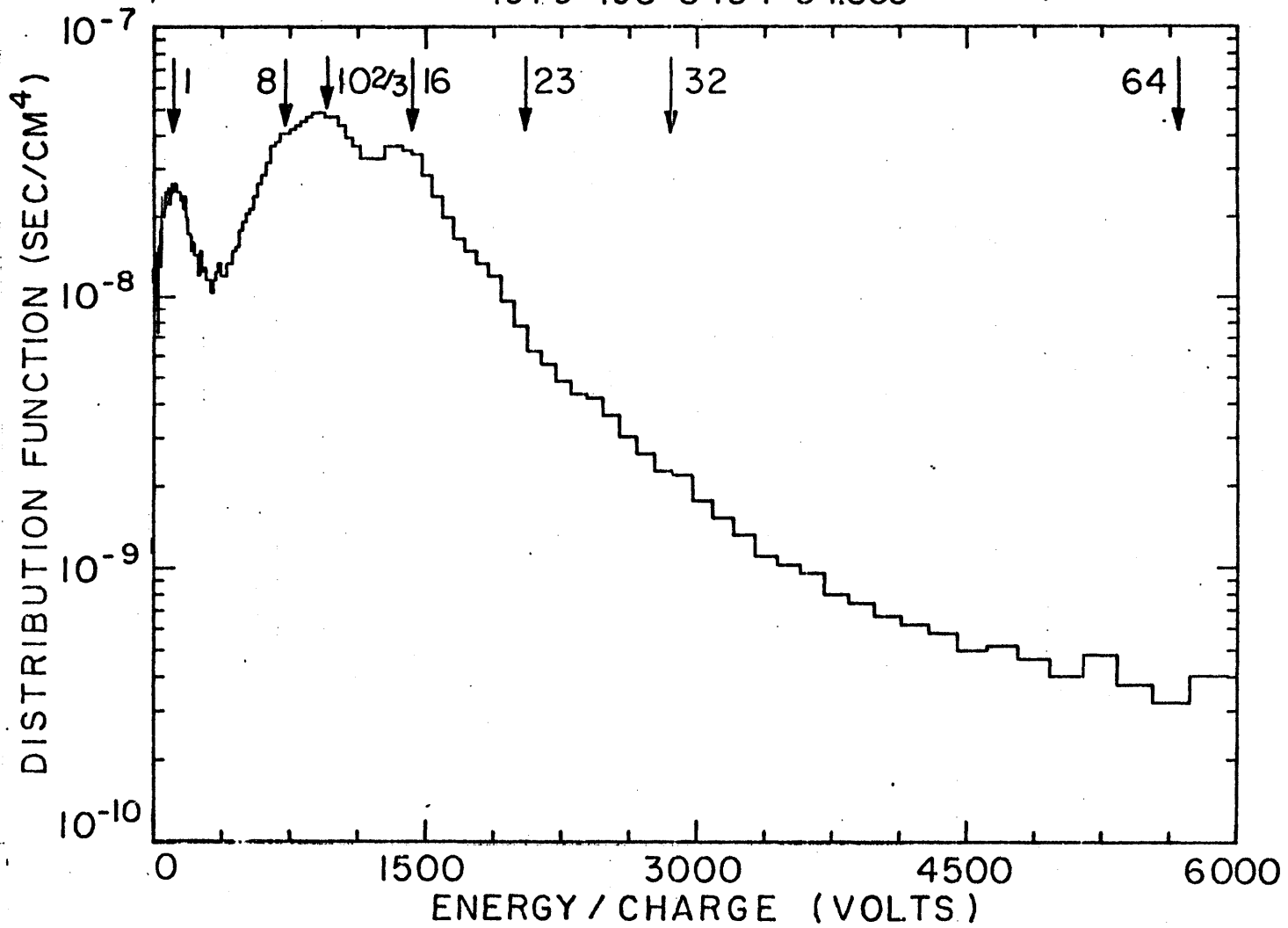


FIGURE 22

1979 190 0454:34.085

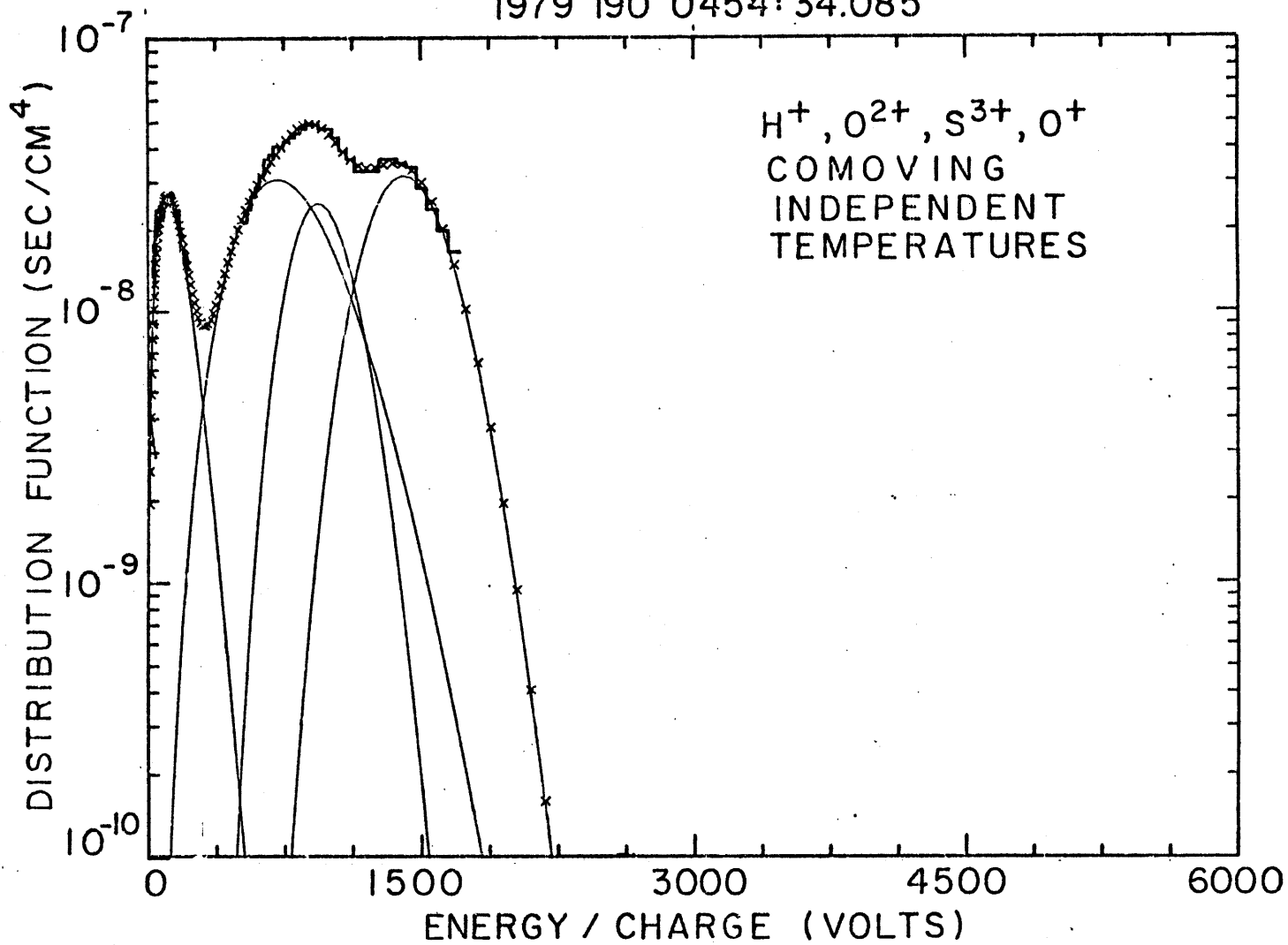


FIGURE 23

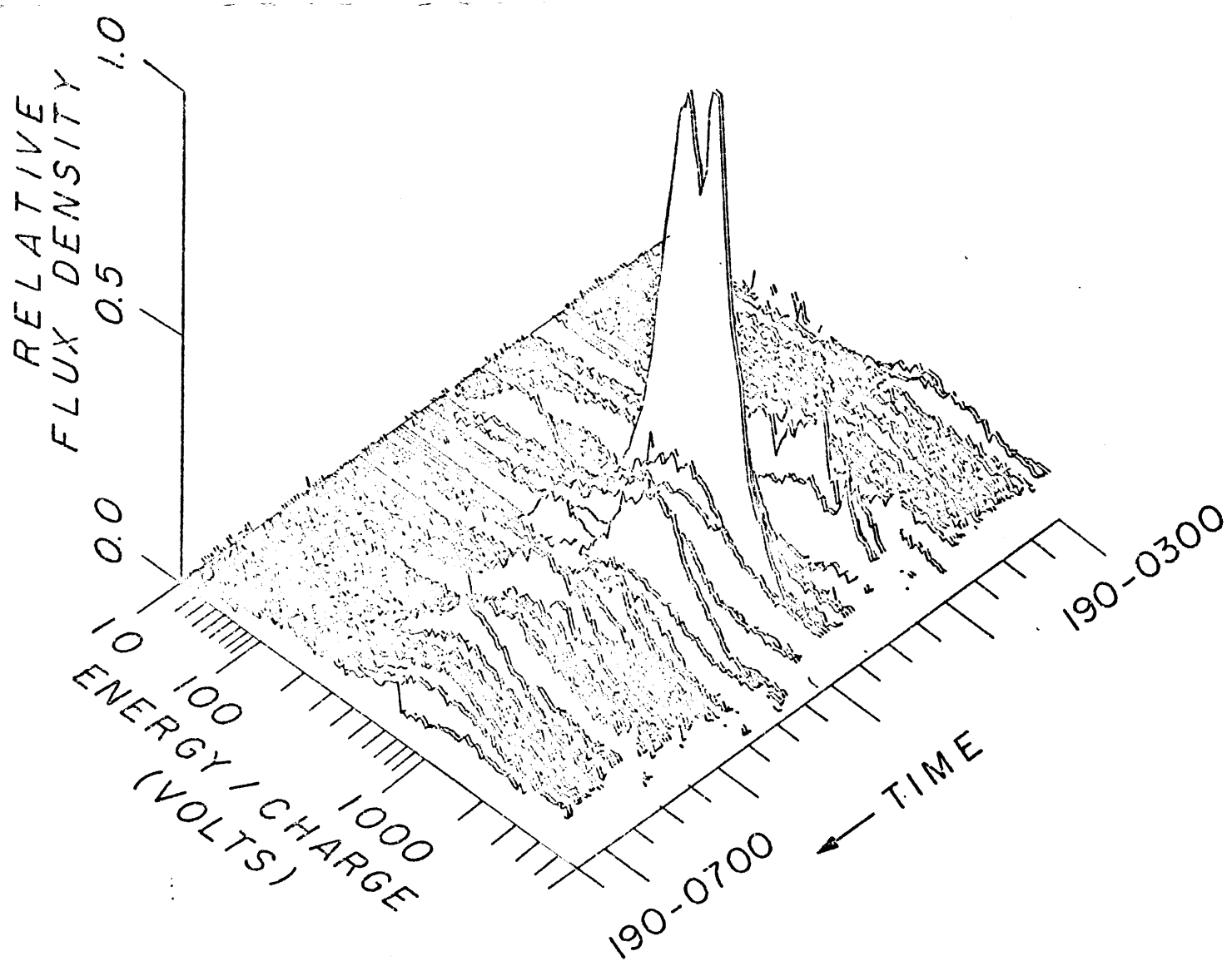


FIGURE 24

VOYAGER 2 INBOUND 16.5 R<sub>J</sub>  
1979 190 0453:59.524

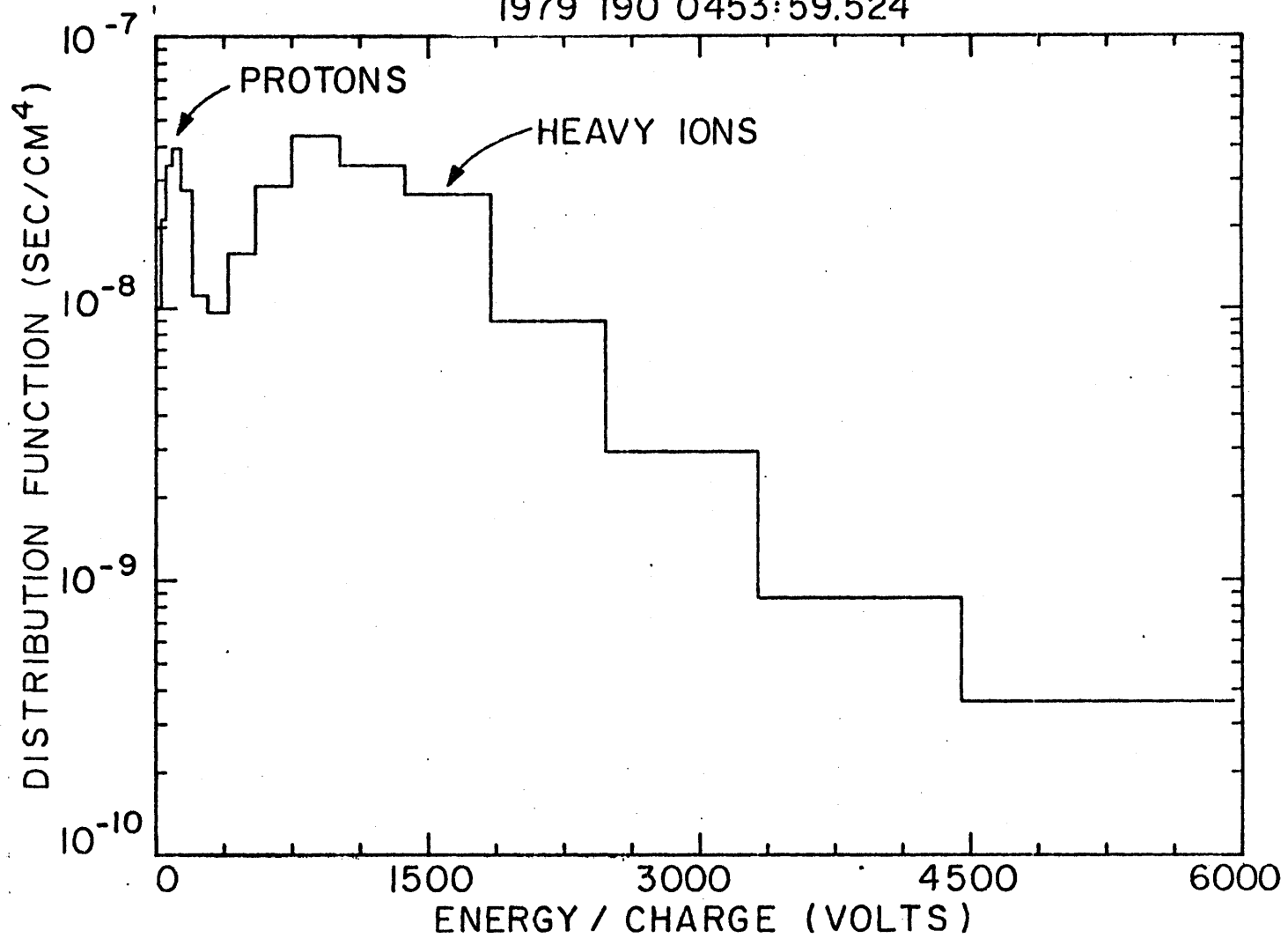


FIGURE 25

1979 190 0453:59.524

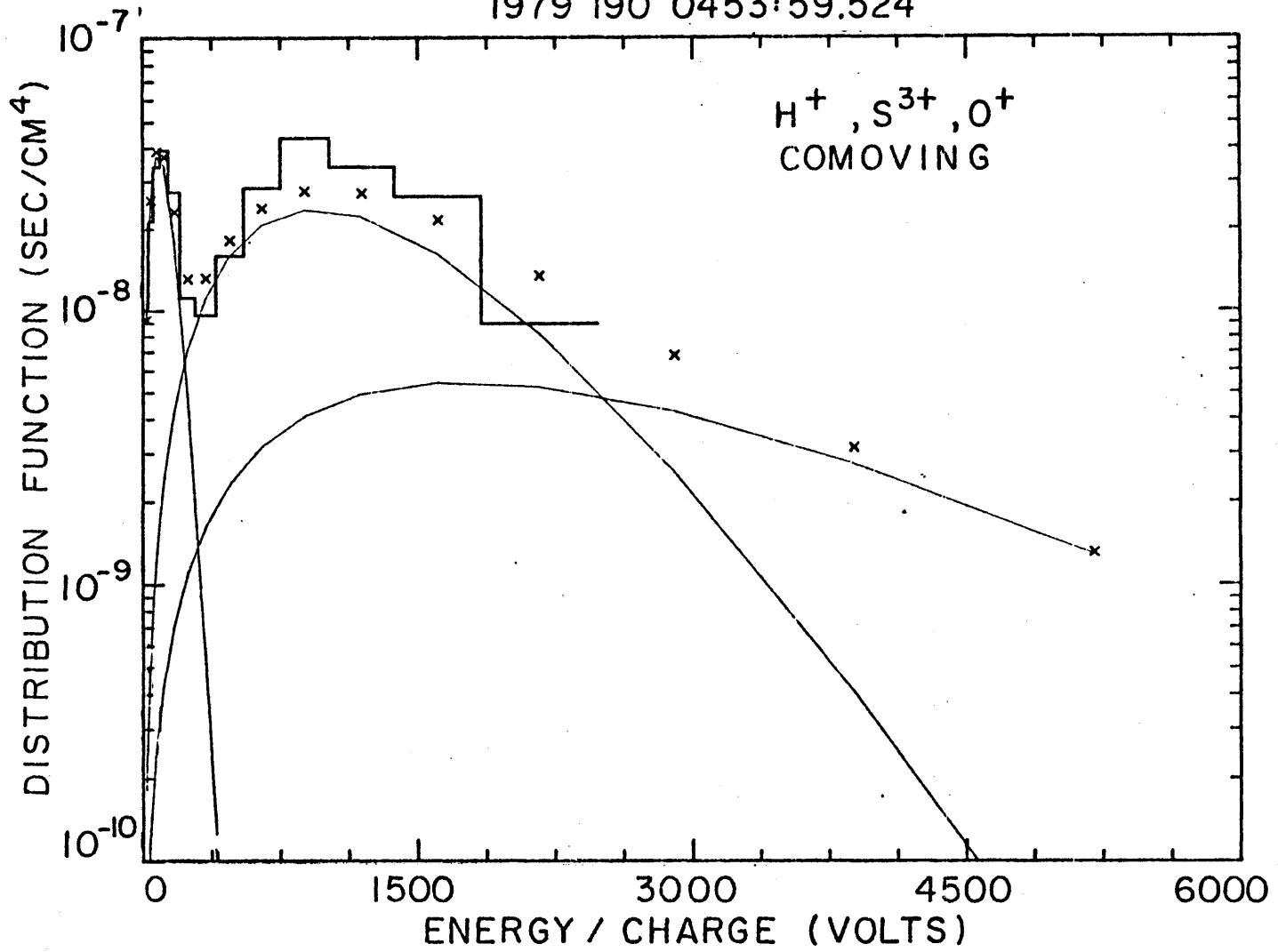


FIGURE 26

VOYAGER 2 INBOUND 16.5 R<sub>J</sub>

1979 190 0455:35.524

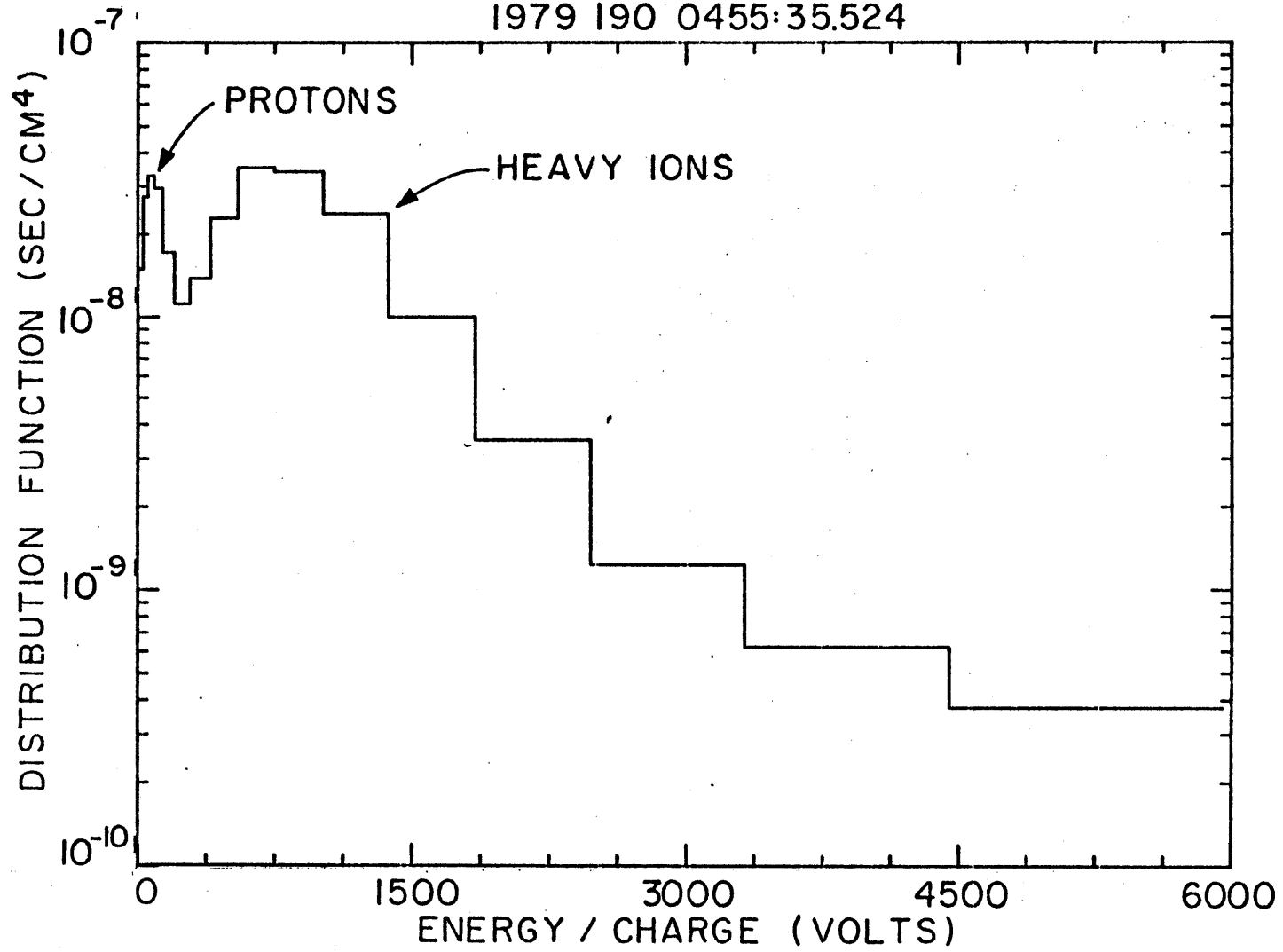


FIGURE 27

1979 190 0455:35.524

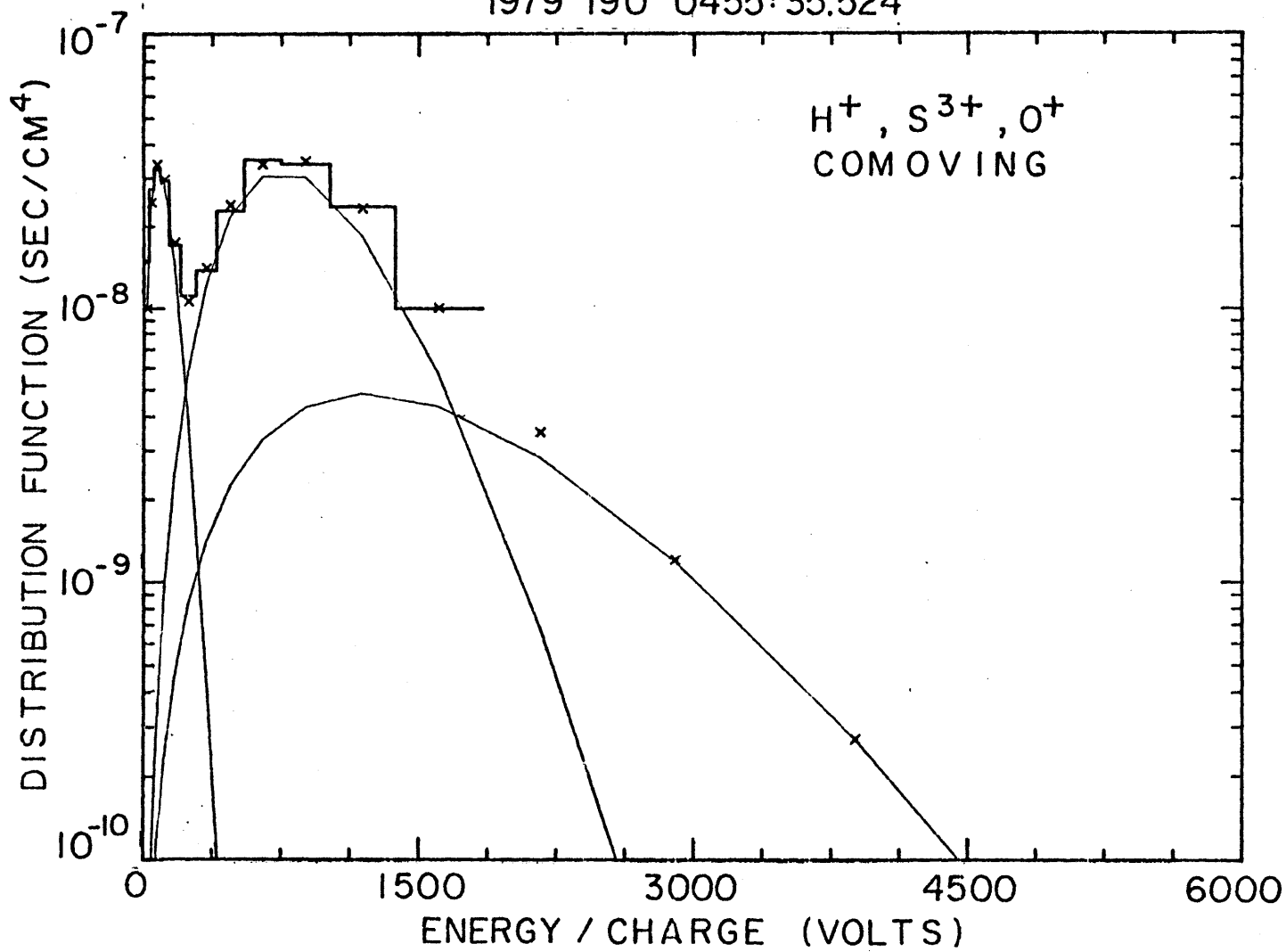


FIGURE 28

VOYAGER 1 INBOUND 16.5 R<sub>J</sub>  
1979 63 1943:59.003

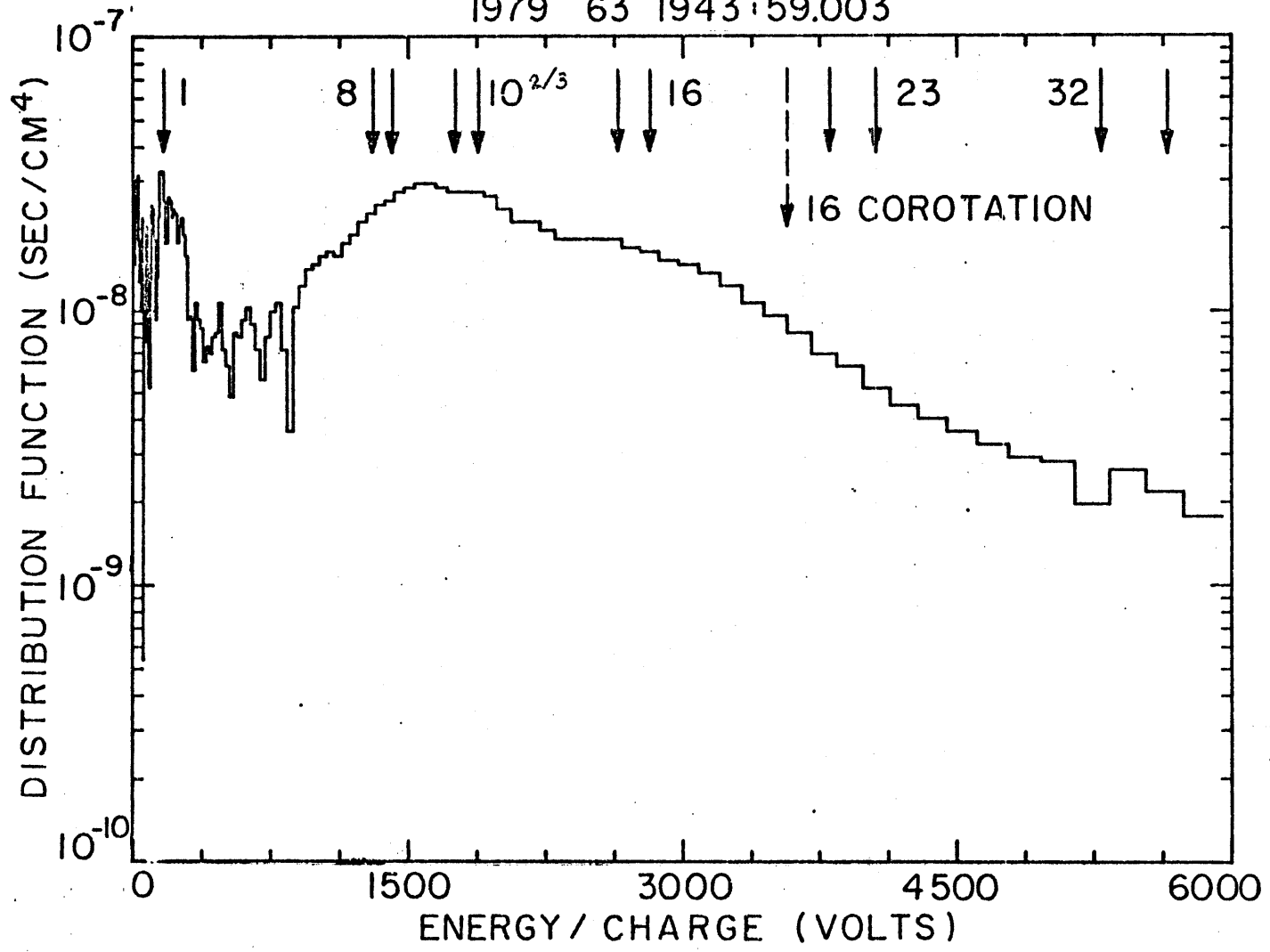


FIGURE 29

1979 63 1943:59.003

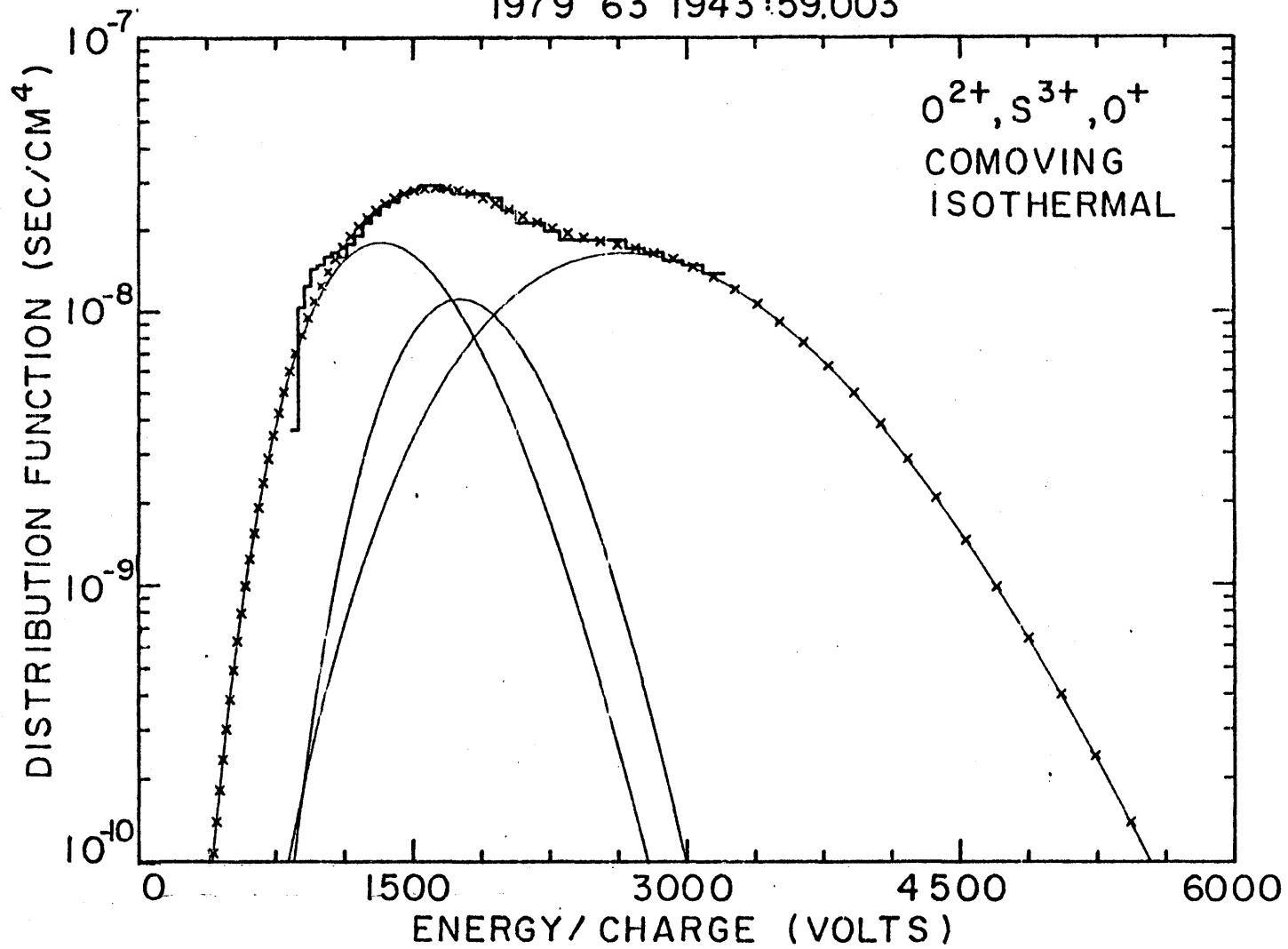


FIGURE 30

1979 63 1943:59.003

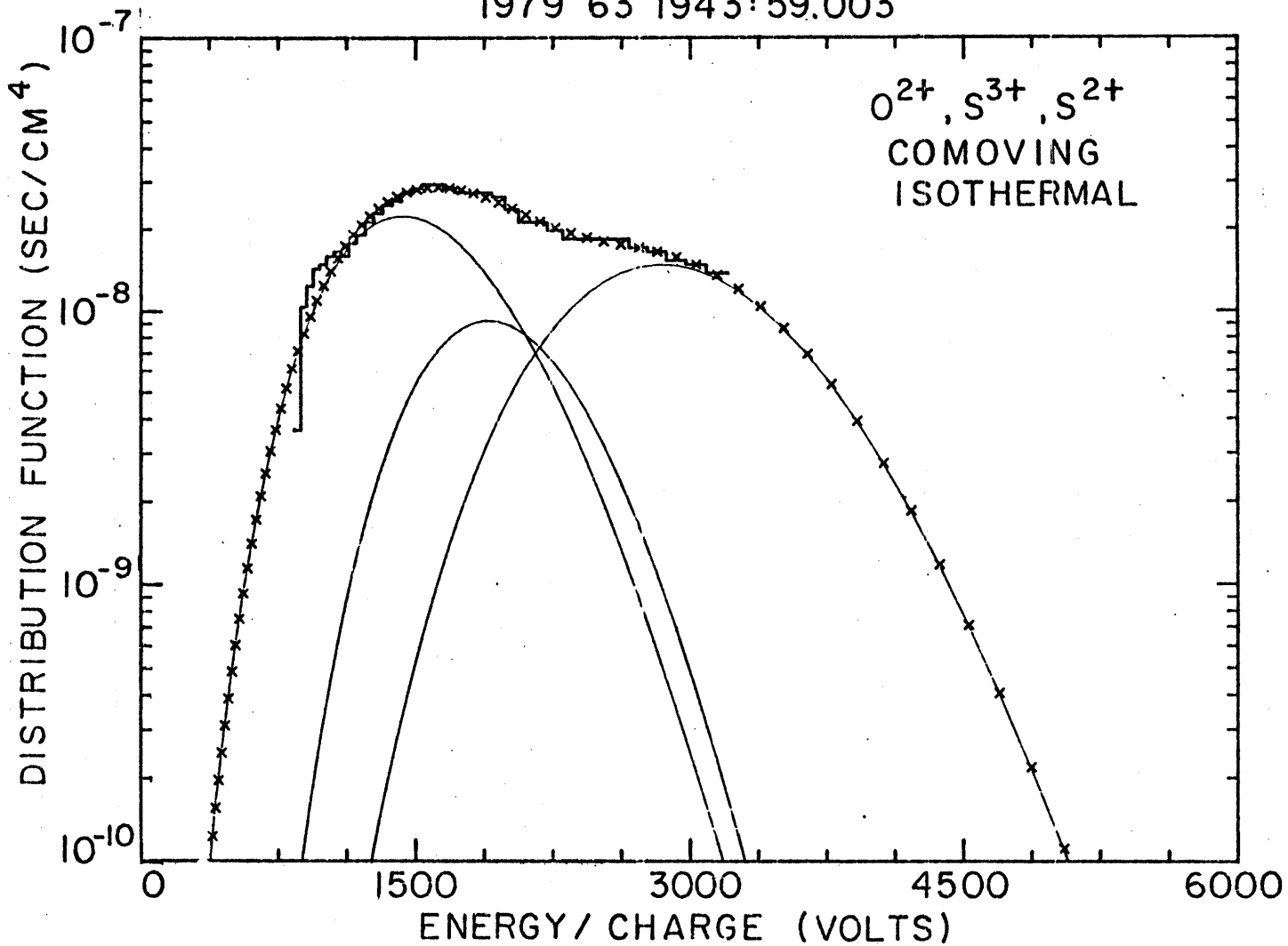


FIGURE 31

VOYAGER 1 INBOUND 16.5 R<sub>J</sub>  
1979 63 1943:24.442

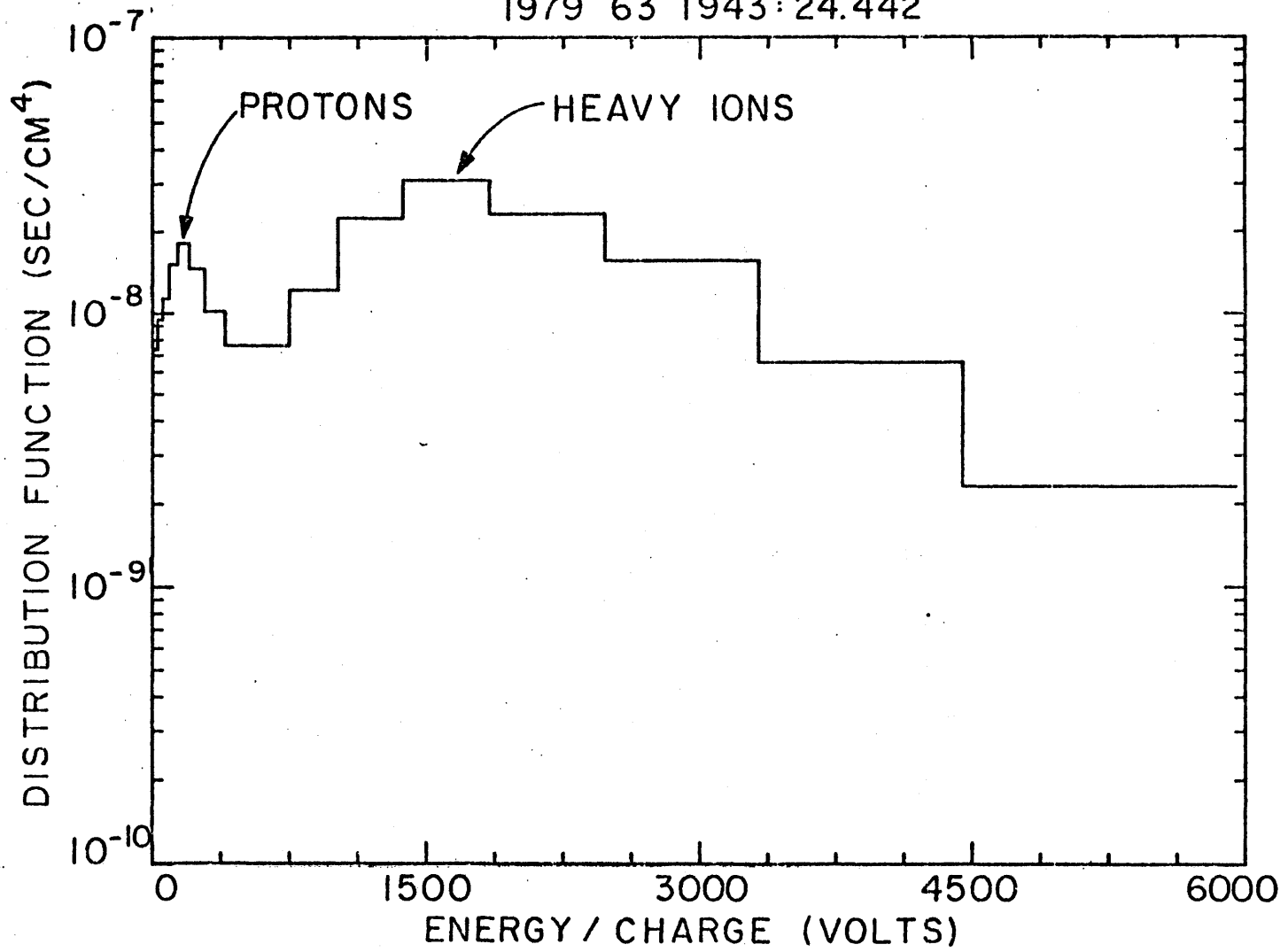


FIGURE 32

1979 63 1943:24.442

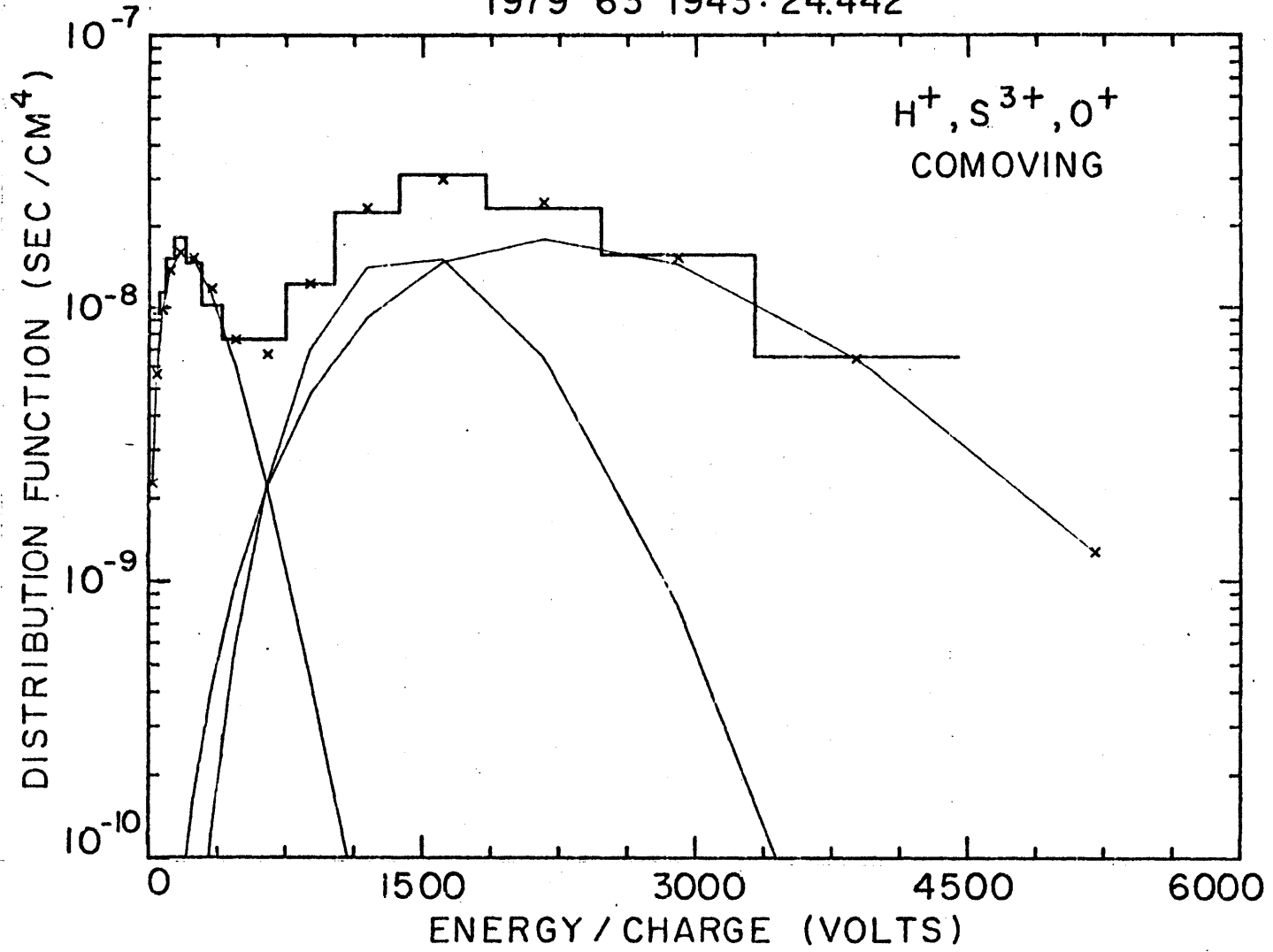


FIGURE 33

1979 63 1943:24.442

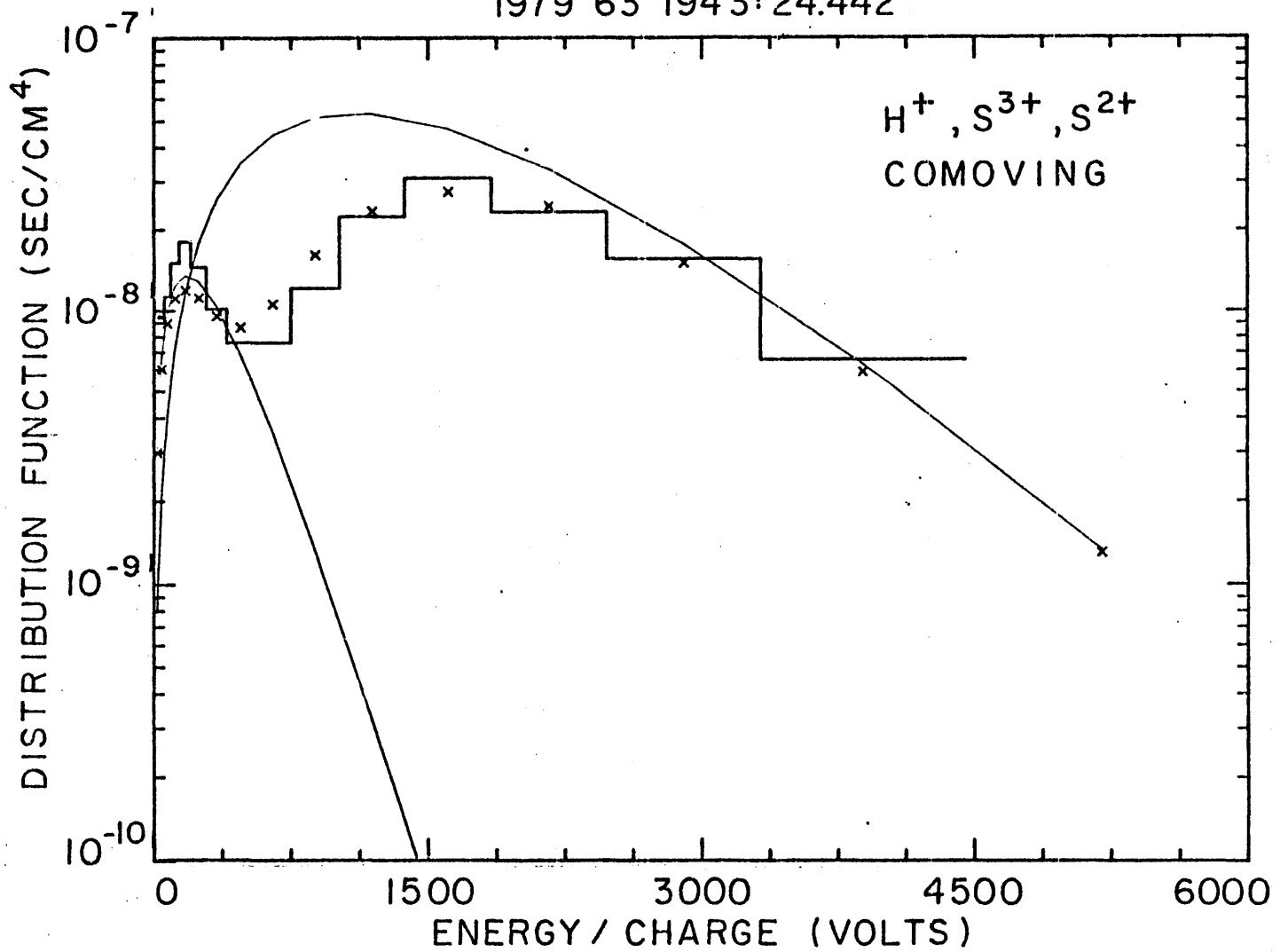


FIGURE 34

1979 63 1943: 24.442

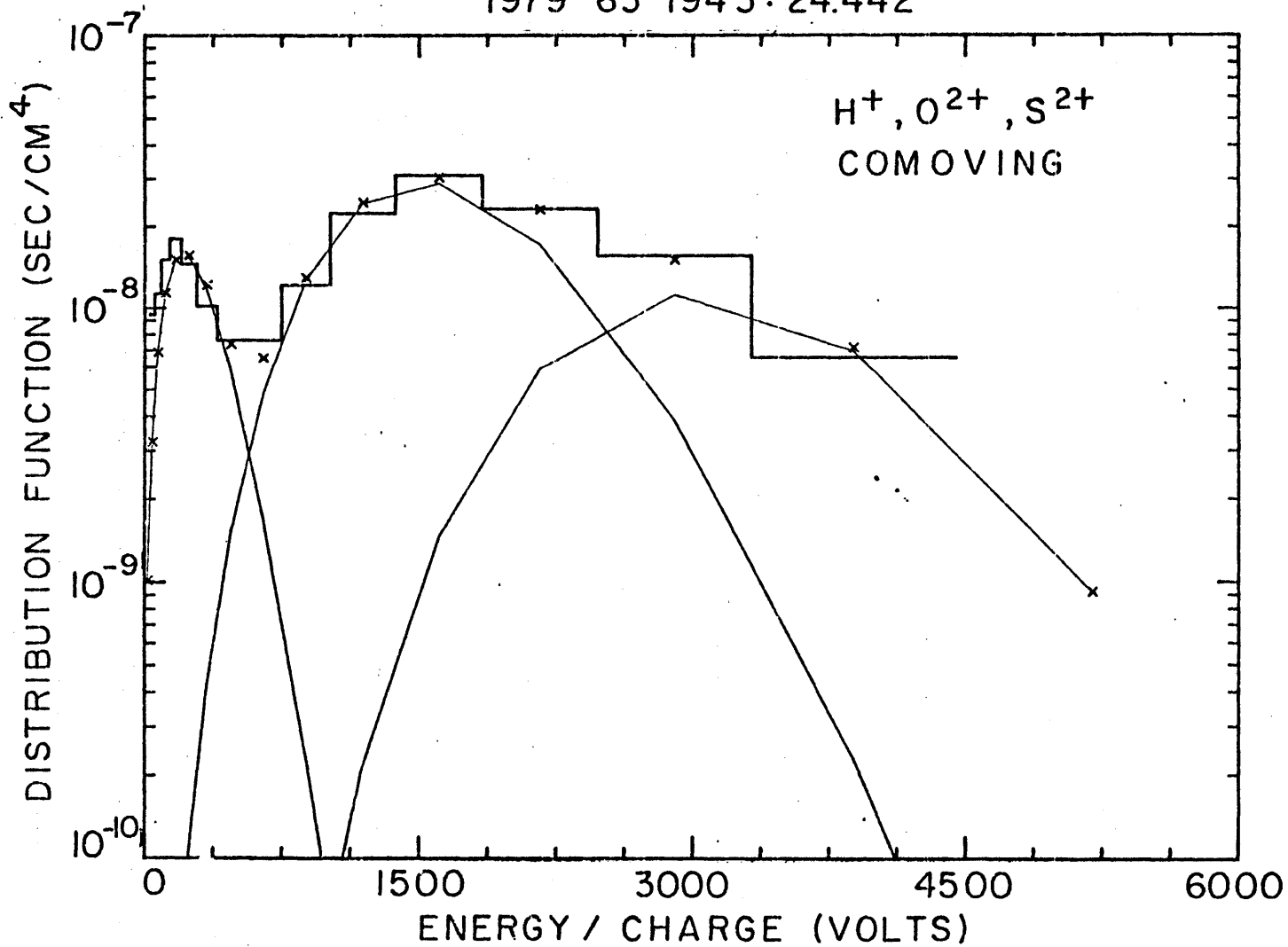


FIGURE 35

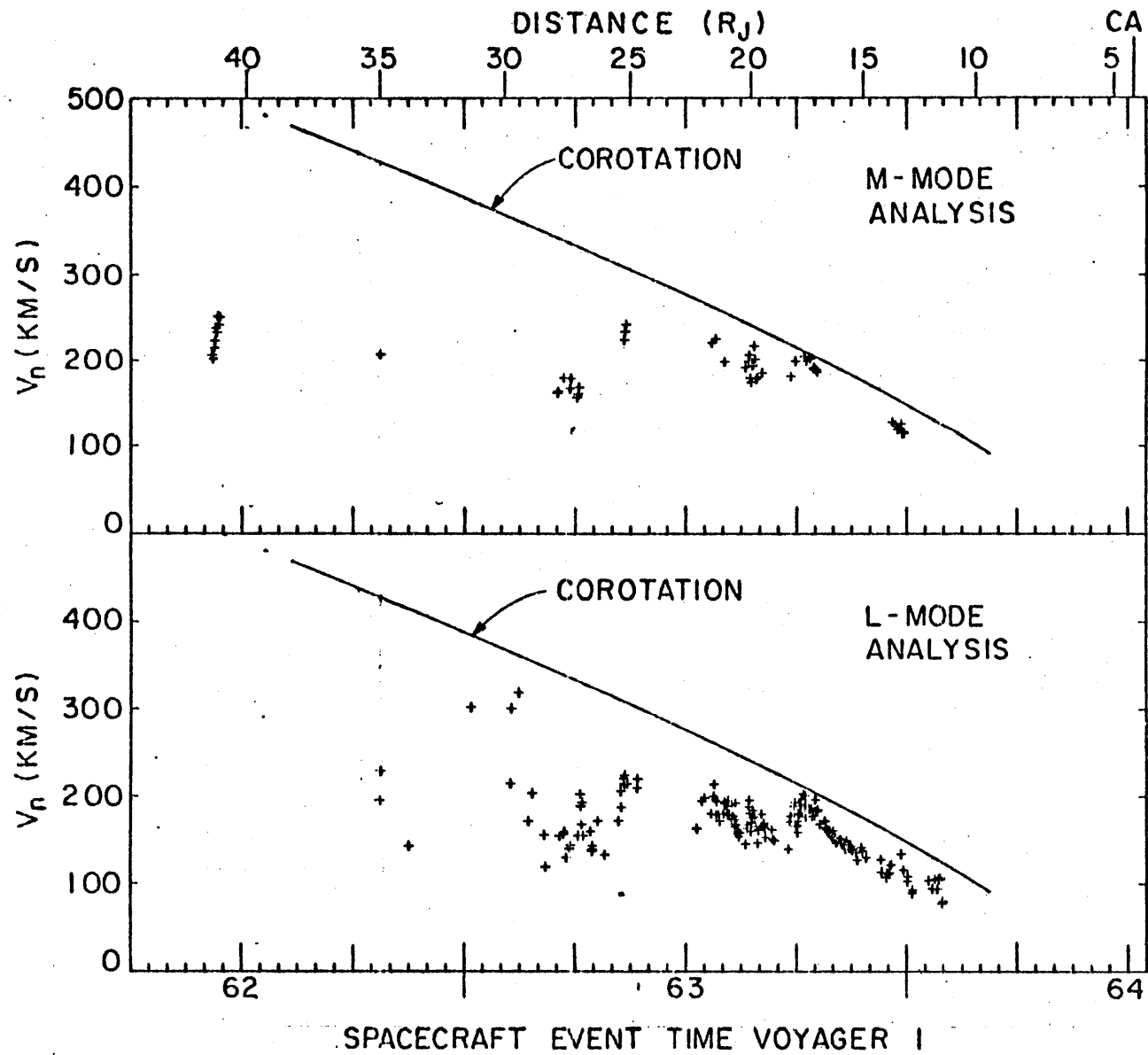


FIGURE 36

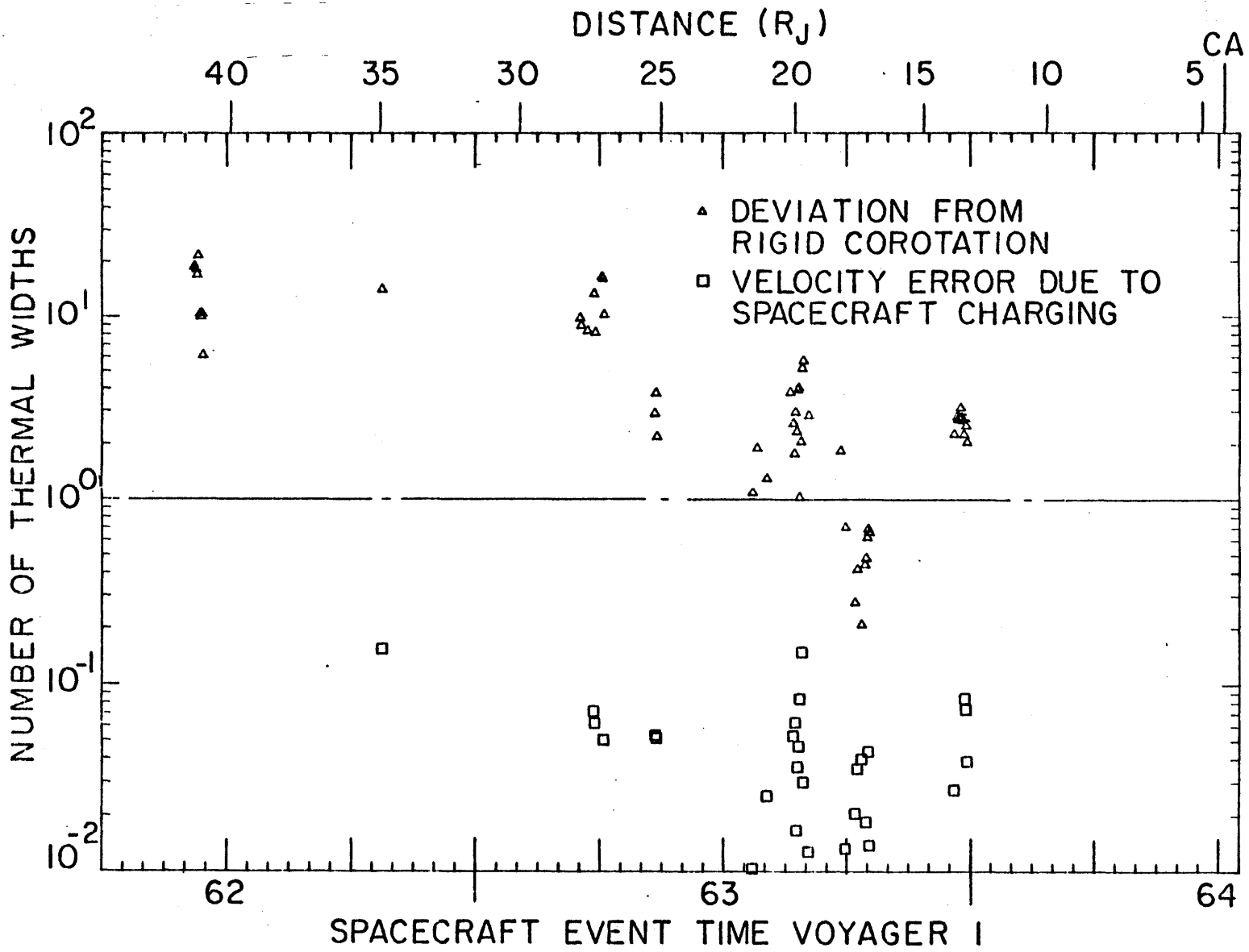


FIGURE 37.

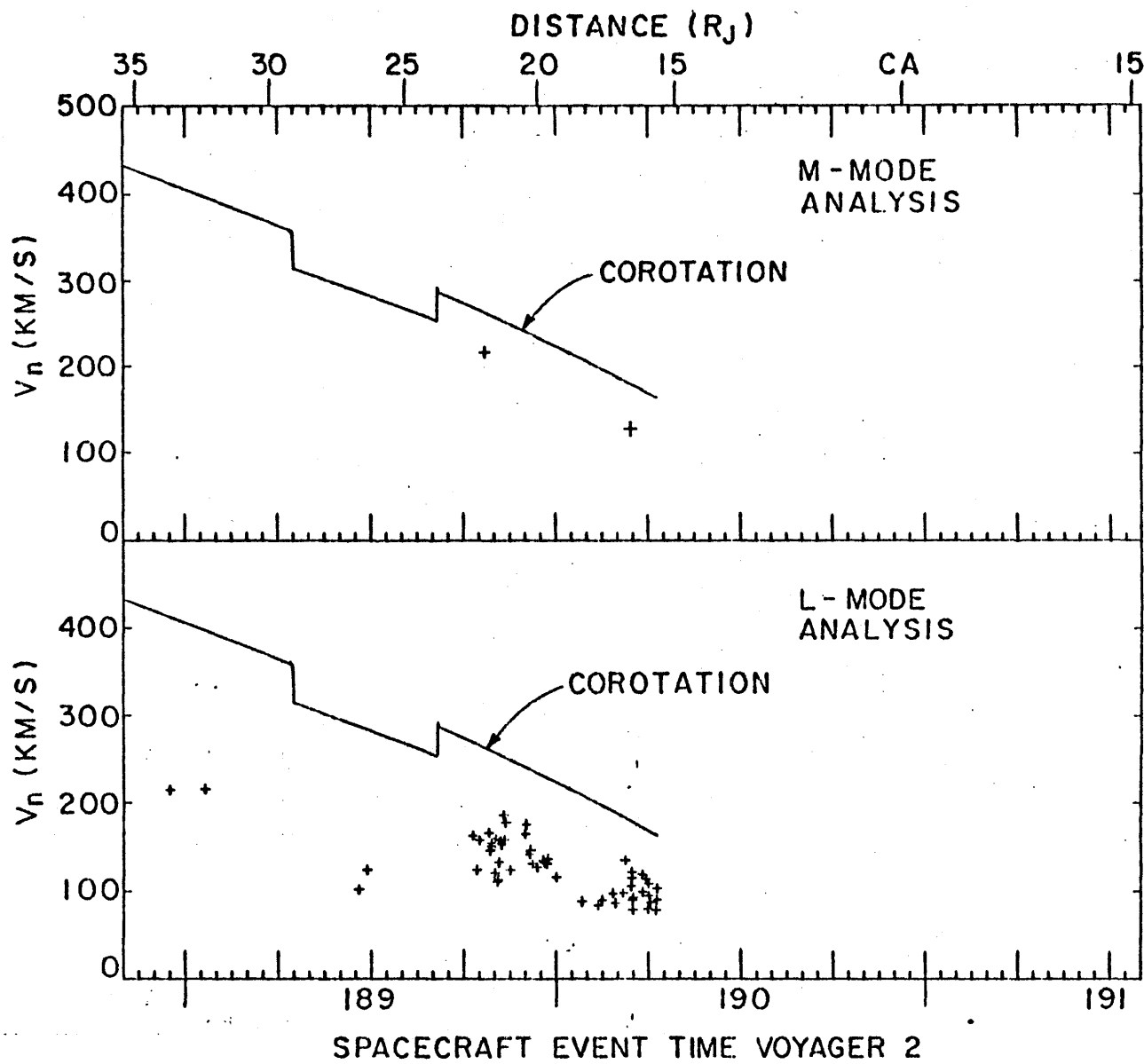


FIGURE 38

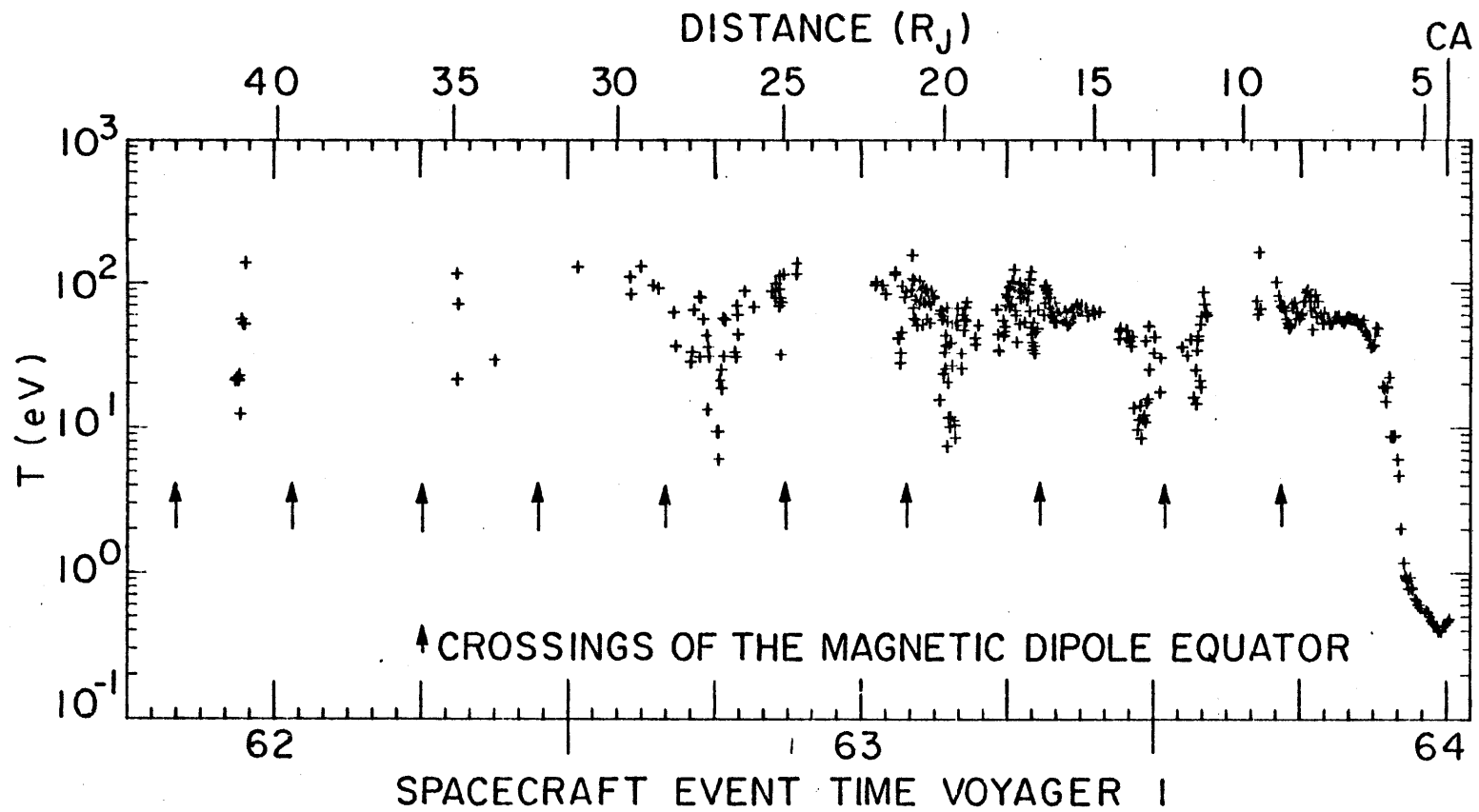
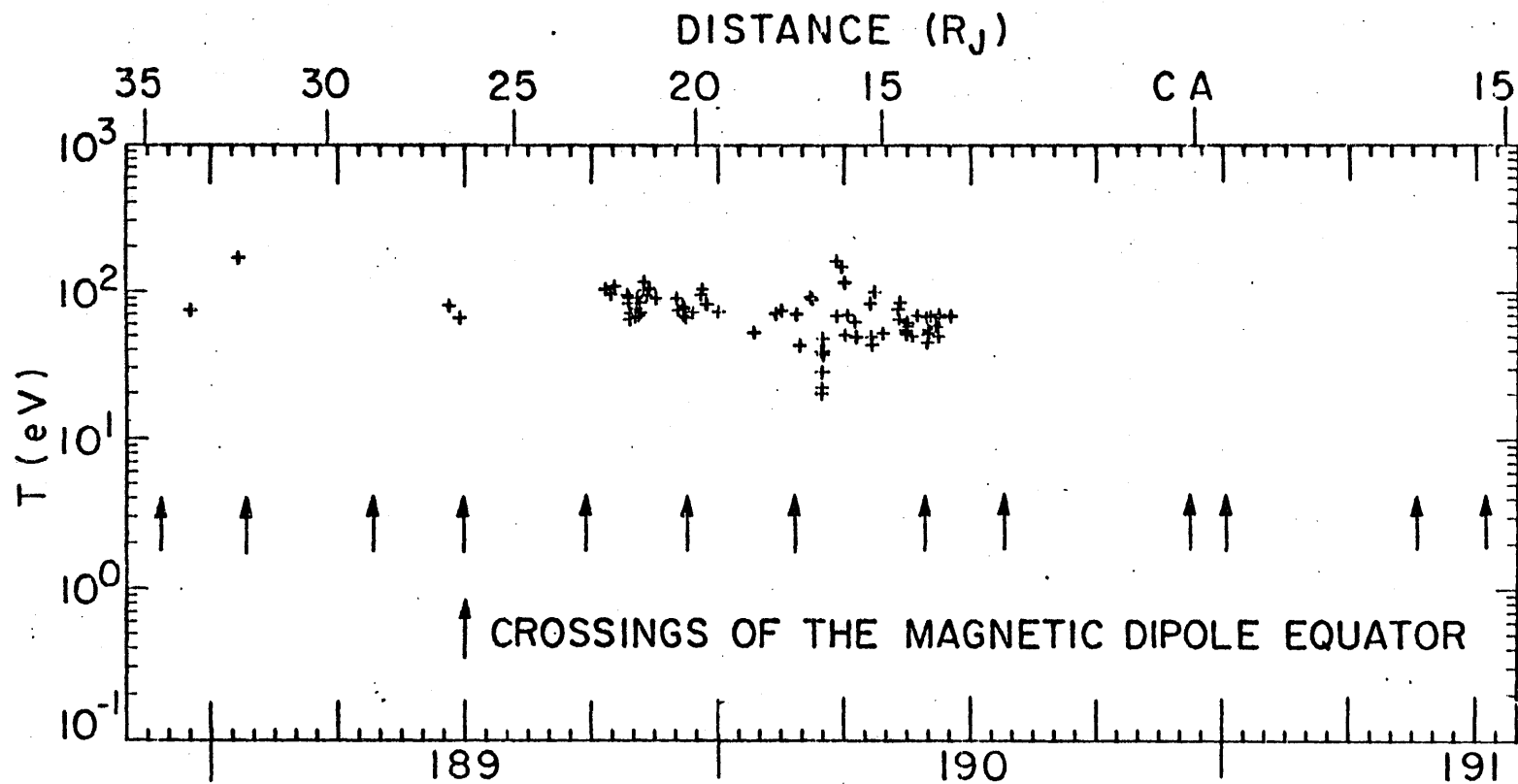


FIGURE 39



SPACECRAFT EVENT TIME VOYAGER 2

FIGURE 40

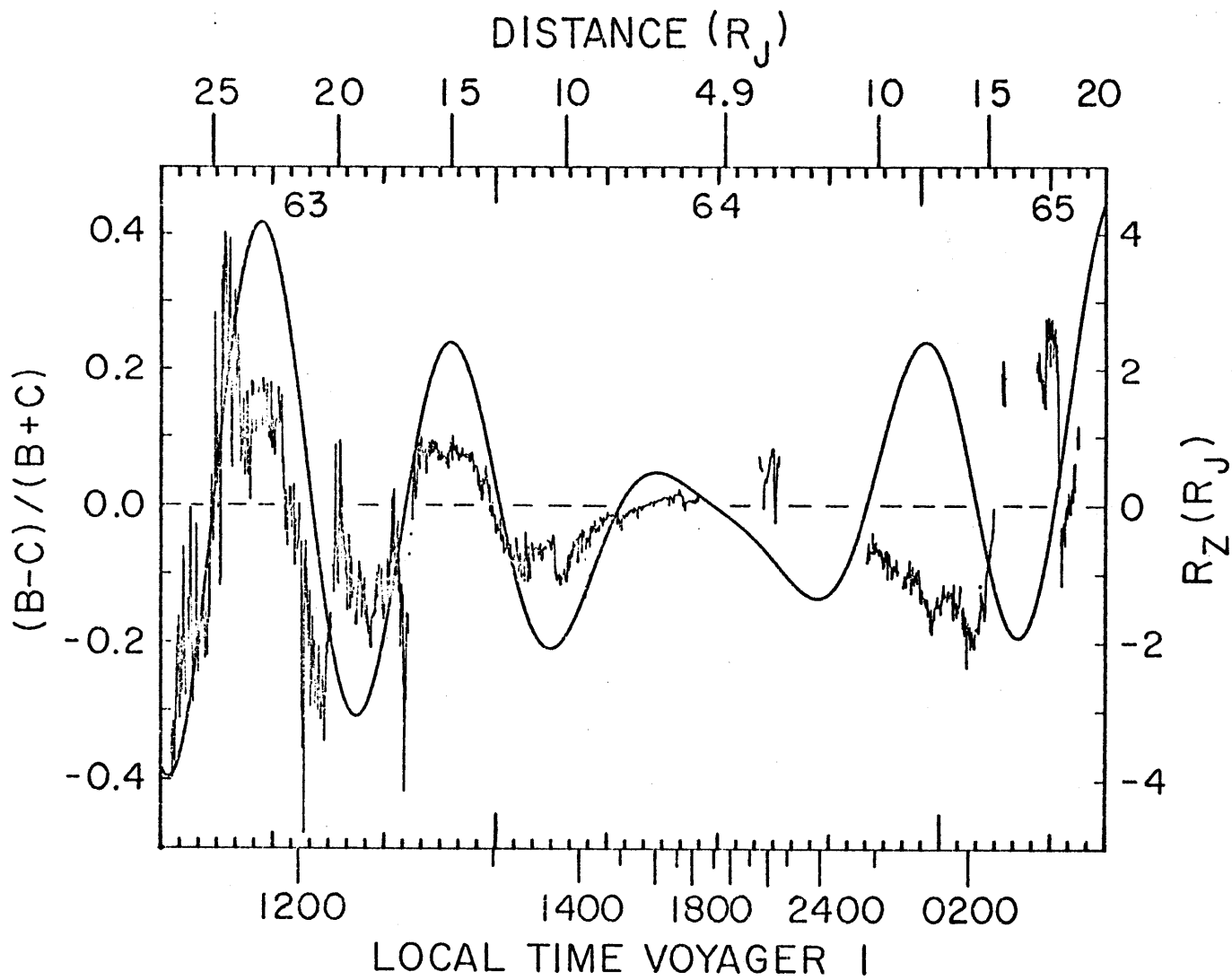


FIGURE 41

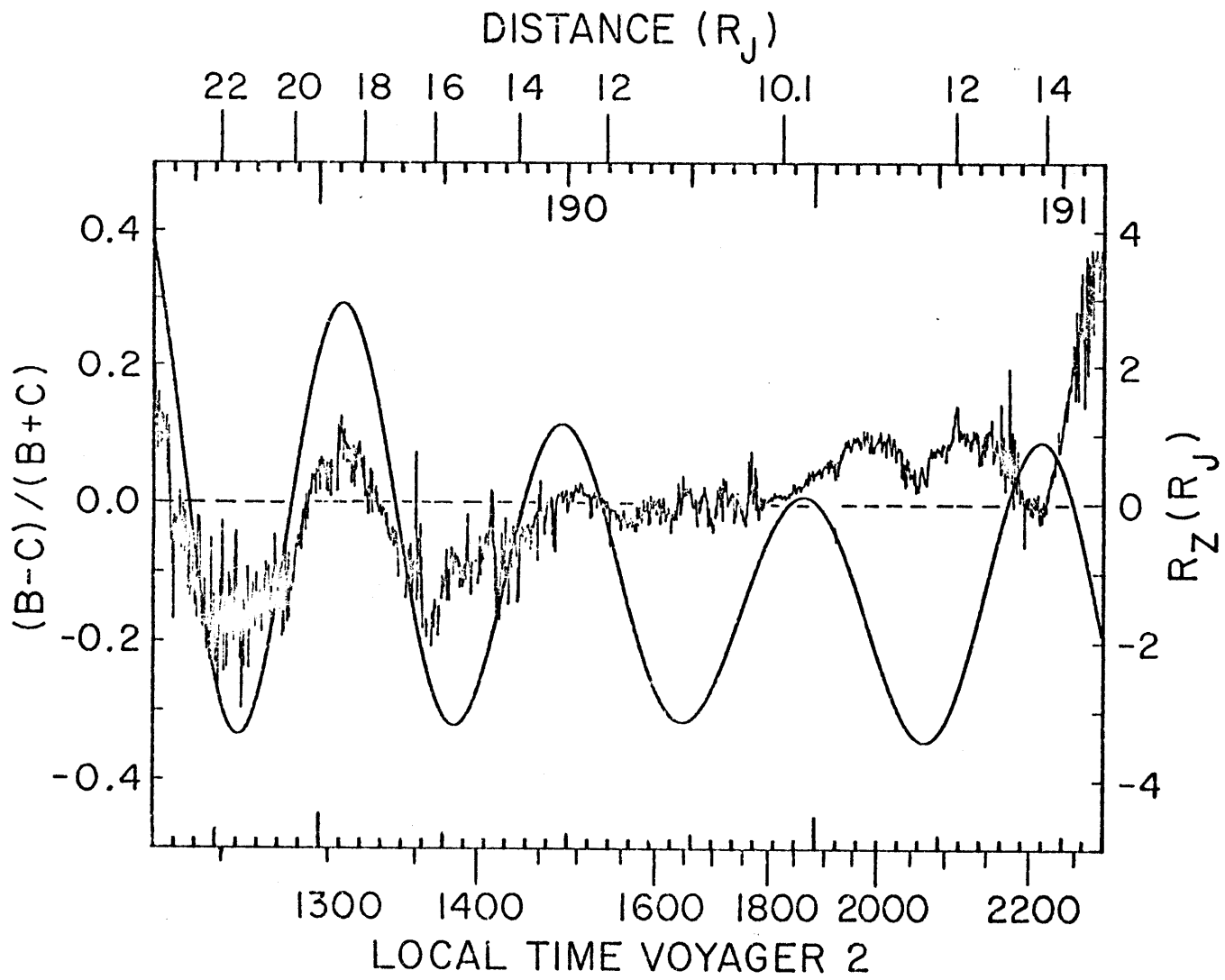


FIGURE 42

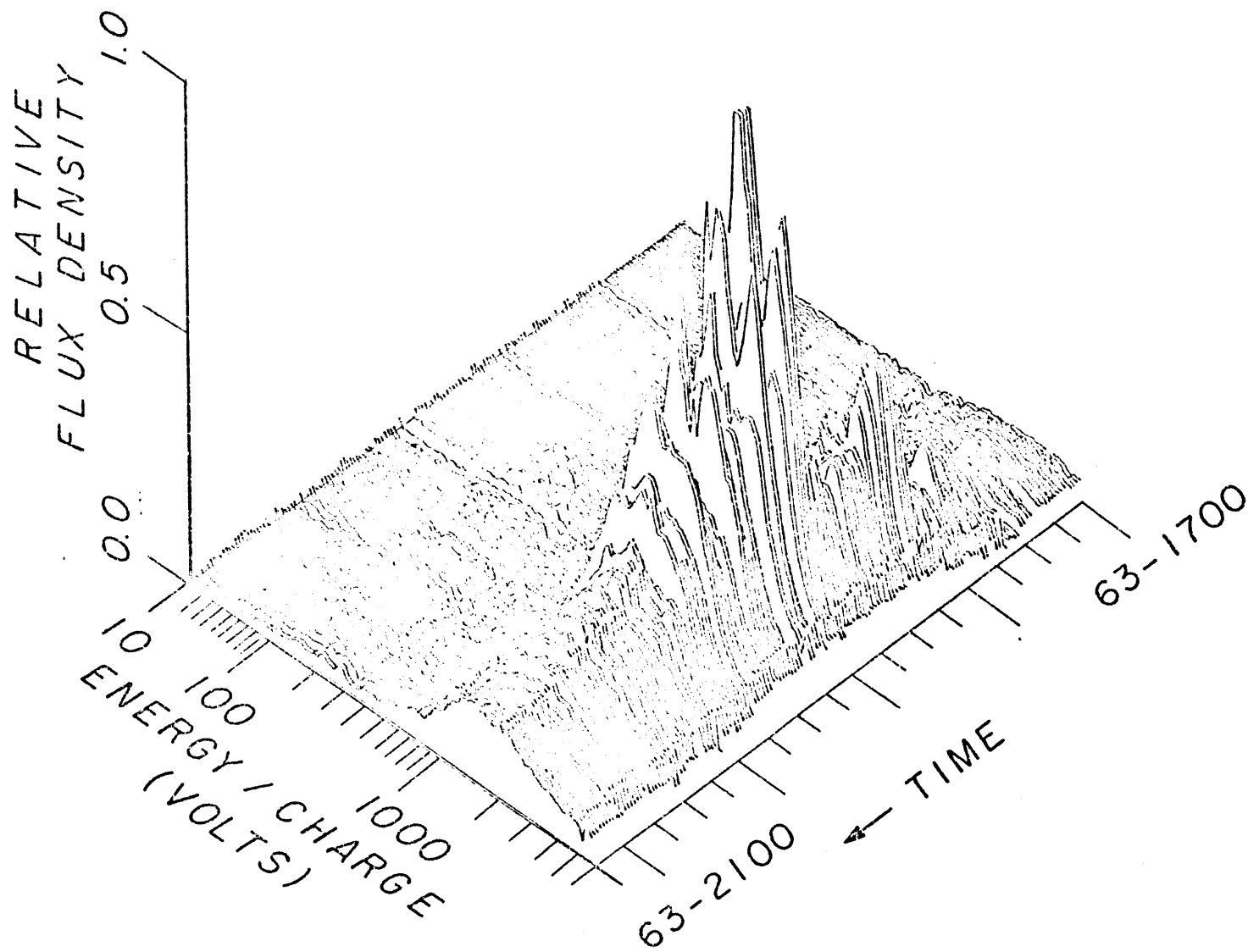


FIGURE 43

# L-MODE SPLINE

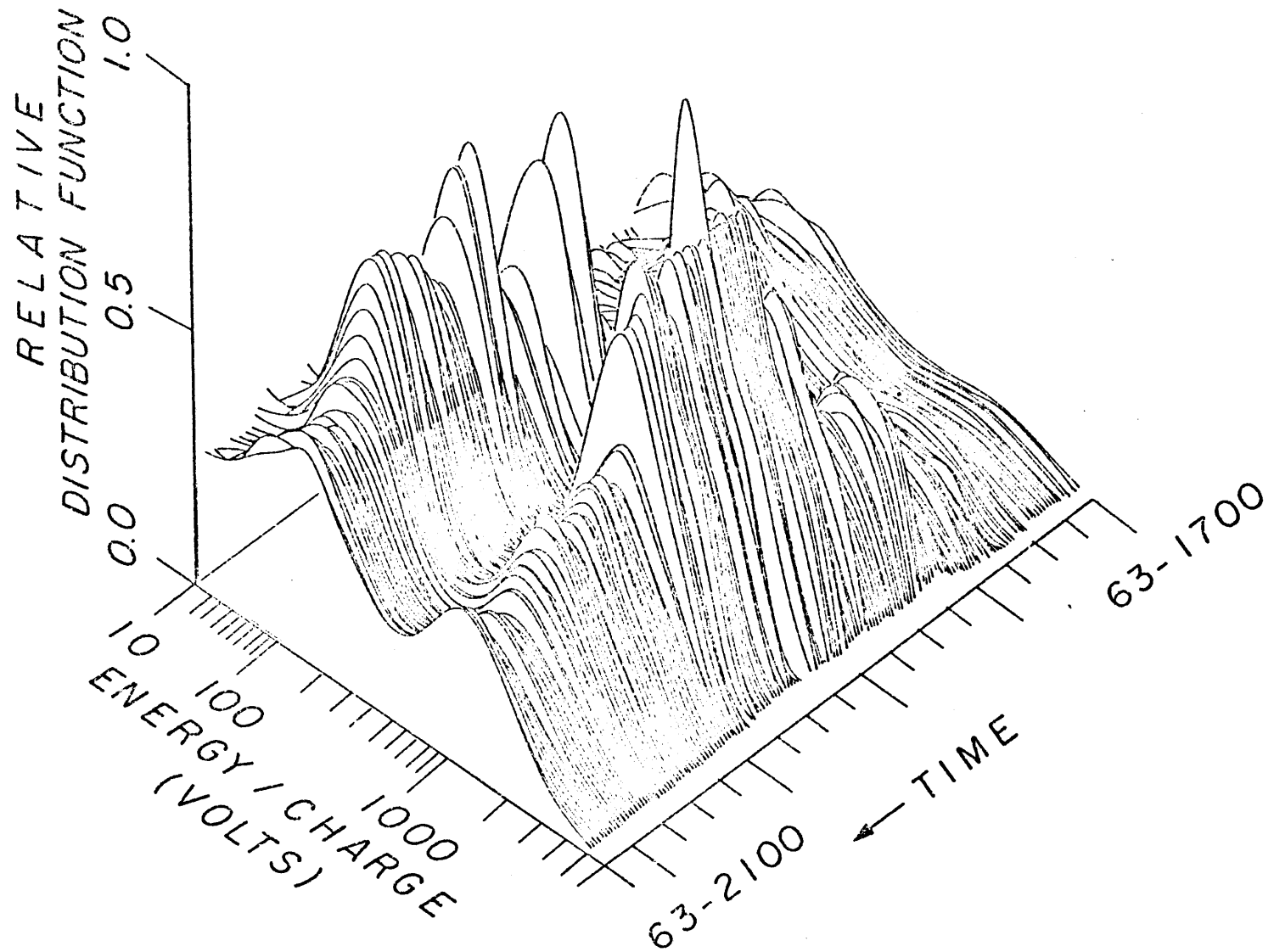


FIGURE 44

## VOYAGER I INBOUND

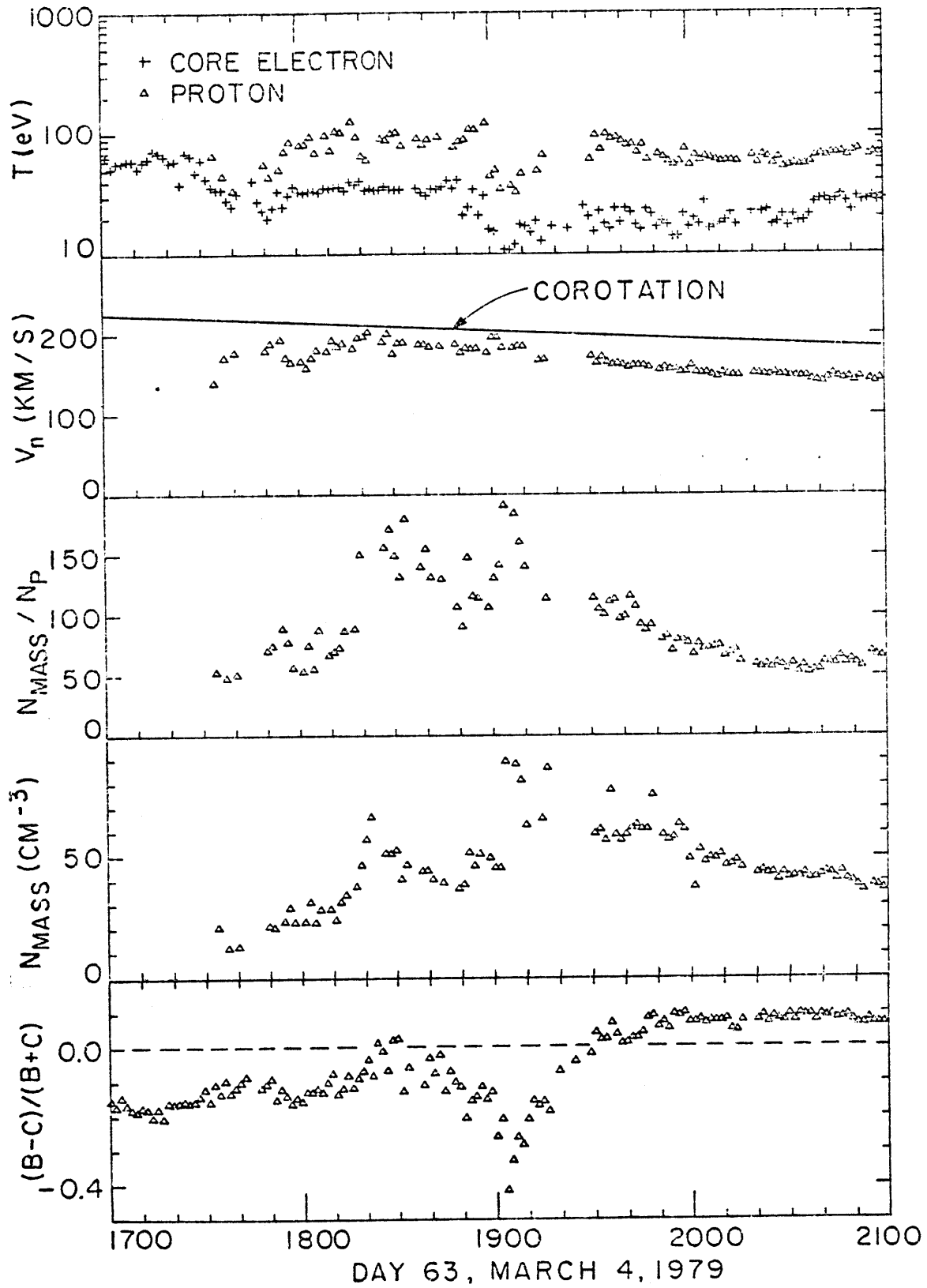


FIGURE 45

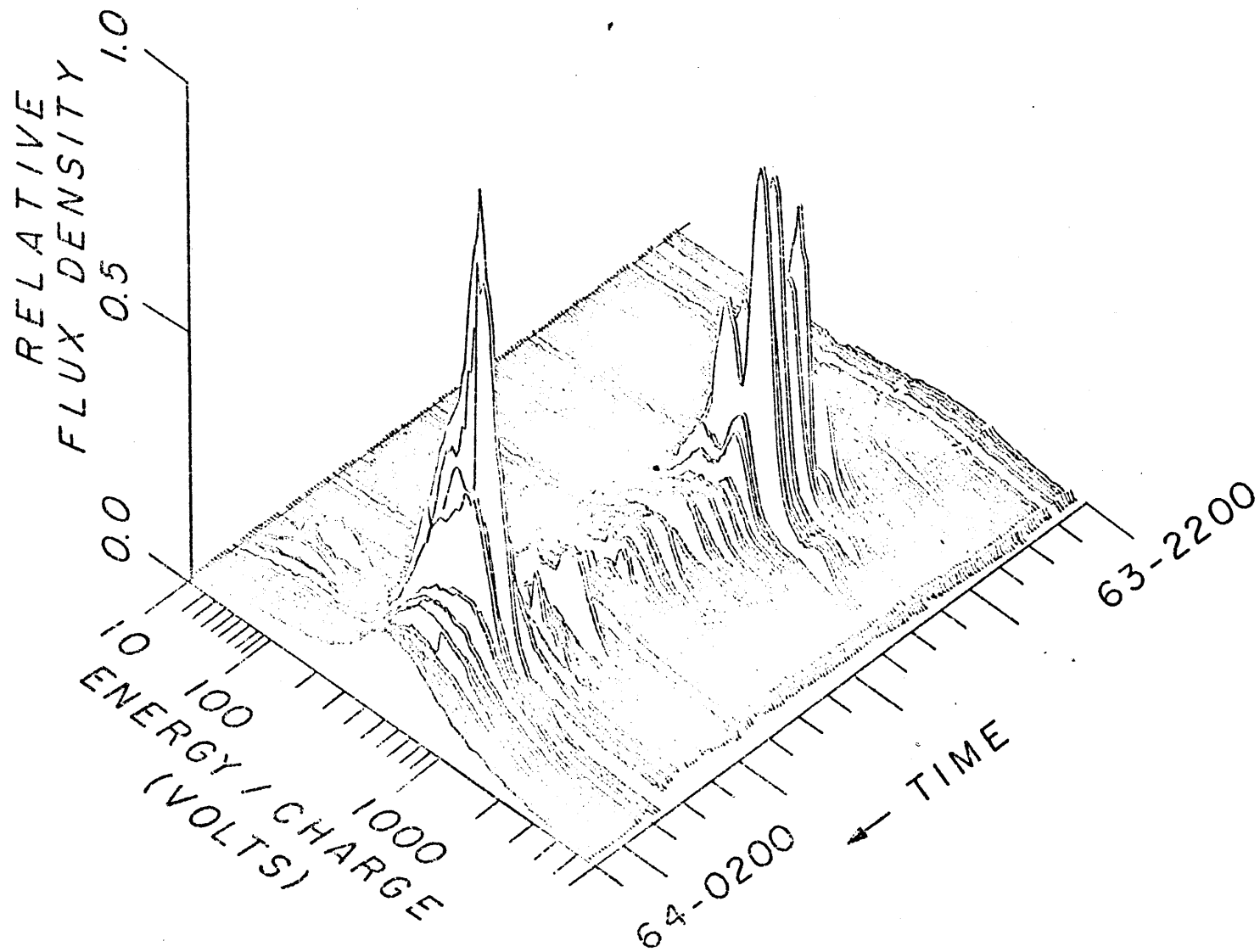


FIGURE 46

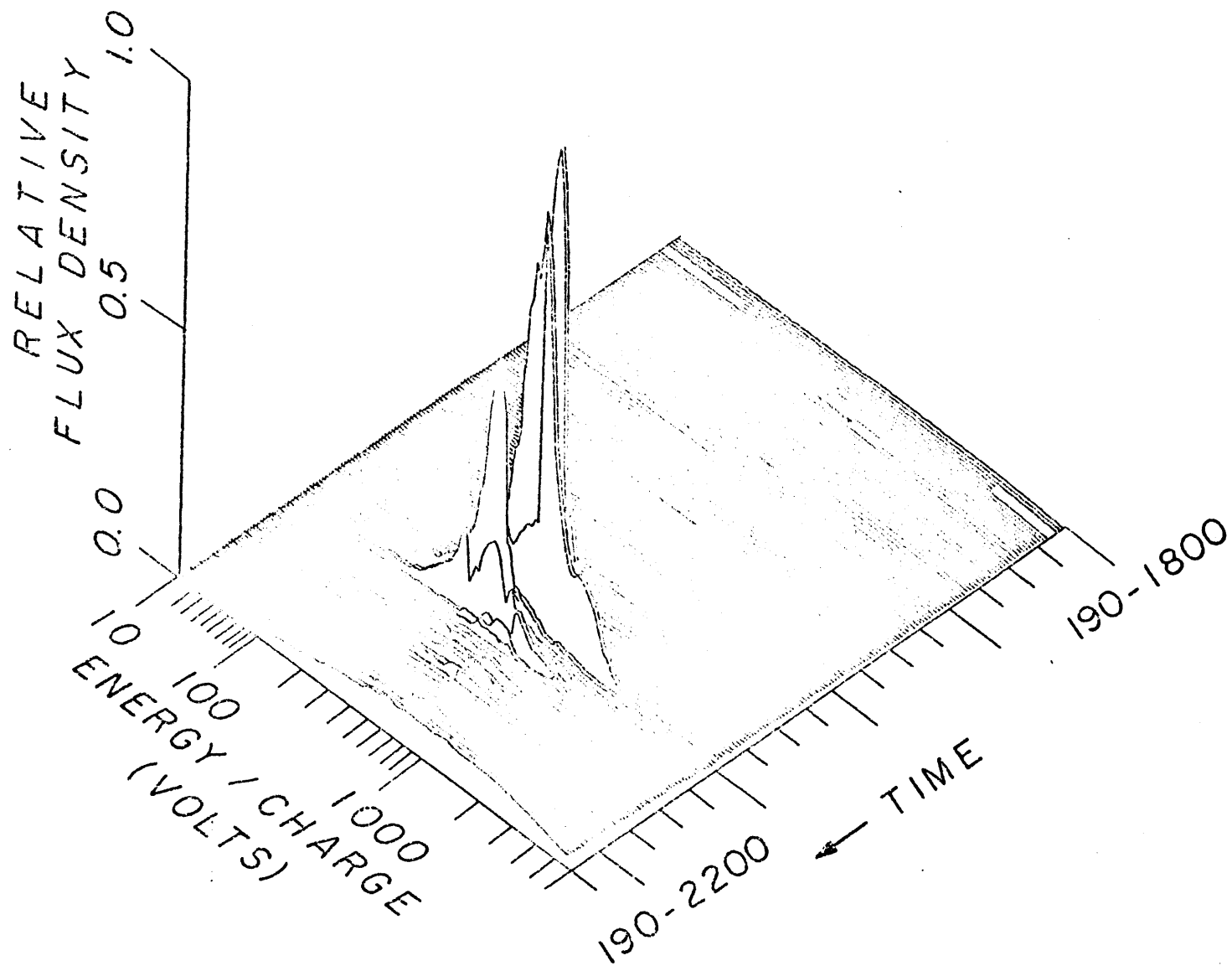


FIGURE 47

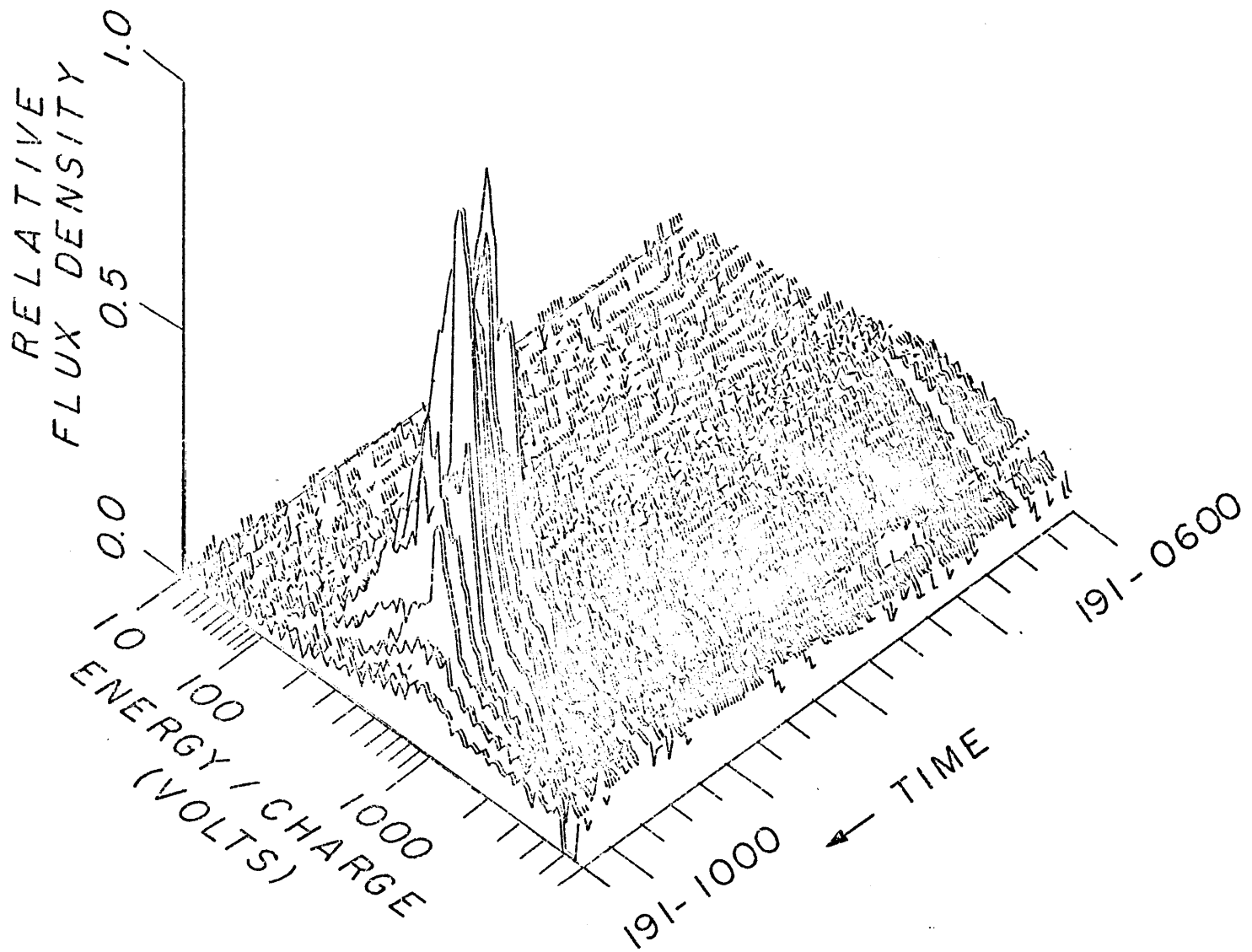


FIGURE 48

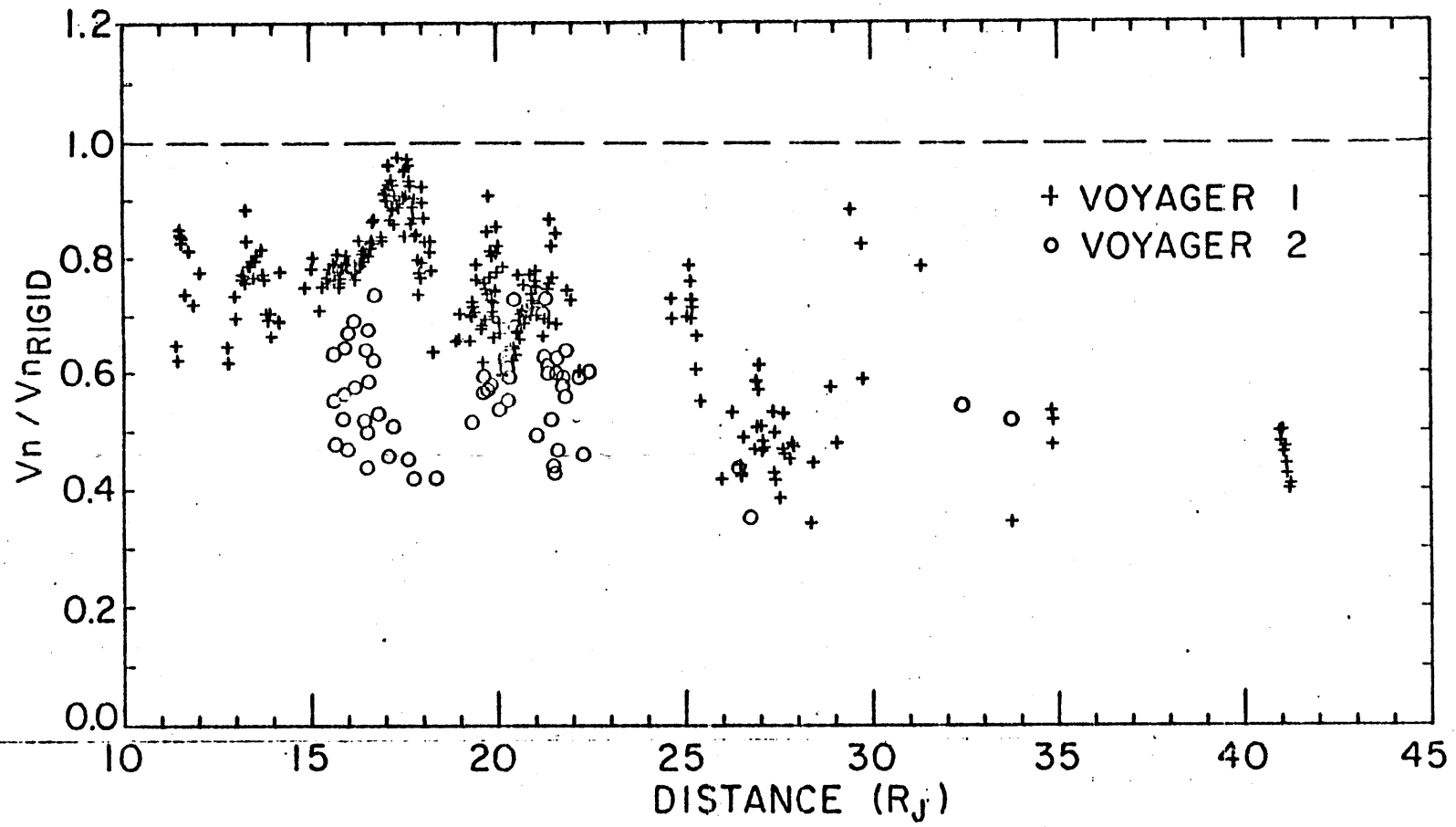


FIGURE 49

# VOYAGER 1 INBOUND

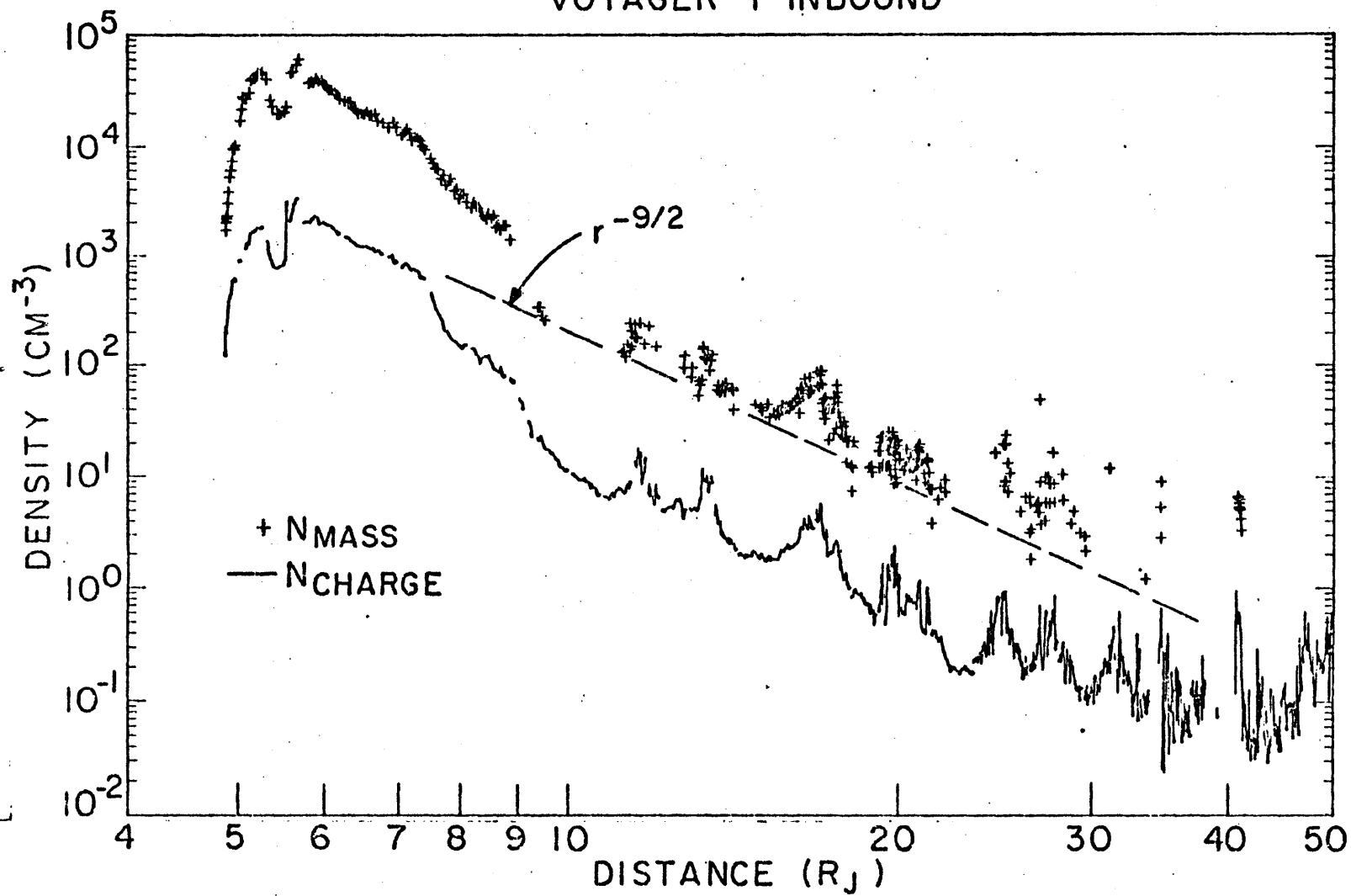


FIGURE 50

# VOYAGER 2 INBOUND

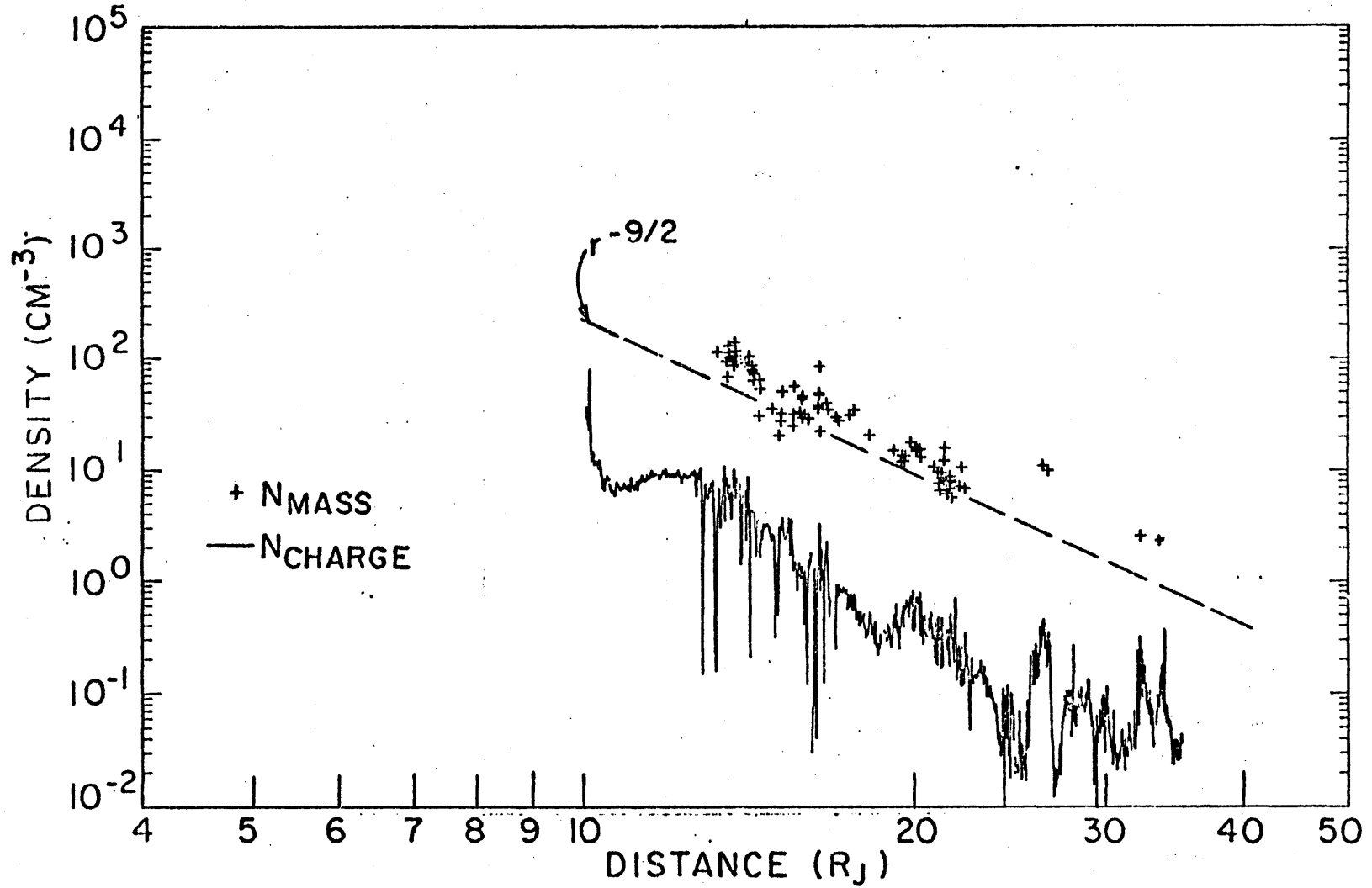


FIGURE 51

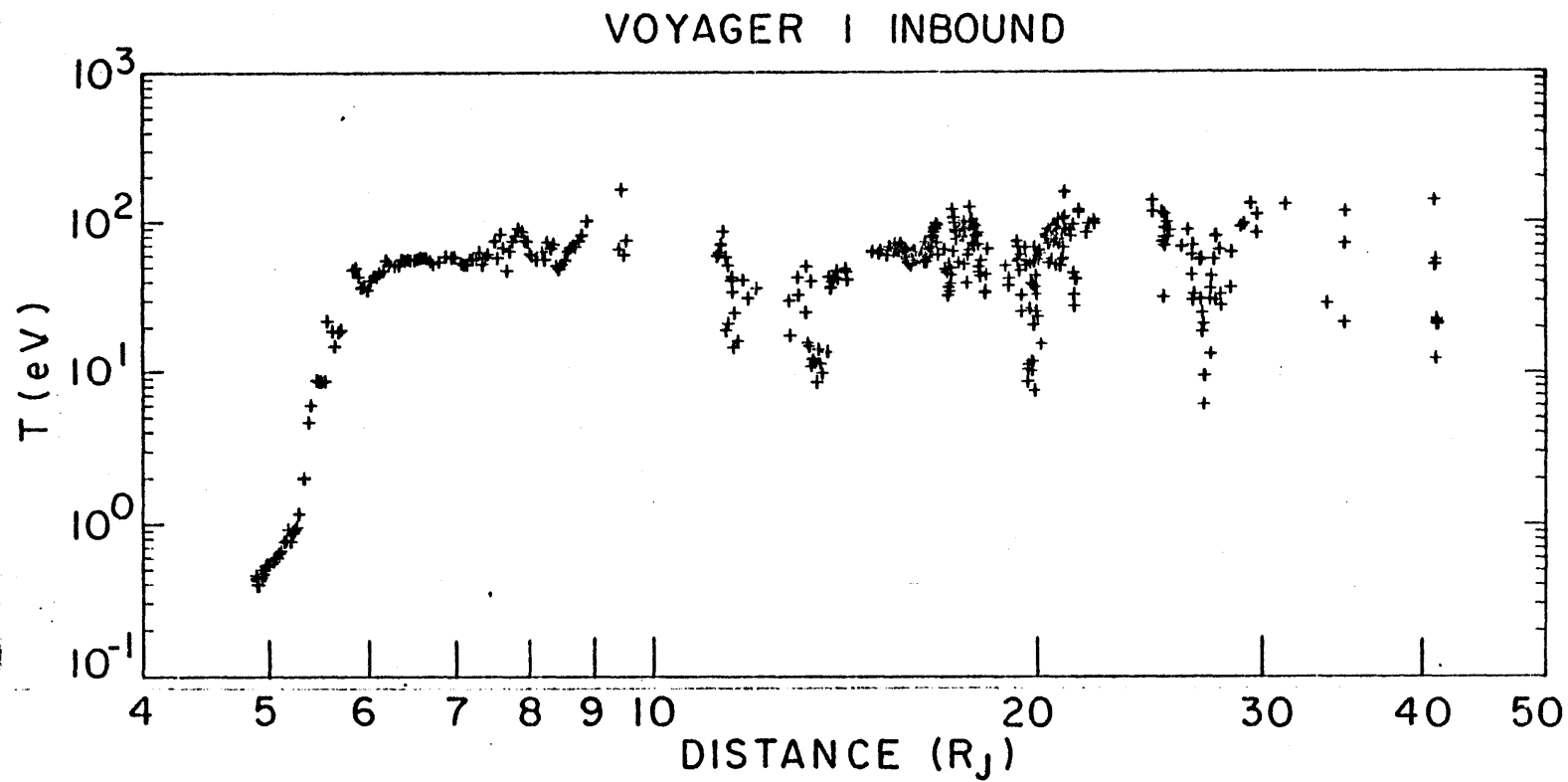


FIGURE 52

VOYAGER 2 INBOUND

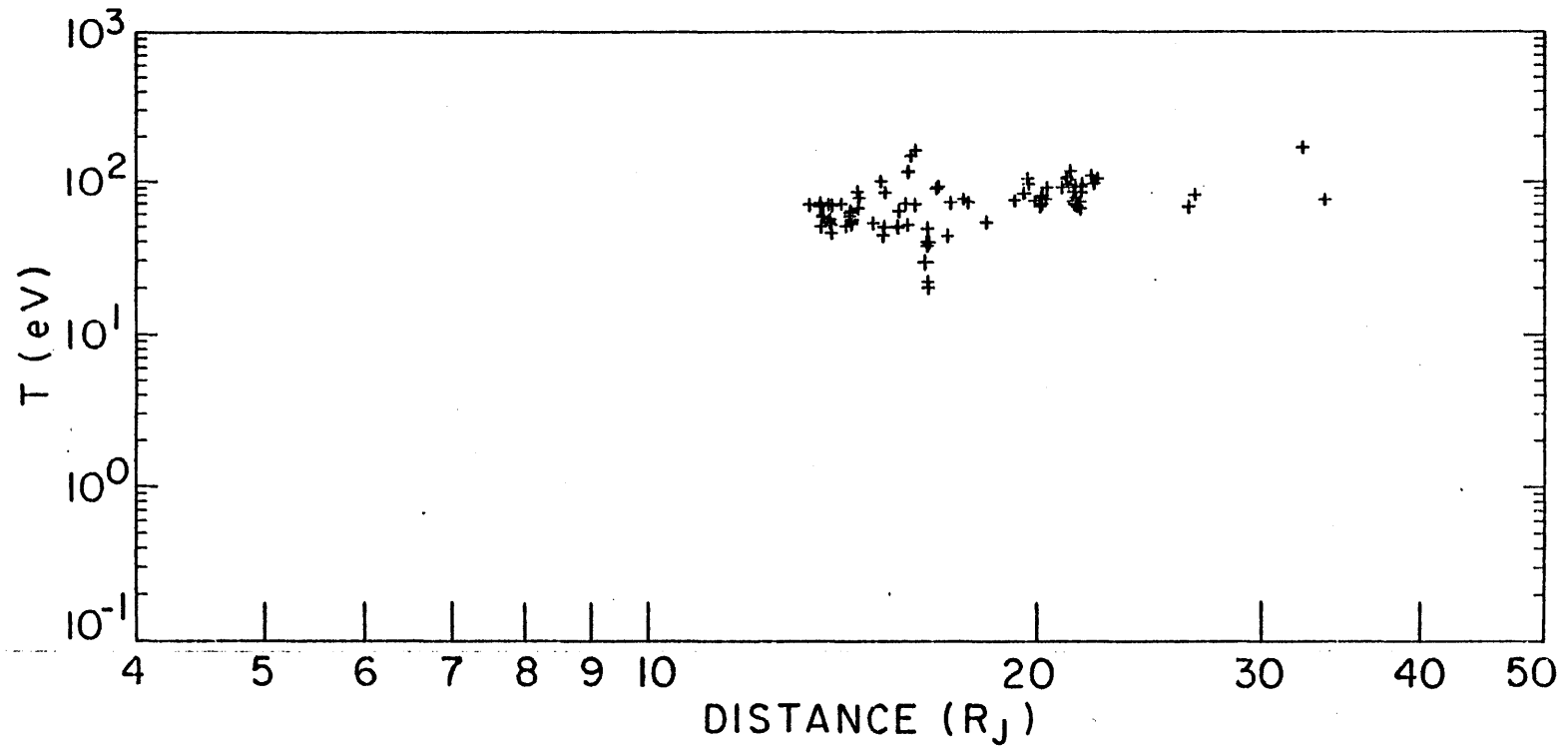


FIGURE 53

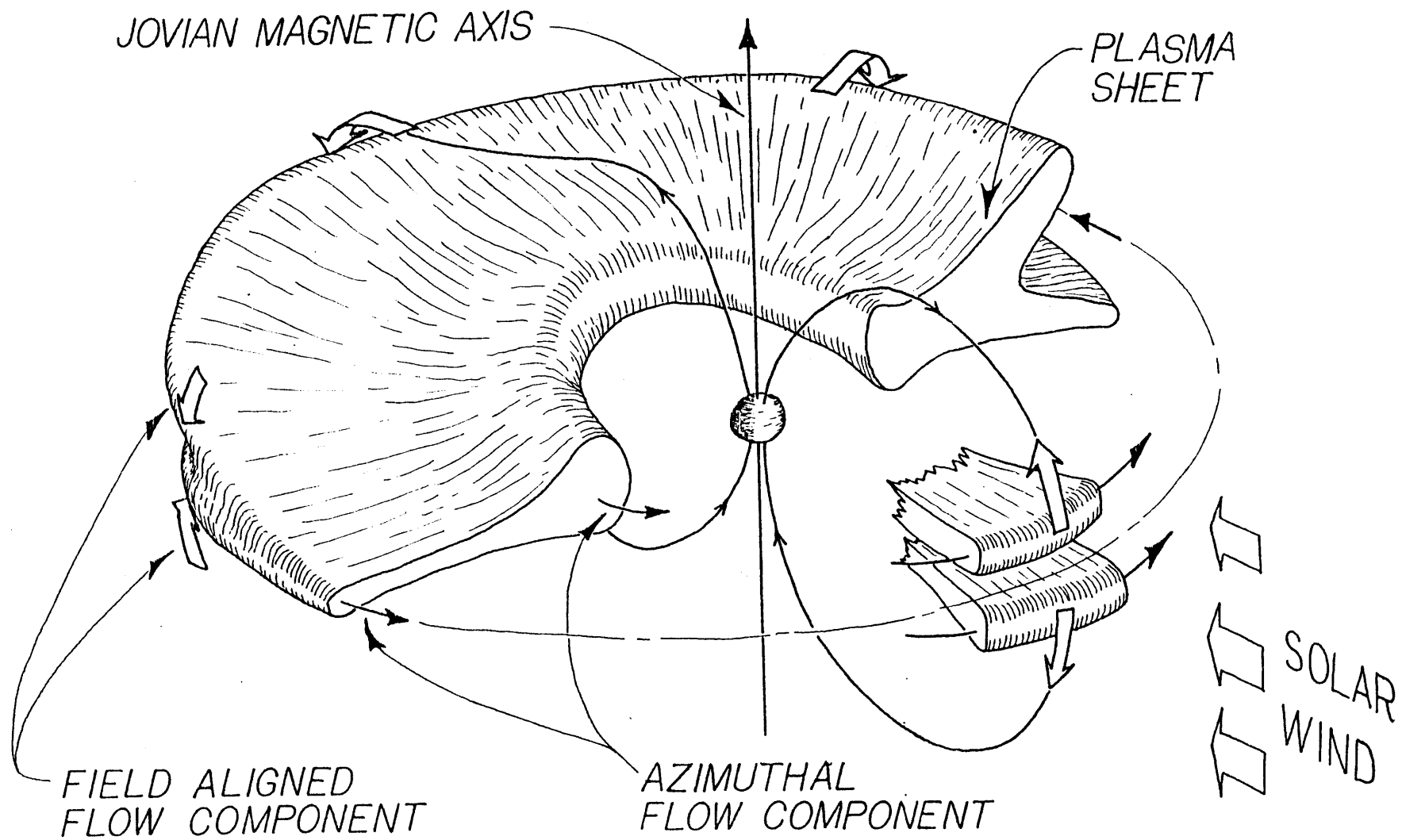


FIGURE 54

## BIOGRAPHICAL NOTE

The author was born on October 29, 1953 in Fort Worth, Texas and attended the public schools there. In May, 1975, he received the B.S. degree in Physics, summa cum laude, from Texas A & M University. He is a member of Phi Kappa Phi, Sigma Xi, and the American Geophysical Union. The author is married to Nancy B. Auclair, D.V.M.